DOE/NASA/0032-23
NASA CR-174674
MTI 84ASE356DR3

Automotive Stirling Engine Development Program

RESD Summary Report

Mechanical Technology Incorporated

May 1984

Prepared for
NATIONAL AERONAUTICS AND SPACE ADMINISTRATION
Lewis Research Center
Under Contract DEN 3-32

for
U.S. DEPARTMENT OF ENERGY
Conservation and Renewable Energy
Office of Vehicle and Engine R&D

DISCLAIMER

Printed in the United States of America

Available from
National Technical Information Service
U.S. Department of Commerce
5285 Port Royal Road
Springfield, VA 22161

NTIS price codes[1]
Printed copy: A10
Microfiche copy: A01

[1]Codes are used for pricing all publications. The code is determined by the number of pages in the publication. Information pertaining to the pricing codes can be found in the current issues of the following publications, which are generally available in most libraries: *Energy Research Abstracts (ERA); Government Reports Announcements* and Index (*GRA* and I); *Scientific and Technical Abstract Reports (STAR);* and publication, NTIS-PR-360 available from NTIS at the above address.

DOE/NASA/0032-23
NASA CR-174674
MTI 84ASE356DR3

Automotive Stirling Engine Development Program

RESD Summary Report

Stirling Engine Systems Division
Mechanical Technology Incorporated
Latham, New York 12110

May 1984

Prepared for
National Aeronautics and Space Administration
Lewis Research Center
Cleveland, Ohio 44135
Under Contract DEN 3-32

for
U.S. DEPARTMENT OF ENERGY
Conservation and Renewable Energy
Office of Vehicle and Engine R&D
Washington, D.C. 20545
Under Interagency Agreement DE-AI01-77CS51040

TABLE OF CONTENTS

TABLE OF CONTENTS (CONT'D)

TABLE OF CONTENTS (CONT'D)

1.0 INTRODUCTION AND SUMMARY

The Reference Engine System Design (RESD) is defined as the best engine design that meets the objectives established for the Automotive Stirling Engine (ASE) Development Program. The engine design must utilize technologies expected to be developed during the course of the ASE Program, which is projected to extend to 1987.

The RESD program objectives are specified as:

- Demonstrate at least 30% improvement in combined metro/highway fuel economy over that of a comparable production, internal-combustion powered vehicle

- Show potential for the following emissions levels in grams per mile after 50,000 miles: $NO_x \leq 0.4$, $HC \leq 0.41$, $CO \leq 3.4$, and total particulates ≤ 0.2

- Achieve a competitive manufacturing cost

- Provide for the ability to use alternative fuels, although the engine will be designed specifically for unleaded gasoline

- Match the reliability and durability of existing automotive power plants

- Provide suitable acceleration for the automotive mission

- Exhibit safety and noise levels that meet Federal standards.

Efforts conducted in the 1983 RESD have focused on reducing the manufacturing cost to a level competitive with the IC/diesel engines, while maintaining emphasis on mileage and emissions. The current 1983 RESD configuration resulting from this study is shown along side the 1981 RESD in Figure 1-1. Highlights of the 1983 RESD are:

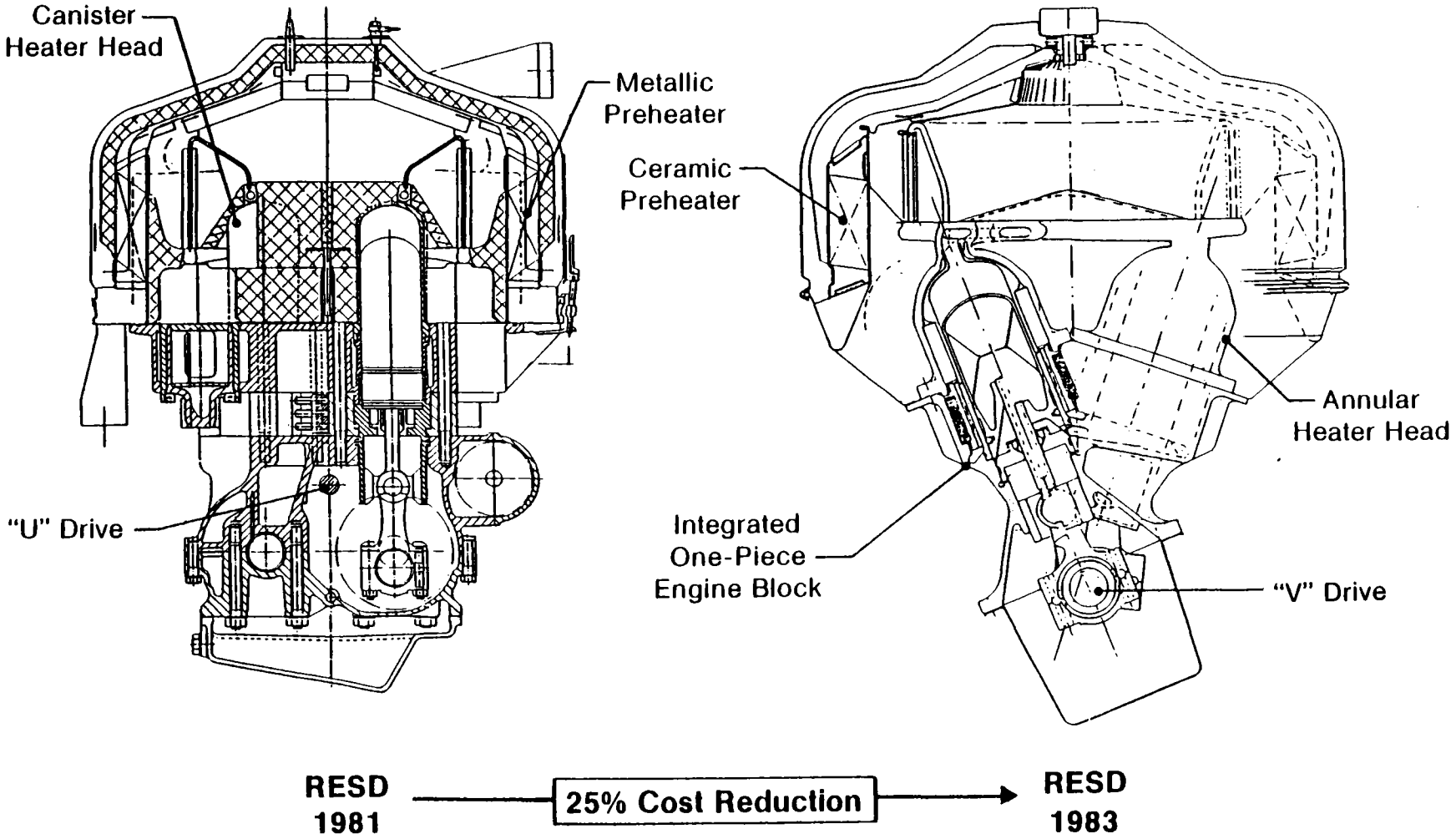

Figure 1-1 Reference Engine Design Concept

832377-1

- Four-cylinder, double-acting engine
- V configuration
- Annular regenerator/cooler
- Ceramic preheater
- Rolling-element drive unit.

This 1983 RESD configuration represents a marked departure from the 1981 RESD, which exhibited the U-drive, canister configuration. The primary driver for this configuration change is, as mentioned, manufacturing cost. Significant gains in manufacturing costs are obtained through the V annular configuration by:

1. Reduction in the number of heater head castings
2. Reduction in the number of rotating parts
3. Simpler block/cold engine structure.

The estimated manufacturing cost for the 1983 RESD, in 1984 dollars, is $1314, representing a reduction of $617 from the 1981 RESD. In addition to the cost reductions achieved by adoption of the V annular configuration, engine system costs have been reduced by incorporation of revised control systems and engine auxiliaries. Major gains in these areas are realized by incorporating a rotating, electrically-driven (rather than translating hydraulically-driven), power-control valve and a positive-displacement combustion air blower. These two components together can eliminate the need for up to three additional systems (the variator, servo-oil system, and possibly the air throttle) and 12 out of 14 check valves.

A comparison of engine performance and weight characteristics for the 1983 RESD and 1981 RESD concepts are shown in Table 1-1. Although the emphasis in the 1983 RESD was placed on manufacturing cost, it should be noted that performance levels of the 1981 RESD were, in general, retained.

The projected fuel economy performance of the 1983 RESD in the chosen vehicle (a 1984 Pontiac Phoenix X-Body) is shown in Table 1-2. The mileage

TABLE 1-1

ENGINE PERFORMANCE SUMMARY

	1981 RESD	1983 V-4 RESD
Maximum Power Point		
Power (kW)	60.1	60.0
(hp)	80.6	80.0
Speed (rpm)	4000	4000
Working Gas Pressure (MPa)	15	15
Efficiency	34.2	34.6
Maximum Efficiency Point		
Power (kW)	22.1	25.5
(hp)	29.6	34.2
Speed (rpm)	1100	1350
Working Gas Pressure (MPa)	15	15
Efficiency	43.5	42.2
Part-Load Point		
Power (kW)	12.2	12.0
(hp)	16.4	16.0
Speed (rpm)	2000	2000
Working Gas Pressure (MPa)	5	5
Efficiency	37.7	37.3
Weight (kg)	180	173
Power Density (lb/hp)	4.9	4.7

TABLE 1-2

PROJECTED RESD VEHICLE FUEL ECONOMY

Urban Without Cold-Start Penalty	41.3 mpg
Urban With Cold-Start Penalty	32.3 mpg
Highway	56.9 mpg
Combined (Gasoline)	40.1 mpg
Combined (Diesel)	46.1 mpg
Comparable IC	31.0 mpg
% Improvement Relative to IC	
With Gasoline	29.4%
With Diesel	48.8%

improvement indicated relative to the equivalent IC system meets the ASE Program goal of 30%.

The selected RESD concept, with its departure from the standard Stirling-engine configurations, indicates the need for development of key technologies; namely:

- Annular Heater Head Configuration - This head design is a relatively new concept, proven conceptually on a P-40 Stirling engine, but one that has had little development work. Specifically, technology development is required to verify the manufacturability of the assembly and development of the partition wall, particularly for minimum head conduction. The configuration and flow pathing of the regenerator and heater manifolds must also be addressed.

- V Configuration - Incorporation of the unitized Vee block to take the place of a water jacket/crankcase/bedplate combination requires that the Vee-block system be developed for castability, and that stress testing be conducted to confirm block integrity. Testing is required on a full block system due to the three-dimensional nature of this design.

- Control System - Simplification of the control system requires development of the rotating power-control valve to ensure attainment of adequate gas sealing and verification of the check valve elimination.

- Combustion Air Blower - Development of this component in conjunction with the control system is required to verify system simplicity with elimination of the servo-oil system and air throttle.

- Hydrogen Compressor System - A hydrogen compressor that would pump the engine charge pressure to a lower level than the current ASE Mod I engines results in elimination of the need for a combustion air blower upstart motor.

- CGR Combustor - The RESD combustor design is only conceptual at this stage; it requires development to ensure low temperature spread and good durability.

Since these key technologies are highly system related, development would be achieved via a full engine system.

2.0 COMPONENT DESIGN DEFINITION

2.1 External Heat System

2.1.1 Preheater

Description

A ceramic recuperative preheater proposed for use in the RESD engine will be a counterflow, corrugated-plate heat exchanger similar to existing preheaters found in the P-40 and Mod I engines; the major differences are the material and flat rather than involute plates. The final material for this component will be developed during the testing program, but should be similar in nature to cordierite (a mixed oxide ceramic made from MgO, Al_2O_3, and SiO_2). The preheater will be composed of a number of rectangular blocks (approximately 10) surrounding the combustor and heater head in an annular array. Each block will be composed of about 50 sets of plates. A plate that allows only the passage of combustion gas, and one that allows only the passage of air, comprise each set. These plates are to be assembled in the pre-fired state to form the blocks. Firing will provide the necessary plate-to-plate sealing for separation of the two gas streams.

Comparison To Existing Technology

The preheater common to the P-40, Mod I, and Upgraded Mod I engines is composed of 1100 stainless-steel plates that are involute in shape in the radial direction and, when assembled together, form an annular ring surrounding the combustor and heater head. Plate-to-plate sealing, and thereby gas stream separation, is provided by seam-welding the thin plates (as thin as 0.004 in. for the Upgraded Mod I engine). Over 2000 of these weld seams are needed to produce a preheater, so it is an extremely time consuming, expensive process. In addition to its high cost, the current preheater material is susceptible to attack by acids formed in the exhaust gas of fuels containing sulfur (i.e., diesel fuel). The third problem is the inability to clean the preheater when fouled. Due to the high-temperature capability of ceramic materials, deposits can be removed from preheater plates by "baking" them off.

Experimental Data

Tests were run in the Preheater Rig on a test section (Figure 2-1) that was available from Coors Porcelain Co. of Golden, Colorado. Although the test section's exhaust gas and air plates differ from an RESD preheater plate, heat-transfer and fluid friction data were generated (Figures 2-2 and 2-3), and performance compatible to Mod I metallic platelets was achieved.

Component Layout

A layout of the RESD ceramic block preheater is shown in Figure 2-4.

2.1.2 Combustor/Fuel Nozzle

Description

The RESD combustion system will include a hairpin combustion gas recirculation (CGR) combustor and a continuously operating, ultrasonic atomizing fuel nozzle. For durability, the flame shield will be ceramic or metal with a ceramic thermal-barrier coating.

Combustor

The hairpin combustor (Figures 2-4 and 2-5) combines the features of the turbulator combustor, with the ejector-flow inducing technique necessary for CGR. The result is a compact, easily fabricated, inexpensive design. The hairpin geometry allows the swirler (turbulator) and ejector to be combined into one piece. The hairpin CGR combustor addresses the concern of mixing intensity by using one pressure drop location to induce recirculation and impart swirl. This will allow wide turndown, low CO/HC emissions, and heater head temperature variation similar to the EGR turbulator combustor. The induced recirculation will limit NO_x. The basic simplicity of the design, combined with a ceramic flame shield, will be cost effective and durable.

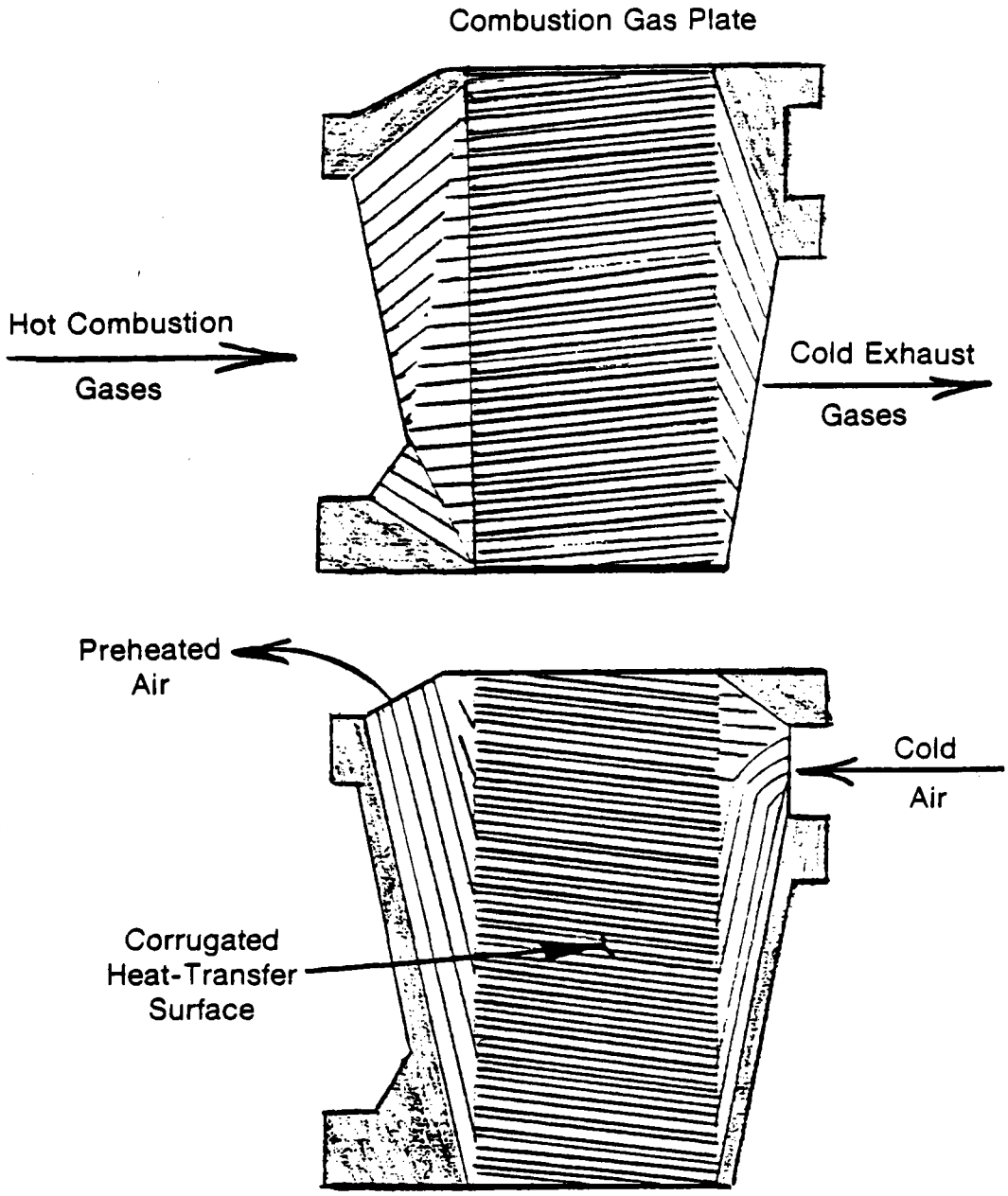

Figure 2-1 Ceramic Preheater Test Section

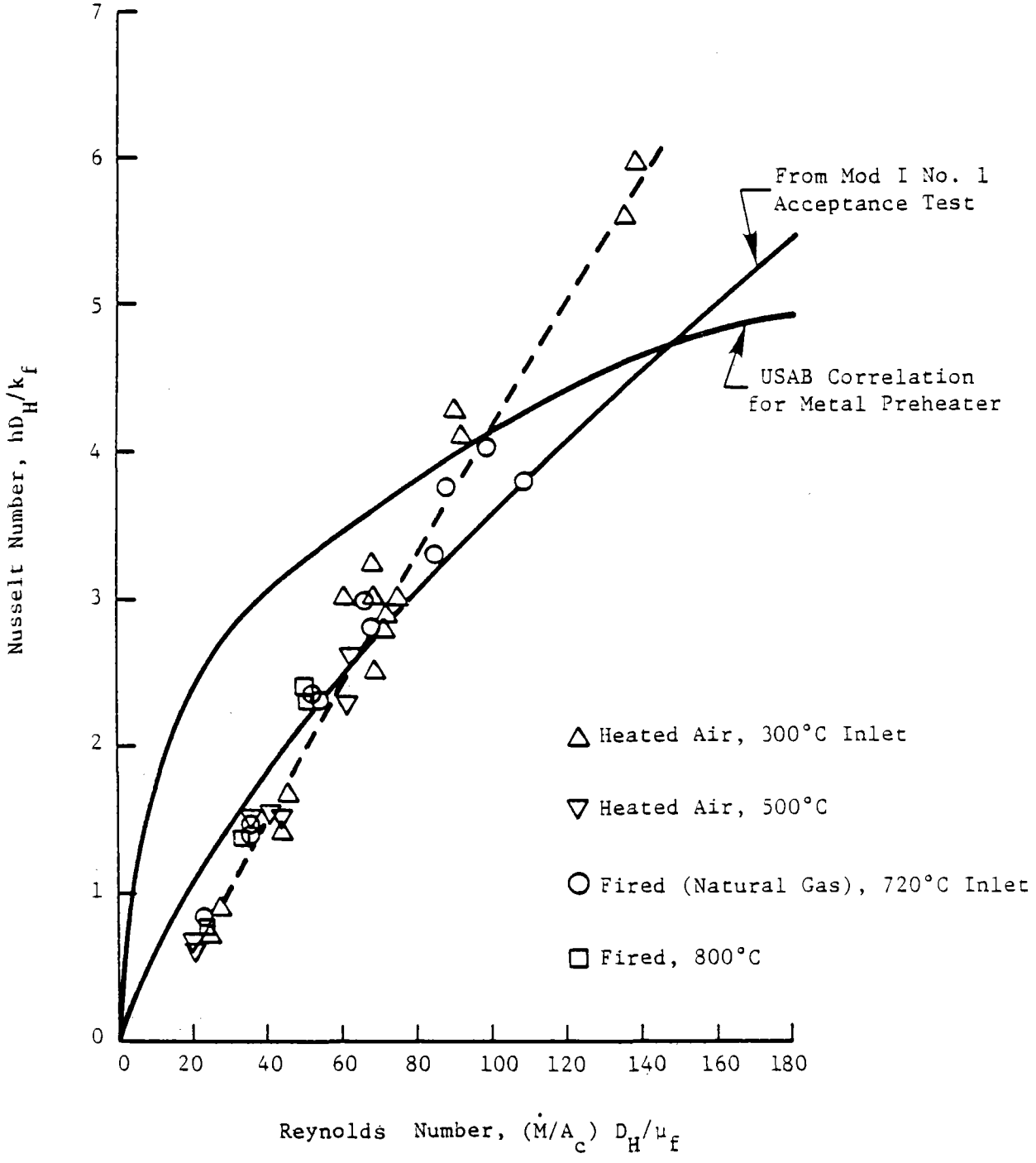

Figure 2-2 Ceramic Preheater Heat-Transfer Results (Test Data from Coors Porcelain Co. Test Section #1)

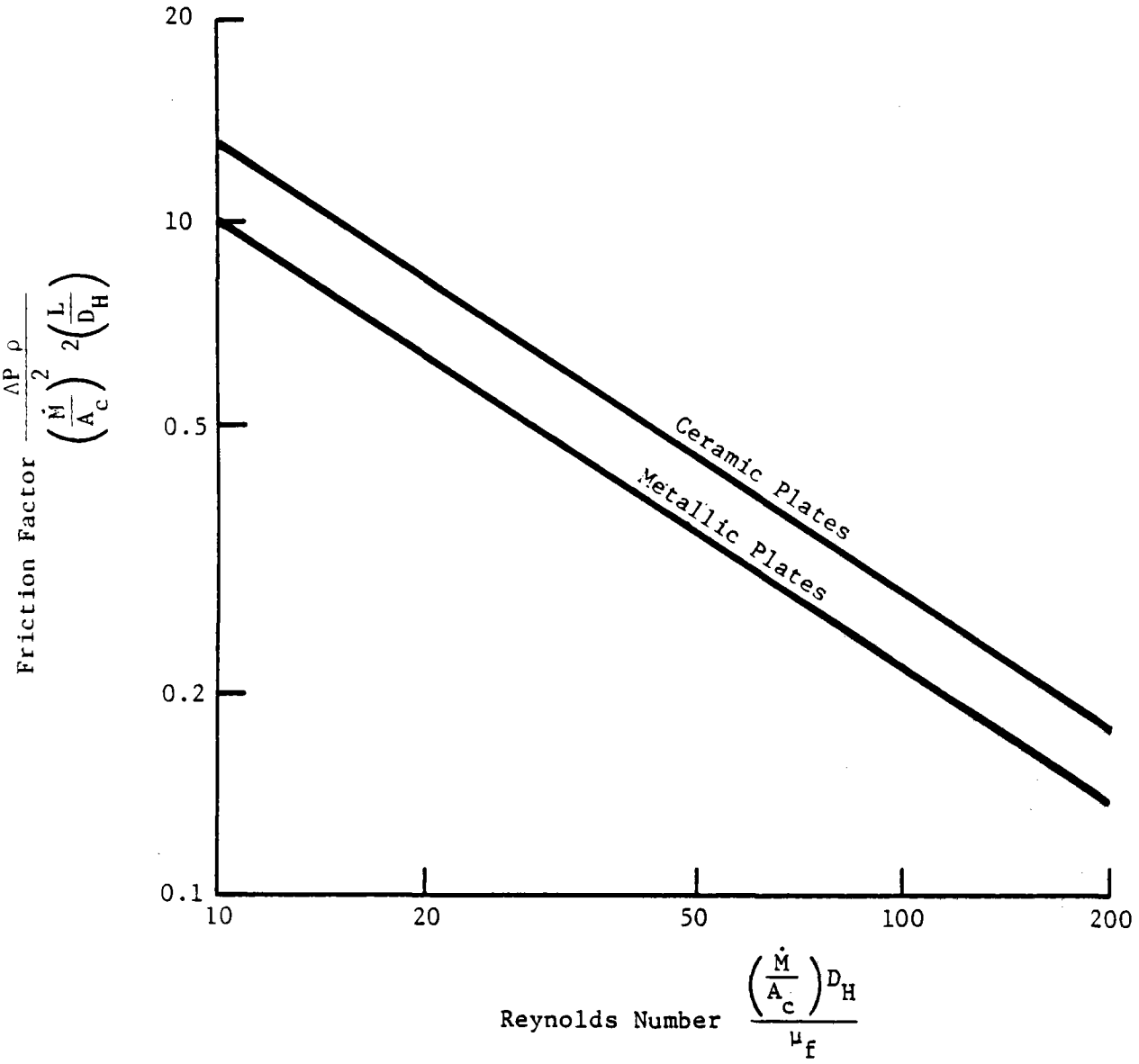

Figure 2-3 Ceramic Preheater Pressure Drop Results

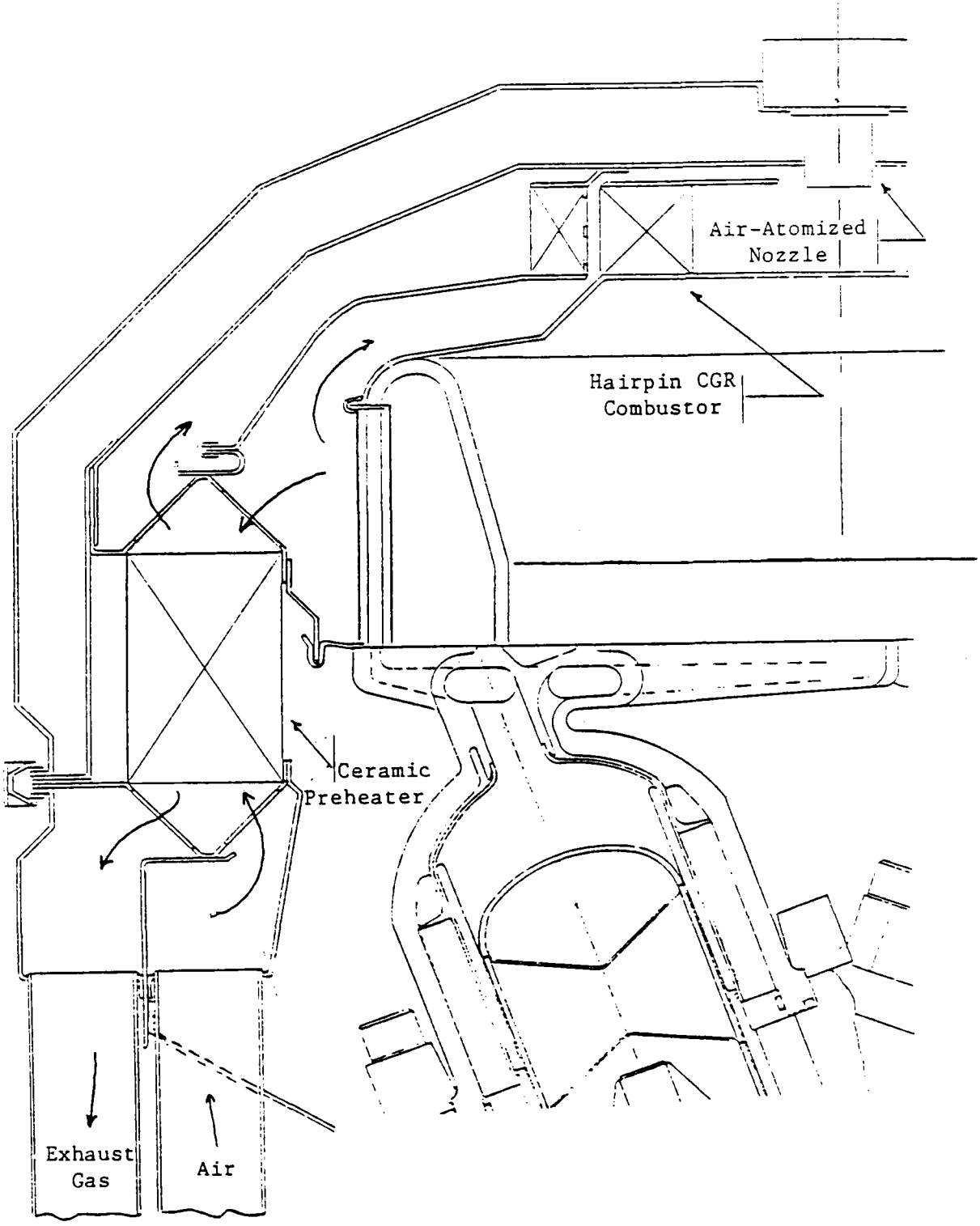

Figure 2-4 RESD External Heat System

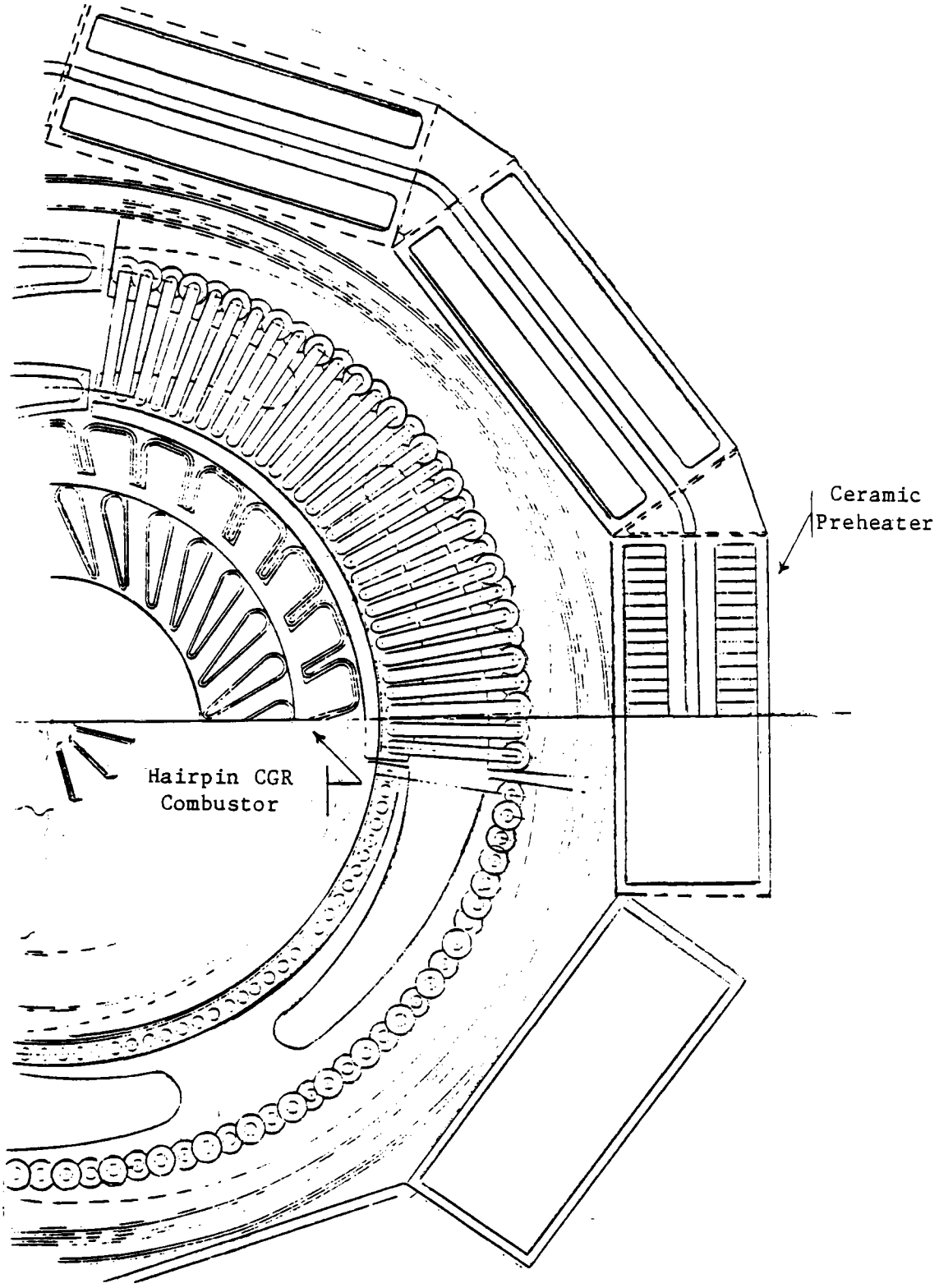

Figure 2-5 RESD External Heat System - Top View

Fuel Nozzle

The sonic fuel nozzle, which is water-cooled, uses a piezoelectric crystal to atomize the fuel. Thirty watts of electric power are required to operate the nozzle. The sonic nozzle (Figure 2-6) is rated high in the performance category, but since it is a new concept, development is required to verify cost and reliability. Its greatest virtues are very small droplets (SMD <15 microns), almost infinite turndown, and an extremely large flow passage that is plug resistant. The large flow passages allow all the alternate fuels to be atomized if adjustments are made to the power supply. The effect on air/fuel control is twofold - the extremely low pressure drop of the nozzle (<1 psi) drastically reduces the pump requirement, but an added control function is needed to adjust the power supply output as nozzle temperature and acoustic characteristics change. The performance potential of this concept results in it being the concept of choice because it provides the best net engine efficiency.

Comparison To Existing Technologies

Both exhaust gas recirculation (EGR) and CGR combustion systems have been used in the P-40, Mod I, and Upgraded Mod I engines. The EGR system (Figure 2-6) utilizes a turbulator combustor with an external gas-recirculation system to supply combustion products from the exhaust to the preheater inlet. EGR has proven to be reliable and capable of meeting ASE Program emissions goals with a uniform heater head temperature profile (ΔT = 15-50°C); however, a problem arises with the amount of EGR required for NO_x compliance, e.g., approximately 70% by volume at low fuel flows, resulting in the pumping requirement to the blower causing a decrease in engine efficiency. The system also adds weight and complexity to the engine because of the piping and EGR valve. The latter must be incorporated into the control system. EGR is also detrimental to preheater life since combustion products flow through the cold side and can cause plugging.

CGR combustors, which recirculate combustion products internally, reduce weight and complexity, and improve the preheater environment; however, problems have been encountered with durability, emissions, and temperature profile. The Mod I CGR combustor (Figures 2-7 and 2-8) consists of two

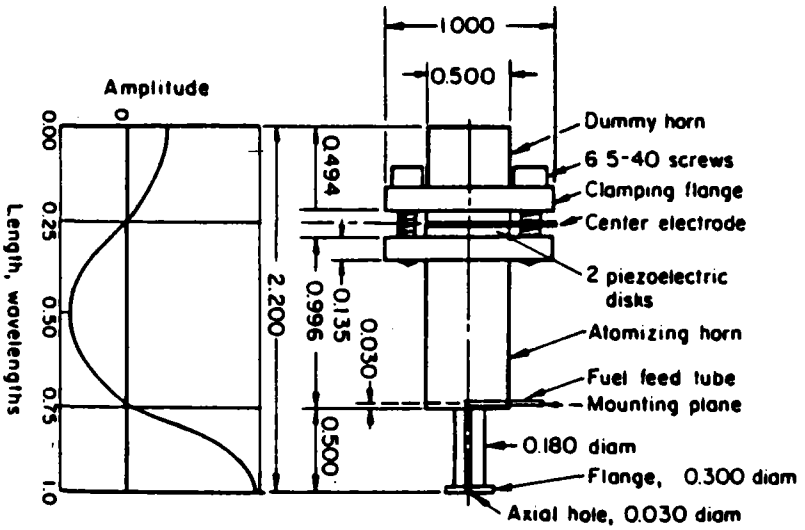

Figure 2-6 Design Details and Amplitude of Axial Vibration for Army/Battelle Ultrasonic Atomizer (Hazard and Hunter, 1966) (Dimensions are in Inches)

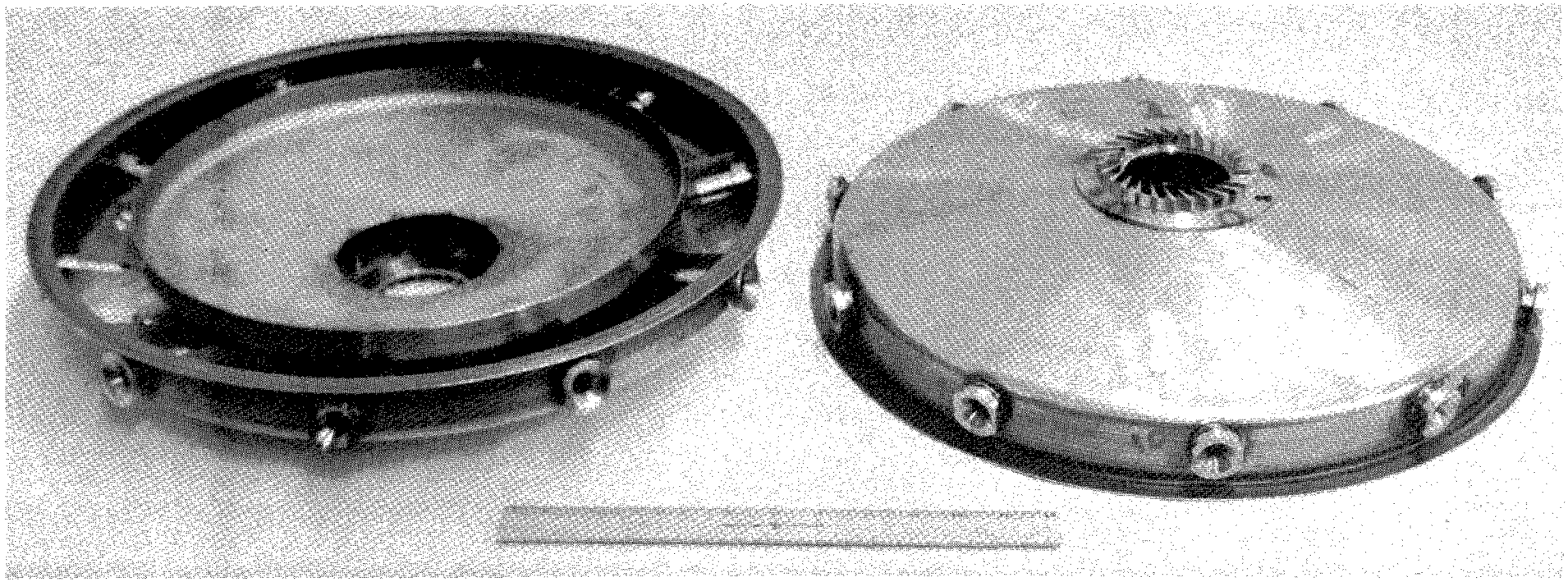

Figure 2-7 Mod I CGR Combustor

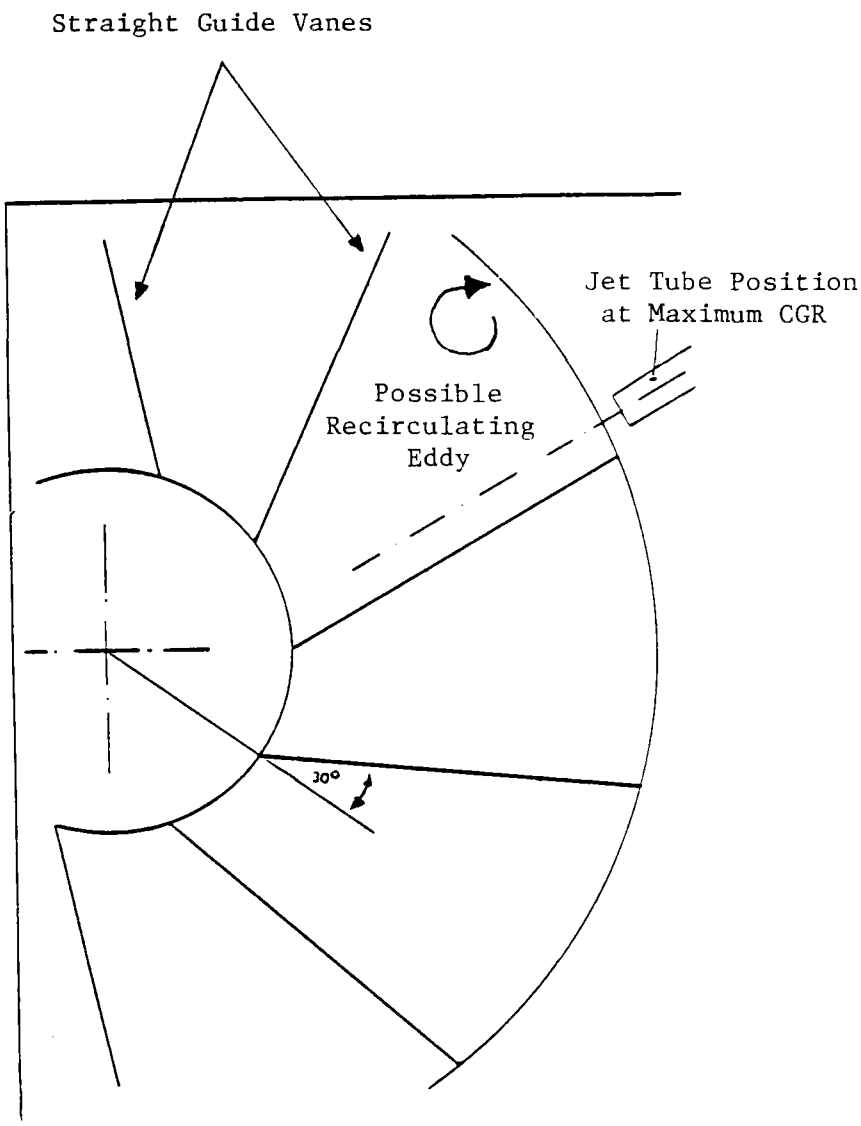

Figure 2-8 Straight Guide Vanes

circular plates divided by vanes into ten converging passageways that exit at a 30° angle to the center line in order to impart swirl to the flow. Each channel has an ejector that uses preheater discharge flow to enduce recirculation. This combustor has a tendency to crack during operation when subjected to start-up thermal transients. CO emissions are high at both low and high power, indicating poor mixing, inadequate volume, and poor heater head temperature distribution, e.g., ΔT = 40-100°C.

The P-40 and Mod I engines use air-atomized fuel nozzles, e.g., an external source of pressurized air is used for atomization. Both nozzles allow air and fuel to mix inside the nozzle, and then exit through a series of holes similar to a shower head. Experience with these internally mixing nozzles indicates that they tend to plug with carbon at low fuel flows which, in turn, adversely affect temperature profile and CO emissions. From a performance standpoint, the injection of cold atomizing air into the combustor degrades EHS efficiency (Figure 2-9). The effect increases at low fuel flow because atomizing airflow is constant (1.5 g/s), and its percent of the total combustor airflow increases as fuel flow and, hence, airflow decrease. In the low flow ranges, typical of the CVS cycle, η_B decreases two points due to atomizing air. Finally, the need for an atomizing air compressor adds weight (4.5 kg) and cost ($150) to the engine. The sonic nozzle provides improvements in each of these areas. Since this nozzle does not require air for fuel atomization, the passages that plug in the air atomized nozzle are eliminated and therefore the nozzle does not plug. There is no impact on η_B, no cold air is injected into the combustor. The power requirement is low (30 watts) and the unit, with its power supply, should be lighter and cost competitive with the air-atomized nozzle.

2.2 Hot Engine System

2.2.1 Heater Head

Description

The heater head proposed for the 1983 RESD is of the annular configuration. It is designed so as to retain the capability of utilizing a single combustor for the engine. To minimize production cost, tube geometry is made as simple

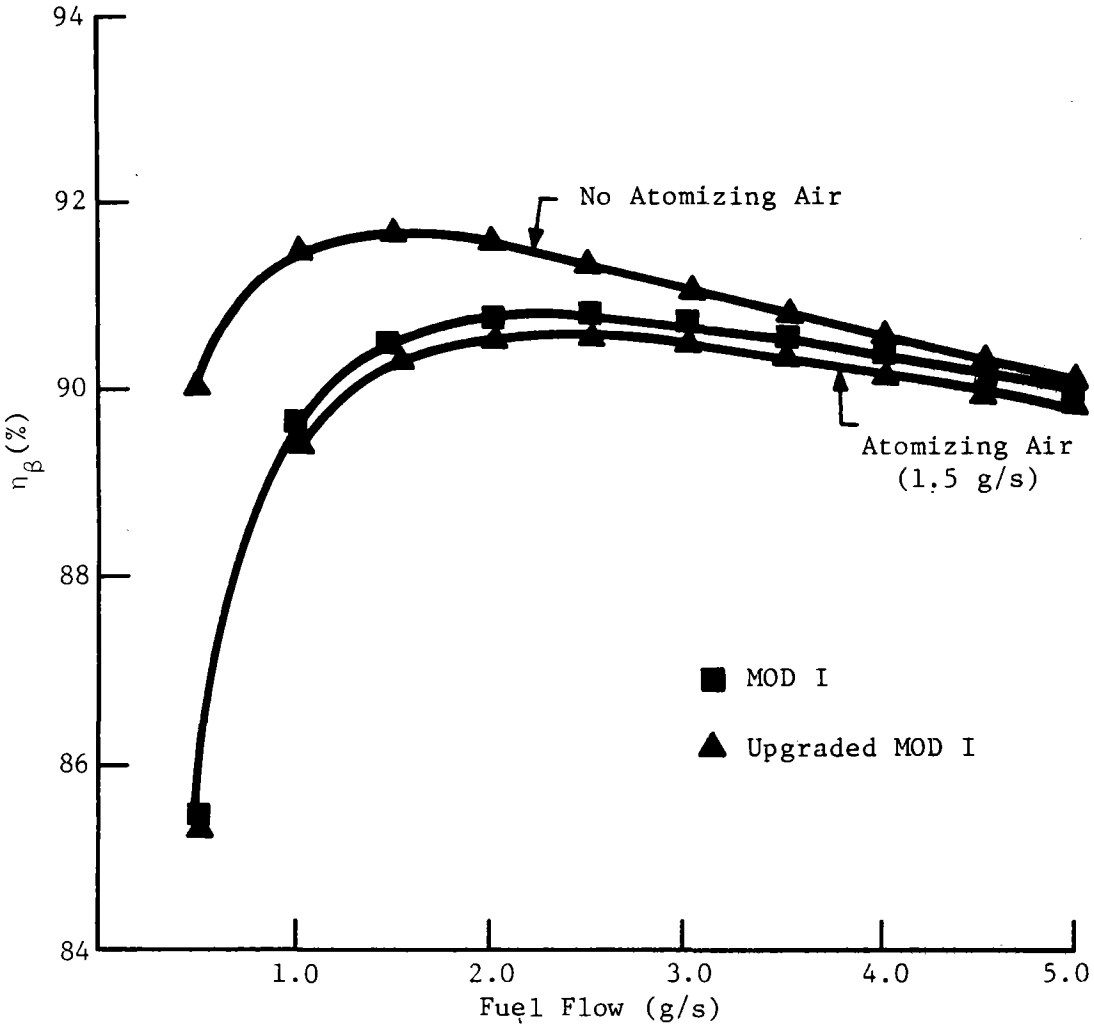

Figure 2-9 EHS Efficiency Versus Fuel Flow - Tubular Combustor

as possible, with bends in one plane only, and with all tubes the same length. The castings are made of a low-cost, iron-based alloy (XF-818) which is also weldable, allowing repair of castings as necessary, and also permitting simpler separate manifold and housing castings which can then be welded together.

In the annular concept (Figure 2-10), the regenerator and cooler are one-piece units concentric to the piston, sharing the same pressure vessel. The regenerator is placed around the dome gap, separated from it by a partition wall, and the cooler is placed around the cylinder liner. A number of geometric options existing on this basic arrangement are outlined below.

Above the regenerator, the pressure vessel closes in to cover the top of the cylinder. This transition must minimize dead volume above the regenerator. To accomplish this, a smoothly formed vessel can be used with a stuffer piece inside occupying unwanted volume (Figure 2-11). The advantage is minimal stress concentrations in the pressure vessel; the penalty is another part, hot and difficult to attach if (to minimize thermal mass) it is ceramic and not metal.

The manifold attaches to the housing by means of single central neck at the housing (Figure 2-11), which was used successfully on Mod I cylinders, and has been expanded to the regenerator housings for the Upgraded Mod I. This arrangement is more difficult to implement with the two manifolds per housing of the annular engine because flow at the regenerator must make a transition between an annular space to a simple pipe before joining the manifold (Figure 2-12). Careful layouts have been made to assure that flow area is adequate and geometry castable. The advantage of such necked manifolds is that their separation from the main housing allows the thermal strains associated with the tube connections to occur in a relatively flexible, free structure, thus minimizing local stresses. A long annular gap between the necks and regenerators assures good flow distribution. Disadvantages are greater dead volume and overall height; however, this is an acceptable penalty for reduction in stress at the most critical sites and for increased manufacturability (as demonstrated on the Upgraded Mod I).

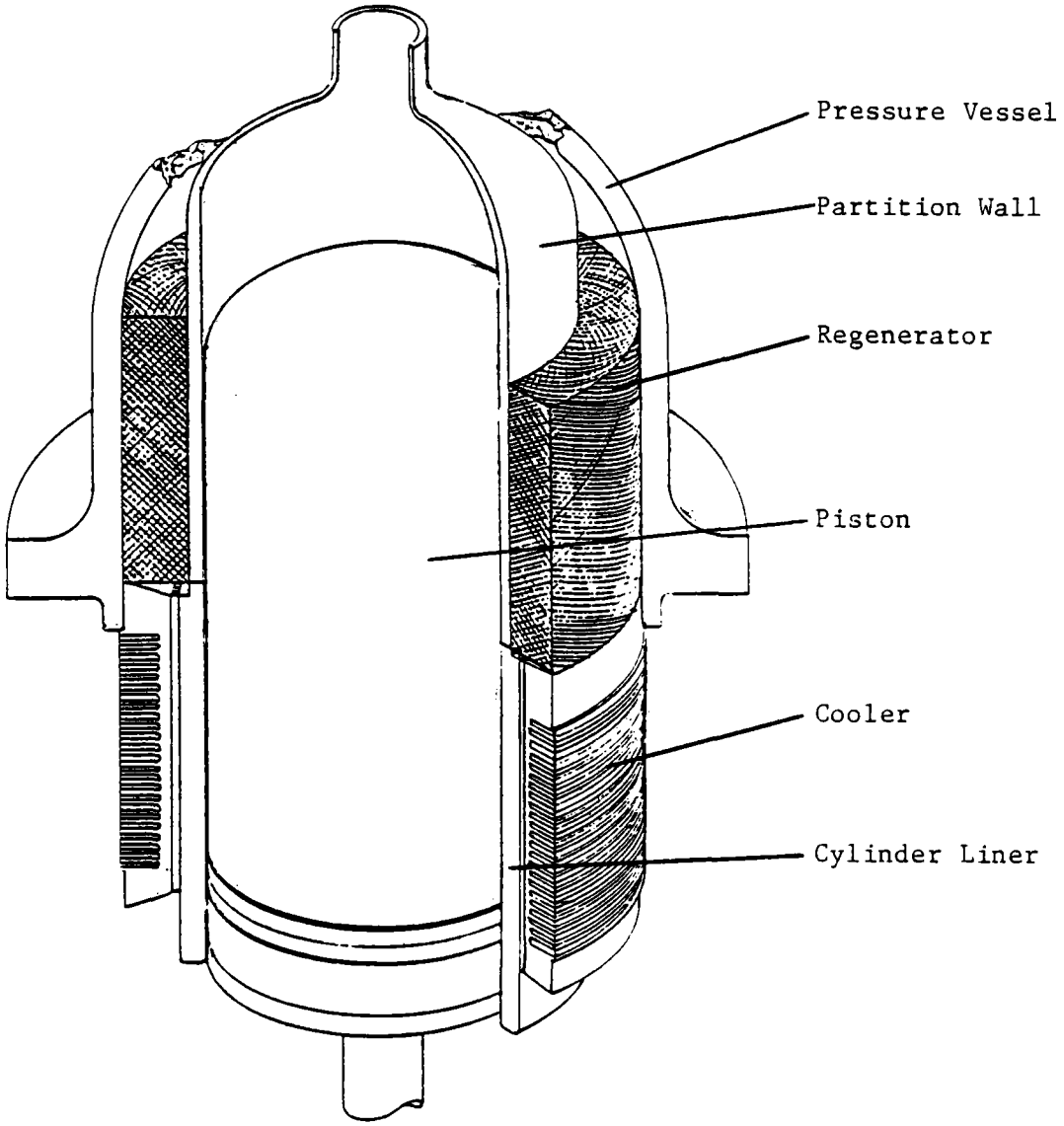

Figure 2-10 Annular Geometry

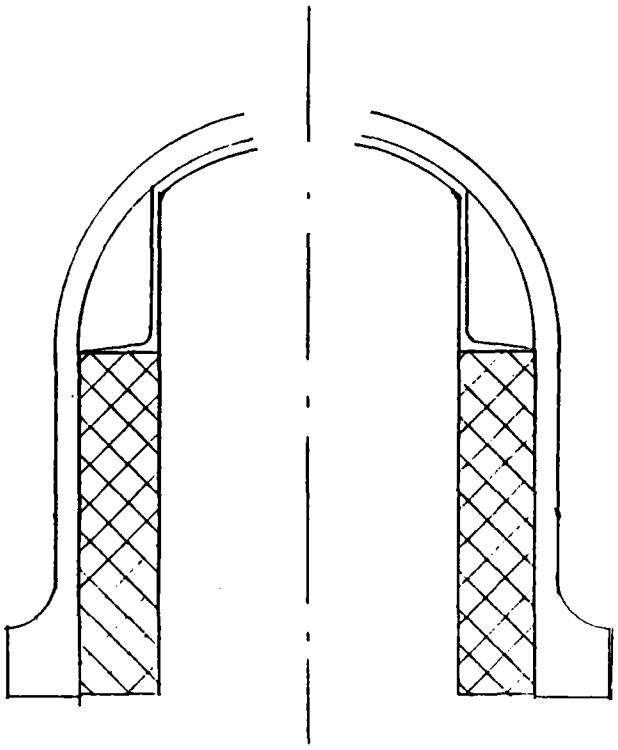

Figure 2-11 Housing/Regenerator Interface Using a Stuffer Piece

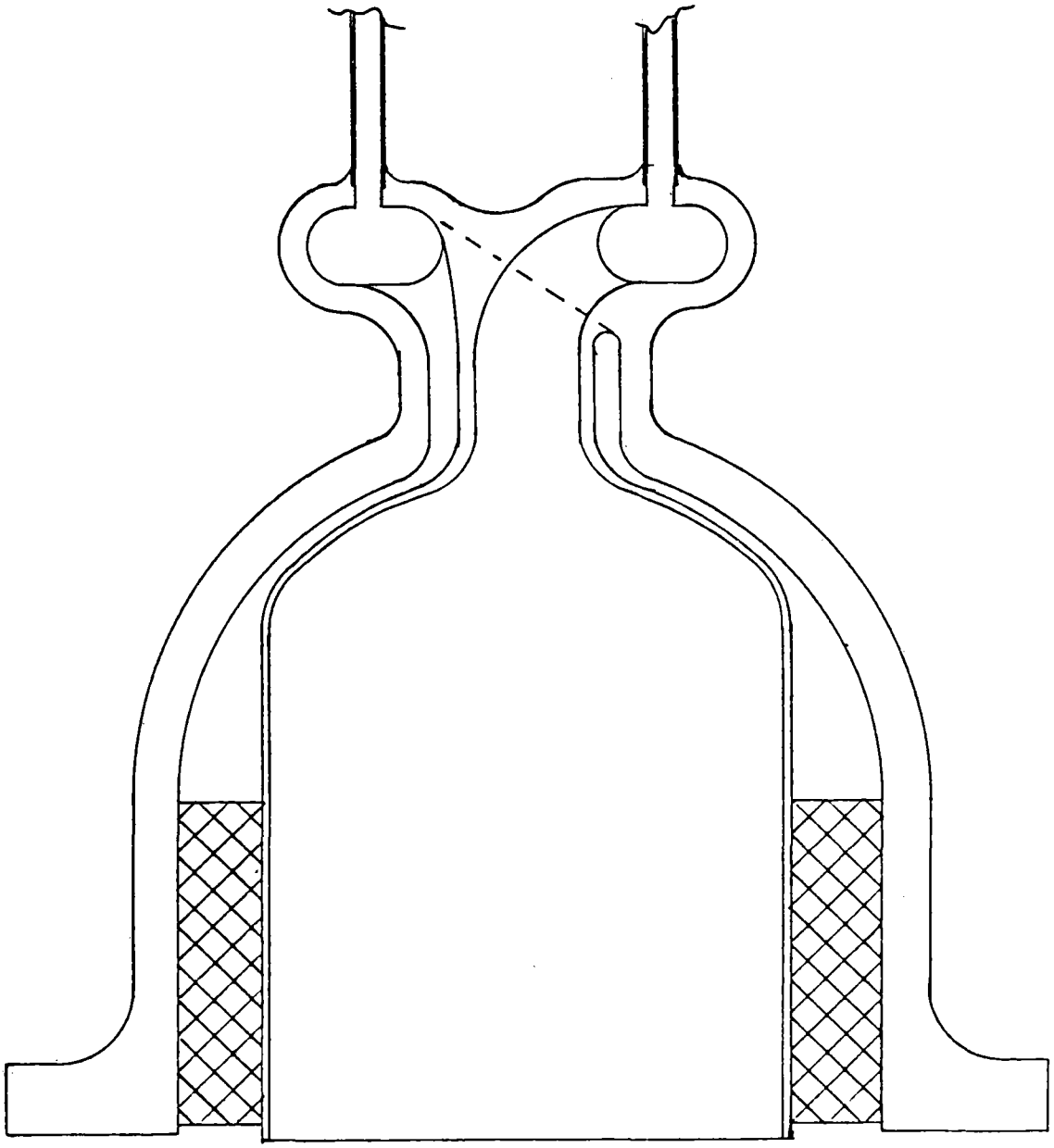

Figure 2-12 Necked Manifolds for Annular Heater

Alternate attachment schemes (direct tubes, entry into the regenerator housing and manifolds integrated with the housing) provide an advantage relative to the chosen design from the stand point of reduced dead volume, but have been shown to have thermal stress and reliability problems.

The partition wall divides the annular gap above the regenerator from the expansion space and the shuttle gap by the piston dome from the regenerator. The mechanical load on the part is small, consisting mainly of pressure drops within one cycle, although it does have important sealing/thermal blocking functions. Gas flow is directed through the heater and regenerator by the partition wall. A seal to the housing is required at the manifold neck (hot) and to the cooler at the regenerator base. Thermal communication between shuttle gap and regenerator must be minimized, as well as axial conduction to the cooler, indicating a material of lowest possible conductivity, i.e., a ceramic. The sealing requirement then becomes very difficult, especially at the hot end where a metal would be better. In either case, dimensional control must be good to maintain the 0.4-mm dome gap.

Combining ceramic and metal in a hybrid design (Figure 2-13) is the configuration of choice for the partition wall. In such a concept, a single metal layer would reach from the neck seal to the cooler seal. Compression fit within that would be a simple ceramic sleeve defining the cylinder, and isolating the thermal gradients. Axial conduction is about half that of an all-metal wall, and radial isolation is 80% of a 4-mm, all-ceramic wall when a 1-mm metal sheet is combined with 3 mm of ceramic. The sealing is metal-to-metal at both ends.

The ceramic material chosen for this application, partially stabilized zirconia, has high-temperature strength (as required) combined with high thermal expansion (near the metal parts) and low conductivity. It has been successfully used for insulating cylinder liners in experimental diesel engines.

Fixture Options - If the heater head structure is to be separable from the remainder of the engine, a fixture means is required. The V-4 RESD has a single cast block that can provide engagement for bolts; the machined decks on the block can also provide for mounting of flanges. The small housing flange/clamping ring system (as on the Mod I) on an integral bolting flange on

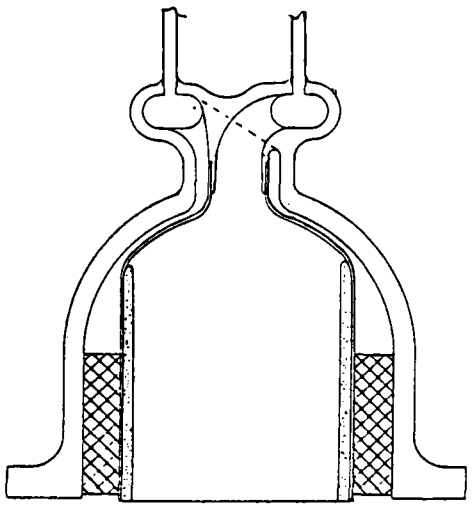

Figure 2-13 Ceramic/Metal Hybrid Partition Wall

the head can also be used. Because of the drive system's reduced volume (relative to the U), material for bolting is not available as far down as the crossheads; thus, more severe constraints on acceptable bolt size and pattern are imposed. Bending stress in the bolts from axial pressure load is increased with shorter bolts, so keeping the bolt circle as small as possible to reduce flange rolling is very important. Minimizing bolt diameter further reduces bending stress, but requires more bolts. Both increased numbers and minimum circles are more easily accomplished with an integral flange than with a separate clamping piece. In addition, the manufacturing, assembly simplicity, and reduced tolerance stack-up support the choice of integral flange for the V-layout.

The thick integral flange, on the other hand, increases conduction losses directly and also indirectly by raising housing thickness above the flange to handle bending stress. As there is little clear advantage for either concept, the design has been kept flexible in this area. Either system can be fitted without impact on any other parts besides the housings.

Existing Technologies and Supporting Designs

Engines built or used in the ASE Program to date (P-40, Mod I, Upgraded Mod I) have heater heads that are similar in many ways to the proposed RESDs. These designs are canister rather than annular, but the tubes and housings provide a solid base of experience for fabrication, performance, and failure modes. Experience with casting difficulties in the Mod I design, and experience with directly entering tubes in the P-40 and Mod I designs has led to the welded and fully necked manifold designs used in this RESD.

Annular technology is not new to the ASE Program - a modified P-40 engine (P-40R) has been tested with good results. This testing has pointed out several problems associated with the annular scheme (regenerator distribution, bypass leakage, and partition wall losses), which in turn has brought attention to these problems in the various schemes considered here.

2.2.2 Regenerator

Description

The prime design for the V-4 RESD regenerator matrix is a sintered wire screen which will be made from 61-μm (0.0024-inch) diameter wire of 304 stainless steel. These screens are stacked, compressed ~30%, and sintered together. The matrix is then brazed to the internal diameter of a stainless-steel tube, and the ends of this tube are rolled over to hold the matrix.

Comparison to Existing Technology

The current regenerator matrix, which is common to the P-40, Mod I, and Upgraded Mod I engines, is fabricated from 50-μm (0.002-inch) diameter wire screen.

Experimental Data

Tests were performed on the sintered screen matrices. Correlations were developed for heat transfer (Nusselt number) and fluid friction (friction factor) characteristics:

$$\text{Nusselt Number} = 0.169\ Re^{0.741};\ \text{and,}$$

$$\text{Friction Factor (f)} = 19.95\ Re^{-0.693} \text{ for } Re \leq 75$$
$$= 3.764\ Re^{-0.307} \text{ for } Re \geq 75,$$

where:

$$\text{Nusselt Number} = h \times 4 \times r_H/k_f$$
$$\text{Friction Factor} = 2 \times g_c/(L/r_H) \times \Delta P \times p/(M/A_c)^2$$
$$\text{Reynolds Number} = 4 \times r_H \times (M/A_c)/\mu_f$$

where:

h = heat-transfer coefficient

r_H = hydraulic radius

k_f = fluid thermal conductivity

g_c = gravitation constant (necessary only for English units)

L = regenerator length

ΔP = regenerator (or test section) pressure drop

p = porosity

M = gas mass flow

A_c = minimum crossflow area = p x frontal area

μ_f = fluid viscosity.

2.2.3 Gas Cooler

Description

Carbon Steel Tube and Shell - The carbon steel tubular cooler concept (baseline design) is similar in most respects to existing ASE coolers. The major difference is that previous units have been cylindrical canisters having one water cross-flow path, while this unit is built around a central strong back that doubles as the cycle cylinder liner (Figure 2-14). Water is still in cross flow, but now splits in two parallel paths, each going halfway around the central cylinder.

These tubular units have typically shown high performance by virtue of their high surface-to-volume ratio and thin pressure-retaining walls.

Description

Relative to existing stainless steel coolers, the carbon steel cooler greatly reduces manufacturing costs. To prevent corrosion, the tubes are surface-treated (before or after assembly) by infusion of chromium to produce a stainless-steel alloy at the surface only. Potential vendors of this process have been contacted. Capacity exists, and in-production estimates of 2¢/tube have been given. This design is much less expensive than the stainless version, but is a slightly higher technical risk, as the surface process is unfamiliar, and actual in-service corrosion resistance is unknown.

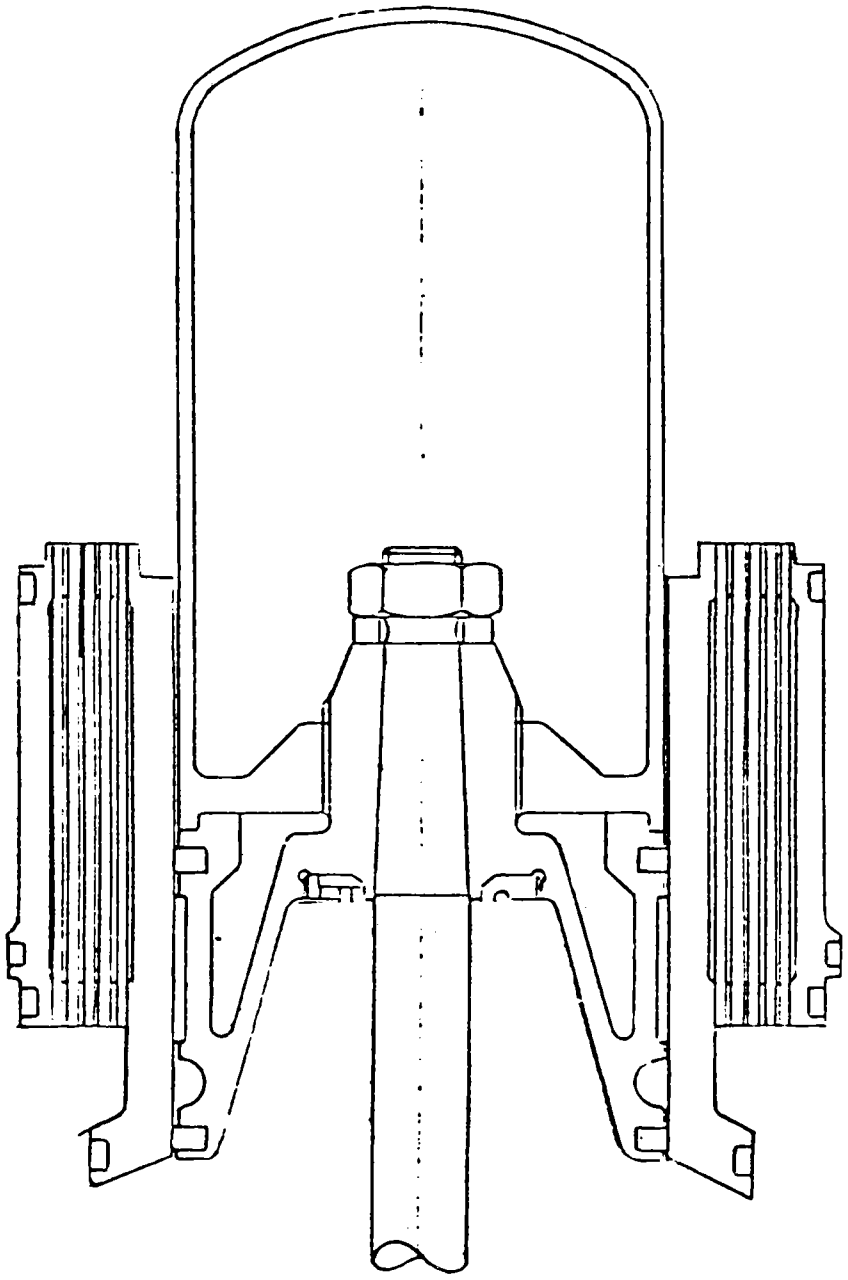

Figure 2-14 Annular Tube Cooler (Around Piston)

2.3 Cold Engine System/Engine Block

2.3.1 Cold Engine/Block Design

Description

V-Drive - This drive is an integrated block, equal angle V-design as seen Figure 2-15. Development of the roller-bearing, reduced-friction drive on the Upgraded Mod I has affirmed its place in the RESD, so this has been incorporated. Also, in order to preserve control options, the block has been reworked to allow space for either a rotary distributor valve or simplified, timed-injection slot drillings. Closer packing of cylinders, combined with improved cylinder/regenerator location, has made the basic block less massive by reducing length and deck height. Block weight is now estimated to be 27 kg.

About one-half of the block mass could be saved by casting in aluminum rather than in iron. On the other hand, the porosity of cast aluminum makes hydrogen retention less certain, although post-casting sealing processes exist. Aluminum has less fatigue resistance than iron, requiring close attention to stresses in the pressurized volumes. It also has a weight savings, but this is coupled with an elevation of risk. Development time for a successful aluminum casting is probably greater than allowed for by the RESD definition; however, the cost would be greater than with iron.

Fitted to the block design was a new, lightweight piston design that takes advantage of the similar part-unifying tolerance control measures. This design (Figure 2-16a) integrates the piston, dome, and rod into a single, welded assembly that assures radial, axial, and concentricity control, and eliminates a required match-fit using the taper joint/threaded dome of earlier designs (Figure 2-16b). A shoulder and thread joint at the crosshead completes the assembly. (The actual crosshead can be a free-riding part to avoid angular error.)

Comparison to Existing Technologies

Mod I CES/EDS - Current Mod I/Upgraded Mod I designs are U-drive engines with canister regenerator/cooler packages. The engines are assembled in a modular

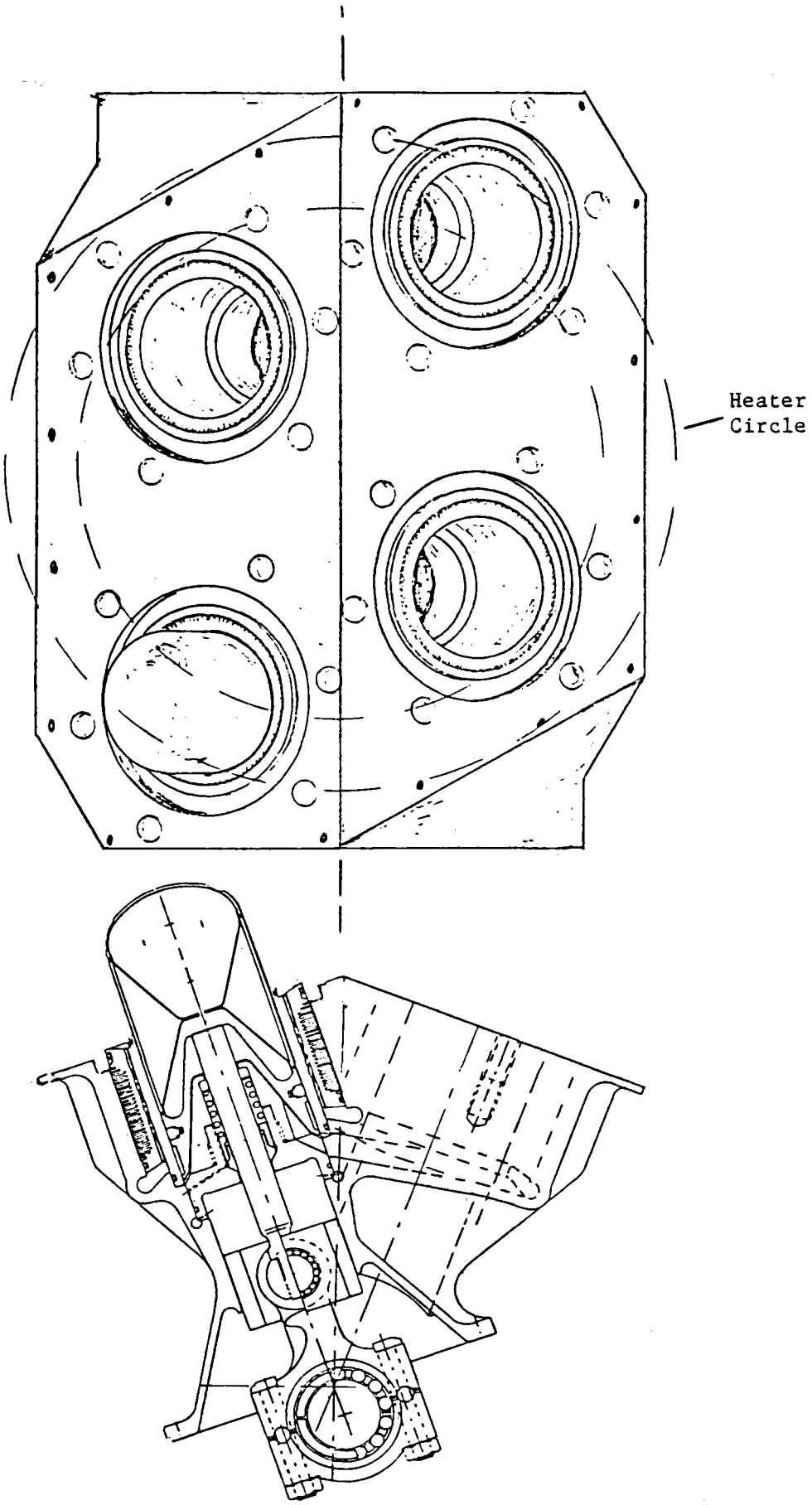

Figure 2-15 60-kW (80-hp) V-Block

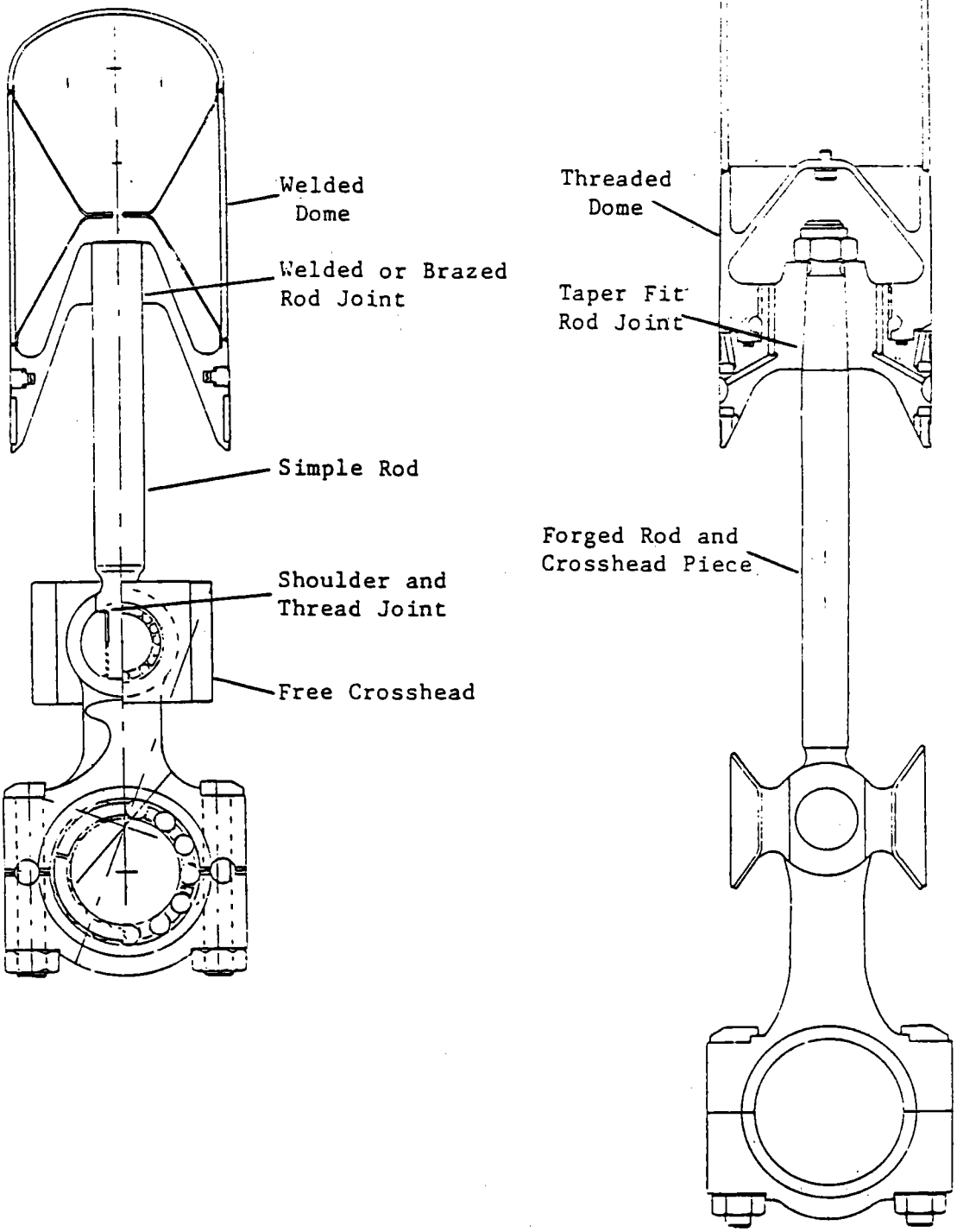

a. V-4 RESD Lightweight Piston Assembly (1.9 kg)

b. Mod I Piston Assembly (2.9 kg)

Figure 2-16 Piston Assembly

fashion with stacks of components held together by long tie bolts. This system is not only massive, costly, and subject to large tolerance stack-up, but reliability is low because of the multiple seals required between parts. In addition, the dual-crankshaft design requires large, noisy, power-transfer gears that carry reversing torque loads. The low-speed torque potential of the engine is limited by this drive design, largely due to the capacity of these gears and the sleeve bearings supporting them and their shafts.

2.3.2 Main Seals and Piston Rings

Main Seals

The main seal is a lubricated sliding seal that can be described as a double-angle seal. There are a number of forms that the seal may take, examples of which are shown in Figure 2-17. The seal itself is made from a polytetrafluorethylene-based (PTFE-based) material or a similar low-modulus material, and is an interference fit on the piston rod. This interference fit maintains intimate contact between the seal and the rod under static conditions, and provides a static gas seal.

The seals shown in Figure 2-17 have different constructions, but are all based on the concept of maintaining a thin but finite film of lubricant between the seal and the rod under dynamic conditions (the convergent entry sections at the upper and lower extremities of the seals play an important role here). The oil film reduces friction and provides an efficient barrier against gas leakage.

Figure 2-18 shows a compound-type seal assembly (for an engine) that has freedom for radial motion during assembly to facilitate rod/seal alignment, and minimize radial loading. When the axial preload is applied by a Belleville-type spring via a loading piece, the seal is clamped against the lower mating surface of the housing. The fully retained O-ring in the base of the seal prevents oil or gas leakage between the seal and mating surface. Oil for cooling/lubrication is supplied to the surface of the piston rod on the crankcase side of the seal.

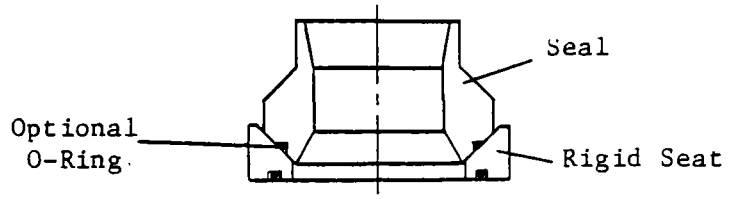

a. Seal With Separate Seat

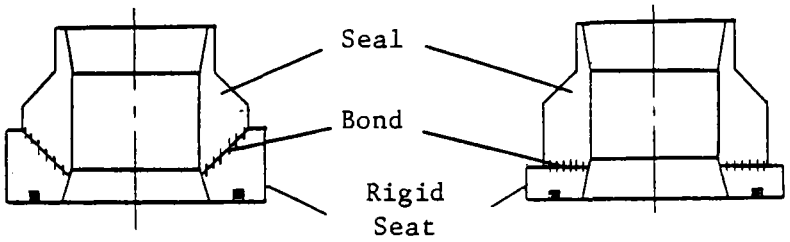

b. Compound Seals c.

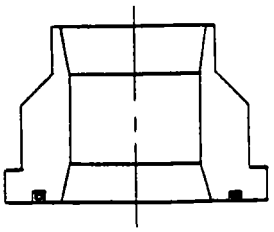

d. One-Piece Seal

Figure 2-17 Double-Angle Main Seals

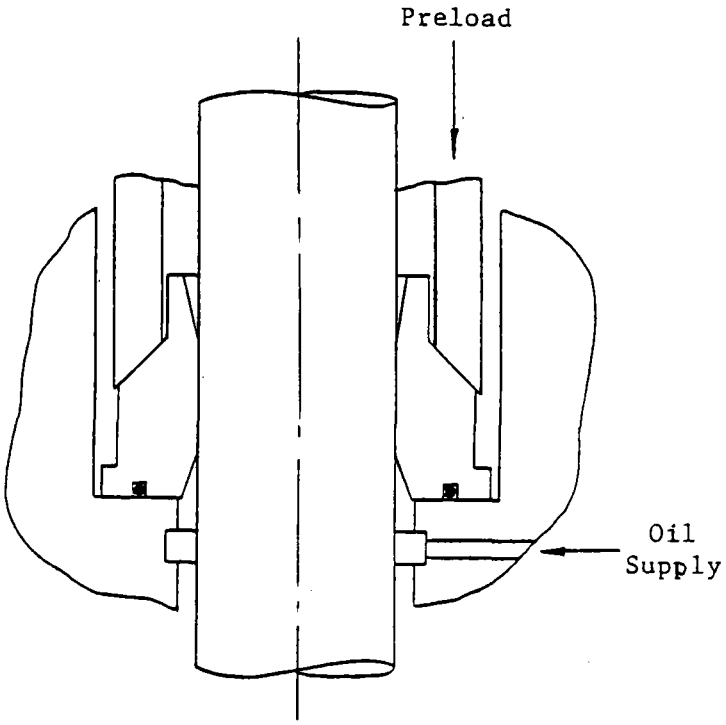

Figure 2-18 Compound-Type Seal Assembly

On the upstroke, oil is drawn into the convergent passage at the inlet to the seal. With the combination of rod motion and inlet passage geometry, a hydrodynamic pressure is generated that expands the seal so that a hydrodynamic oil film separates rod and seal surfaces. This process is repeated on the downstroke; however, the hydrodynamic film is formed from the oil on the surface of the rod that passes through the seal on the upstroke. Oil film thickness and the volume of oil that passes through the seal on the up/downstrokes are dependent on the geometries of the convergent inlet passages. To ensure a zero net flow of oil into the working cycles of the engine, the seal is designed so that its pumping capacity on the upstroke is less than that on the downstroke.

Comparison to Existing Technology

Prior designs of Stirling engine piston rod seals fall into two categories - hermetic and sliding. The large pressure difference across the hermetic seal, and its long rod stroke, are extremely demanding. Some measure of success was achieved with the roll-sock seal, but this involved a critical pressure balancing system, and the seal's reliability and life did not approach the requirements for a Stirling-engine application. With current technology or projected developments, a hermetic seal is not a viable concept for the piston rods.

In sliding seal designs such as the Leningrader seal, lubrication of the seal was necessary so that it would not destroy itself thermally as a result of high rod/seal friction. The seal was designed, however, to act as a scraper to remove oil from the surface of the rod on the upstroke, and prevent it from entering the working cycles. The effectiveness of this scraping action was variable, with the result that some seals were inadequately lubricated, and others allowed excessive oil leakage. Overall, performance of the Leningrader seal was erratic, and its life was mainly short.

In the Pumping Leningrader (PL) seal design, the concept of a lubricated seal was taken one step further. It was recognized that it was impossible to remove all traces of oil from the surface of the rod on the upstroke; therefore, some oil would always pass through a lubricated seal. In an attempt to ensure that the oil passing through the seal did not accumulate on the gas

side, a pumping ring was added to the basic Leningrader seal, as shown in Figure 2-19. On the downstroke, oil on the surface of the rod enters the pumping ring and flows back to the crankcase side of the seal. The addition of the pumping ring does not affect the operation of the seal on the upstroke, and the nominally sharp edge of the seal on the crankcase side acts as a scraper.

Operation of the PL seal is critically dependent on the effectiveness of the scraping action. If the scraper is very effective in removing oil from the surface of the rod, the seal will be inadequately lubricated, and will fail due to high friction. At the other extreme, if the scraper is ineffective, the seal will be adequately lubricated, but the amount of oil passing through the seal on the upstroke will exceed the pumping capacity of the pumping ring on the downstroke. In this case, the seal will fail due to oil leakage into the working cycles. Between these two extremes a situation exists where oil flow through the seal on the upstroke is sufficient for lubrication, but does not exceed the capacity of the pumping ring on the downstroke. Under these conditions, the PL seal will be an efficient gas/oil seal.

The effectiveness of the scraping action in the PL seal is dependent on the geometry of the seal in the area where it contacts the rod on the crankcase side. If there is any form of convergent passage between the rod and seal surfaces in this entry region, it will promote hydrodynamic action on the upstroke. A very short, convergent passage can generate a strong hydrodynamic pumping action and, in practice, this could very easily occur. Normal variations in manufactured seals may produce a convergent passage when the seal is installed. Any rounding of the lower edge of the seal, or a slight taper in the bore, could form a convergent passage, as shown in Figure 2-20. Deformation or deflection of the slightly overhung section of the seal would have a similar effect, as shown in Figure 2-21.

The operation of the PL seal and failure modes described above are consistent with their performance in engines and test rigs. Nominally, identical seals give radically different performances. Some seals fail due to high gas leakage after a very short time, while others leak oil but not gas. There are also many examples of seals that have performed well for thousands of hours. These random variations in performance must be expected when the seal design does not produce consistent lubrication of the seal.

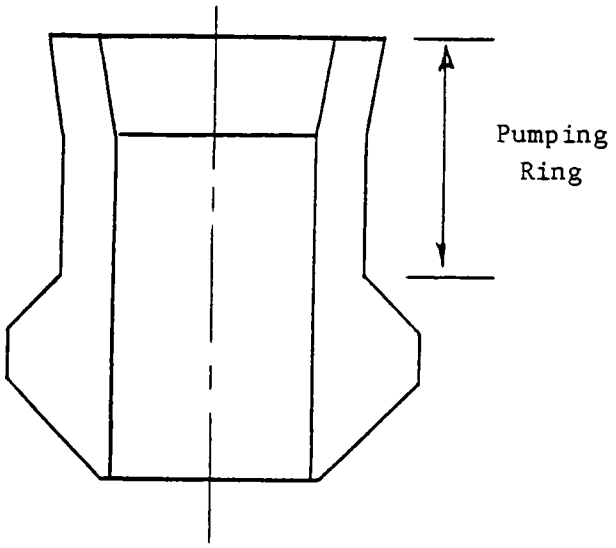

Figure 2-19 Pumping Leningrader Seal

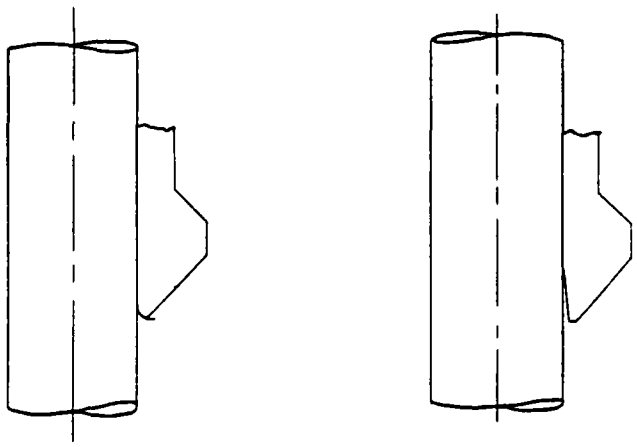

Figure 2-20 Convergent Inlet Passages on Seal Formed by Rounded Edge/Bore Taper

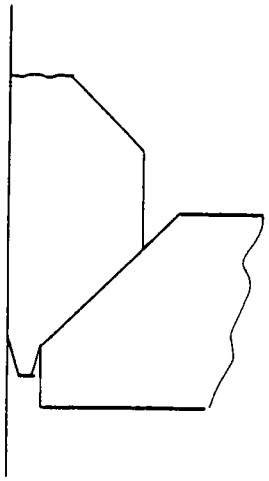

Figure 2-21 Convergent Inlet Passage on Seal Formed by Deflection/Deformation of Overhung Seal Tip

In the double-angle seal design, there is no variable scraping action. The seal is provided with a convergent, reproducible entry section on the crankcase side that is designed to generate a controlled, hydrodynamic oil film between the seal and the rod on the upstroke. A similar but not identical entry section on the gas side of the seal produces the same effect on the downstroke. The two entry sections are designed such that the hydrodynamic pumping capacity on the downstroke is greater than that on the upstroke, thus ensuring that there is no net flow of oil to the gas side of the seal.

An analytical study of the operation of a double-angle seal has been conducted. This analysis was based on a simplified model of the seal (shown in Figure 2-22). Basically, the model is a stepped, elastic tube with the larger diameter section representing the trapezoidal section of the seal shown in Figure 2-17. The convergent inlet passages at the upper and lower ends of the seal are formed by plain chamfers on the seal. Assuming that the oil was isoviscous, and that squeeze-film effects were negligible, a quasistatic, elastohydrodynamic solution was derived. Examples of the operating conditions predicted by this analysis are given in Figures 2-23 and 2-24. For the example chosen, the following parameters are fixed:

D_1	= 18 mm
D_2	= 22 mm
α	= 5°
Interference fit on rod	= 0.15 mm
Stroke	= 34 mm
Speed	= 4000 rpm
P_{min}	= 10 MPa.

Figure 2-23 shows the volumetric flow rate of oil through the seal as a function of crank angle, with positive flow toward the crankcase. With crank angles in the range of 180-360°, negative flows are those through the seal to the gas side. With the chosen values of β, flow rates are all less than the maximum flow rate, which can be generated by the 5° inlet angle on the downstroke (see Figure 2-22); therefore, on the downstroke (0-180°), the 5° inlet operates under starved conditions, the flow rates are mirror images of those on the upstroke, and net flow of oil through the seal is zero. With the chosen seal geometry and operating condition, the pumping capacity on the upstroke

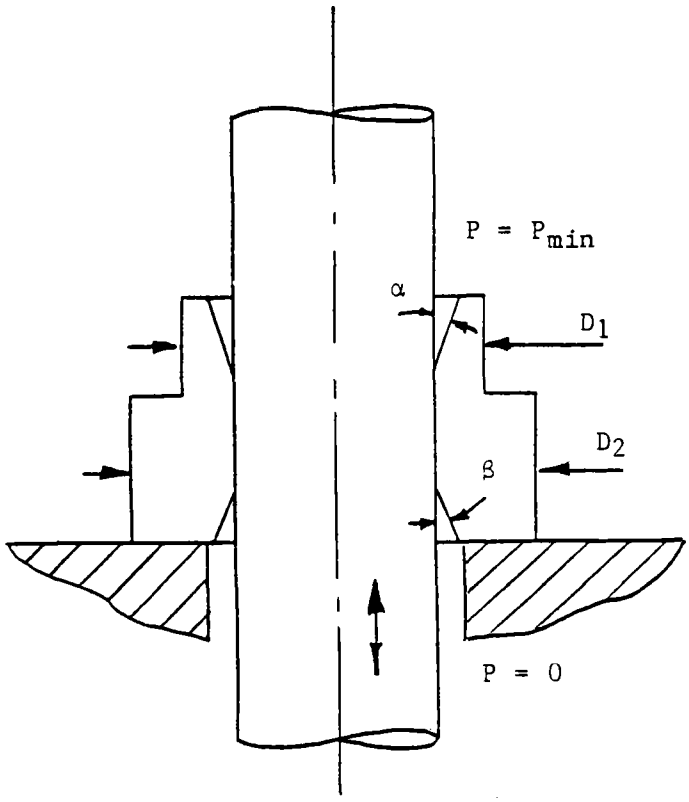

Figure 2-22 Simple Model of Double-Angle Seal

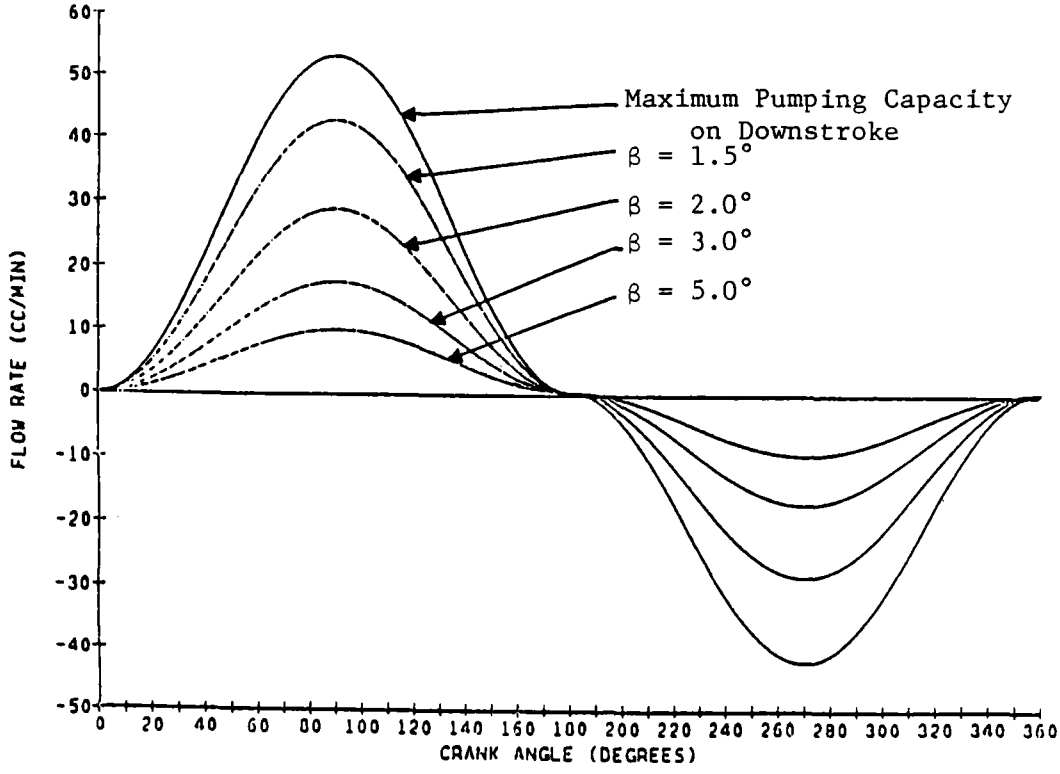

Figure 2-23 Operating Conditions Predicted by Analysis of Double-Angle Seal - Flow Rate Versus Crank Angle

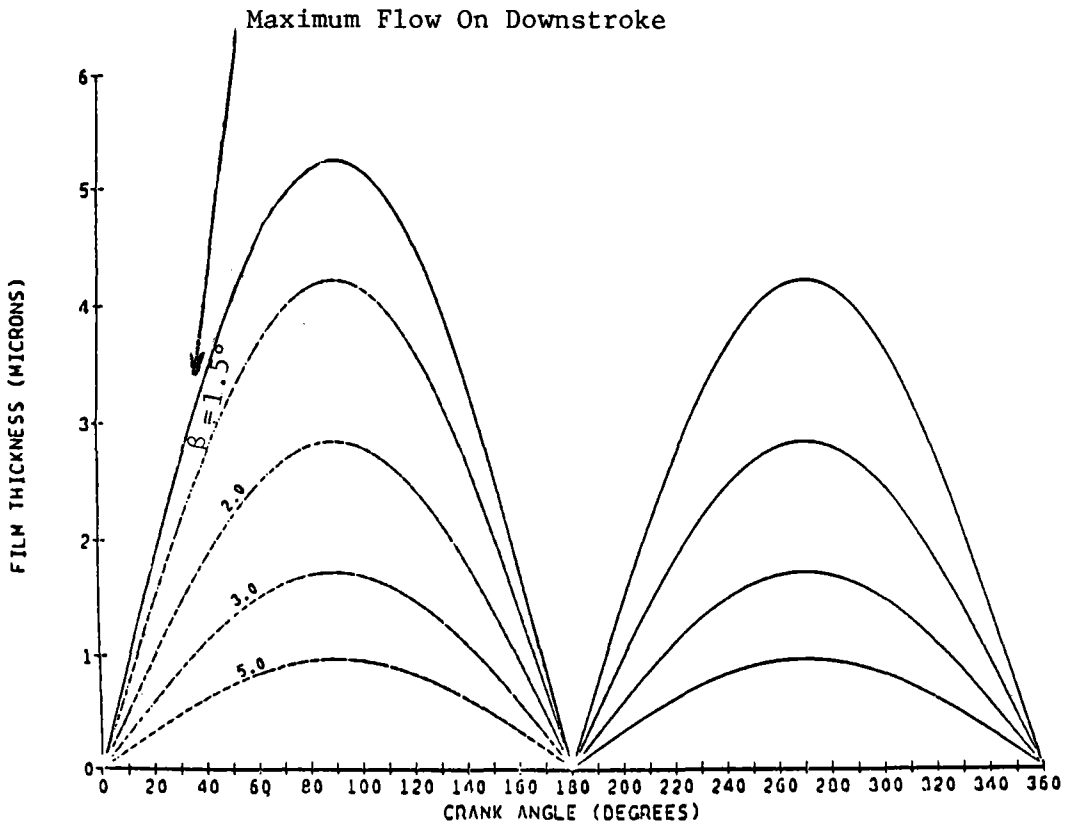

Figure 2-24 Operating Conditions Predicted by Analysis of Double-Angle Seal - Film Thickness versus Crank Angle

would exceed the maximum pumping capacity on the downstroke if β was less than 1.25°.

For the same seal and operating conditions, the thickness of the oil film separating the rod and seal is shown in Figure 2-24 as a function of crank angle. The film thicknesses are small, but would be more than adequate with a good surface finish on the rod. The analysis predicts zero oil film thickness at top and bottom dead centers but, in practice, a thin film would probably be retained due to squeeze-film effects, which were not taken into account in the analysis.

Double-angle seals of the type shown in Figure 2-25 (made from PTFE-based materials) have been tested in the Exploratory Seals Rig. All the seals performed well for an initial period with minimal gas leakage and no detectable oil leakage, but then suddenly started to leak oil. When this occurred, it was found that the inlet chamfer on the low-pressure side of the seal had almost or completely disappeared due to deformation of the seal. From this, it is reasonable to conclude that during the deformation process, the geometry of the lower entry section changed in such a way that oil flow to the gas side of the seal exceeded the seal's capacity for pumping in the opposite direction. With a reduced preload, one pair of seals ran for 528 hours with no noticeable deformation. Over this period, gas leakage was low, and total oil leakage was small (comparable to that which occurred with PL-type seals over a much shorter time).

Rig modifications have been made to allow testing of seals of the types shown in Figure 2-17. These seal designs are all aimed at minimizing or eliminating seal deformation, and maintaining the required inlet geometry on the low-pressure side of the seal.

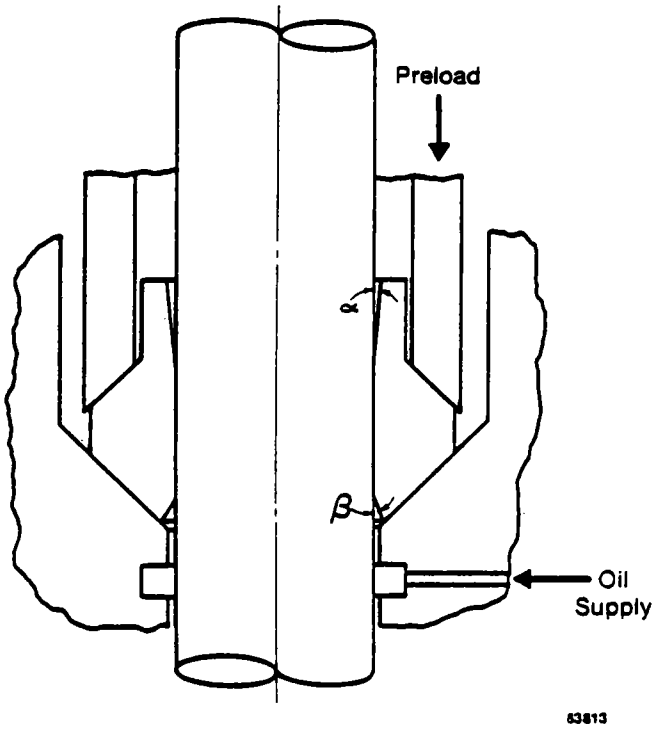

Figure 2-25 Double-Angle Seal in Exploratory Rig

Piston Rings

The RESD has one piston ring per piston of the form shown in Figure 2-26. The piston ring is made from a PTFE-based material, or a similar low-modulus, dry-bearing material. Radial holes in the mid-plane of the ring communicate the pressure at the mid-point of the leak path between the surfaces of the ring and cylinder to the inner surface of the piston ring for pressure balancing. Contact between the ring and cylinder is maintained by an internal expander ring that exerts a predictable controlled force. The leakage path around the back of the piston ring is sealed by two O-rings that straddle the piston ring.

Pressure-balancing of the piston ring makes the friction independent of gas pressure in the engine. Contact force and ring friction are dependent only on the load exerted by the expander ring, but this will also affect gas leakage past the rings. Pressure-balancing of the piston ring also makes the contact pressure independent of the gas pressure in the engine, and dependent only on the force exerted by the expander ring. Reducing the contact force and pressure will reduce both friction and wear of the rings, which is advantageous. However, this reduction will usually be accompanied by increased piston ring leakage, which will reduce the power developed by the engine. A compromise is therefore necessary to ensure that the benefits of reduced friction are greater than the adverse effects of increased piston ring leakage.

The single-ring system allows leakage from cycle to cycle; therefore, it is impossible for the pressure in any one cycle to be significantly and consistently different from the pressures in adjacent cycles. As a result, the system provides automatic balancing of the cycle pressures. By positioning the single ring near the base of the piston, the overall height of the piston/dome assembly may be reduced without subjecting the ring to a higher-temperature environment than the upper ring in a two-ring system. This should reduce the weight of the piston assembly, and a more significant weight reduction may be achieved if this permits reduction in the overall height of the engine.

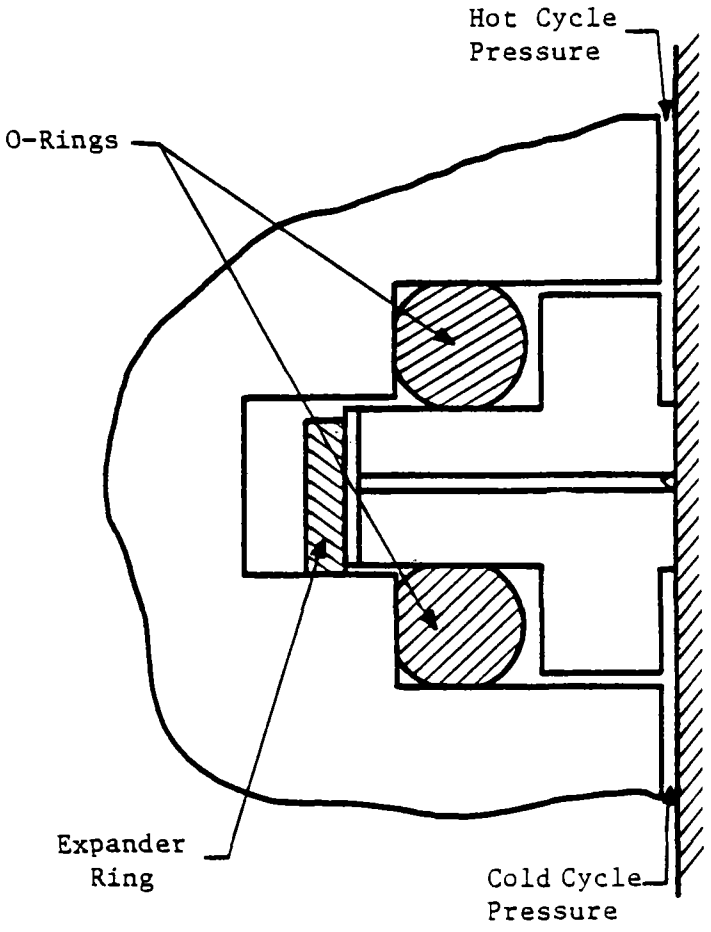

Figure 2-26 1983 RESD Piston Ring

Comparison to Existing Technologies

In the Mod I engine, the piston rings are a major source of friction power loss, and their effective life is limited by their inability to seal at start-up, or their limited ability to compensate for wear. The original Mod I piston ring system employed two solid, Rulon LD piston rings per piston. The space between the two piston rings was connected to the piston dome, and the pressure in this space was maintained at or close to the minimum cycle pressure by the check valve action of the piston rings (shown in Figure 2-27). The piston rings were machined to be an interference fit in the cylinders to provide a seal at start-up. Under operating conditions, the seal was augmented by pressure loading from the cycle pressure action on the inner surface of the piston rings.

Rig tests showed that once the solid rings had been energized, they gave low gas leakage under both static and dynamic conditions. No ring failures occurred during testing after the initial seal had been affected; failures were due to the rings' inability to seal at start-up. These failures only occurred after the rings had gone through a period of testing. Examination of failed rings showed that dimensional changes had occurred, particularly a reduction in the O.D. of the rings, so that they were no longer an interference fit in the cylinder. Piston ring wear (loss of weight) was not sufficient to account for the change in diameter, so it was concluded that the rings had suffered permanent deformation under the loads, and thermal cycles imposed on them during intermittent testing. With this deformation, a situation was eventually reached in which there was a large clearance between the piston rings and cylinders under cold-start conditions. With virtually no resistance to leakage flow, it was impossible to build up sufficient pressure to energize the rings. The test rig experience with solid rings was borne out in the engines where the rings would perform well for some time, and then suddenly fail to seal at start-up. Measurements of piston ring friction under rig conditions were in close agreement with predicted values (see Figure 2-28).

To overcome the problems with the solid rings, a modified piston ring system was introduced and is currently used in the Mod I engine. In this system, each piston has two piston ring grooves, and each groove houses two Rulon LD piston rings (shown in Figure 2-29). The ring closest to the cycle pressure is split with a 15° scarf joint, while the second ring is solid. The rubber backup ring

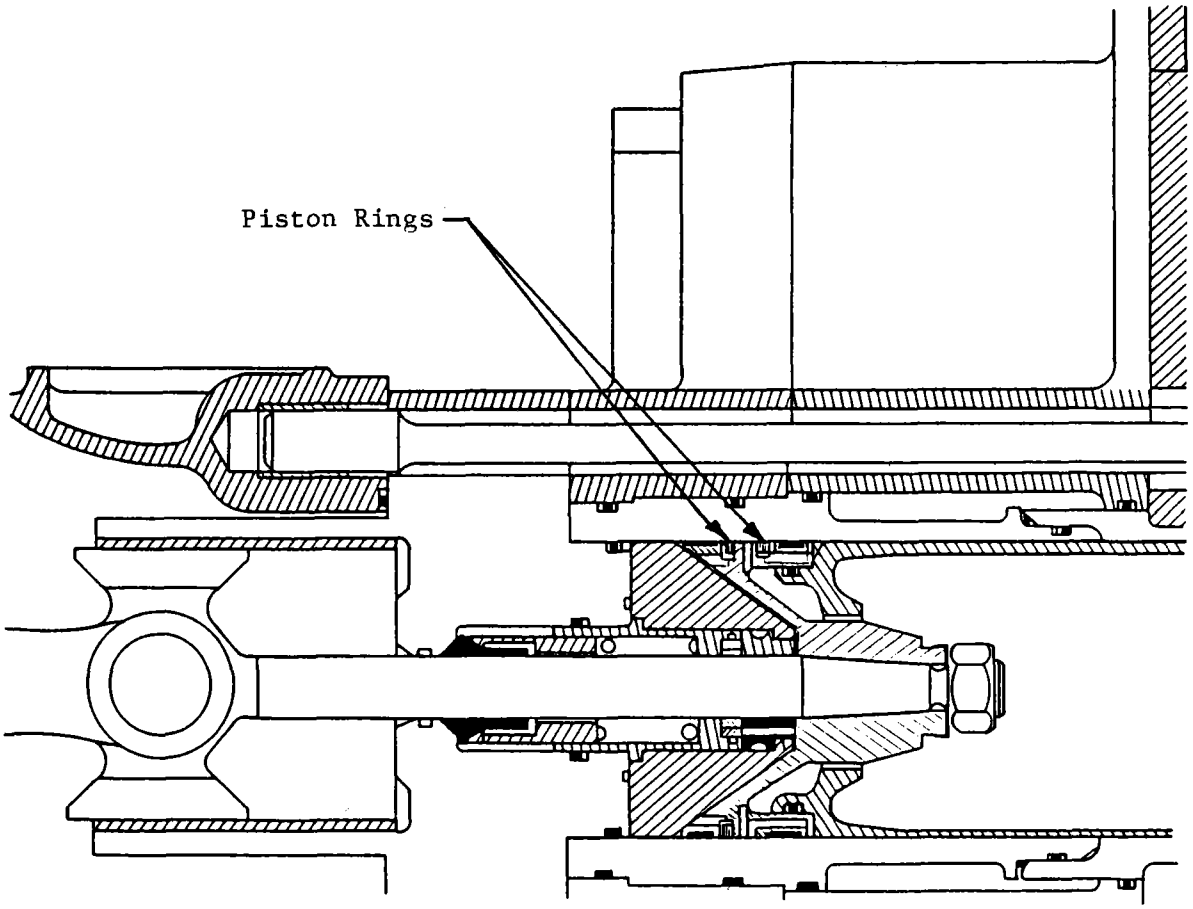

Fig. 2-27 Solid Piston Rings with Check Valve Action

832406

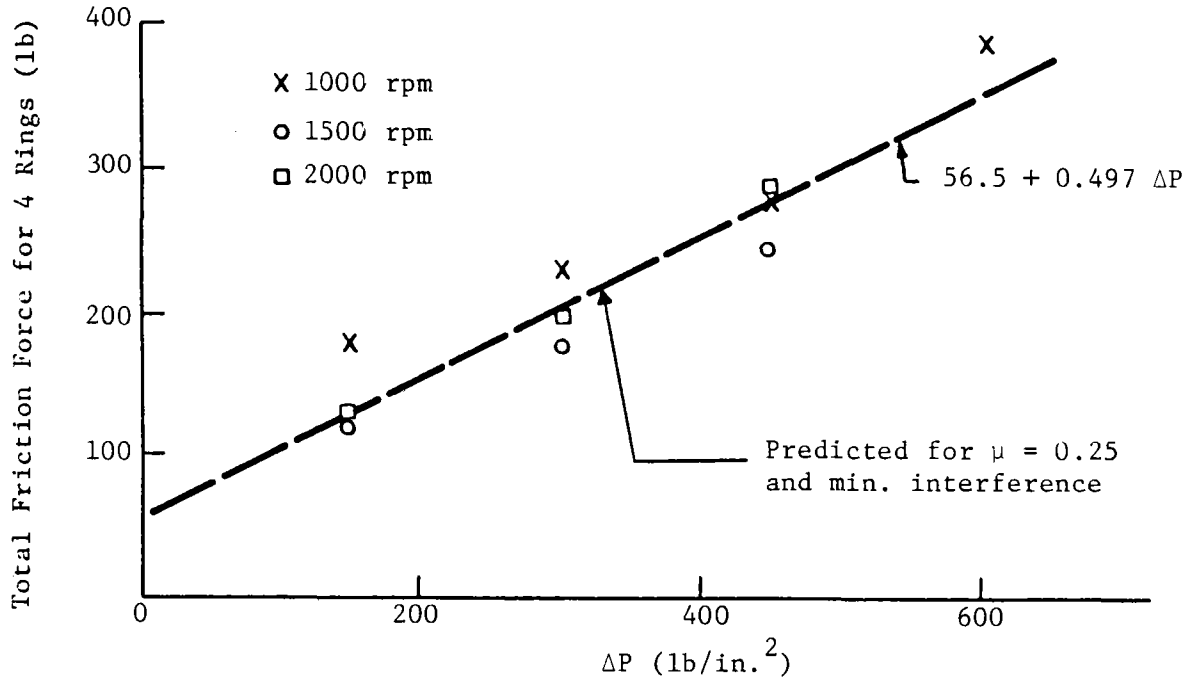

Figure 2-28 Mod I Rulon LD Solid Rings - Hydrogen

832405

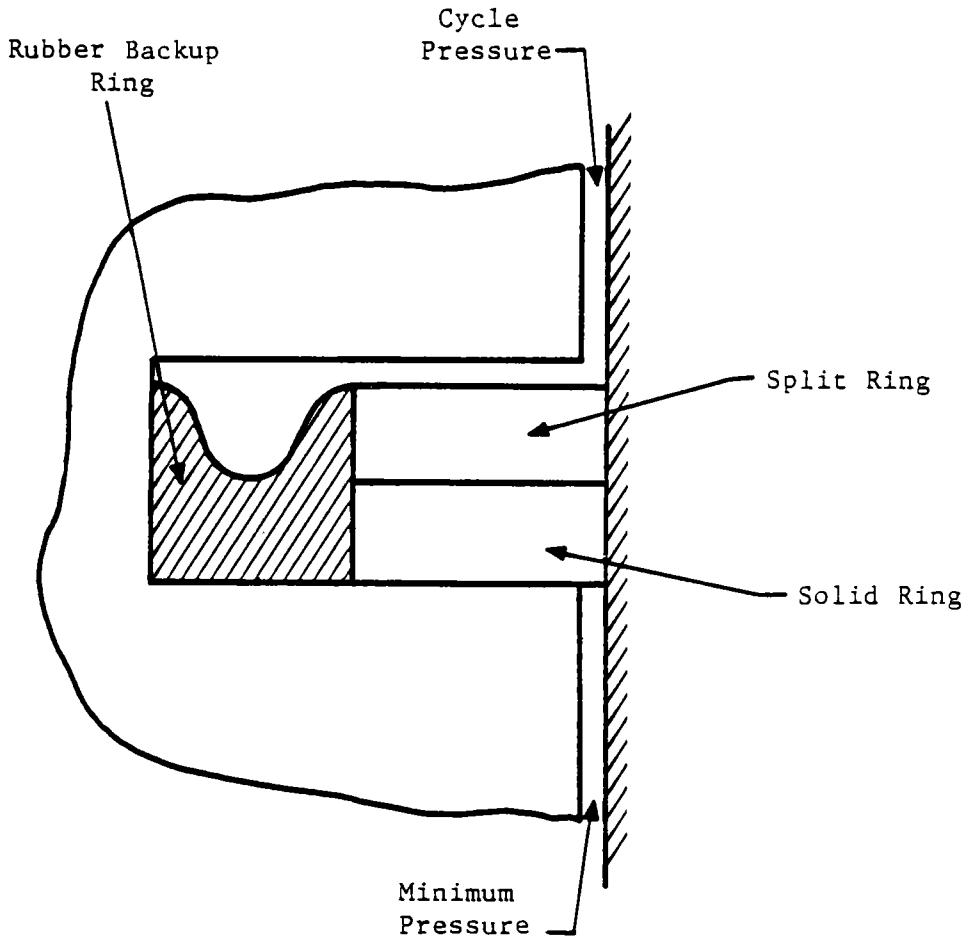

Figure 2-29 Modified Piston Ring System

with its U-shaped cross section exerts a radial force on the piston rings, and seals the leak path around the back of the piston rings. Under free conditions, the backup ring has the asymmetrical form shown in Figure 2-30. When the piston rings are installed, the outer lip of the backup ring is deflected inward by the split piston ring, thus exerting a light radial force on the split ring that is sufficient to hold it in contact with the cylinder wall. The split ring provides a sufficiently good seal at start-up to allow a pressure difference to be generated across the piston rings, and then the cycle pressure acting on the backup ring exerts additional radial loads in both piston rings to provide a fully activated seal.

The spaces between the piston ring grooves on each piston are connected to the chambers between the main and cap seals via the piston domes and hollow piston rods. These chambers are maintained at the minimum cycle pressure by check valves; therefore, the space between the piston ring grooves is also maintained at or close to minimum cycle pressure. As a result, there should be no reversal of pressure difference across the rings under steady-state conditions.

Test rig and engine experience has shown that the split/solid ring arrangement generally provides an effective seal when new. This is maintained for some time, but then progressively deteriorates as the capacity of the backup ring diminishes to compensate for piston ring wear. This principal mode of failure with the split/solid rings limits the effective life of the piston rings, although it does not constitute a catastrophic failure. The deterioration in performance due to piston ring wear results in longer start-up times and reduced engine efficiency.

Since pressure loading of the split/solid rings gives undesirably high friction (see Figure 2-31), the contact area has been minimized by using thin rings (0.9-mm nominal) to keep the friction within acceptable limits, but this makes the rings more susceptible to damage, particularly during installation.

With the inter-ring space maintained at minimum cycle pressure, the engine's four working cycles are effectively isolated from each other, and the conditions within each cycle are independent of those in the other cycles. Gas leakage from the cycles will always flow into the inter-ring space, and the

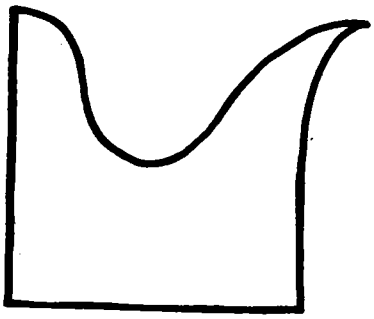

Figure 2-30 Asymmetrical Form of Backup Ring

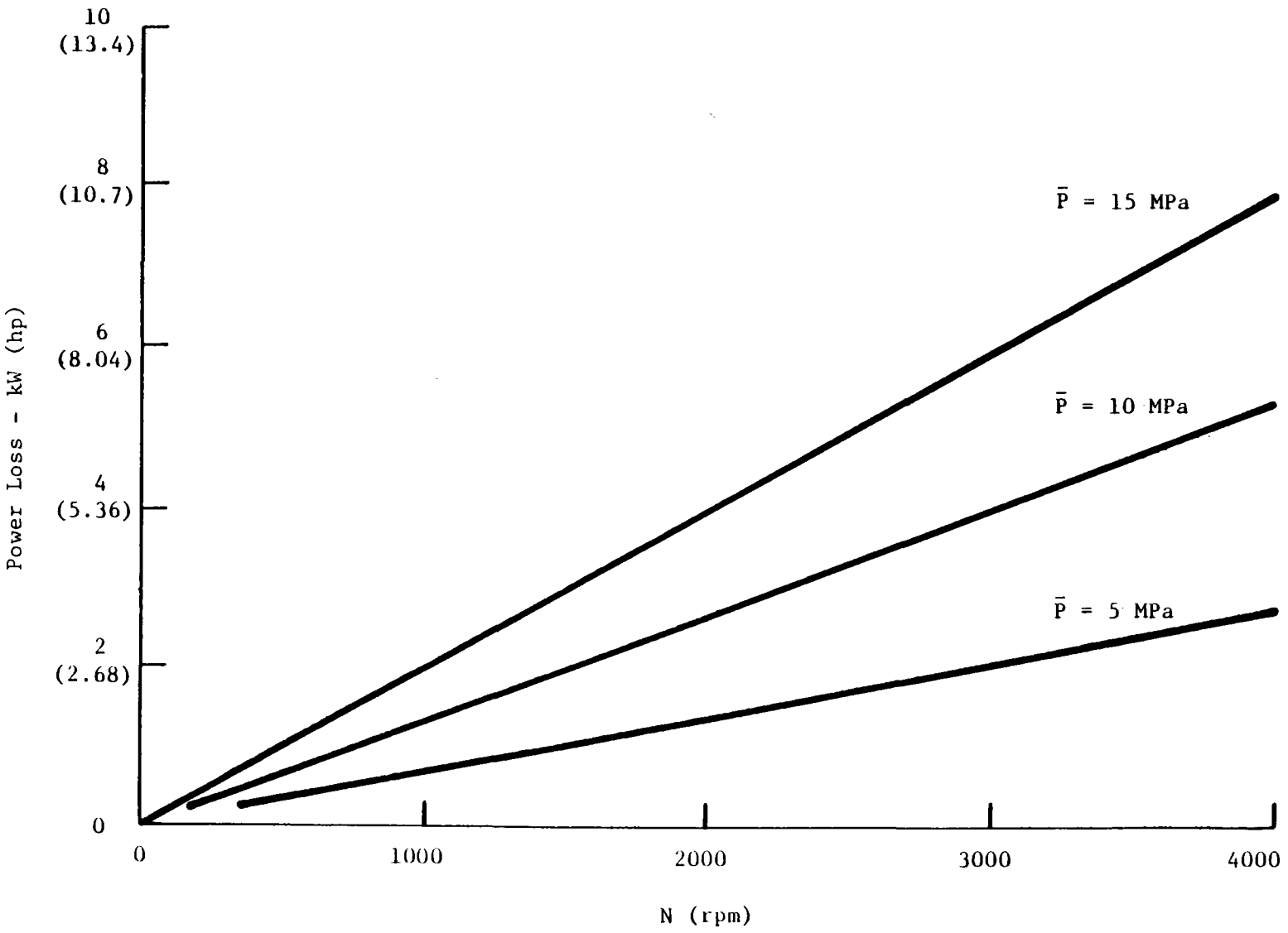

Figure 2-31 Friction Power Loss for Mod I Split/Solid Piston Rings

system that controls the inter-ring pressure must have the capacity to vent this leakage. To maintain steady-state operating conditions, the gas supply system to each cycle must be able to make up for the gas leakage out of the cycles past the piston rings. While gas leakage past the piston rings is not lost from the system, it does impose a number of penalties such as:

- Energy loss associated with the piston ring leakage
- Leakage flow that must be returned to the supply bottle by the hydrogen compressor, thus requiring additional energy input
- Additional heat input required for the replacement gas to maintain engine conditions.

Since leakage past individual rings will always differ, total leak rates from the individual cycles will never be identical; therefore, mean pressure and pressure amplitude will vary from cycle to cycle.

Initial attempts to generate an improved piston ring design were based on the existing Mod I arrangement, i.e., two piston ring grooves per piston. From the outset, it was clear that any form of pressure-loaded ring would have friction similar to that in the existing ring design. To avoid the effects of pressure loading, a pressure-balanced ring design was evolved (the H-ring shown in Figure 2-32). The jointed ring has a number of radial holes spaced around the circumference in the mid-plane of the ring. These holes communicate the pressure at the mid-point of the leak path between the ring and cylinder to the inner surface of the ring. With this arrangement, the pressure on the inner surface of the ring is equal to the mean pressure on the outer surface, and there is no net radial force due to the gas pressure. The O-ring on the cycle side of the piston ring isolates the cavity behind the piston ring from the cycle pressure, and holds the ring in contact with the opposite side of the groove. An expander ring on the I.D. of the piston ring provides the only radial force holding the piston ring in contact with the cylinder. Piston ring friction is directly proportional to the force exerted by the expander ring, thus providing flexibility to vary the expansion force to attain an acceptable compromise between friction and leakage.

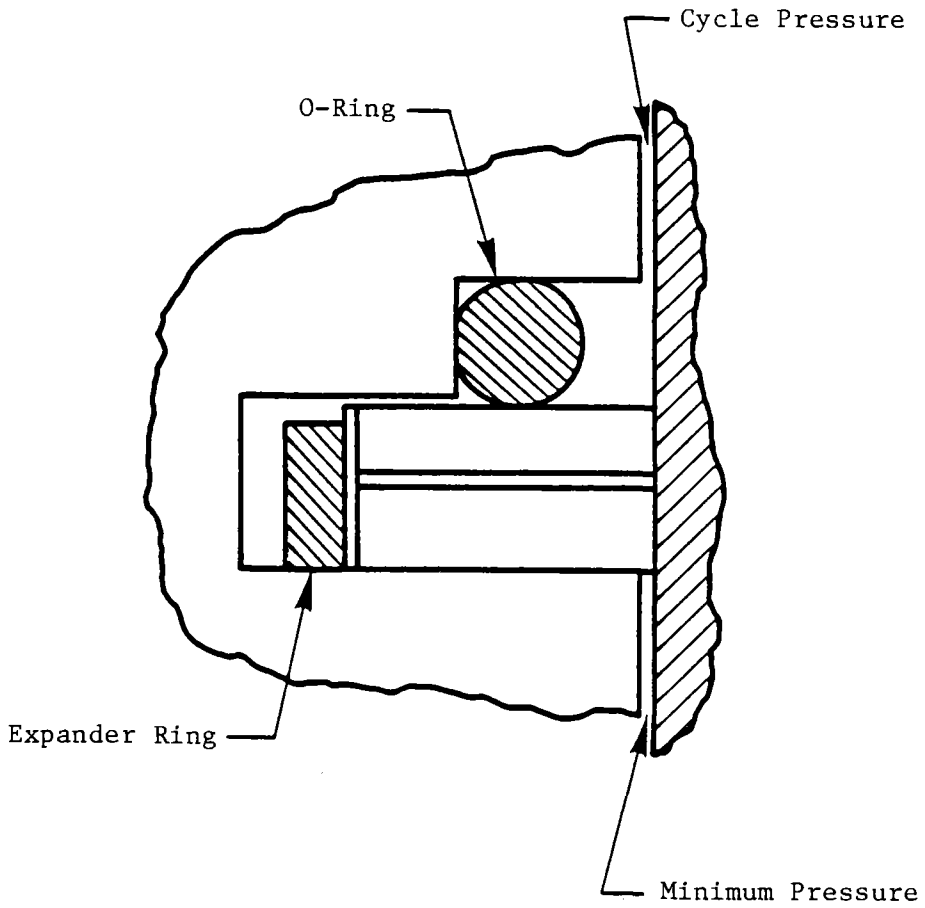

Figure 2-32 Pressure-Balanced H-Ring

Piston rings have been evaluated in rig tests. Measurements showed that piston ring friction was basically independent of the gas pressure, as expected, and close to the predicted values (Figure 2-33). With H-rings, hydrogen leakage was ~10 ℓ/min, which was approximately an order of magnitude greater than that previously measured with solid rings of the same dimensions. An analytical study showed that gas leakage of 10 ℓ/min across each piston ring would have negligible effect on the power developed by a Mod I engine, implying that the H-ring design tested would be an acceptable alternative. In Figure 2-34, frictional power loss with H-rings is compared to that for the split/solid rings in the Mod I engine, indicating the advantage of the H-ring.

No testing has been carried out with a single pressure-balanced ring, but it would be expected to show similar friction characteristics when compared to the two ring designs. By reducing the number of piston rings in the engine from eight to four, a further reduction in power loss should be achieved. With the same major dimensions and loading, leakage across a single pressure-balanced ring should be comparable to that measured with the two ring designs.

2.3.3 Engine Drive System

Description

The 1983 RESD Engine Drive System (EDS) is based on the rolling-element bearing technology developed and demonstrated on the Upgraded Mod I engine. (Figures 2-35 and 2-36 show the general arrangement of the system.) The basic layout is a 40°-V, four-cylinder engine with a three-main-bearing crankshaft. Cylinders 1 and 4 are in the left bank, and cylinders 2 and 3 are in the right bank, as viewed from the flywheel end of the engine. The front and center main bearings are split-cage roller bearings that run directly on hardened journals on the crankshaft. Half-shell outer races are captured at the crankcase/bearing cap interface in a manner similar to conventional journal bearings. Front and center main bearing dimensions are 34.93 mm (1.375 in.) x 46.05 mm (1.813 in.) x 19.05 mm (0.750 in.).

The rear main bearing is a combination roller/ball bearing assembly (Figure 2-37) with an integral outer race and a two-piece inner race split through the

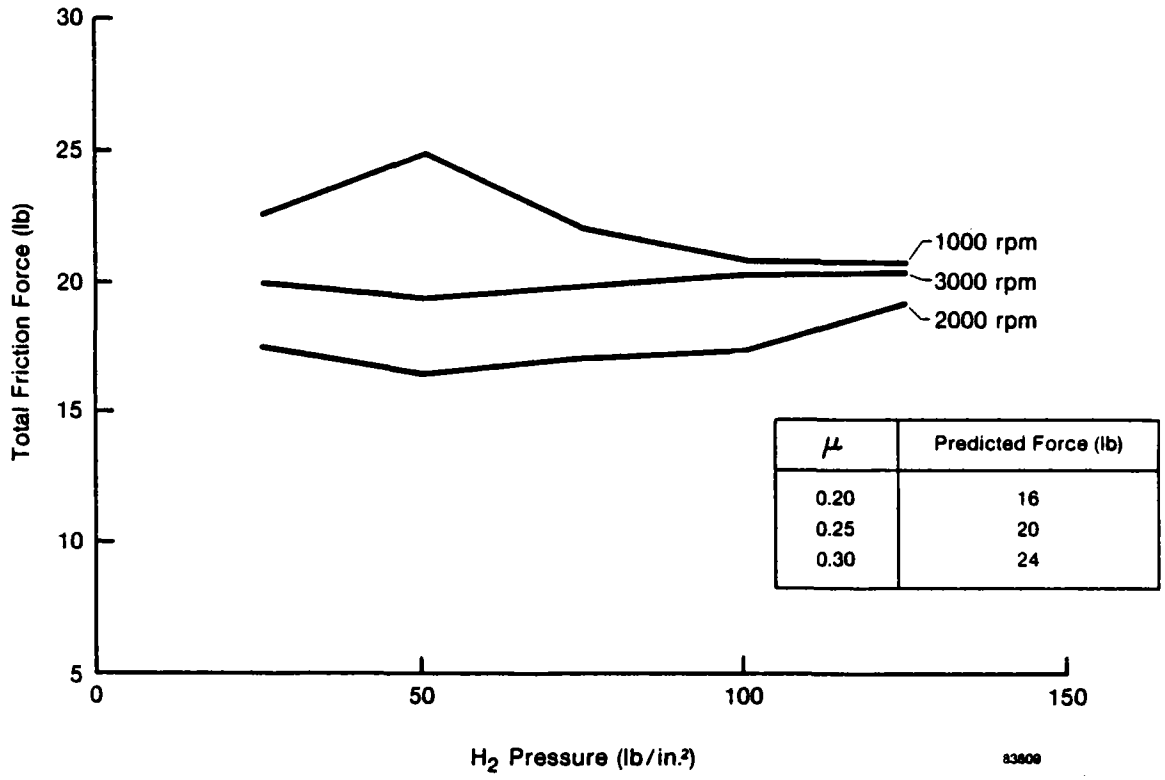

Figure 2-33 Total Friction Force for 4 H-Rings

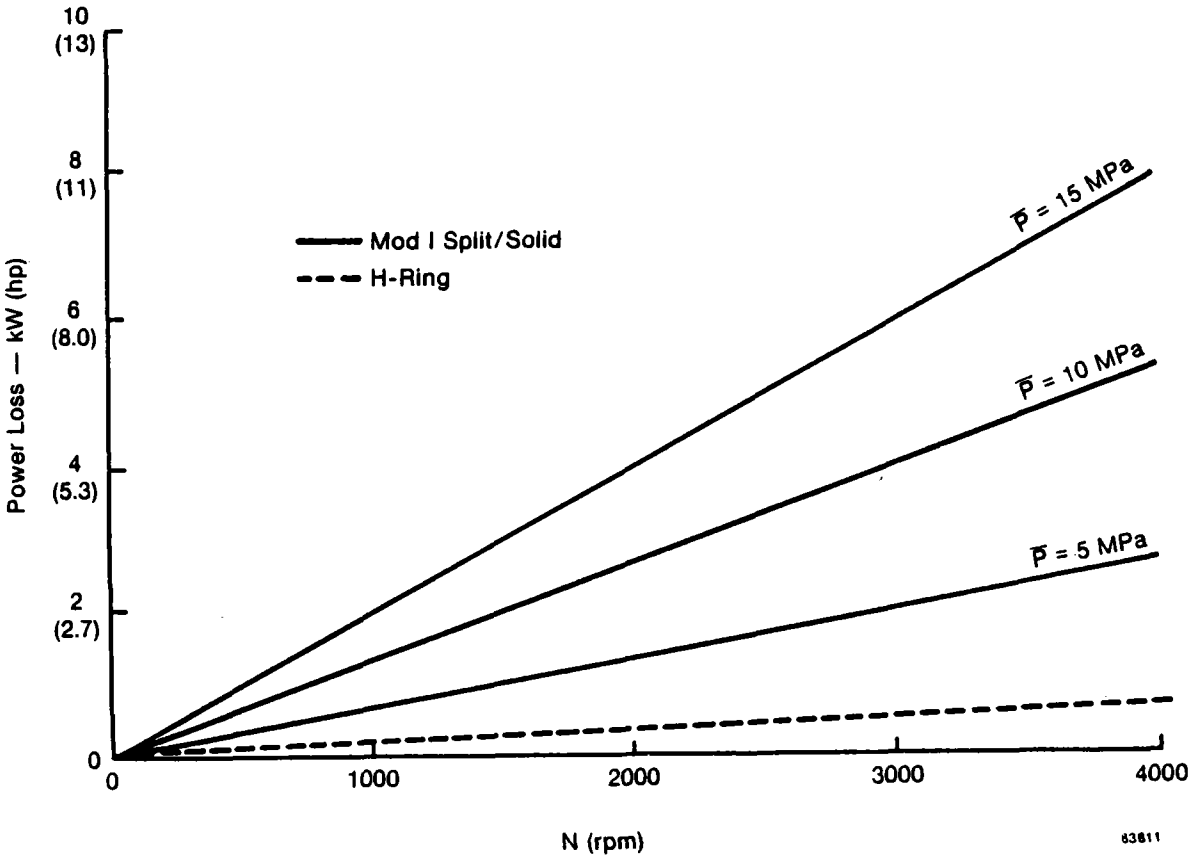

Figure 2-34 Comparison of Total Piston Ring Power Loss for Mod I Split/Solid and H-Rings

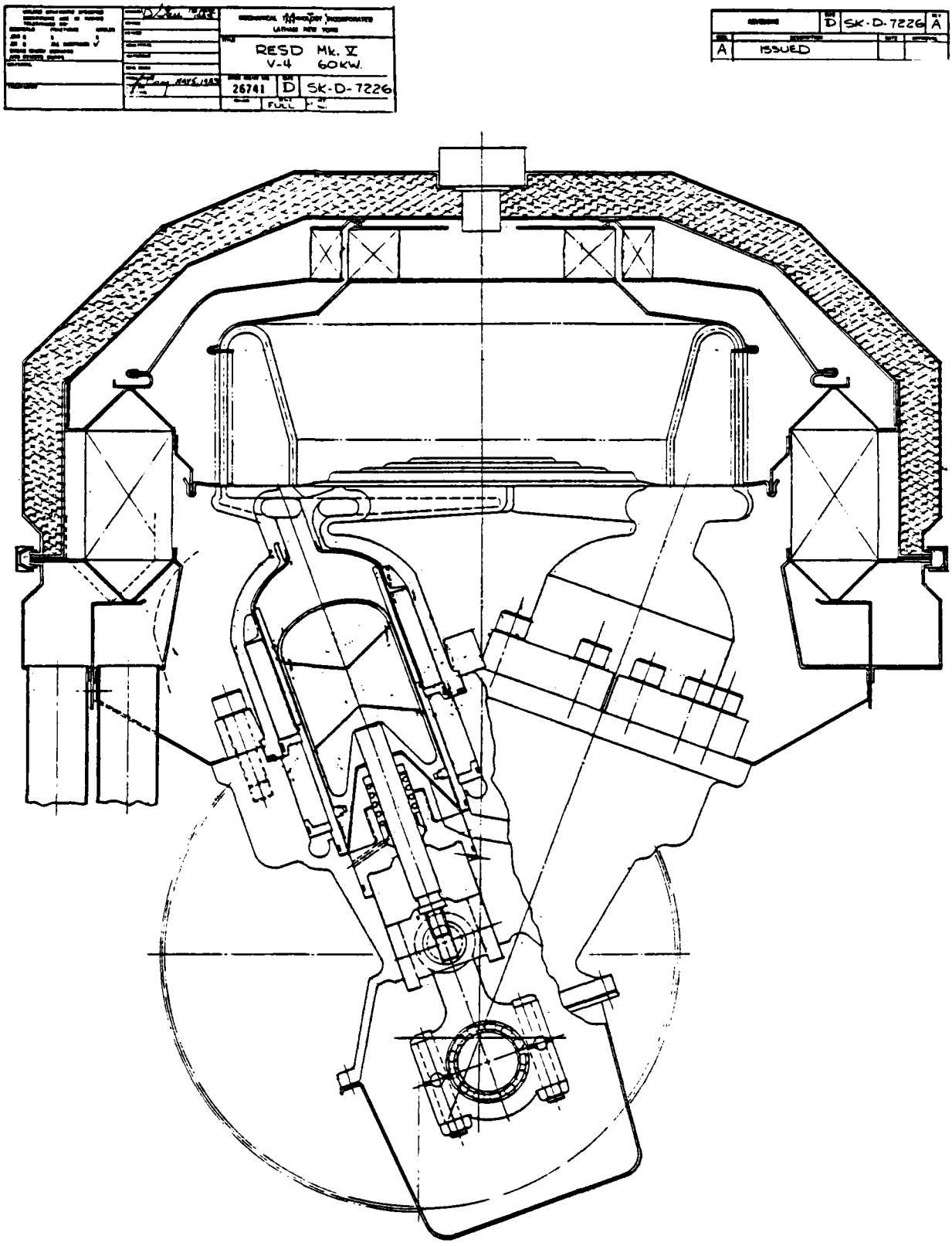

Figure 2-35 General Arrangement of RESD Engine Drive System (Cross Section, Front View)

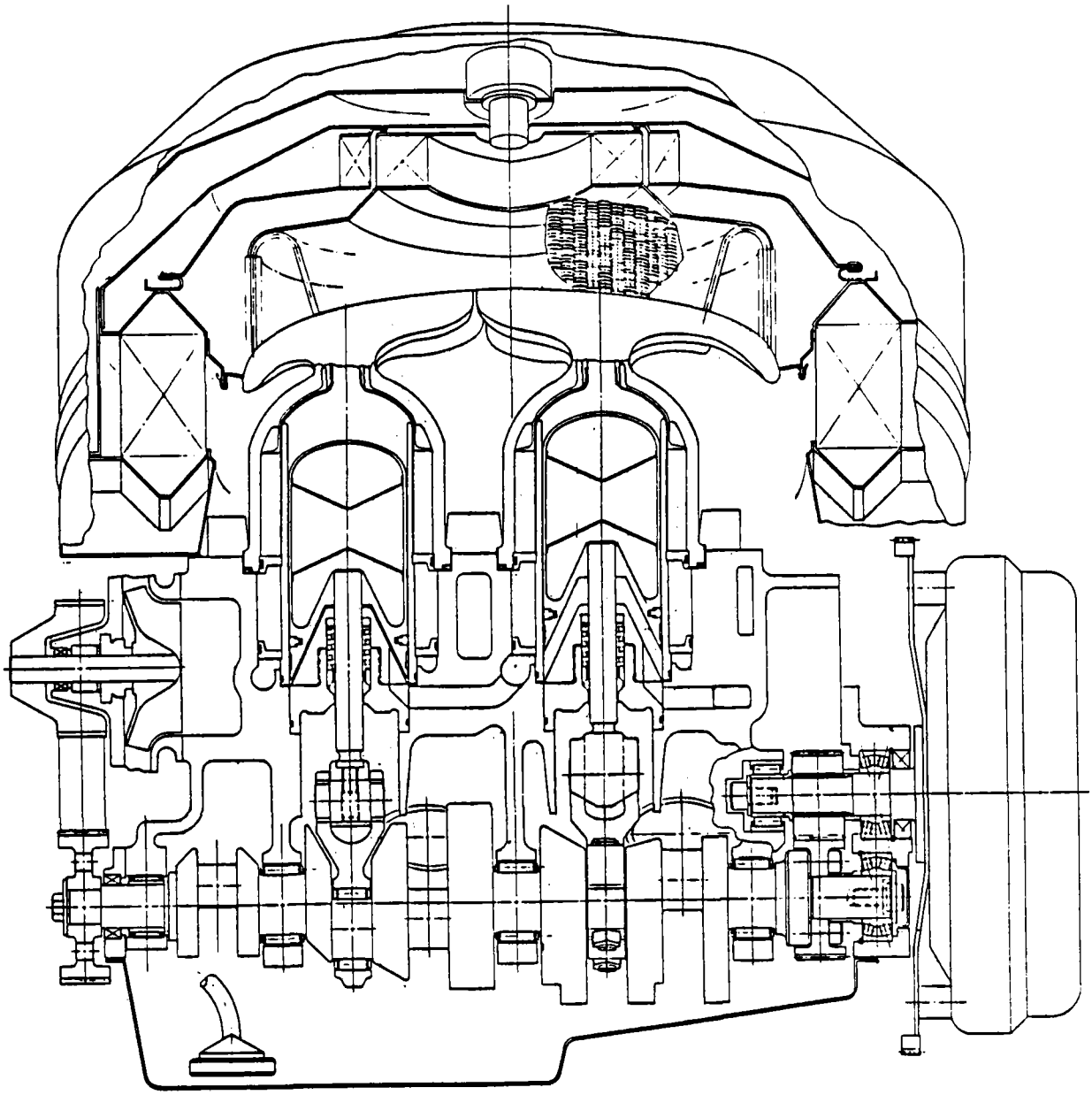

Figure 2-36 General Arrangement of RESD Engine Drive System (Cross Section, Side View)

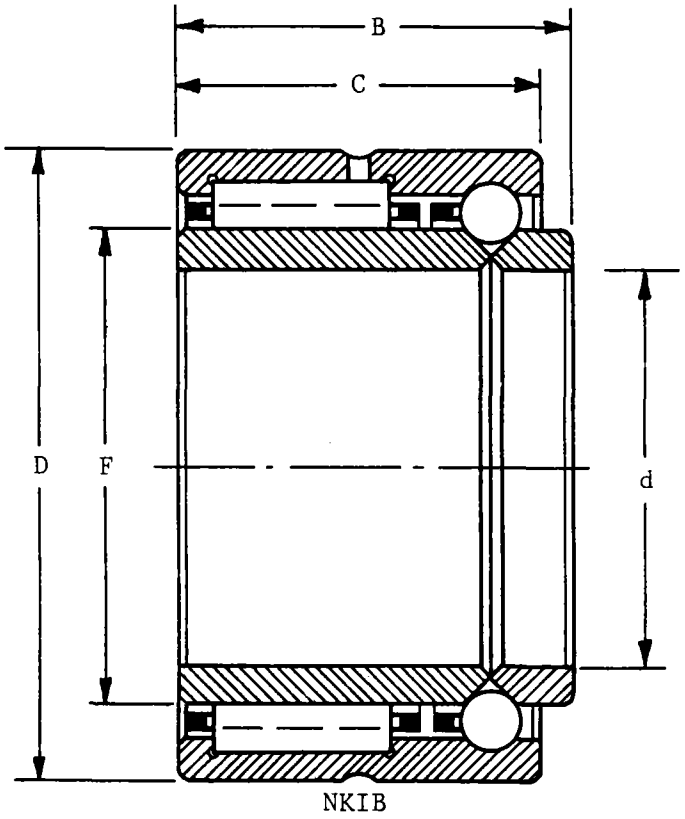

Figure 2-37 Rear Main Bearing

ball groove. The bearing assembly is installed on the shaft between the rear crank cheek and the flywheel. The rear bearing bore in the crankcase is flanged to provide axial location for the crankshaft. The big end connecting rod bearings are split-cage roller bearings that run directly on hardened crankpins. The big end bores of the connecting rods are hardened and ground to provide the outer race running surface. Perfect alignment of the cap to the rod is obtained by fracturing the rod at the cap interface, and bolting the parts together to the specified assembly torque prior to final machining of the big end bore. The rear main bearing dimensions are 35 mm (1.378 in.) x 48 mm (1.890 in.) x 20.8 mm (0.819 in.). Two full-complement, drawn-cup roller bearings are used on the connecting rod wrist pins - one on each side of the crosshead. The wrist pins are retained in the crosshead by a press fit. The wrist pin bearing dimensions are 20.64 (0.813 in.) x 26.99 mm (1.063 in.) x 12.7 mm (0.500 in.).

The hydrogen pump connecting rod is similar to the power piston connecting rods except that the wrist pin is press-fitted to the rod, and a single, drawn-cup bearing that runs directly on the hardened wrist pin is installed in the crosshead. The bearing on the wrist pin is a 15.82 mm (0.625 in.) x 11.11 mm (0.438 in.) x 11.13 mm (0.438 in.), full-complement design; the big end bearing is 22.23 mm (0.815 in.) x 30.16 mm (1.182 in.) x 15.82 mm (0.625 in.), split-cage design running on a hardened shaft journal inside a fractured rod bore. The rolling-element bearings are lubricated by jet sprays directed at each bearing (a direct-drive, gerotor-type oil pump is used).

Comparison to Existing Technologies

Extensive use of rolling-element bearings has been made in the field of high specific output, IC engines, particularly outboard marine and motorcycle engines. The need for rolling-element bearings in these applications was originally dictated by marginal lubrication conditions rather than by the desire to reduce mechanical losses. Outboard marine engines are almost exclusively two-stroke cycle machines that are lubricated by an oil mist entrained in the fuel/air mixture as it passes through the crankcase. Many motorcycle engines were two-stroke cycle machines initially, and required rolling-element bearings for the same reasons as the marine engines. Emissions regulations have forced most motorcycle manufacturers to adopt

four-stroke cycle engines for highway motorcycles; however, many of these engines have retained rolling-element bearings, presumably for the performance advantages.

Two Mod I Stirling engines have been modified to incorporate rolling-element bearings throughout. Figure 2-38 is a cross section through the Mod I Lightweight Reduced Friction Drive (LRFD) showing the bearing details. Both of the Reduced Friction Drives (RFD) have been run extensively as motoring rigs, and have demonstrated a significant reduction of mechanical friction power versus the journal bearing baseline engine. The original RFD unit is currently being used to support the seals development effort, and has accumulated more than 67 hours of test time. The LRFD was run as a motored rig for more than 50 hours.

Experimental Data

Extensive motoring tests were conducted with the baseline EDS, RFD, and LRFD Motoring Rigs. The baseline unit was used to characterize various mechanical loss mechanisms in the drive system, and to predict performance improvements that could be expected through substitution of rolling-element bearings. (Figure 2-39 shows the breakdown of mechanical losses determined from this effort, and Table 2-1 shows the predicted loss reduction with rolling-element bearings.) The RFD's with rolling-element bearings were tested to determine the validity of the performance predictions. Figures 2-40 and 2-41 show comparative results for various operating conditions for the baseline versus the RFD's.

Extensive analysis of equivalent bearing loads/speeds was conducted to determine proper sizing of bearings. Table 2-2 shows calculated bearing loads and equivalent data over the life of the engine for the loads, speeds, and times shown. These forces were used to calculate the equivalent main bearing/crankpin bearing loads shown in Table 2-3. The equivalent speed/load and required life were used to calculate the required dynamic capacity shown in Table 2-4. Table 2-5 shows the recommended bearing and weighted L-10 life for the crankpins and each main journal. Tables 2-6 and 2-7 show the maximum crankshaft loads at the connecting rod throws and main journals for the RESD. The equivalent speed for the RESD is the same as for the Mod I (1429 rpm). The

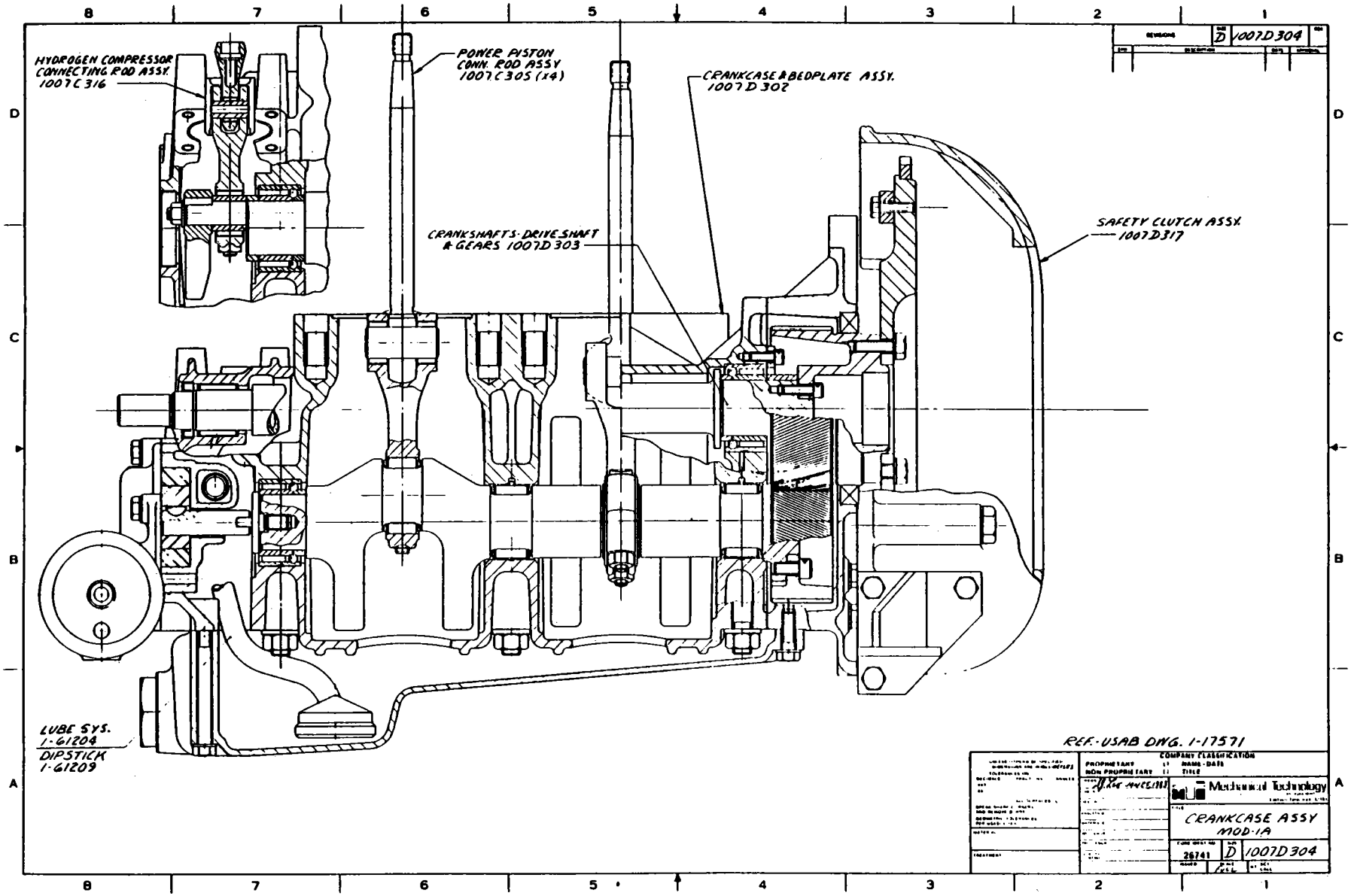

Figure 2-38 Mod I Lightweight Reduced Friction Drive Cross Section

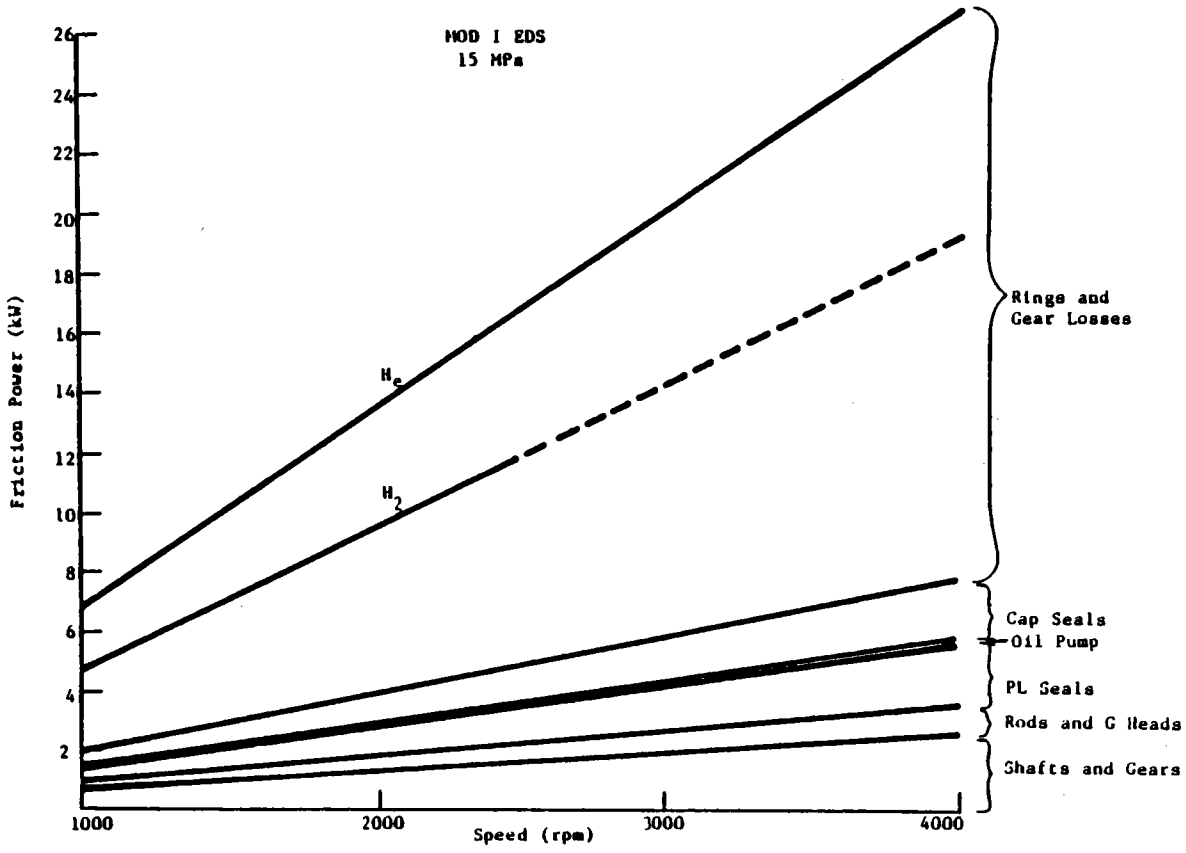

Figure 2-39 Loss Breakdown Curves for 15-MPa Mean Pressure

TABLE 2-1

PREDICTED MECHANICAL LOSS REDUCTION FOR REDUCED FRICTION DRIVE

Bearing	Mod I - kW (hp)	RFD - kW (hp)	Δ - kW (hp)
Crossheads	0.570 (0.764)	0.570 (0.764)	0.0 (0.0)
Drive Shaft Thrust	0.334 (0.448)	0.0 (0.0)	-0.334 (-0.448)
2 Crankshaft Thrust	0.668 (0.896)	0.0 (0.0)	-0.668 (-0.896)
Drive Shaft Front	0.090 (0.121)	0.090 (0.121)	0.0 (0.0)
Drive Shaft Rear	0.290 (0.389)	0.260 (0.349)	-0.030 (-0.040)
4 Crank Pin	0.760 (1.019)	0.660 (0.885)	-0.100 (-0.134)
6 Main	1.600 (2.146)	1.132 (1.518)	-0.468 (-0.627)
Total	4.312 (5.782)	2.712 (3.637)	-1.600 (-2.146)

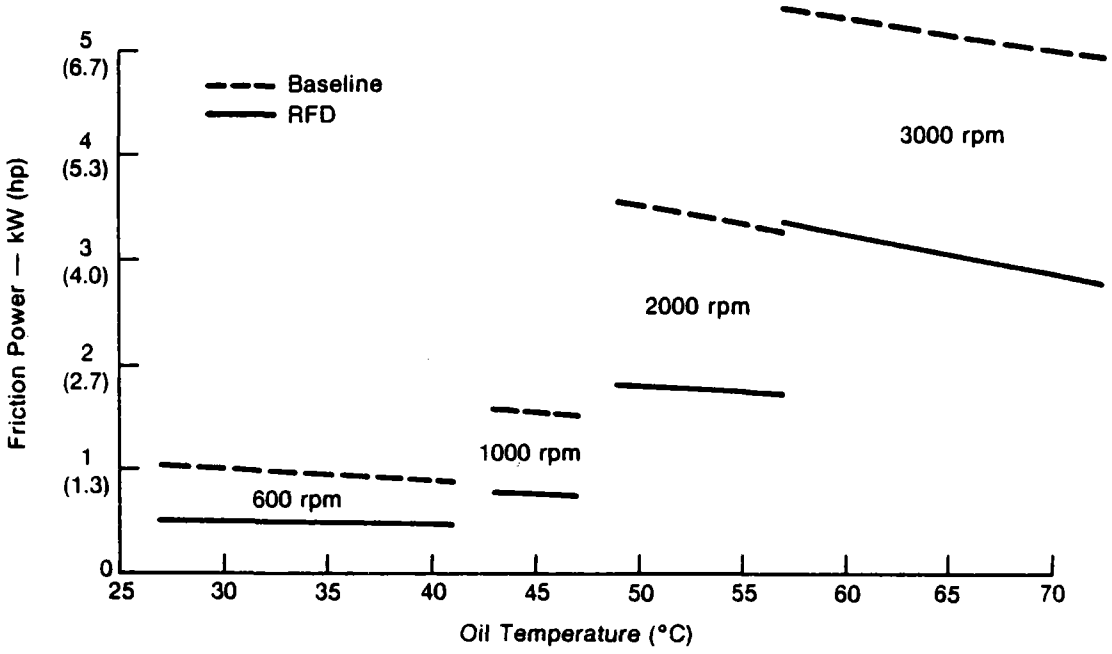

Figure 2-40a Mod I EDS (System Complete - No Gas) 831484

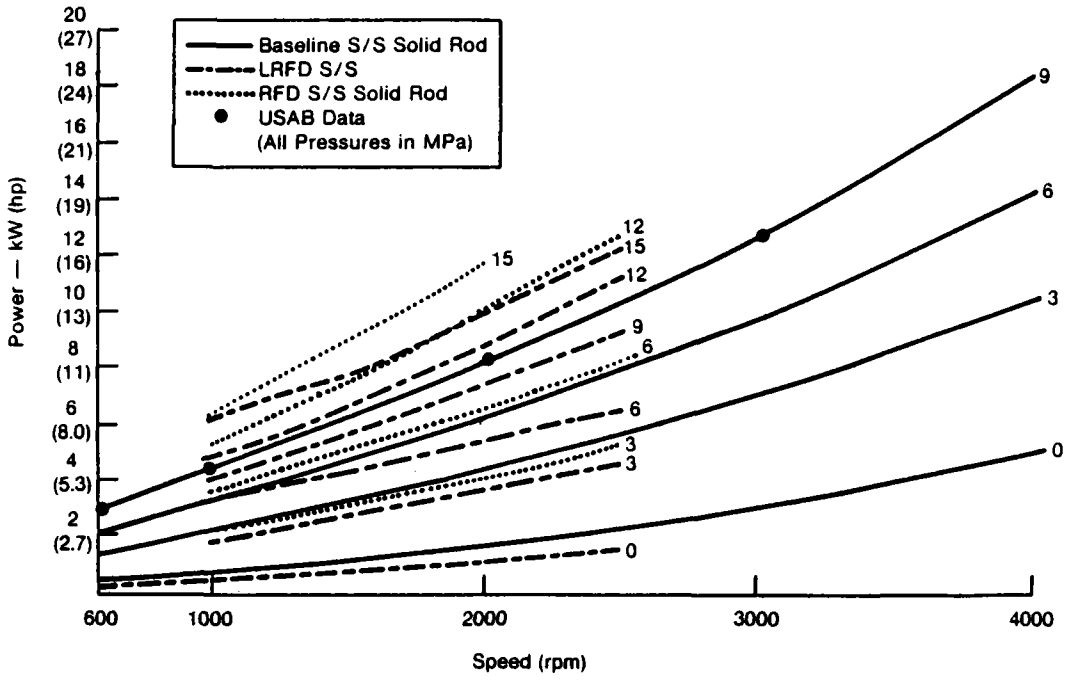

Figure 2-40b Mod I EDS (Helium)

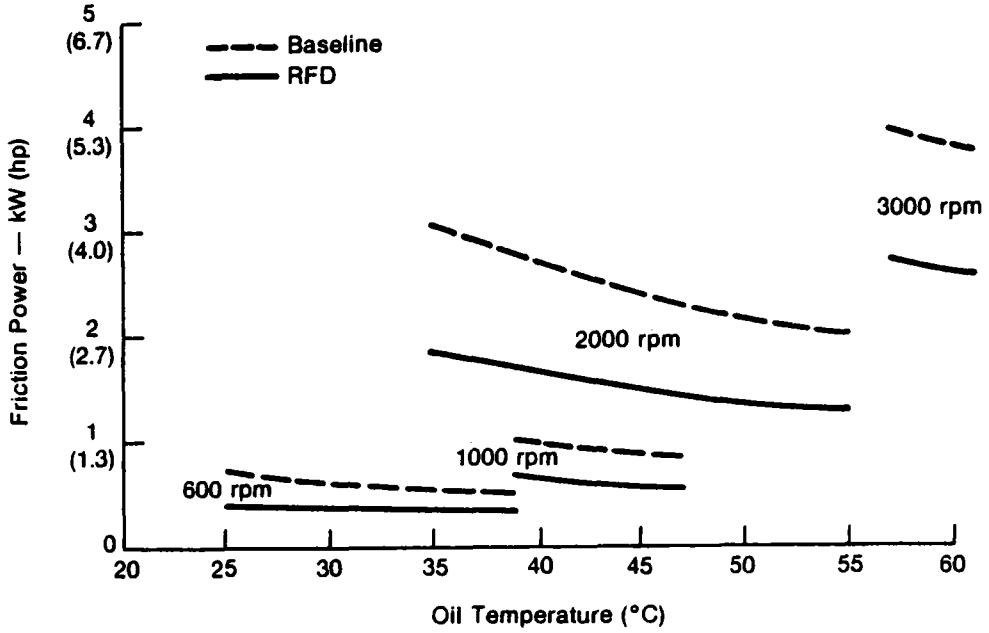

Figure 2-41a Mod I EDS (No Cylinders)

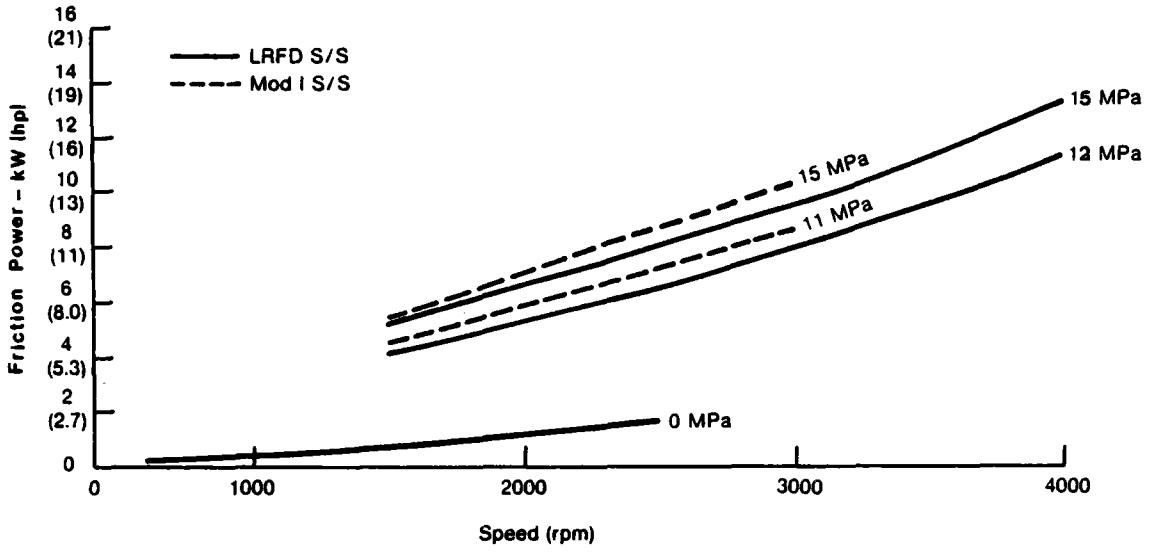

Figure 2-41b Mod I EDS (Hydrogen)

831557

TABLE 2-2

MOD I LIGHTWEIGHT REDUCED FRICTION DRIVE

Calculated Bearing Loads (N)

% of Torque	% of Load	Time (hrs)	Speed (rpm)	Crank-pin	Crank 1&2 Main #1	Crank 1&2 Main #2	Crank 1 Main #3	Crank 2 Main #3	Output Shaft Front Support (Radial)	Output Shaft Front Support (Axial)
10	25.0	19	500	3800	1625	2525	2375	2000	1750	675
10	25.0	543	1000	3800	1625	2525	2375	2000	1750	675
20	40.0	543	1000	6080	2600	4040	3800	3200	2800	1080
30	50.0	150	1000	7600	3250	5050	4750	4000	3500	1350
40	60.0	146	1000	9120	3900	6060	5700	4800	4200	1620
50	68.5	66	1000	10412	4453	6919	6508	5480	4795	1850
60	75.0	4	1000	11400	4875	7575	7125	6000	5250	2025
10	25.0	145	1500	3800	1625	2525	2375	2000	1750	675
20	40.0	100	1500	6080	2600	4040	3800	3200	2800	1080
30	50.0	234	1500	7600	3250	5050	4750	4000	3500	1350
40	60.0	156	1500	9120	3900	6060	5700	4800	4200	1620
50	68.5	156	1500	10412	4453	6919	6508	5480	4795	1850
60	75.0	134	1500	11400	4875	7575	7125	6000	5250	2025
70	82.5	66	1500	12540	5363	8333	7838	6600	5775	2228
80	89.0	33	1500	13528	5785	8989	8455	7120	6230	2403
90	95.0	16	1500	14440	6175	9595	9025	7600	6650	2565
100	100.0	3	1500	15200	6500	10100	9500	8000	7000	2700
10	25.0	63	2000	3800	1625	2525	2375	2000	1750	675
20	40.0	103	2000	6080	2600	4040	3800	3200	2800	1080
30	50.0	274	2000	7600	3250	5050	4750	4000	3500	1350
40	60.0	332	2000	9120	3900	6060	5700	4800	4200	1620
50	68.5	133	2000	10412	4453	6919	6508	5480	4795	1850
60	75.0	66	2000	11400	4875	7575	7125	6000	5250	2025
70	82.5	10	2000	12540	5363	8333	7838	6600	5775	2228
80	89.0	8	2000	13528	5785	8989	8455	7120	6230	2403
90	95.0	3	2000	14440	6175	9595	9025	7600	6650	2565
100	100.0	3	2000	15200	6500	10100	9500	8000	7000	2700
Equivalent			1429	8690	3716	5774	5431	4574	4002	1544

TABLE 2-3

MOD I LIGHTWEIGHT REDUCED FRICTION DRIVE

Equivalent Maximum Bearing Load Calculation

Main Bearing Loads (N)

	Crank 1&2 Main #1	Crank 1&2 Main #2	Crank 1 Main #3	Crank 2 Main #3
1	0	0	3330	11030
2	3470	5670	2670	6730
3	7100	11070	4930	3400
4	3500	16600	8070	3030
5	85	11160	11400	6360
6	3585	5670	14830	9930
7	7000	1165	12000	7670
8	10830	5530	8500	6065
9	6800	11000	4700	7000
10	3460	5630	1570	9170
Equivalent	6500	10100	9500	8000

Crankpin Bearing Load (N)

Equivalent Load = 15200 N

Output Shaft Front Support Loads (N)

Gear Force per Gear Set	- 5000 N
Angle Between Gear Reactions	- 88.68°
Total Output Gear Force	- 7000 N
Maximum Thrust Force	- 2700 N

TABLE 2-4

MOD I LIGHTWEIGHT REDUCED FRICTION DRIVE

Required Bearing Capacities

Position	Equivalent Speed (rpm)	Equivalent Load (N)	Required Life (hrs)	Dynamic Capacity (N)
Crankpin	1429	8690	3500	48100
Main #1	1429	3716	3500	20600
Main #2	1429	5774	3500	32000
Main #3 (Crank 1)	1429	5431	3500	30100
Main #3 (Crank 2)	1429	4574	3500	25300
Output Shaft	1429	4002	3500	22200*
Front Support	1429	1544	3500	8550**

*radial
**axial

TABLE 2-5

MOD I LIGHTWEIGHT REDUCED FRICTION DRIVE

INA Recommended Bearings

Position	INA P/N	Dynamic Capacity (N)	Static Capacity (N)	Weighted L-10 Life (hrs)
Crankpin	F 95915 (K35 x 48 x 20.8)	50000	63000	3984
	K42 x 47 x 27*	33500	75000	1050
Main #1	FC 65798	36000	57000	22610
Main #2	F 57777**	46000	62000	11780
Main #3	F 57777**	46000	62000	14450 (Crank 1) 25610 (Crank 2)
Output Shaft	NKIB 5907	31500	50000	11310***
Front Support		6000	8500	1076****

*Currently Supplied Bearing
**To be used with FC 65978 shell halves
***Radial
****Axial

TABLE 2-6

1983 RESD CRANKTHROW FORCES (lb) ON ROTATING AXES

CRANK	THROW #4		THROW #1		THROW #3		THROW #1		GEAR	
ANGLE	FY	FZ	FY	FZ	FY	FZ	FY	FZ	FY	FZ
0.0	-2806.0	-541.1	-4137.7	1505.9	-3639.6	1324.8	634.9	-117.2	0.0	-415.0
10.0	-1895.8	-34.9	-4096.8	2517.4	-3326.8	2044.4	59.1	-22.3	17.7	100.6
20.0	-863.0	129.5	-3739.3	3498.6	-2765.7	2587.6	-450.1	270.4	163.8	450.1
30.0	147.6	-47.6	-3082.9	4326.4	-2057.0	2886.3	-833.2	741.6	335.0	580.3
40.0	1007.9	-512.3	-2193.6	4885.9	-1310.4	2918.9	-1122.0	1250.0	441.5	526.2
50.0	1624.2	-1172.4	-1180.7	5091.5	-627.1	2704.2	-1012.8	2050.1	378.0	317.3
60.0	1948.4	-1916.3	-183.7	4905.3	1942.3	-1220.1	-739.5	2760.4	-1315.8	-759.8
70.0	1978.1	-2633.5	652.2	4349.5	1326.2	-1171.7	-211.9	3403.0	-1428.2	-520.0
80.0	1749.1	-3230.3	1202.6	3504.7	765.2	-946.8	544.1	3892.1	-1477.2	-260.6
90.0	1325.2	-3639.4	1388.9	2497.4	313.9	-564.3	1471.9	4149.8	-1468.1	-0.2
100.0	783.8	-3825.3	1634.9	1396.6	20.5	-59.8	2483.7	4117.3	-1449.8	255.5
110.0	205.0	-3781.9	654.0	578.1	-78.0	519.4	3467.7	3767.8	-1339.3	487.3
120.0	-337.5	-3528.2	-131.4	-82.7	41.4	1114.7	4301.0	3118.4	-1241.9	716.7
130.0	-782.9	-3102.3	-1031.6	-450.1	384.4	1659.9	4867.8	2233.5	-1118.2	938.0
140.0	-1086.5	-2554.5	-1941.9	-490.8	935.9	2086.1	5081.5	1222.4	-961.2	1145.1
150.0	-1219.9	-1942.5	-2720.3	-261.2	1735.8	2372.7	4903.6	224.1	-757.2	1310.9
160.0	-1171.6	-1326.3	-3288.8	177.2	2489.2	2329.9	4354.6	-616.3	-522.6	1434.8
170.0	-946.7	-765.3	-3598.9	735.9	3347.8	2058.4	3514.5	-1173.8	-262.9	1489.3
180.0	-564.2	-314.0	-3639.9	1324.0	4137.4	1506.9	2508.8	-1368.3	-0.3	1484.3
190.0	-59.8	-20.5	-3434.2	1858.0	4756.4	706.0	1484.5	-1179.6	252.6	1434.3
200.0	519.4	78.0	-3029.0	2273.5	5113.5	-275.2	583.2	-649.0	492.9	1355.4
210.0	1114.7	-41.3	-2486.1	2526.0	5142.9	-1331.1	-83.6	130.6	723.7	1254.2
220.0	1659.9	-384.2	-1873.5	2593.6	4821.4	-2331.7	-451.3	1036.5	945.1	1126.9
230.0	2086.2	-935.7	-1258.8	2474.2	4178.2	-3140.1	-506.9	1937.9	1147.8	963.7
240.0	2327.9	-1657.6	-704.1	2182.9	3294.5	-3638.7	-283.5	2718.3	1314.5	759.5
250.0	2330.2	-2489.0	-263.1	1750.0	2297.0	-3750.4	150.2	3290.2	1427.2	520.0
260.0	2058.7	-3347.6	21.9	1216.9	1332.4	-3457.6	706.4	3604.8	1477.0	260.9
270.0	1507.4	-4137.2	122.0	634.1	542.1	-2805.8	1293.8	3650.6	1469.2	0.5
280.0	706.6	-4756.3	22.7	59.1	35.6	-1895.8	1829.9	3449.4	1419.2	-249.7
290.0	-274.6	-5113.5	-273.9	-447.9	-129.2	-863.0	2248.5	3047.8	1342.3	-488.0
300.0	-1330.6	-5143.1	-748.1	-827.2	47.5	147.7	2505.5	2506.8	1245.0	-718.1
310.0	-2331.1	-4821.7	-1361.2	-1024.7	511.9	1008.1	2578.1	1894.8	1121.9	-940.7
320.0	-3139.9	-4178.3	-2057.8	-996.9	1171.9	1624.6	2463.8	1279.0	962.8	-1146.5
330.0	-3638.3	-3294.9	-2766.1	-718.1	1915.7	1949.1	2177.0	722.0	761.2	-1317.2
340.0	-3788.6	-2191.7	-3404.3	-185.6	2632.8	1979.0	1747.8	277.6	522.6	-1434.0
350.0	-3457.6	-1332.1	-3887.8	574.4	3229.6	1750.2	1217.0	-12.0	262.9	-1487.3

TABLE 2-7

1983 RESD CRANKSHAFT BEARING LOAD (lb)

CRANK ANGLE	MAIN BRG #1		MAIN BRG #2		MAIN BRG #3		FRONT END BRG		FLYWHEEL END BRG		CRANKSHAFT TORQUE(IN-LB)
	FY	FZ	FY	FZ	FY	FZ	FY	FZ	FY	FZ	
0.	-3860.	41.	-6607.	1890.	-384.	136.	747.	-24.	156.	-285.	572.
10.	-3084.	909.	-6191.	3294.	-837.	726.	620.	-228.	235.	-124.	-141.
20.	-2095.	1469.	-5311.	4518.	-1082.	1327.	451.	-376.	341.	-49.	-660.
30.	-1012.	1669.	-4080.	5424.	-1163.	1872.	258.	-453.	428.	-75.	-924.
40.	46.	1511.	-2674.	5882.	-1191.	2259.	62.	-456.	469.	-167.	-947.
50.	940.	1009.	-1170.	5956.	-1001.	2742.	-110.	-379.	386.	-351.	-681.
60.	1383.	609.	1731.	3170.	-632.	811.	-204.	-316.	-696.	-475.	2093.
70.	1826.	-329.	2113.	2760.	-671.	1663.	-302.	-125.	-722.	-493.	2093.
80.	1907.	-1317.	2299.	2243.	-393.	2520.	-332.	91.	-770.	-510.	2066.
90.	1638.	-2229.	2275.	1695.	182.	3274.	-291.	303.	-840.	-517.	2022.
100.	1277.	-2987.	2397.	1151.	916.	3834.	-239.	491.	-938.	-499.	2027.
110.	300.	-3414.	1704.	805.	1938.	4113.	-41.	613.	-1045.	-451.	1963.
120.	-574.	-3559.	1276.	570.	2909.	4101.	131.	676.	-1161.	-354.	1974.
130.	-1433.	-3390.	862.	498.	3792.	3803.	304.	668.	-1259.	-210.	2010.
140.	-2183.	-2931.	515.	587.	4493.	3273.	460.	592.	-1319.	-27.	2059.
150.	-2738.	-2265.	368.	817.	4983.	2611.	578.	465.	-1328.	163.	2085.
160.	-3021.	-1459.	286.	1030.	5114.	1853.	644.	300.	-1262.	363.	2103.
170.	-3033.	-627.	439.	1264.	5014.	1161.	656.	123.	-1146.	526.	2083.
180.	-2771.	142.	751.	1420.	4687.	601.	614.	-46.	-987.	647.	2044.
190.	-2273.	759.	1173.	1443.	4205.	230.	525.	-187.	-798.	722.	2006.
200.	-1594.	1154.	1638.	1306.	3652.	72.	401.	-285.	-593.	755.	1986.
210.	-808.	1278.	2067.	1004.	3106.	116.	254.	-327.	-378.	745.	1994.
220.	-0.	1104.	2390.	565.	2626.	325.	101.	-307.	-164.	691.	2026.
230.	740.	634.	2553.	43.	2251.	649.	-41.	-225.	39.	591.	2064.
240.	1323.	-105.	2529.	-496.	1997.	1040.	-156.	-84.	214.	443.	2091.
250.	1670.	-1053.	2319.	-985.	1870.	1455.	-229.	104.	346.	254.	2092.
260.	1719.	-2124.	1951.	-1369.	1872.	1860.	-249.	322.	423.	36.	2065.
270.	1436.	-3209.	1466.	-1611.	2003.	2219.	-210.	549.	440.	-192.	2023.
280.	826.	-4184.	914.	-1695.	2258.	2494.	-111.	759.	402.	-413.	1984.
290.	-66.	-4925.	337.	-1623.	2614.	2643.	39.	927.	318.	-614.	1967.
300.	-1150.	-5328.	-222.	-1406.	3028.	2627.	227.	1029.	198.	-783.	1979.
310.	-2304.	-5322.	-731.	-1062.	3434.	2429.	431.	1050.	54.	-913.	2016.
320.	-3383.	-4892.	-1160.	-611.	3758.	2057.	626.	983.	-105.	-996.	2062.
330.	-4246.	-4079.	-1484.	-74.	3930.	1547.	789.	833.	-266.	-1027.	2095.
340.	-4817.	-2892.	-1696.	560.	3908.	952.	904.	601.	-416.	-1003.	2102.
350.	-4901.	-1734.	-1727.	1158.	3660.	371.	938.	359.	-537.	-938.	2080.

equivalent loads are ~10% higher for the RESD than for the Mod I; however, the same bearings are used in both engines since the Mod I bearing design is conservative.

Figure 2-42 shows the 3-D beam model used for calculating shaft deflections at the main journals. Table 2-8 summarizes the results of the deflection analysis. No calculable reduction of bearing life is predicted as a result of the deflections determined by the analysis.

2.4 RESD Controls and Auxiliaries

The controls and auxiliaries of any engine system must provide reliable control of engine parameters forsteady-state and transient operation (including start-up and shutdown cycles) while giving desirable engine transient response characteristics. While the P-40, Mod I, and Upgraded Mod I control systems satisfy these requirements, this effort is primarily directed at identifying a system with improved reliability, fewer parts, lower cost, and increased serviceability.

The controls and auxiliaries for a Stirling-engine system can be divided into four functions. The power control is required to regulate engine output across the operating range. The torque output regulation is done in response to a continuously variable input signal (in this case, a vehicle accelerator pedal), and must be capable of rapid transient response. The combustion control system regulates the mixture of air and fuel to ensure proper combustion, maintaining appropriate emissions levels through transient and steady-state operation. The temperature control operates to keep the external heating system operational at the highest possible efficiency. Engine output can be controlled by modulating the heat input to the engine, but this results in poor efficiency, slow transient response (because of the thermal inertia of the heater system), and poor emissions for the systems currently used. The temperature control, therefore, holds a constant heater head temperature, as high as possible to facilitate heat transfer to the working gas without exceeding the temperature capability of the materials. The fourth function is the auxiliaries - those components required to support the operation of the engine systems. This study addressed these four functions, and selected an

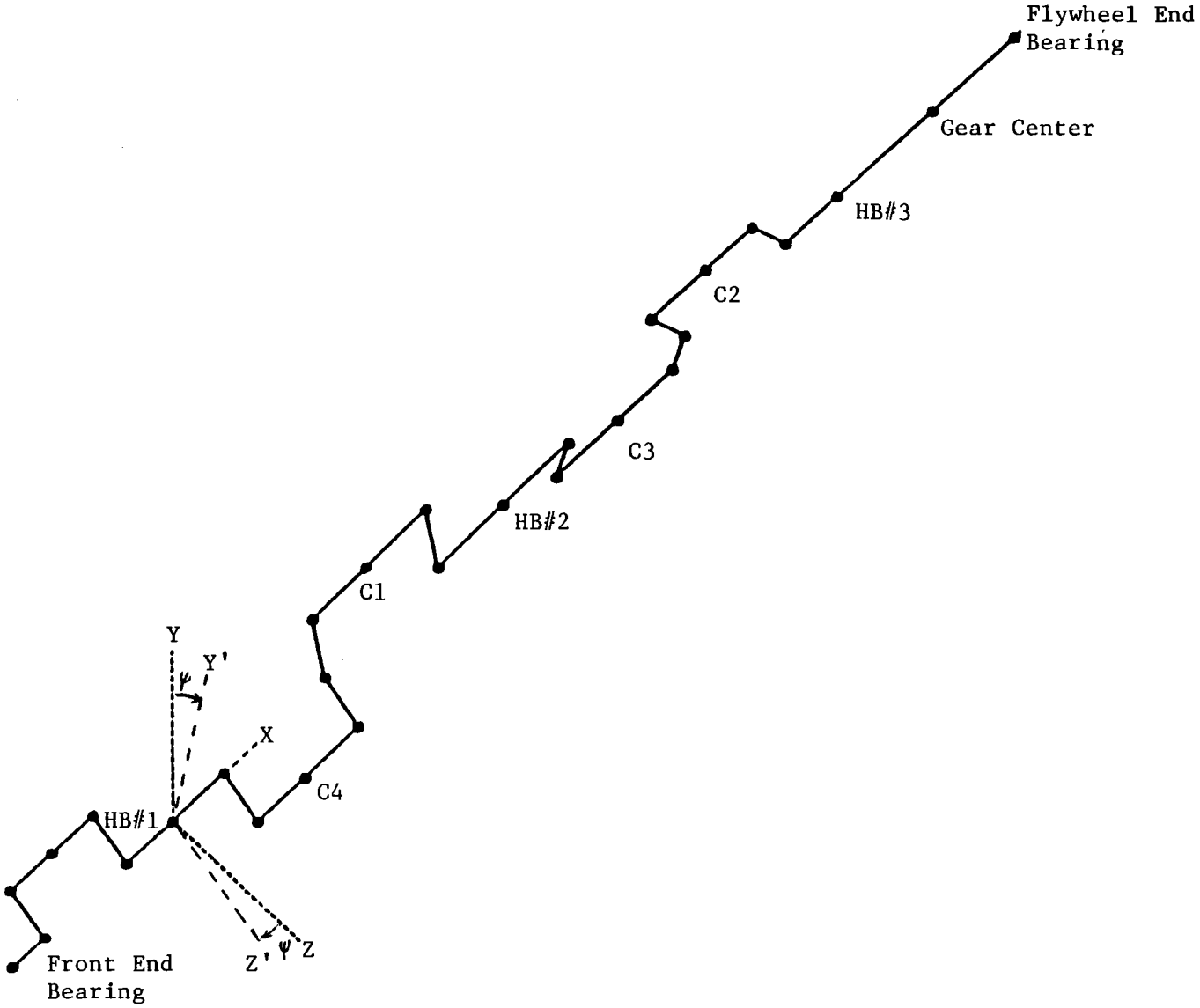

Figure 2-42 1983 RESD 3-D Beam Model

TABLE 2-8

1983 RESD CRANKSHAFT ANGULAR DISPLACEMENT (MINUTES)

CRANK ANGLE	MAIN BRG #1		MAIN BRG #2		MAIN BRG #3		FRONT END BRG		FLYWHEEL END BRG	
	THY	THZ	THY	THZ	THY	THZ	THY	THZ	THY	THZ
0.	-0.03	-3.14	-0.10	1.59	0.44	0.42	0.06	0.63	-0.41	-0.19
10.	-0.68	-2.58	0.24	1.20	0.44	0.65	0.15	0.55	-0.10	-0.26
20.	-1.16	-1.85	0.47	0.74	0.55	0.84	0.22	0.43	0.08	-0.39
30.	-1.40	-1.02	0.55	0.23	0.75	0.95	0.27	0.28	0.11	-0.51
40.	-1.40	-0.18	0.51	-0.28	0.98	0.99	0.28	0.12	0.01	-0.57
50.	-1.14	0.54	0.24	-0.67	1.35	0.81	0.26	-0.03	-0.21	-0.46
60.	-0.93	0.92	1.25	-0.05	0.75	-0.78	0.24	-0.11	-0.62	1.12
70.	-0.31	1.32	0.58	-0.57	1.03	-0.77	0.16	-0.21	-0.55	1.17
80.	0.39	1.41	-0.23	-0.76	1.33	-0.89	0.06	-0.26	-0.47	1.20
90.	1.07	1.22	-1.06	-0.59	1.59	-1.12	-0.04	-0.24	-0.40	1.24
100.	1.67	0.97	-1.83	-0.31	1.76	-1.45	-0.13	-0.22	-0.30	1.30
110.	2.07	0.13	-2.38	0.67	1.82	-1.88	-0.19	-0.05	-0.20	1.35
120.	2.27	-0.60	-2.70	1.58	1.73	-2.32	-0.23	0.10	-0.05	1.41
130.	2.24	-1.32	-2.75	2.52	1.49	-2.73	-0.24	0.25	0.13	1.45
140.	2.00	-1.97	-2.52	3.40	1.12	-3.04	-0.21	0.39	0.34	1.46
150.	1.59	-2.45	-2.09	4.14	0.69	-3.24	-0.17	0.51	0.55	1.42
160.	1.05	-2.70	-1.45	4.56	0.21	-3.23	-0.10	0.57	0.76	1.30
170.	0.48	-2.72	-0.75	4.75	-0.21	-3.10	-0.03	0.60	0.93	1.14
180.	-0.08	-2.52	-0.04	4.67	-0.56	-2.84	0.05	0.57	1.04	0.94
190.	-0.54	-2.13	0.60	4.33	-0.81	-2.49	0.11	0.51	1.11	0.71
200.	-0.86	-1.59	1.11	3.79	-0.94	-2.08	0.16	0.41	1.14	0.47
210.	-1.01	-0.96	1.45	3.10	-0.96	-1.65	0.18	0.29	1.13	0.21
220.	-0.95	-0.32	1.58	2.33	-0.88	-1.22	0.18	0.16	1.08	-0.06
230.	-0.69	0.27	1.47	1.54	-0.69	-0.83	0.15	0.04	0.97	-0.32
240.	-0.23	0.73	1.13	0.83	-0.41	-0.49	0.10	-0.06	0.79	-0.55
250.	0.39	1.01	0.57	0.27	-0.05	-0.24	0.03	-0.13	0.55	-0.74
260.	1.10	1.06	-0.16	-0.07	0.36	-0.10	-0.06	-0.16	0.27	-0.85
270.	1.85	0.86	-0.99	-0.13	0.79	-0.08	-0.15	-0.14	-0.03	-0.90
280.	2.55	0.40	-1.82	0.11	1.20	-0.19	-0.24	-0.07	-0.33	-0.87
290.	3.12	-0.27	-2.57	0.64	1.54	-0.39	-0.31	0.04	-0.62	-0.78
300.	3.47	-1.09	-3.13	1.38	1.80	-0.68	-0.37	0.18	-0.87	-0.65
310.	3.55	-1.96	-3.42	2.26	1.95	-1.01	-0.39	0.34	-1.09	-0.48
320.	3.35	-2.79	-3.41	3.16	1.97	-1.34	-0.37	0.50	-1.26	-0.28
330.	2.87	-3.45	-3.08	3.96	1.87	-1.63	-0.32	0.64	-1.37	-0.06
340.	2.11	-3.90	-2.44	4.57	1.66	-1.85	-0.24	0.74	-1.40	0.17
350.	1.33	-3.99	-1.67	4.85	1.39	-1.96	-0.14	0.79	-1.37	0.38

RESD system that satisfies the system requirements with appropriate size and weight considerations.

2.4.1 Controls

Power-Control System

The Power-Control System must be capable of up-power transients consistent with current IC-engine performance, and down-power transients that control engine speed from full power at full speed to idle load at idle speed. It must also provide smooth idling operation. The most popular power-control schemes in existence today, and the one used on the P-40, Mod I, and Upgraded Mod I, is probably the mean pressure control (MPC). This system modulates the working gas pressure (mass) as a function of engine speed and power demand. Those relations depend on the desired engine "driving characteristic." To properly handle low-power (idle) operation and down-power transients, a short-circuiting capability must be added to working gas mean pressure control. Short-circuiting essentially ports high working gas pressure to low working gas pressure, causing the engine to work against itself. This function is intended to be included when reference is made to MPC in this study. Experience with MPC power control has shown it to provide good engine control, but to require a costly and complex working gas management system to increase or decrease engine pressure.

Description

Control System - An MPC power-control system was selected as the prime concept. The current MPC (Upgraded Mod I) is shown in Figure 2-43. Elements of that system identified as areas for improvement were the:

- Servo Valve - a costly element ($1400) requiring a servo-oil system that is prone to fouling, resulting in loss of control
- Check Valves - have a history of relatively high failure rate, resulting in loss of engine performance; fourteen are currently used in the system.

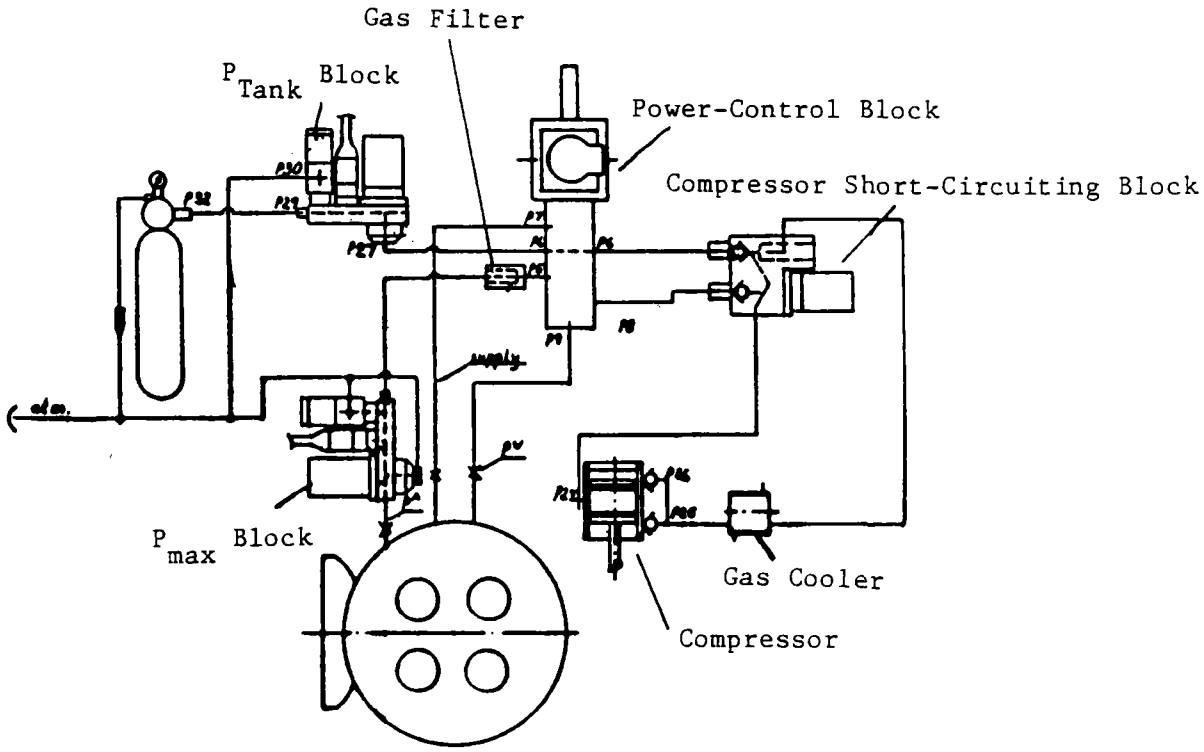

Figure 2-43 Current MPC (Upgraded Mod I)

Power Control Valve - A rotary working gas control valve was selected for the control system (see Figure 2-44). Since the valve does not time the injection, timed injection slots are required. Experience with the timed injection slots on the Mod I and Upgraded Mod I has shown them to be reliable. Locating the rotary valve close to the cycles, as with the distributor valve, will allow running without check valves if the dead volume between the valve and injection slots is kept acceptably small. The rotary valve is integrated into the engine block, reducing dead volume to a minimum, and keeping weight down by using the block as the valve's outer housing. The rotary valve will perform functionally the same as the linear hydrogen control valve found on the Upgraded Mod I, but it will be positioned via an electric motor drive instead of requiring a servo valve and servo-oil supply. Inside, the valve porting will be to the individual cycles.

The rotary working gas control valve was selected as the prime system because it eliminates the need for the servo valve and check valves - two components that have displayed reliability problems.

Combustion Control - The system selected, uses a positive-displacement combustion air blower (described in Section 2.4.2) with speed and eccentricity feedback, as well as ambient temperature and pressure compensation, to determine combustion airflow. Fuel flow is metered by a valve system. The valve would be operated by a stepper motor, and pressure differential across the valve would be held constant. The system must be capable of a flow resolution of 5% of minimum flow to hold an air/fuel ratio (λ) value within 5% at low flows, i.e., for a 20:1 turndown, a flow resolution of one quarter of 1% of the maximum flow must be achieved. To do this, the valve must have a nonlinear characteristic so that a stepper motor resolution of 1% (motor rotation divided into 100 steps) gives the desired low flow resolution. Fuel flow is, therefore, open loop, eliminating the costly fuel flow sensor.

To complete the prime system, an oxygen sensor located upstream of the preheater is added. (Current automotive oxygen sensor designs operate from 350 to 800°C to keep response time on the order of milliseconds.) This closes the combustion control loop, and fine tunes the fuel flow. To enhance transient response of the combustion control, the current scheme of waiting for a sensed airflow change before initiating a fuel flow change would be modified.

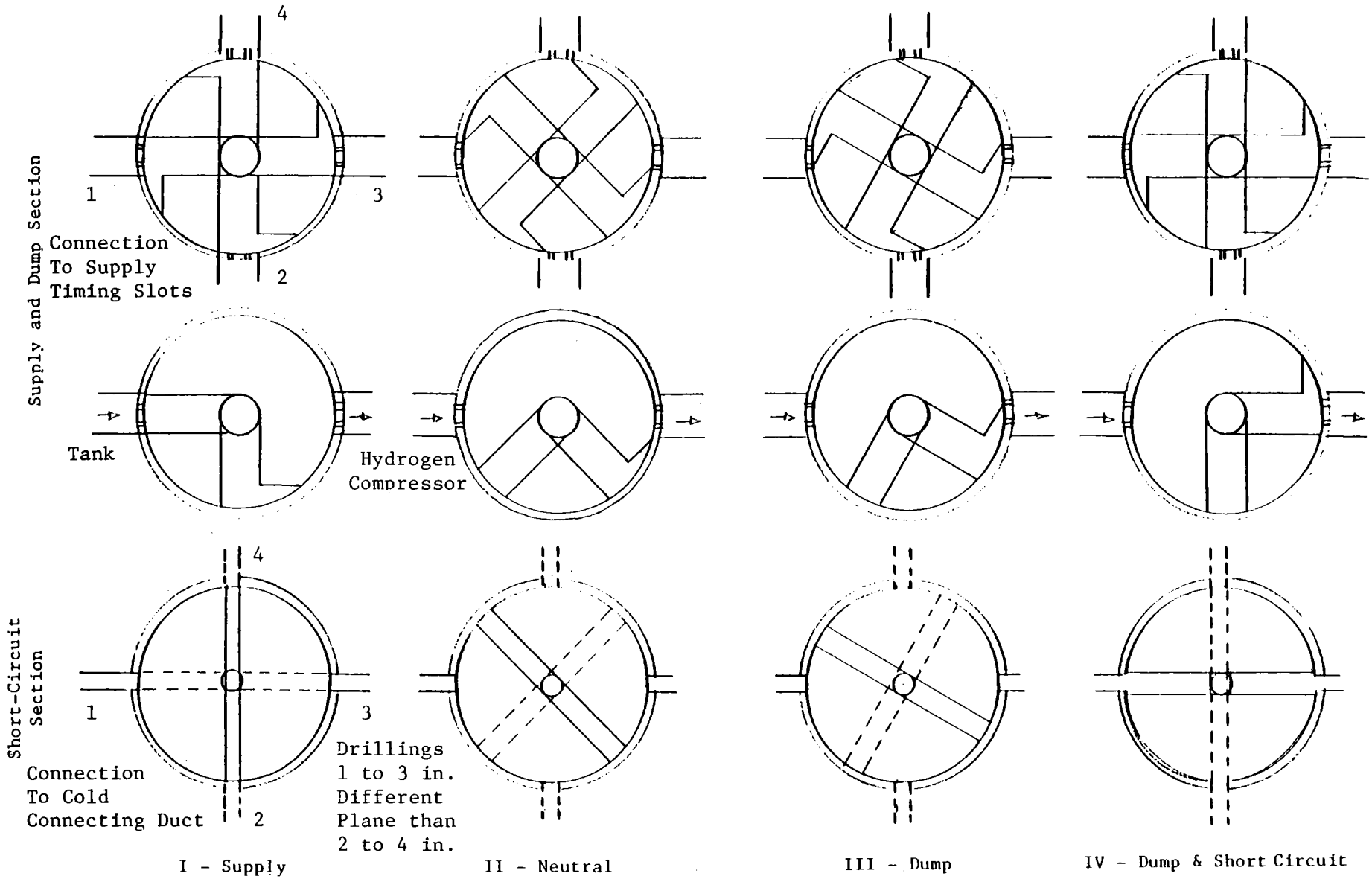

Figure 2-44 Rotary Hydrogen Control Valve Concept

Since desired airflow and fuel flow signals originate from the same microprocessor, the command to change those flows would be sent at the same time, eliminating transport lag and sensor lag times.

The combustion control system selected eliminates several costly components, and increases transient response/steady-state performance over the present combustion controls. The airflow pressure drop introduced by the K-Jetronic does not exist. Airflow and fuel flow sensors are eliminated, and performance is increased by enhanced transient response, closed-loop combustion control, and low flow resolution.

Temperature Control - The system retains tube temperature measurement with temperature controls (T/Cs). New designs for fixing the T/Cs to the tubes are required. A wedge-shaped cap design would improve the contact of the T/C tip to the tube surface.

2.4.2 Auxiliaries

The auxiliaries mentioned here are those that differ from the ones used on the current Upgraded Mod I design, i.e., the fuel pump, batteries, and after-cooling pump will remain the same and, as such, will not be described.

Combustion Air Blower

A major departure from the Upgraded Mod I system is the variable, positive-displacement combustion air blower. One of the objectives of this design change was to eliminate the need to vary blower speed relative to engine speed. This is done on the Upgraded Mod I via a hydraulically actuated variator. A second component that could be deleted through use of the variable, positive-displacement blower is the Upgraded Mod I's air throttle valve, if the blower design provided predictable, repeatable airflows for a given operating point, independent of changes in combustor or system pressure drops. Blower speed and displacement would then indicate combustion airflow.

A blower design concept is currently being developed to meet the above three objectives. The blower is driven directly by the engine, and airflow is changed by increasing or decreasing the eccentricity of the "piston" assembly

to change the blower displacement. This design can therefore change airflow independent of engine speed. The positive-displacement-type blower will deliver repeatable flows for the same displacement and rotating speed, therefore eliminating the need for both the air throttle and airflow sensor.

Upstart Motor and Starter Motor

Data taken on the Motoring Rig of the Upgraded Mod I design showed that the torque required to rotate an engine bottom end at low working gas pressures was very small (see Figure 2-45). If it were small enough to permit a single motor to run the auxiliaries required for start-up (combustion and atomizing air blowers - the servo-oil system is not required) and crank the engine, then three benefits would be realized: 1) one motor would be eliminated; 2) working gas would be circulating during combustor warm-up, thus reducing the thermal shock to the heater tubes and housing, and reducing low-cycle fatigue of those parts; and, 3) there would be a reduction in the start-up energy required, because as soon as the engine was able to put out some power, it would reduce the starter load, and as soon as the engine was able to maintain engine speed, the starter would disengage independent of tube temperature. The Upgraded Mod I design does not engage the starter until the rear-row tube temperature has reached 475°C, at which point the engine is capable of producing sufficient torque to maintain idle speed. A summary of the estimated combined starting motor loads is shown in Table 2-9.

To reduce the engine working gas pressure to approximately 1.0 MPa on shutdown, it will be necessary to increase the pumping capability of the current hydrogen compressor. The Mod I and Upgraded Mod I use a single-stage, double-acting compressor design. With proper valving, either external or internal to the compressor, it could be made to operate as a two-stage compressor when the pressure ratio across it exceeds its capability as a single-stage compressor.

Cooling Fan

Since the engine will be mounted transversely, an electric-motor-driven cooling fan that replaces the clutch coupling of the fan to the engine is required; cooling fan logic and control will remain the same. The relay

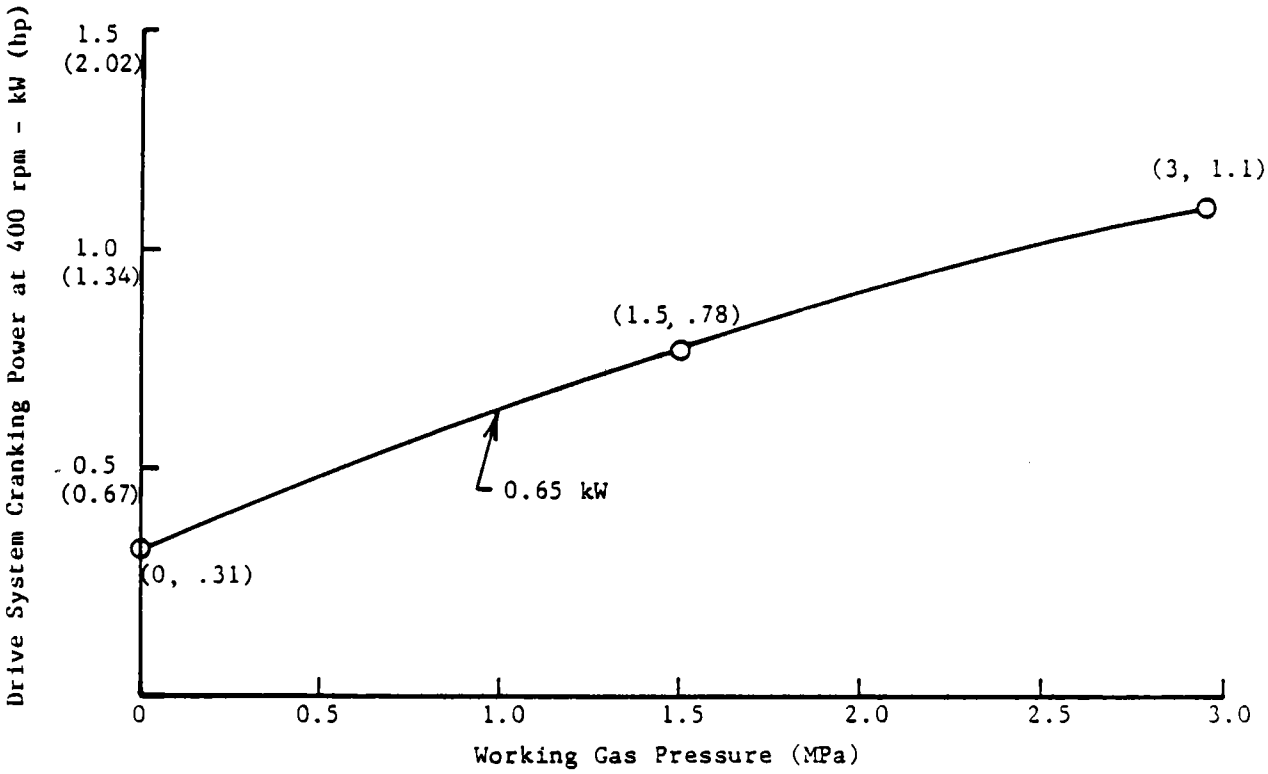

Engine Oil Temperature = 19°C

Figure 2-45 Testing with Split/Solid Rings - Upgraded Mod I Reduced Friction Drive

TABLE 2-9

ESTIMATED STARTING MOTOR LOADS

System	Load	Comment
Engine Cranking	650 Watts	Based on data taken on Updated Mod I Reduced Friction Drive.
Combustion Blower	250 Watts	No ΔP load introduced by the K-Jetronic or air throttle valve.
Atomizing Air Compressor	100 Watts	Estimated on one half Updated Mod I size.
Servo-Oil System	0	Not required.
Total Cold Engine Cranking and Auxiliary Load	1000 Watts	Current upstart motor is rated 1000 Watts; as heater temperature increases, the engine will reduce the starting motor load.

function that energizes the fan clutch on the Upgraded Mod I will be used to operate the fan motor.

Controls and Auxiliaries Summary

The system designs selected for the RESD result in a significant savings in hardware complexity and weight over the Upgraded Mod I designs. Table 2-10 lists the components and systems that are altered or eliminated. Elimination of the servo-oil system reduces component weight (by about 20 pounds), power consumption, and hardware. Eliminating the air throttle valve reduces the power consumption represented by the pressure drop it introduces to the airflow. The need for airflow and fuel flow sensing represents costs that are not part of the RESD system. (Table 2-10 is a summary of the primary designs selected.) The objectives of achieving improved reliability, fewer parts, lower cost, and reduced complexity have been addressed with system designs that are within the scope of near-term technology development. The objective of serviceability must be addressed during the detailed design phase. With the systems identified, complex alignment and adjustments should not be required.

Electronic Controls

The electronic controls portion of the engine control will continue to be a microprocessor-based control. The functions will be changed from the Upgraded Mod I system as required by the RESD.

TABLE 2-10

SUMMARY TABLE OF PRIMARY SYSTEM DESIGNS SELECTED FOR THE RESD

System	Comparison With Updated Mod I	Comments
Working Gas Control	Rotary valve with porting to each cycle located on the engine block instead of linear valve. Motor drive instead of servo valve found on Updated Mod I.	No supply and dump check valves required. No servo-oil supply required. Simplified hydrogen plumbing. Reduction in system cost.
Combustion Control	Variable, positive-displacement blower instead of Updated Mod I centrifugal blower. Fuel flow control valve instead of Updated Mod I metering pump.	No servo-oil system required. No variator required. No airflow or fuel flow sensor required. No air throttle valve required.
Temperature Control	Heater tube T/Cs for both Updated Mod I and RESD.	
Starter/Upstart Motor	Combined functions into one motor approximately the same as Updated Mod I upstart motor.	Elimination of one motor. Requires hydrogen compressor capable of lowering engine pressure to 1 MPa on shutdown. Reduces thermal stresses.
Cooling Fan Drive	Electric motor drive instead of Updated Mod I system where it is driven by engine through a clutch.	Change is required because of engine mounting in vehicle.
Electronic Controls	Electronic controls will remain a microprocessor-based system.	Modifications will be made to accommodate engine system functional requirements.
Atomizing Air Pressure Regulator	Atomizing air pressure (flow will be regulated in proportion to combustor air inlet pressure (flow)), minimizing atomizing airflow at the low fuel flows instead of regulating atomizing air pressure to a fixed value.	This will minimize the performance losses associated with an air-atomized fuel system.

3.0 MATERIALS' SELECTION SUMMARY
1983 RESD

3.1 Part Materials

This subsection describes the material selected for each main engine part. Any treatments applied to the materials are also specifically identified. Rationale for the selections is largely based on material effectiveness and cost. In addition, special attention was given to minimizing the use of strategic materials, (see subsection 3.2 for more detail).

Outer Shroud

Material: Deep-Drawn Quality Steel (0.5-mm KK)
Treatments: Paint

The outer shroud will encapsulate the shroud insulation on the top of the engine. A high-temperature paint will finish the part.

Inner Shroud

Material: 18-SR
Treatments: None

The inner shroud will encapsulate the shroud insulation; 18-SR is a cost-effective, oxidation resistant material, that is readily weldable.

Flame Shield

Material: 310 Stainless Steel
Treatments: Thermal Barrier Coatings

A thermal-barrier coating applied to 310 stainless steel will reduce the oxidation/corrosion effects, as well as the temperature, of the air-cooled flame shield. 310 stainless steel will have sufficient strength at operating

temperatures (estimated at 800-850°C) to resist bulging from the internal pressure.

Preheater (1 of 2) (Primary Option)

Material: Coors Ceramic (Proprietary)
Treatments: None Identified

The ceramic material will have a very low coefficient of thermal expansion, which will allow a high level of thermal shock resistance when compared to other ceramics. The lighter weight and lower material cost of ceramic are definite advantages over the traditional 310 stainless steel. In addition, the Coors ceramic may be more corrosion/oxidation resistant than 310 stainless steel.

Preheater (2 of 2) (Secondary Option)

Material: 310 Stainless Steel or 18-SR
Treatments: Welded Assembly

As a backup to the Coors ceramic material, 310 stainless steel or, if a stamping process can be worked out on time, 18-SR or 12-SR may be used. 12-SR would be preferred because of its lower chromium content.

Support for Ceramic Preheater

Material: 18-SR
Treatments: None

18-SR will have sufficient elevated temperature strength (800°C) to provide hold-down support for the air preheater ceramic blocks.

Retainer for Ceramic Preheater

Material: 18-SR
Treatments: None

A low-strength, oxidation-resistant material is required to hold the ceramic block in place. 12-SR has no strength at elevated temperatures; however, 18-SR has some elevated temperature stength, and good oxidation-resistance.

Combustor Liner

Material: 18-SR (0.5-0.7-mm KK)
Treatments: Thermal Barrier Coating

All combustor sheet-metal parts, including the swirler, will be fabricated from 18-SR. The flame tube will be coated with a thermal-barrier coating to reduce temperature gradients around the circumference of the combustor, thereby reducing warpage. The back side of the flame tube will be "cooled" by the recirculated exhaust gas. The coating will also reduce oxidation and corrosion.

CGR Nozzle Assembly

Material: 304 Stainless Steel
Treatments: None

The CGR nozzle assembly will be made from 304 stainless steel, which is required to prevent oxidation.

Insulation - Shroud

Material: Molded Ceramic Wool
Treatments: Canned, Between Inner and Outer Shroud
Al_2O_3, 51%, SIO_2, 49%

This material, the same as that used in the Mod I engine, can be molded to shape. The insulation is "canned" to prevent mechanical damage and erosion.

Intake Manifold

Material: Steel (45 x F)
Treatments: Corrosion/Rust-Resistant Coating
Galvanize/Aluminize

The intake manifold will experience temperatures up to 200°C. It also shares a common wall with the exhaust manifold. The parts that do not come in contact with corrosive exhaust gases can be made from a deep-drawn quality, low-alloy steel with a corrosion/rust-resistant coating on the air side.

Exhaust Manifold

Material: 12-SR
Treatments: None

Alloy 12-SR is a 12% chromium ferritic stainless steel which has adequate corrosion resistance to the cooled gasoline exhaust. Its current use on catalytic converter cases demonstrates this potential.

Transition Flange

Material: Aluminized Steel
Treatments: None

To withstand the higher combustion-gas temperatures, the transition flange must be of 310 stainless steel to provide the corrosion/oxidation resistance needed.

Loose Insulation

Material: Al_2O_3, 51%; SiO_2, 49%
Treatments: None

Any loose-bulk insulation containing aluminum and silica fibers is adequate.

Heater Tubes

Material: CG-27
Treatments: Nickel Plating; Heat Treatment After Braze

A comprehensive alloy selection criteria was established and used for alternative low-cost heater tube material. Alloy CG-27 is the preferred heater tube material because of its lower strategic-material content and exceptionally high creep strength. The design stress is based on a creep rupture life of 3500 hours at 850°C at a minimum stress of 28.125 N/mm^2. Based on the latest data, CG-27 far exceeds this criteria with an estimated stress for rupture at 3500 hours at 850°C at a stress of 51 N/mm^2. This, together with exceptional oxidation resistance and low H_2 permeability, make CG-27 an excellent selection.

Fins

Material: 310 Stainless Steel
Treatments: None - Diffusion-Bonded During Braze Cycle

Current fin material (must be corrosion/oxidation resistant at high temperatures) is 310 Stainless Steel. The Mod I engine's 310 SS fins are plated with electroless nickel (Ni-P), which is used as a brazing alloy to join the fin to the tube. It is believed that Ni-P plating causes accelerated oxidation of the fins; this would be eliminated with diffusion bonding.

Manifolds

Material: XF-818 - Investment-Cast
Treatments: To be Welded to Housings

A comprehensive alloy selection was performed for the heater head castings. Alternative materials included XF-818, CRM-6D and SAF-11. Alloy XF-818 was selected over CRM-6D mainly because of its inherent weldability and slightly lower strategic-element content. SAF-11 experienced some problems during casting, and was removed from consideration. The fatigue stength of XF-818

and CRM-6D are basically the same, and both alloys meet the current Upgraded Mod I requirements. The manifolds will be investment-cast and then welded to the housings, which will be cast by a less expensive method.

Housings

Material: XF-818 - Shell-Cast
Treatments: To be Welded to Manifolds

The same selection criteria used for the manifolds applies to the housings, which will be cast by the shell-casting method, and then welded to the manifolds (cost effective when compared to casting a monolith investment-casting).

Partition Wall Assembly

Material: Partially Stabilized Zirconia (PSZ)/CG-27
Treatments: Interference Fit

A material with low thermal conductivity and a thermal expansion that is close to the mating metal is needed. PSZ is the ceramic that comes closest to these requirements. The thermal conductivity of PSZ is 1 to 2 Btu/hr-ft-°F from room temperature to 2000°F (cast iron is 80 Btu/hr-ft-°F at room temperature). The thermal expansion of PSZ is between 4 to 8.5 x 10^{-6} from room temperature to 2400°F; the thermal expansion of CG-27 is 9.5 from room temperature to 1500°F. SiC and Si_3N_4 have lower thermal expansions and higher thermal conductivities - both undesirable. PSZ has been effective in the adiabatic diesel-engine program in a similar application.

Regenerator

Material: 304 SS Screen
Treatments: Sintered

The current material of choice is 304 stainless-steel screen, pressed and sintered. This material provides the best engine efficiency of any other

material tried, and it has adequate corrosion-resistance when the environment is free from chlorine-containing substances.

Manifold Flow Guides

Material: 18-SR
Treatments: None

18-SR, which withstands high temperature, and offers good oxidation-resistance, will be used for the flow guides between the inner and outer manifolds.

Block

Material: Cast Ductile Iron
Treatments: Heat-Treat

The material choice here is between ductile iron and aluminum. There is a large potential for having interconnected porosity (microshrinkage) in cast aluminum, especially with hydrogen. This, combined with the high pressure, rules out as-cast aluminum. Cast ductile iron can perform in this environment.

Crankshaft

Material: Ductile Cast Iron
Treatments: Heat-Treat, BHN 187-269, Harden Journals

The crankshaft shall be cast from ductile iron, which is a standard, inexpensive, reliable material for this application, and is currently used in most automotive applications.

Connecting Rod

Material: Pearlitic Malleable Cast Iron
Treatments: Heat-Treat, BHN 241-269

A standard, low-cost material in common use by today's automotive manufacturers is pearlitic, malleable cast iron; no other alternatives are known.

Crosshead

Material: Steel
Treatments: High Compressive Modulus to Reduce Cyclic Load in Piston Rod

The higher compressive modulus of steel is required to withstand the joint stress and cyclic loading imposed on the crosshead.

Seal Housing Assembly

Material: 4140
Treatments: Heat-Treat

Low-alloy steel 4140 is a preferred material for this assembly because of its low cost, higher strength, and good machinability.

Oil Pump/Filter Assembly

Material: Cast Aluminum (Steel, Medium Carbon, Harden Surfaces)
Treatments: None

Cast aluminum will provide a lightweight, low-cost oil pump housing/filter assembly. Pump parts will be made from surface-hardened, medium-carbon steel. Powder metallurgy may play a cost-competitive role in making these parts.

Oil Pan

Material: Fiber-Reinforced Nylon (Allied STX)
Treatments: None

On a cost basis, nylon is about equal to steel; however, there is a weight advantage with nylon, so it is the preferred material.

Cylinder Liner/Cooler

Material: Low-Carbon Steel
Treatments: Surface Treatment, Chromium Diffusion

The cooler will be made from low-carbon steel. The surface will be treated with a chromium diffusion process to prevent rusting. This will result in a 50% reduction in chromium content and a cost savings.

Piston Dome

Material: CG-27
Treatments: Heat-Treat; Dome Welding

Piston dome material will be CG-27, which has a cost/strategic-material advantage over Inconel 718, but has equivalent high-temperature strength. The dome will be made in two pieces - a formed top and cylindrical section - that will be welded together.

Internal Piston Heat Shield Assembly

Material: 316 SS
Treatments: None

Internal heat shields will be made of 316 stainless steel, and will be stamped. Top and bottom shields will be identical, and act as an alignment tool during EB-welding.

Piston Rod/Base

Material: 4063/4140 Steel
Treatments: Pre/Post-Heat During Welding

The piston base, a 4140 alloy steel, will be EB-welded to the cylindrical dome part. The piston rod, will be a low-alloy steel such as 4063, which has no chrome, is hardenable to Rc50 for the wear surface, and is low in cost.

Water Pump

Material: Fiber-Reinforced Plastic (Dupont)
Treatments: None

Current technology in fiber-reinforced, molded plastics allows water pumps to be made from this material, resulting in a high cost savings with reduced machining, and a substantial weight savings.

3.2 Strategic Materials Accounting

Careful attention has been given in selecting the least possible amount of strategic materials for use in the V-4 RESD. With the current configuration and materials selection, the following amounts of strategic elements are present in the 1983 RESD:

Element	Weight (kg)	Percentage of Total Engine Weight (%)
Cobalt	0.0	0
Chromium	6.047	7.0
Columbium	0.108	0.1
Tantalum	0.0	0

4.0 QUALITY ASSURANCE

Quality-assurance aspects of the 1983 RESD design have been addressed by utilizing the experience obtained during Mod I engine system testing. In the ASE Program, the quality-assurance program includes a quality assurance reporting system to document individual part failures and discrepancies. The information gathered via these quality assurance reports (QARs) over a two-year test period is the basis for identifying improvements desired in the design from a quality-assurance standpoint.

Mod I QAR Experience

A summary of problems documented via the QAR system is presented in Figure 4-1. The problems are defined as items which: 1) cause an engine to stop running; 2) prevent an engine from being started; and 3) cause degradation in engine performance. It is considered that problems which fall into these categories must be minimized to provide acceptable engine performance and mean time between failure (MTBF) data. A summary of the major problems which have occurred in the Mod I is presented in Table 4-1.

1983 RESD Design Changes

Design changes in the 1983 RESD strongly reflect the Mod I experience. These changes are summarized by the major engine systems described below:

- External Heat System - The combustor design has been changed to minimize buckling due to thermal transients. Also, the RESD CGR ejector design will minimize variations in ejector performance that create temperature nonuniformities. The nozzle design also reduces nozzle plugging problems with the incorporation of water cooling and change to the externally atomized fuel nozzle. The RESD flame shield will be ceramic or metal with a ceramic thermal-barrier coating to improve durability. The Upgraded Mod I engine has incorporated a separate fuel nozzle igniter, rather than the integrated Mod I unit. This system has provided both improved durability and engine starting. This concept

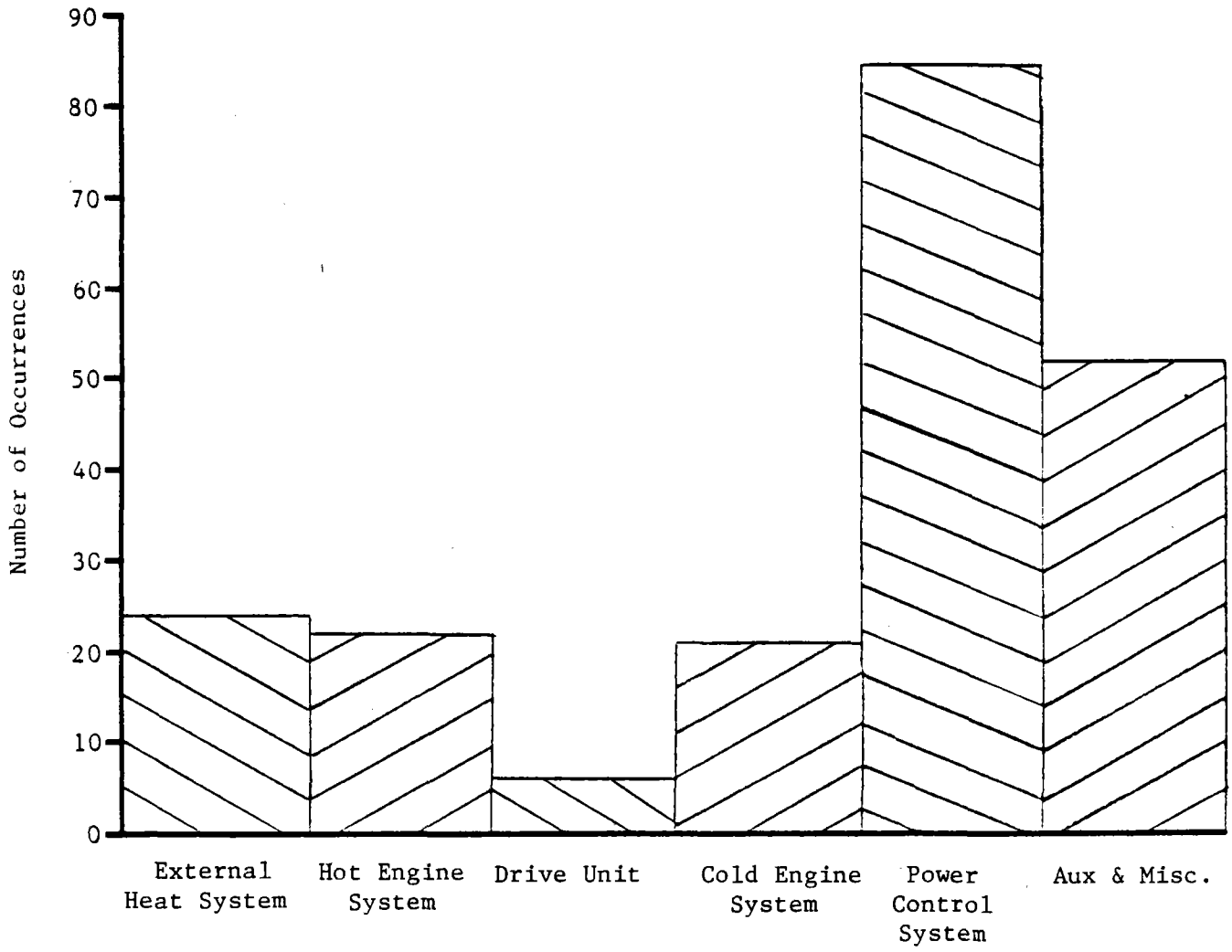

Figure 4-1 Mod I QAR History: Failures/Discrepancies of Major Systems Through April 27, 1983

TABLE 4-1

MAJOR PROBLEMS IDENTIFIED FOR INDIVIDUAL UNITS OR ASSEMBLIES

- Moog Valve
- Heater Head
- Check Valves
- Combustion Air Blower
- Fuel Nozzle
- Igniter
- Preheater
- Atomizing Air Compressor/Servo-Oil Pumps
- Combustor
- Flame Shield

has been retained for the RESD. The metallic preheater of current Stirling engines has been replaced with a ceramic preheater composed of ten separate units. In the event of plugging, only the affected section needs to be removed for cleaning.

- Hot Engine System - The heater head design for the RESD is completely new, an annular rather than canister design. Materials for the housing and tubes will be XF-818 and CG-27, respectively, which are the materials selected for the Upgraded Mod I. The confidence level of the design will be elevated relative to the Mod I and Upgraded Mod I designs with the incorporation of more extensive stress analysis.

- Controls - Most of the control system problems have been with the check valves, servo-oil pump, and Moog valve. In the RESD, the servo-oil system is eliminated by removing the requirement for the hydraulically-driven variator, and by replacing the hydraulically-actuated Moog valve with an electrically-operated rotary valve. The RESD control system also revises the entire working-gas plumbing scheme to eliminate 12 of the 14 check valves in the current ASE system.

- Auxiliaries - The combustion air blower with its flat-belt, high-speed drive will be replaced on the RESD with a variable-displacement blower.

5.0 STRESS ANALYSIS

The most critical component in the Stirling engine, in terms of stress, is the heater head. Prolonged operation at elevated temperature and pressure is required. Cyclical operation between 3 MPa and 15 MPa engine charge pressure imposes an additional stress criteria on this component. The third most important facet of engine operation is in the thermal transients encountered during an engine start. The design criteria to insure that adequate strength is acquired in the design is well established and has been presented previously (Automotive Stirling Engine Mod I Design Review Report, Volume 1 DOE/NASA/0032-16). The stress analysis that has been performed for the RESD heater head is presented in subsections 5.1 and 5.2. A more detailed analysis will be required as refinements are made during the final design process. Experimental verification of temperature gradients during starting transients is required to guide the design. These can be obtained on existing engines and compared to similar calculated gradients for these existing engines.

An additional component that has been analyzed is the piston rod/crosshead attachment. The design selected for the RESD is a considerable departure from the Mod I design. Preliminary stress analysis performed for this component is also included in this section.

5.1 Stress Analysis of Components

This subsection presents stress analyses performed on several major components in the RESD. Different design alternatives have been studied with respect to strength requirements.

5.1.1 Heater Tubes

The most probable failure mode of the heater tubes is creep rupture due to a combination of high temperature and high internal pressure. Consequently, the wall thickness of the tubes has to be selected based on a creep rupture analysis.

Loadings

The pressure loading is based on a combined driving cycle (55% metro/45% highway). The mean pressure variation was taken from driving simulations corresponding to 1981 RESD installed in X-car which is an approximation of the pressure loading in the 1983 RESD installed in the X-car. The creep rupture analysis was therefore based on the following mean pressure levels.

Mean Pressure (MPa)	Time Period (hours)
2	177.3
3	1077.8
4	341.9
5	569.7
6	496.5
7	305.9
8	186.4
9	140.7
10	95.6
11	43.8
12	27.3
13	20.2
14	9.7
15	7.0
	3500 TOTAL HOURS

Another load requirement is 100 hours at maximal power. Consequently, the heater tubes have to be designed to meet the worst of the above mentioned load requirements. With a set temperature of 820°C, it is assumed that the maximal heater tube temperature is 870°C. The creep rupture analysis is based on this temperature.

Material Data

The heater tube material selected is CG-27. Based on presently known data, the creep rupture curve for CG-27 can be approximated by the following relationship between the creep rupture stress (σ_{CR}) and the time to creep rupture (t_{CR}).

$$\sigma_{CR} = 710\ (t_{CR})^{-0.35} \text{ at } T = 870°C$$

The stress σ_{CR} is expressed in MPa and the time t_{CR} in hours. The stress refers to "the mean diameter formula"

$$\sigma = \frac{p(D-h)}{2h}$$

where

p = internal pressure

D = outer diameter of the tube

h = wall thickness

Creep Rupture Analysis

The creep rupture analysis was based on the linear damage rule, which for the mean pressure variation corresponding to the combined metro/highway driving cycle resulted in the following equivalent pressure:

$$p_{eq} = 6.1 \text{ MPa} \simeq 0.41 \times p_{max}$$

The creep rupture curve gives,

$$t = 3500 \text{ h} \rightarrow \sigma_{CR} = 40.8 \text{ MPa}$$

$$\sigma_{CR}/1.5 = 27 \text{ MPa}$$

Allowable stress,

$$h_{min} = \frac{D}{1 + \frac{2\sigma}{peq}}$$

$$\left.\begin{array}{l} D = 4.5 \text{ mm} \\ \sigma = 27 \text{ MPa} \\ Peq = 6.1 \text{ MPa} \end{array}\right\} \rightarrow \quad h_{min} = 0.46 \text{ mm}$$

For the second criteria

$t = 100$ h the creep rupture curve gives,
$\sigma_{CR} = 142$ MPa and the allowable stress,
$\sigma = 94$ MPa

Thus,

$$\left.\begin{array}{l} D = 4.5 \text{ mm} \\ \sigma = 94 \text{ MPa} \\ p = 15 \text{ MPa} \end{array}\right\} \rightarrow \quad h_{min} = 0.33 \text{ mm}$$

The analysis above shows that from the creep rupture point of view, it seems possible to decrease the wall thickness of 0.75 mm to 0.50 mm and still contain the safety factor 1.5 on the creep rupture stress.

Comments

To decrease the wall thickness of the heater tubes from 0.75 mm to 0.50 mm is connected with a certain risk due to the following uncertainties:

- The creep rupture curve is based on a small number of data points, because the material testing is not completed yet.
- The way in which the brazing cycle will affect the creep rupture properties of CG-27 is still unknown because it has not been tested.
- Material properties such as yield strength, ultimate tensile strength, or fatigue limit are not known for a 870°C design temperature.

- The creep rupture curve is based on testing in air. However, in the actual application, the tubes will be exposed to hydrogen at high pressure on the inside and combustion gases on the outside, which probably will heighten corrosion or oxidation.

Some of the questions indicated above will be addressed through HT-P40 testing, which, to date, is incomplete. In addition, the thinner walls of the heater tubes will impose a higher sensitivity to tolerances, porosity, ovality and so on, and probably will increase the need for good quality assurance.

Result

The data points from the creep rupture testing of CG-27 indicate the possibility of decreasing the wall thickness of the heater tubes from 0.75 mm to 0.50 mm. However, because of uncertainties concerning the material properties, a reduction of the wall thickness may weaken it. Consequently, the present design retains the original dimensions of the heater tubes.

5.1.2 Flange Arrangements of the Heater Housings

During the design process of the RESD, different types of flange arrangements have been studied. Thus, stress analyses have been done on both loose flanges and integral flanges with different dimensions. The result of the stress analysis for each step in the design process is given in the following discussion.

Loose Flange Arrangements

In the case of loose flanges, the heater housings are completely axisymmetric in the cold end. Also the contact forces between the housing and the loose flange are axisymmetric. These factors make the stress analysis a straight forward procedure which, in turn, decreases the uncertainties of the result.

The stress analysis was based on the finite element method and the housings were modelled with axisymmetric elements, which were isoparametric with 8 nodes and a quadratic displacement function. The geometry, loading

conditions, and boundary conditions for typical models with different cold end geometry are shown in Figure 5-1.

Integral Flanges

A flange that is integrated with the heater housing, displays a geometry not completely axisymmetric; neither is the load that is transferred to the cylinder block axisymmetric. The preloaded bolts create a contact pressure between the flange and the cylinder block. However, during operation some relative motion occurs between the contact surfaces, resulting in nonlinear behavior. These facts indicate that an adequate stress analysis should be based on a nonlinear 3-dimensional structural analysis. Such an analysis would be expensive and time consuming and could not be justified in this study. Therefore, the compromise in this case, was to use an axisymmetric model and run it with different types of boundary conditions to get an estimation of an upper and a lower limit of the stresses. Thus, the same type of finite element analysis, as in the case of loose flanges, was done. The geometry, the loading conditions, and the boundary conditions for typical models with different cold end geometry are shown in Figures 5-2 through 5-5.

Loadings

As indicated in the figures, the models were loaded with an internal pressure (p) of 20 MPa combined with an axial temperature gradient (T) between 750°C and 70°C. Basically, three different load cases were run, temperature load only (T), pressure load only (p), and the combination (p + T).

Stresses

The stresses in the fillet radius between the flange and the cylindrical housing for the models are shown in Table 5-1. The stress components σ_1, σ_2, and σ_3 refer to principal stresses and σ_1 is the component in the hoop direction. The stress component σ_{eq} is the equivalent stress according to von Mises yield criterion.

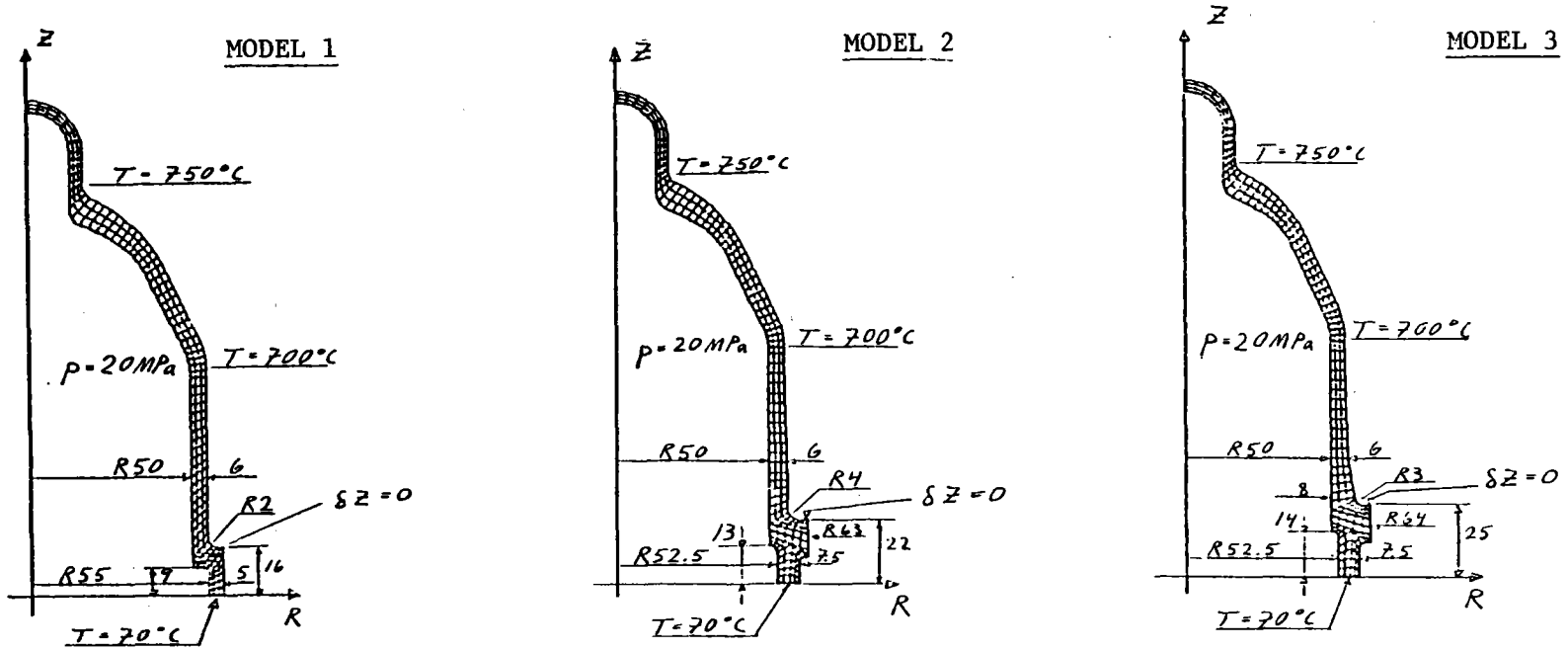

Figure 5-1 Models 1, 2, and 3 - Geometry, Loading Conditions and Boundary Conditions (Loose Flanges)

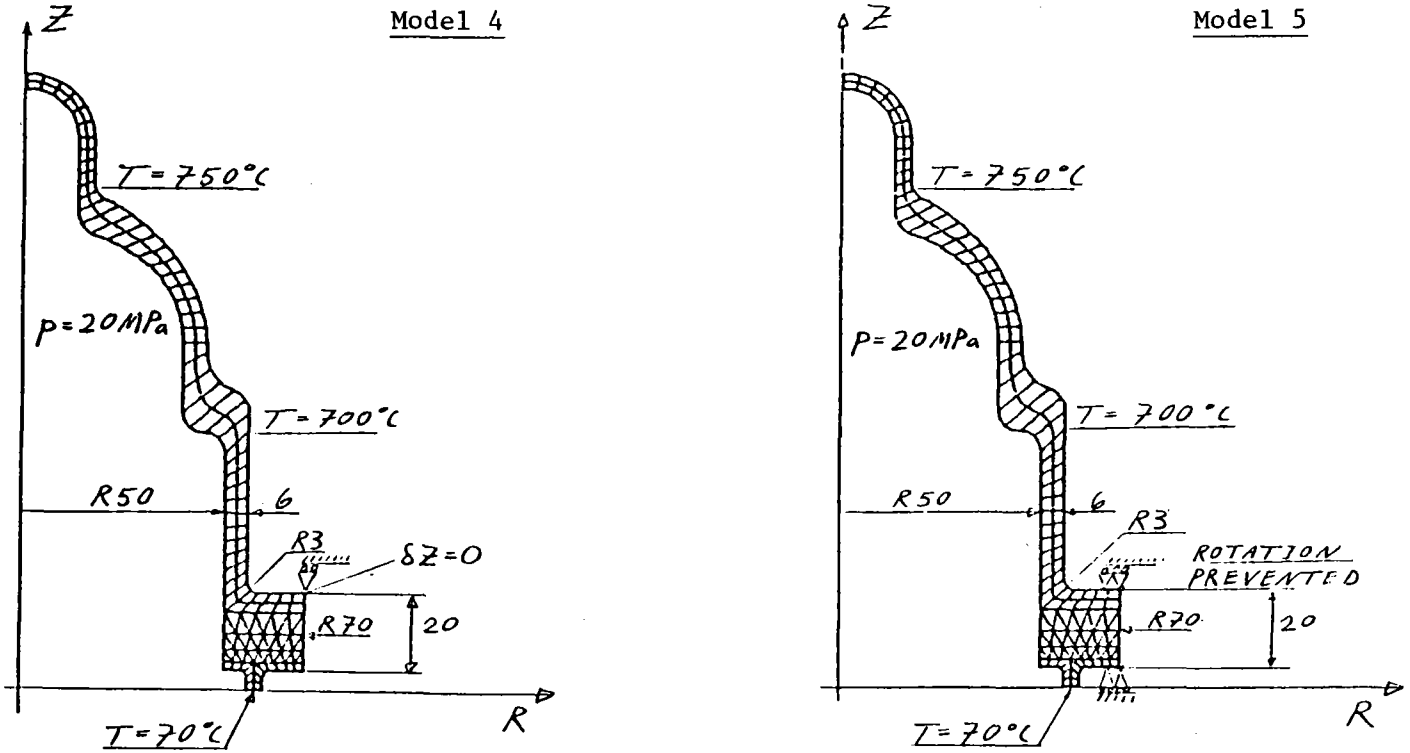

Figure 5-2 Models 4 and 5 - Geometry, Loading Conditions, and Boundary Conditions (Integral Flanges)

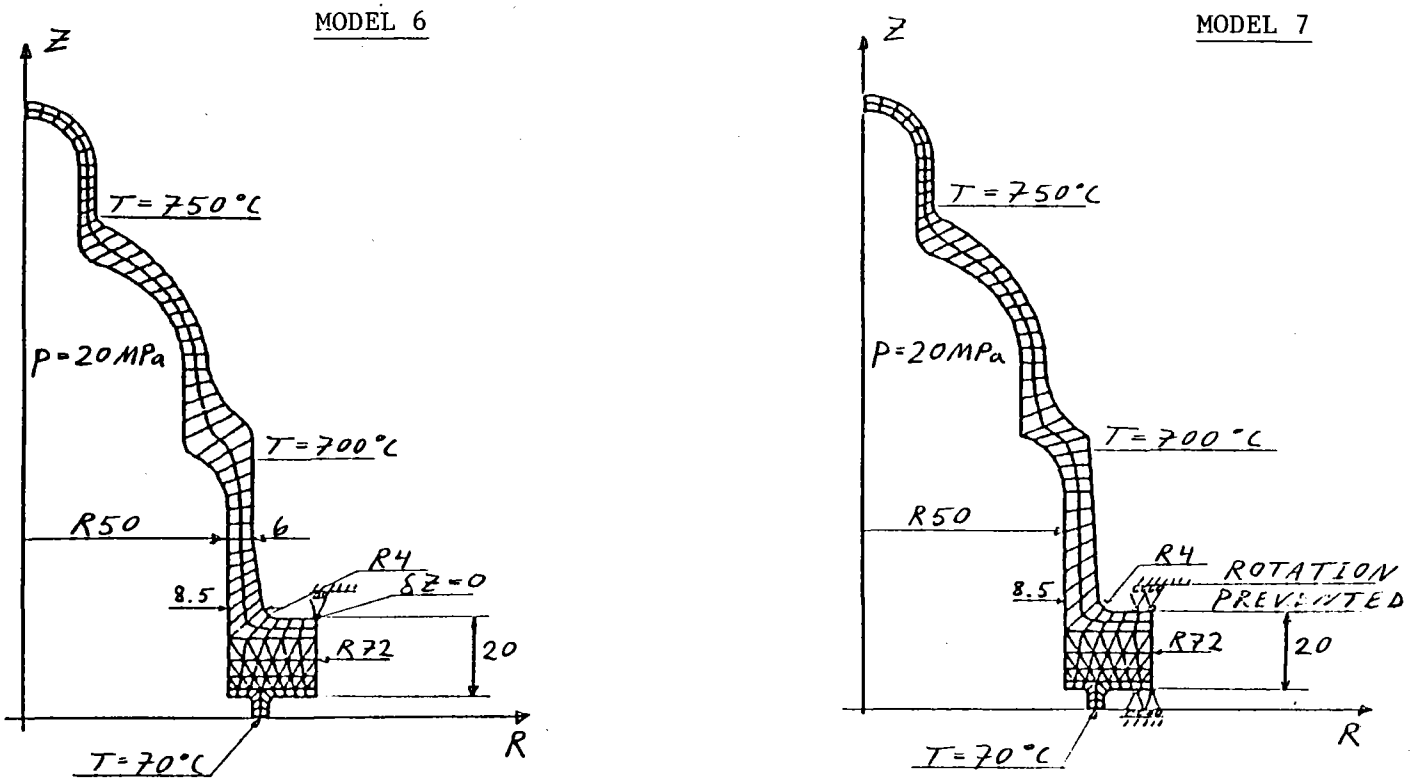

Figure 5-3 Models 6 and 7 (Integral Flanges)

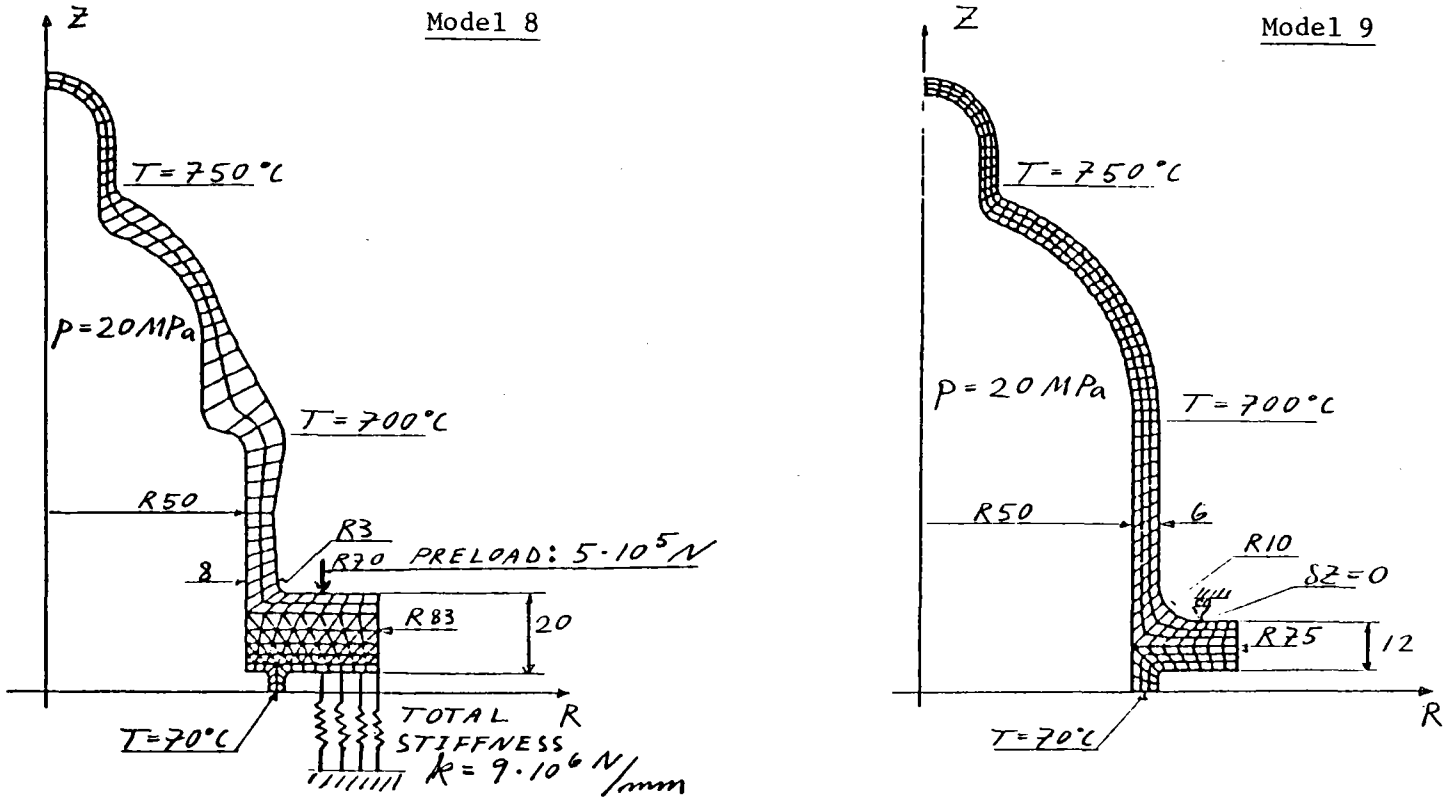

Figure 5-4 Models 8 and 9 (Integral Flanges)

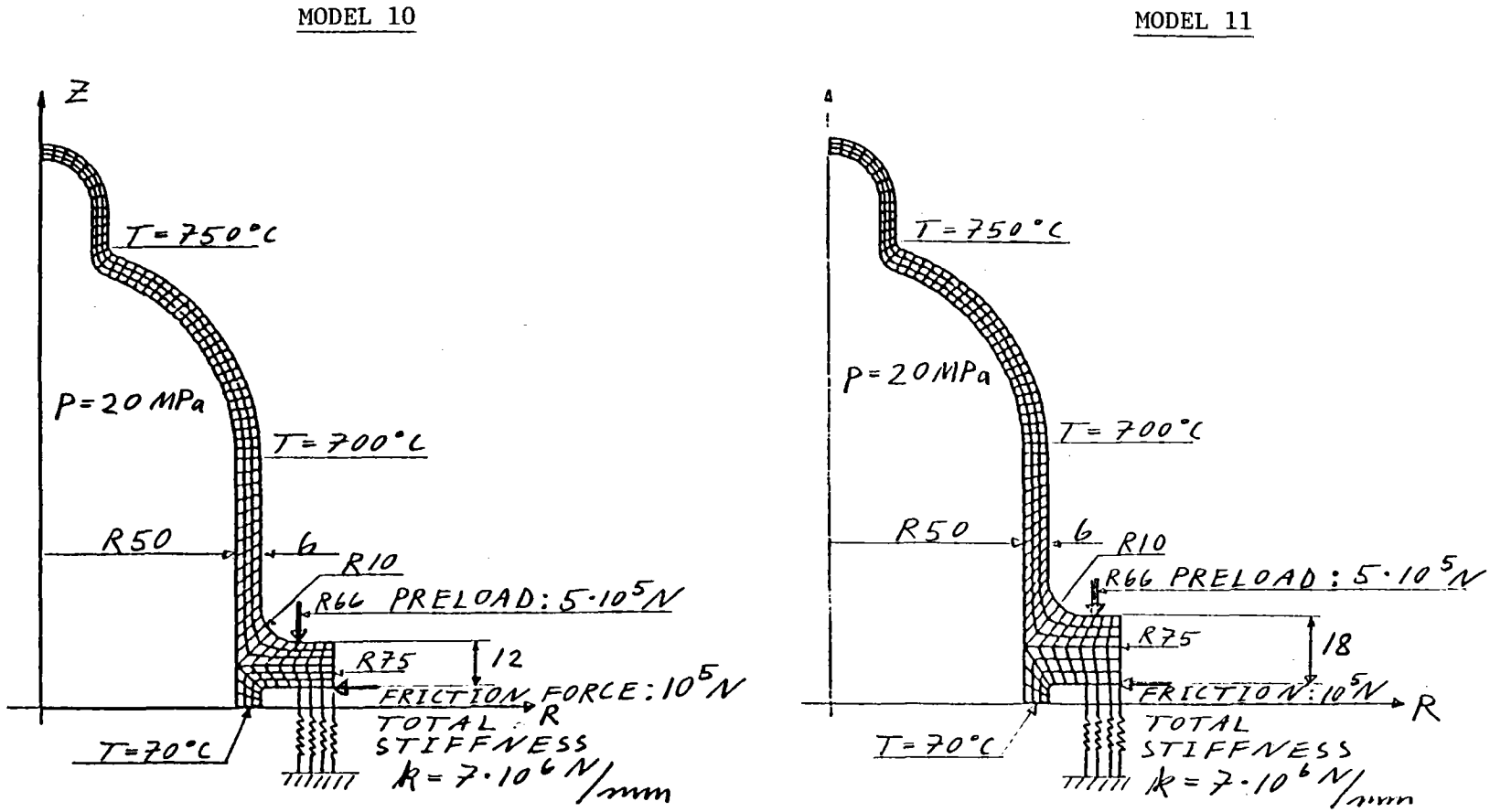

Figure 5-5 Models 10 and 11 (Integral Flanges)

TABLE 5-1

STRESSES IN FILLET RADIUS BETWEEN FLANGE AND CYLINDRICAL HOUSING

Model No.	Load Case	Stresses (MPa) σ^1	σ^2	σ^3	σ^{eq}
1	T	9	-23	-4	28
	p	384	597	≈0	524
	T+p	393	573	-4	511
2	p	309	433	48	340
3	p	210	292	48	215
4	T	-59	-265	-69	202
	p	446	652	150	436
	T+p	387	387	81	306
5	T	-91	-345	-89	255
	p	333	462	106	313
	T+p	242	118	16	196
6	T	-	-	-	175
	p	-	-	-	289
	T+p	-	-	-	228
7	T	-	-	-	252
	p	-	-	-	182
	T+p	-	-	-	161
8	T	-	-	-	258
	p	-	-	-	159
	T+p	-	-	-	245
9	T	-	-	-	110
	p	-	-	-	343
	T+p	-	-	-	286
10	T	-144	-321	-8	272
	p	199	255	6	226
	T+p	184	114	2	159
11	T	-83	-288	-8	252
	p	200	229	7	209
	T+p	199	42	2	181

Material Data

The selected material is XF-818. The temperature is about 200 to 300°C on the upper surface of the flange. At this temperature XF-818 has the following strength properties.

Yield strength (MPa):	290
Ultimate tensile strength (MPa):	475
Estimated fatigue limit in bending (MPa):	±150

Stress Analysis

The most probable failure mode of the cold part of the housings is fatigue failure in the small radius, between the flange and the cylindrical part. One way to compare the different designs is, therefore, to check their strength by looking at the risk of high cycle fatigue failure.

Based on the fatigue limit and the ultimate tensile strength, it is possible to define an approximative Haigh diagram. A 1.7 pressure ratio in the engine corresponds to the line $R = 0.59$ ($R = \sigma_{min}/\sigma_{max}$) in the Haigh diagram. In case of pressure loading only, the working point corresponding to the stress cycle will fall on this line. In some cases, in particular those with an integral flange, the axial temperature gradient tends to decrease the stresses due to the pressure loading. In addition, the mean stress value of the stress cycle will decrease. However, the amplitude of the stress components depends only on the pressure amplitude. Having these aspects in mind and looking at the Haigh diagram with a safety factor of at least 1.5 leads to the conclusion that the maximal stress should be about 200 N/mm^2 to be acceptable.

In a loose flange arrangement, the flange of the housing is free to rotate. This means that the stresses caused by the axial temperature gradient are rather small, which can be seen for model 1 in Table 5-1. For this reason, models 2 and 3 were analyzed for pressure loading only. As can be seen in the table, only the design corresponding to model 3 exhibits an acceptable stress level.

Models 4 and 5 represent the case with integrated flanges. Both models have the same geometry but different boundary conditions. In model 4 the flange is free to rotate and in model 5 the rotation is completely prevented. The actual behavior of such a flange is assumed to be within these limits. Thus, the equivalent stress corresponding to (T + p) - loading is probably between 306 N/mm^2 and 196 N/mm^2, which is too high. Models 6 and 7 represent a slightly modified design, which reduces the stress to a value between 228 N/mm^2 and 161 N/mm^2. Thus, the design corresponding to these models exhibit an acceptable level of strength.

Model 8 represents the same flange as in models 6 and 7. However, in this case a somewhat different boundary condition has been used. The preloading from the bolts has been included with the force 5×10^5N. The contact between the flange and the cylinder block has been modelled with springs having a total stiffness of 9×10^6 N/mm. As a realistic boundary condition should have only compressive forces in the springs, the number of springs or their extension in radial direction was varied in order to obtain this condition. The result in terms of stresses can be seen in the stress table. The equivalent stress in this case was 245 N/mm^2 corresponding to the load case (T + p). This stress value is higher than in model 6 with rotation allowed, which indicates that the latter model is probably not as conservative as it first appeared. However, one geometric difference exists between models 6 and 8. The radius between the flange and the cylindrical part was 4.0 mm in model 6 compared to 3.0 in model 8.

Models 9 to 11 represent a somewhat different type of integrated flange. The radius between the flange and the cylindrical part is comparatively big (10 mm). The bolt head is intended to be counter sunk into this radius meaning that the bending moment can be reduced because of the smaller distance between the bolt and the cylindrical part. In model 9 the flange is free to rotate but prevented from axial displacement at the point where the bolts are located. In models 10 and 11 preloading from the bolts is included. The contact with the cylinder block is modelled by springs in the same way as in model 8. However, in this case a friction force between the flange and the cylinder block is included. The geometry of the flange is the same in models 9 and 10, but in model 11 the height of the flange has been increased from 12 to 18 mm.

The equivalent stress corresponding to model 10 seems low and well below the allowable stress limit. However, the holes in the flange caused by the counter sunk bolt heads have not been included in the model. The effect of the holes represents a stress concentration which will increase the stresses considerably. To evaluate the stress concentration factor, in this case, is very difficult. However, a rough estimation can be done in the following way. A biaxial stress state exists in the critical point, with say σ_1 200 N/mm^2 and σ_2 100 N/mm2. A circular hole in the biaxially stressed plate has a stress concentration factor of 2.5, and if the hole is elliptical, the factor will be even higher. In our case, the counter sunk hole is not perpendicular to the surface and consequently the hole edge will be somewhat elliptical. This means that the stress concentration factor could be greater than 2.5. However, even with a stress concentration factor of 2.0 the allowable stress limit will be exceeded.

In the cases with integrated flanges, there exists another effect that has not been included in the axisymmetric finite element models, namely the stress distribution in the hoop direction. The load is transferred from the flange to the bolts at discrete locations corresponding to the bolt positions. This means that the stresses in the flange will be higher in a point near the bolt, compared to a point between two bolts. Consequently, the stress values from the axisymmetric models have to be multiplied with a certain factor depending on the number of bolts and their distribution in circumferential direction. Many bolts evenly distributed will of course reduce this factor. Thus, the unquantified stress distribution in the hoop direction increases the uncertainties in the stress analysis and it emphasizes the need of low stress levels in the case of integrated flanges.

Result

Different types of flanges have been studied to determine their strength. The best alternative is a loose flange arrangement for the following reasons. The flange is free to rotate, which means no extra stresses in the flange or in the bolts due to the axial temperature gradient in the housing. The axisymmetric flange and the axisymmetric loading mean that the stresses can be evaluated with high precision, minimizing the risks from inadequate strength.

5.1.3 Bolt Joint Between Heater Housing and Cylinder Block

This section contains sizing and stress analyses of the bolts holding the heater housing and cylinder block together. It contains also an estimation of the additional stresses caused by the flange rotation due to the axial temperature gradient combined with the pressure loading. Finally the dependency between bolt dimension and fatigue life is studied.

Sizing and Number of Bolts

During the design process of the RESD, the diameter of the sealing O-ring has varied. In this case an O-ring diameter of 110 mm has been assumed.

Maximal pressure: 20 MPa

Area: $A = \frac{\pi \cdot 110^2}{4} = 9503 \text{ mm}^2$

Maximal gas force: $F_A = 19 \times 10^4$ N

If k_B is the stiffness of the bolt and k_C is the stiffness of the clamped material, the stiffness ratio is:

$$\phi = \frac{1}{\frac{K_C}{K_B} + 1}$$

Assume: $\phi = 1/3$

Maximal gas force in the bolts: $F_{SA} = \Phi F_A = 6.34 \times 10^4$N

Assume bolt quality 12.9, which has yield strength $\sigma_y = 1080$ N/mm^2

For the dimension M14 the "stress area": $A_S = 115$ mm^2

n = number of bolts

Static requirement (according to VDI 2230):

$$\frac{F_{SA}}{n} \leq 0.1 \cdot \sigma_y \cdot A_S$$

$$n \geq 5.1$$

Consequently, 6 x M14 12.9 is needed.

Maximal pressure cycle: (15 ±5) MPa

Load amplitude:

$$F_{SAa} = \frac{5}{20} \cdot \phi \cdot \frac{FA}{6} = 2639 \text{ N}$$

Minimum bolt area: $A_m = 105 \text{ mm}^2$

Stress amplitude:

$$\sigma_a = \frac{F_{SAa}}{Am} = \pm 25 \text{ N/mm}$$

This can be compared with the allowable stress amplitude of approximately $\pm 35 \text{ N/mm}^2$.

The allowable stress amplitude is based on Figure 5-6 (taken from ASME, Section VIII - Division 2), which shows the design fatigue curve for high-strength steel bolting for temperatures not exceeding 700°F. As an alternative to 6 x M14 bolts, it is possible to use 8 x M12 bolts, which are nearly equivalent in strength.

Estimation of Bending Stresses

As mentioned earlier in the section containing the flange analysis, the rotation of the integral flanges will cause bending moments on the bolts. In this section the bending stress in the bolt has been estimated based on the angular deflection of the flange surface in contact with the bolt head. Table 5-2 shows the angle corresponding to some different finite element models shown earlier in the section containing the stress analyses of the flanges.

The following equation assumes that the bolt is beam fixed at one end and exposed to a bending moment at the other.

$$\left.\begin{aligned} \gamma &= \frac{M \cdot L}{E \cdot I} \\ \sigma_b &= \frac{M \cdot D}{2 \cdot I} \end{aligned}\right\} \rightarrow \sigma_b = \frac{\gamma \cdot E \cdot D}{2 \cdot L}$$

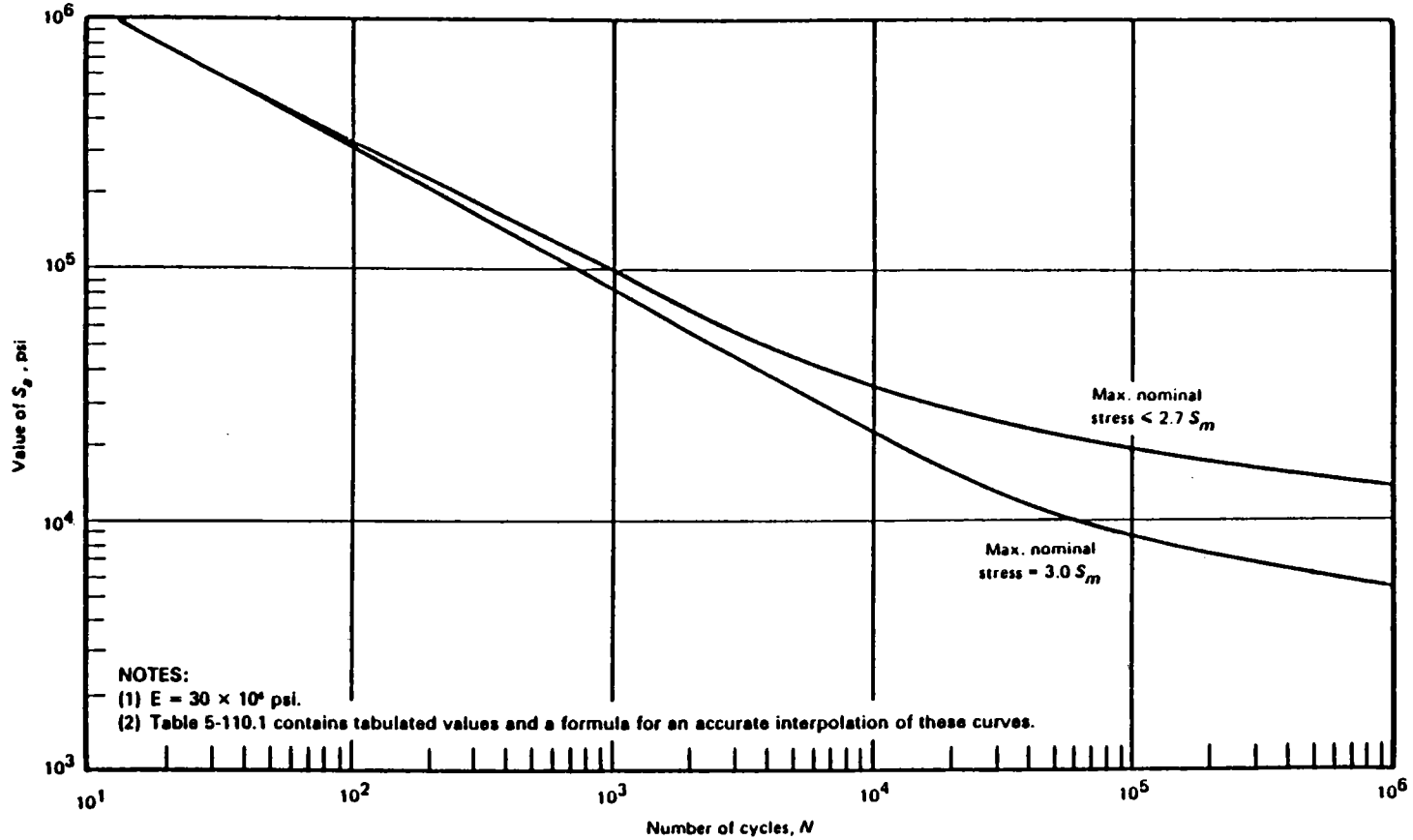

Figure 5-6 Design Fatigue Curve for High-Strength Bolting for Temperatures not Exceeding 700°F (Taken from ASME Section VIII, Division 2)

TABLE 5-2

ANGULAR DEFLECTION OF THE FLANGE SURFACE
FOR SOME DIFFERENT LOAD CASES

Model No.	Angle Deflection (rad)		
	T	p	T + p
4	57.7×10^{-4}	66.4×10^{-4}	111×10^{-4}
8	56.6×10^{-4}*	9.39×10^{-4}	66.1×10^{-4}
10	19.5	29.2×10^{-4}	80.2×10^{-4}
11	-	-	69.3×10^{-4}

where,

M = bending moment

L = bolt length

E = modulus of elasticity

α = angular deflection

D = bolt diameter

σ_b = bending stress

Assume,

$\alpha = 70 \times 10^{-4}$ rad

$E = 210{,}000$ N/mm^2

$D = 14$ mm

which gives $\sigma_b = \frac{10290}{L}$

or the stress amplitude $\sigma = \frac{5145}{L}$

Thus,

$L = 30$ mm $\rightarrow \sigma = 172$ N/mm^2

$L = 50$ mm $\rightarrow \sigma = 103$ N/mm^2

The axial stress must be added to this bending stress amplitude. The axial stress amplitude corresponding to the high frequent pressure variation p = (15 ±5) MPa earlier has been evaluated to ±25 N/mm^2. The low frequency pressure cycle p = (10 ±10) MPa corresponding to the start/stop cycle of the engine will give an axial stress amplitude of ±50 N/mm^2. The total stress amplitude for the bolt is then,

for,

$L = 30$ mm $\quad \sigma = \pm 222$ N/mm^2

$L = 50$ mm $\quad \sigma = \pm 153$ N/mm^2

The earlier mentioned design fatigue curve for high-strength steel bolting gives the following life times expressed in number of cycles.

$\sigma = \pm 85$ N/mm^2 $\rightarrow N = 30{,}000$

$\sigma = \pm 160$ N/mm^2 $\rightarrow N = 10{,}000$

$\sigma = \pm 270$ N/mm^2 $\rightarrow N = 4{,}000$

In the automotive application the life time requirement is in the order of 10,000 start/stop cycles. This means that the stress amplitude in the bolts must be ±160 N/mm^2. The analysis indicates that this requirement can be met only if the free length of the bolts is around 50 mm.

Result

The analysis shows that with the assumed O-ring diameter of 110 mm, the strength requirement of the bolts is met with 6 x M14 bolts or 8 x M12 bolts in 12.9 quality. In case of integral flanges the stress design criteria are met for both static loading and the high frequent pressure loading. However, low cycle fatigue problems related to the start/stop cycle can only be avoided if the integral flanges are combined with rather long bolts. The analysis has indicated that a free length of about 50 mm is necessary to meet a life time requirement of 10,000 start/stop cycles.

5.1.4 Hot End of the Heater Housings

The stress levels at the hot end of some of these housings have been studied. (The finite element models of the different housing have already been shown in Subsection 5.1.2, Flange Arrangements of the Heater Housings.) The loading and boundary conditions for the different models have been shown earlier. Models 3 and 10 represent housings with two manifolds, see Figure 5-7.

The models have been analyzed for three different load cases, stationary temperature load (T), internal pressure (p) of 20 MPa and the combination (T + p). The equivalent stress according to von Mises yield criterion for the different models is shown in the following pages.

Discussion of Stress Levels

The first stress limit requirement that has to be fulfilled concerns the primary membrane stresses, which must have a safety factor 1.5 against yielding. With a set temperature on the heater tubes of 820°C, the maximal temperature of the housing is expected to be about 700°C to 750°C. At this

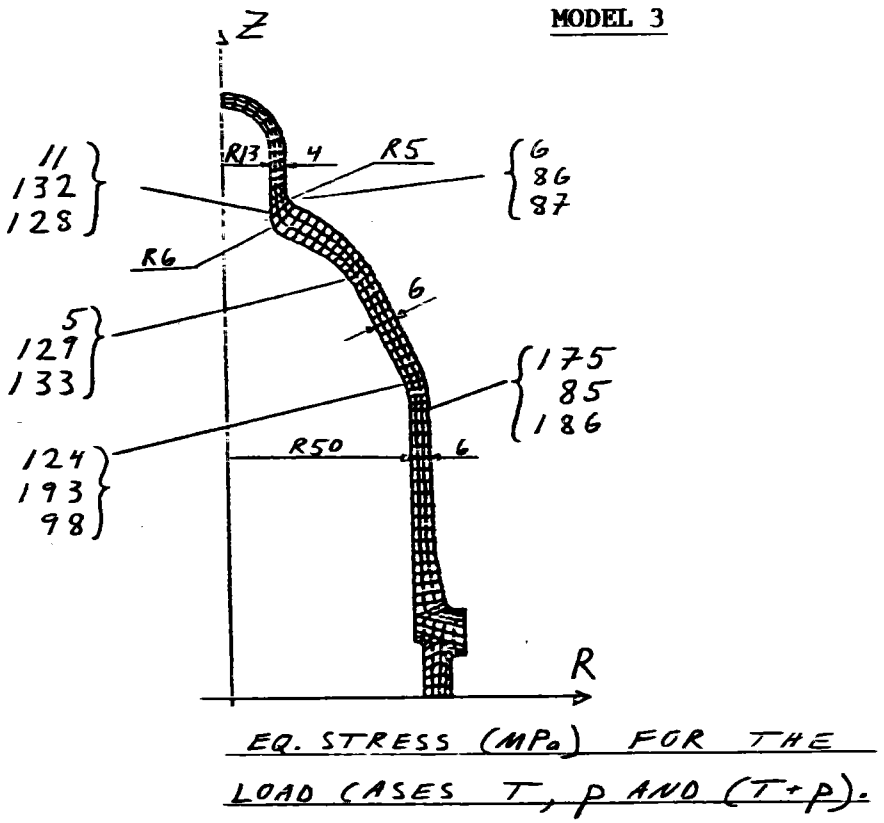

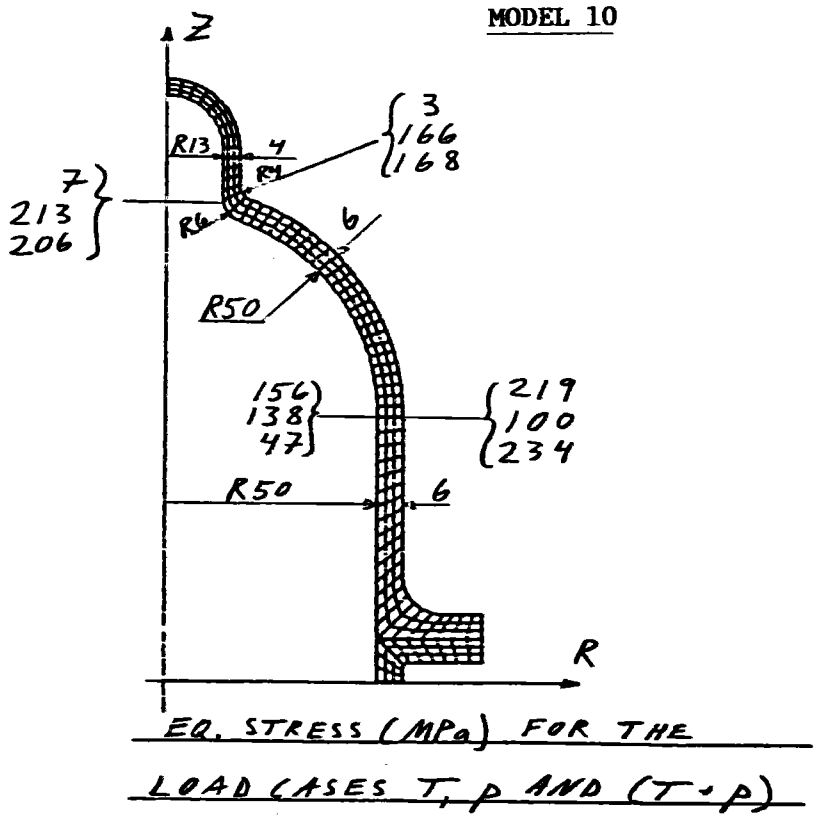

Figure 5-7 Stress Analysis for Models 3 and 10
(Housings have Two Manifolds)

temperature XF-818 has a yield strength of approximately 250 N/mm^2, which gives an allowable primary membrane stress of 167 N/mm^2. The primary membrane stress in the cylindrical part of the pressure vessel can be evaluated based on the following formula:

$$\sigma = \frac{p(D - t)}{2 \cdot t}$$

where,

p = internal pressure, 20 MPa

D = diameter, 100 mm

t = wall thickness, 6 mm

This gives a primary membrane stress of 177 N/mm^2 and consequently the requirement on the primary membrane stresses is approximately fulfilled for all the models.

Another stress criterion concerns the primary stresses (membrane stresses + bending stresses), which shall be below the yield strength of the material. In applying this criterion, stress concentration effects are excluded, which means that only the linear part of the stress distribution over the wall thickness is considered. The primary stresses corresponding to an internal pressure of 20 MPa are less than the yield strength of the materials for all models and consequently also this stress criterion in fulfilled.

The next stress criterion concerns the primary plus secondary stresses caused by the pressure loading combined with the stationary temperature loading. This type of stress should be below the yield strength of the material. Also in applying this criterion, the stress concentration effects must be excluded. The stress values from the finite element analysis represent maximum values and therefore include stress concentration effects. This means that for most of the points the primary plus secondary stresses are somewhat lower than the stress values shown for the different models. The stress limit requirement on primary and secondary stress therefore is likely fulfilled for all models.

To eliminate the risk of failure due to creep rupture, the primary membrane stresses must be limited. A set temperature of 820°C on the heater tubes, corresponds approximately to a maximal temperature of 750°C at the hot end of the heater housing. At this temperature, the creep rupture curve for XF-818 in air can be expressed in the following way:

$$\sigma_{CR} = 400 \times t_{CR}^{-0.106}$$

where σ_{CR} (MPa) is the stress level, which causes creep rupture after the time t_{CR} (h). The pressure levels corresponding to a 3500 h combined driving cycle have already been shown in Subsection 5.1.1, Heater Tubes. A creep rupture analysis based on the linear damage rule gives an equivalent pressure of 9 MPa. The creep rupture curve gives a stress value of 168 N/mm2 corresponding to 3500 h. With a safety factor of 1.5, the allowable primary membrane stress is 112 N/mm^2, corresponding to an internal pressure of 9 MPa. For the loadcase p = 20 MPa, the corresponding stress level is 249 N/mm^2. Another load requirement is 100 h at full load corresponding to a mean pressure of 15 MPa. For the time 100 h the creep rupture curve gives a stress value of 245 N/mm^2. With a safety factor of 1.5 the allowable primary membrane stress is 163 N/mm^2 corresponding to a pressure of 15 MPa. For the load case p = 20 MPa the corresponding stress limit is 217 N/mm^2. Evidently, the 100 h at 15 MPa is worse from the perspective of creep damage than 3500 h with a combined metro/highway cycle. It has been mentioned earlier that the maximal primary membrane stress is about 177 N/mm^2 and consequently, from the perspective of creep rupture, this stress level is acceptable.

The requirement for the primary stress is a safety factor of 1.2 to the creep rupture stress. For the case p = 20 MPa, the stress limit is then 217 x 1.5/1.2 = 271 N/mm^2. This stress limit is not exceeded for any of the different models and consequently the requirement is fulfilled even with the stress concentration effects included.

Just as a precaution, it is recommended to use the previously mentioned criterion on the primary and secondary stresses, corresponding to loadcase (T + p). The stress values of the different models are in general less than the limit

271 N/mm^2. One point in models 4 and 7 has a stress value of 280 N/mm^2 and 283 N/mm^2 respectively. However, again this is the maximum value, which includes stress concentration effects, and consequently the pure primary plus secondary stress is somewhat less. In summary, the overall impression is that the stress levels are acceptable from the creep rupture point of view.

Finally the stress values of the different models have to be analyzed from the aspect of fatigue. Based on earlier experience for example stress analysis of the Upgraded Mod I heater housings, it can be concluded that the safety factor against low cycle fatigue failure due to the mean pressure variations is higher than the safety factor against high cycle fatigue failure due to the high frequent pressure variations. Thus the fatigue analysis is limited to the case p = (15 ±5) MPa.

Based on the material testing of XF-818 at 800°C, the fatigue limit is considered to be around ±110 N/mm^2. The ultimate tensile strength is then about 425 N/mm^2. Based on the fatigue limit and the ultimate tensile strength, it is possible to define an approximative Haigh diagram. A 1.7 pressure ratio in the engine corresponds to the line R = 0.59 ($R = \sigma_{min}/\sigma_{max}$) in the Haigh diagram. In case of pressure loading only the working point corresponding to the stress cycle will fall along this line. The intersection between this line and the line defining a Haigh diagram reduced with a safety factor 1.5 on the amplitude represents a point corresponding to a maximal stress value of 177 N/mm^2. This can be considered as an approximative value of the maximal stress that can be accepted from the fatigue point of view. It can be compared with the maximal stresses in the Mod I Update heater design, in which all stress values are less than 200 N/mm^2 in the hot end of both the cylinder and regenerator housing.

An acceptable stress value around 175 to 200 N/mm^2 means that one point in model 3 is at the limit. Model 10 has two critical points. However, in both cases the design can be made acceptable in terms of fatigue by small changes.

Summary

Some different designs of heater housings have been analyzed from the strength point of view. The most critical failure mode is fatigue. The low fatigue limit of XF-818 makes it impossible to accept design concepts with large geometric discontinuities. The best solution with respect to the low fatigue limit of XF-818 is probably a cylindrical pressure vessel, without geometric discontinuities or other stress raisers, connected to a hemispherical head with an integral axisymmetric neck connected to the manifold.

5.1.5 The Connection Between the Piston Rod and the Con-Rod

The selected design concept for the connection between the piston rod and the con-rod was analyzed. The piston rod is threaded into a pin, which is guided in the small end of the con-rod, see Figure 5-8. This subsection contains a study of the stress situation in the threaded connection.

Stress Analysis

The analysis is based on the axial force in the piston rod of the Mod I engine. The maximal value of this force alternates between +15300 N and -22950 N. The corresponding force in the RESD will be of approximately the same magnitude. The threaded part of the piston rod has a dimension corresponding to M10. The clamped material will have an outer diameter of two to three times the threaded diameter. The clamped material will have an axial length of probably less than two times the threaded diameter. These conditions result in a force ratio ϕ in the order of 0.3 to 0.4 and therefore the analysis is based on $\phi = 0.35$.

The basic static requirement that should be fulfilled is:

$$\phi F_A \leq 0.1 \times \sigma_y \times A_s$$

where

F_A = maximal axial force

σ_y = yield strength of the material

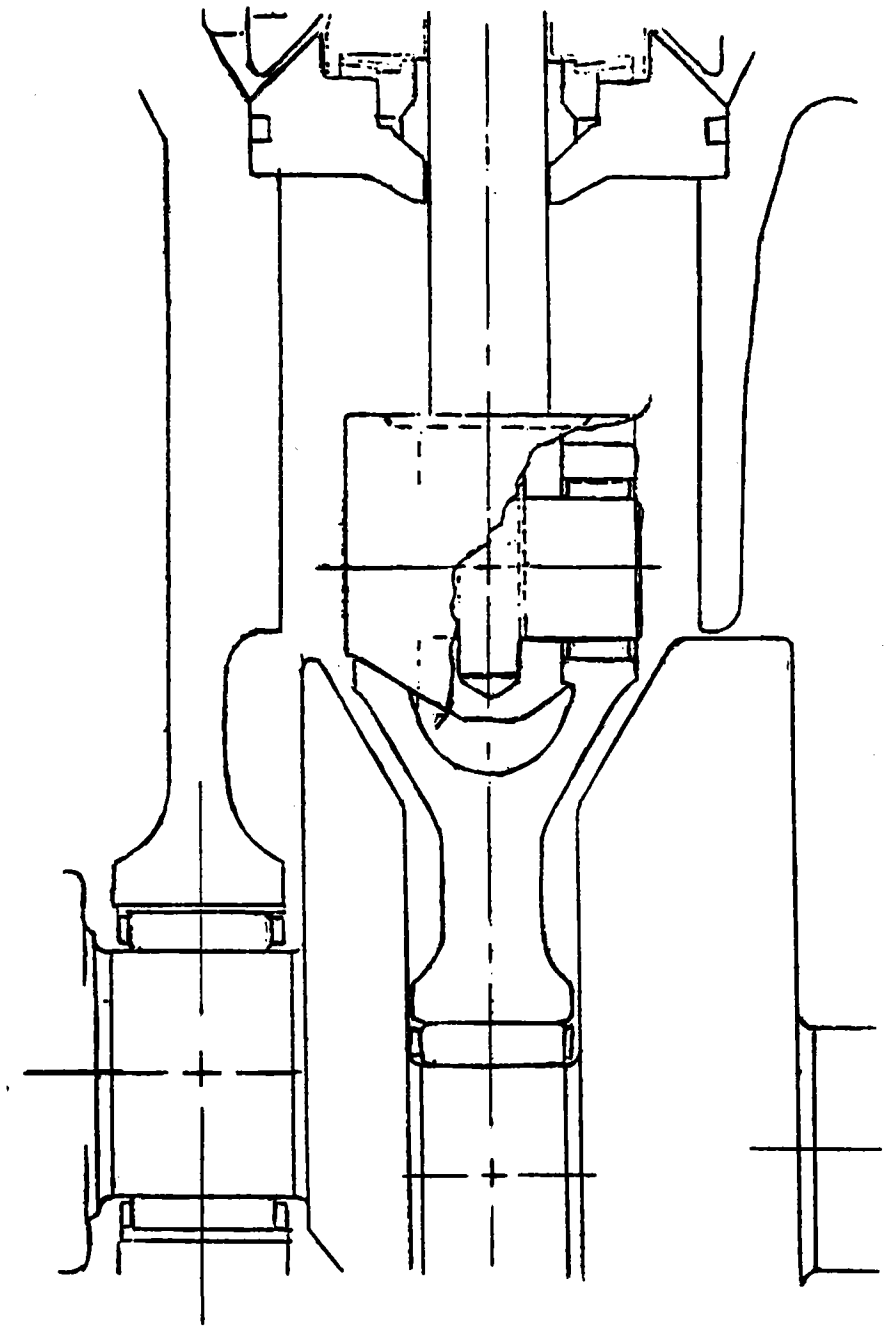

Figure 5-8 Design Showing Connection Between Piston Rod and Con-Rod

A_S = cross section area of the bolt

$\phi F_A = 5355$ N

If 12.9 quality is assumed, then

$\sigma_y = 1080$ N/mm^2 and, $0.1 \times \sigma_y \times A_S = 6264$ N.

Consequently, the first requirement is met.

According to VDI 2230 the needed preload can be expressed in the following way:

$$F_{Mmax} = \sigma_A[F_{kerf} + (1 - \phi) \times F_A + F_Z]$$

where,

α_A is a factor dependent on the tightening procedure, the type of tool, and so on.

F_{kerf} is the smallest preload that is needed to prevent the clamped parts from separating.

F_Z is the loss in preloading due to local yielding in the threads.

$\alpha_A = 1.6$
$F_{Kerf} = 15{,}300$ N
$\phi = 0.35$
$F_A = 15{,}300$ N
$F_Z = 1000$ N

$\rightarrow F_{Mmax} = 42{,}000$ N

This needed preload can be compared to the preload corresponding to a normal tightening moment for a M10 bolt in quality 12.9. For a normal value of the friction coefficient ($\mu = 0.14$), the tightening moment is 83 Nm corresponding to a prelaod of 44,300 N. This force is evidently of the same magnitude as the needed preload, and consequently a normal tightening moment is needed.

The stress amplitude in the threaded part of the piston rod σ_a is evaluated in the following way:

$$\sigma_a = \pm \phi \frac{F_{max} - F_{min}}{2 \cdot A_{min}}$$

A_{min} is the minimum cross section area, in this case 52.3 mm^2.

Thus,

$$\sigma_a = \pm 128 \text{ N/mm}^2.$$

This value can be compared to the allowable stress amplitude of approximately ± 35 N/mm^2 for high-strength steel bolting (compare with the fatigue curve given in subsection 5.1.3. The analysis shows that the design can not be accepted due to the risk of fatigue failure. However, the situation can be improved in different ways. First, the fatigue curve mentioned is based on high-strength steel bolting in general, which means that it may be possible to select a material with a higher fatigue limit.

Second, the fatigue strength can be increased considerably by rolling the threads after heat treatment. For the third, the fatigue properties can also be increased by using nonstandard threads with a bigger root radius.

The allowable sterss amplitude can also be increased by decreasing the preload. However, a reduced tightening torque seems impossible in this case, according to the analysis above. Another problem, related to the high tightening torque, is the risk of damage to the bearings in the crankshaft during the tightening operation. Maybe this can be solved by fixing the con-rod during the tightening.

Summary

The design concept based on a threaded connection of size M10 between the piston rod and a pin guided in the con-rod can not be shown to exhibit acceptable fatigue strength, as based on a stress analysis. However, an acceptable design can be made by using a material with good fatigue properties, using nonstandard threads with higher fatigue resistance and/or rolling the threads

after heat treatment. Fatigue testing should be conducted to verify acceptability.

5.2 Thermal Transients

The start transients in a Stirling engine represent a severe loading condition. When the manifolds and the top of the heater housings are exposed to the hot gas, high transient temperature gradients will be created in the walls of the pressure vessel. If the corresponding thermal stresses exceed the yield strength of the material, creep ratching effects can occur due to the start/stop cycle in combination with the high operating temperature. The early appearance of cracks in the regenerator housing of the Mod I has probably been caused by this phenomenon. Consequently, the transient loading conditions, especially during the start, represent a potential problem from the perspective of material strength and life requirement. For this reason, great emphasis has been put on the transient loading conditions in the stress analysis work for the RESD. This section discusses the thermal transient analyses and the corresponding stress analyses, which have been accomplished for the RESD.

5.2.1 Tube-Manifold Junction

Transient Loading Conditions

During the time period studied, the outer surface of the heater tube was exposed to a heat flux of 200 kW/m^2. During the first 10 seconds, the inner surfaces of the tube and the top of the manifold were thermally isolated and consequently had no heat exchange with the working gas. After the first 10 seconds, cranking of the engine is started. start. At this time the gas temperature (Tg) is considered to be 450°C. In the following time period, the gas temperature slowly increases to a temperature level of 600°C, which it reaches 20 seconds later at t = 30 seconds. The surface heat transfer coefficiency (α) between the gas and the inner surface of the tube-manifold structure was assumed to 2000 $W/m^2/°C$. The gas temperature function was based on measured gas temperature in a heater tube during a start of the Mod I engine. The initial temperature in the tube-manifold structure was 20°C.

Material Property Data

The heater tube material is assumed to be CG-27 and the material in the manifold is assumed to be XF-818. All the material data required for the analysis were not available. In addition, some properties didn't differ much between CG-27 and XF-818. Therefore, the same material data were used for both CG-27 and XF-818 in the analysis. The used material property data are listed below.

Thermal Conductivity ($W/m^2/°C$):	16.0
Density (kg/m^3):	8,000
Elastic modulus (N/mm^2):	170,000
Poisson's ratio:	0.3
Coefficiency of thermal expansion ($1/°C$):	16.0×10^{-6}
Specific heat ($J/kg/°C$):	420

Finite Element Model

The purpose in creating the finite element model was to study the thermal transients in the tube-manifold junction. Of special interest is of course the stress in the large geometric discontinuity where the tube meets the much thicker material of the manifold. The analysis was based on an axisymmetric finite element model, in which the actual part of the manifold was modelled as an equivalent thick-walled cylinder. The manifold with the largest distance between the tubes has the biggest material discontinuity in the tube-manifold junction. A typical maximal spacing of the tubes is about 11 mm, which gives an equivalent cylinder with an outer radius of 5.5 mm. The height of the cylinder corresponds to the wall thickness in the top of the manifold, which in this case was 7 mm. The free length of the tube was 10 mm. The finite element model consisted of 138 isoparametric axisymmetric elements with 8 nodes. The total model had 994 D.O.F. Figure 5-9 shows the geometry and the loading conditions for the model.

Transient Temperature Distribution

Figure 5-10 shows the temperature in some points as a function of time. Figure 5-11 shows the temperature distribution along the outer surface of the tube-manifold junction at time, t = 10 seconds.

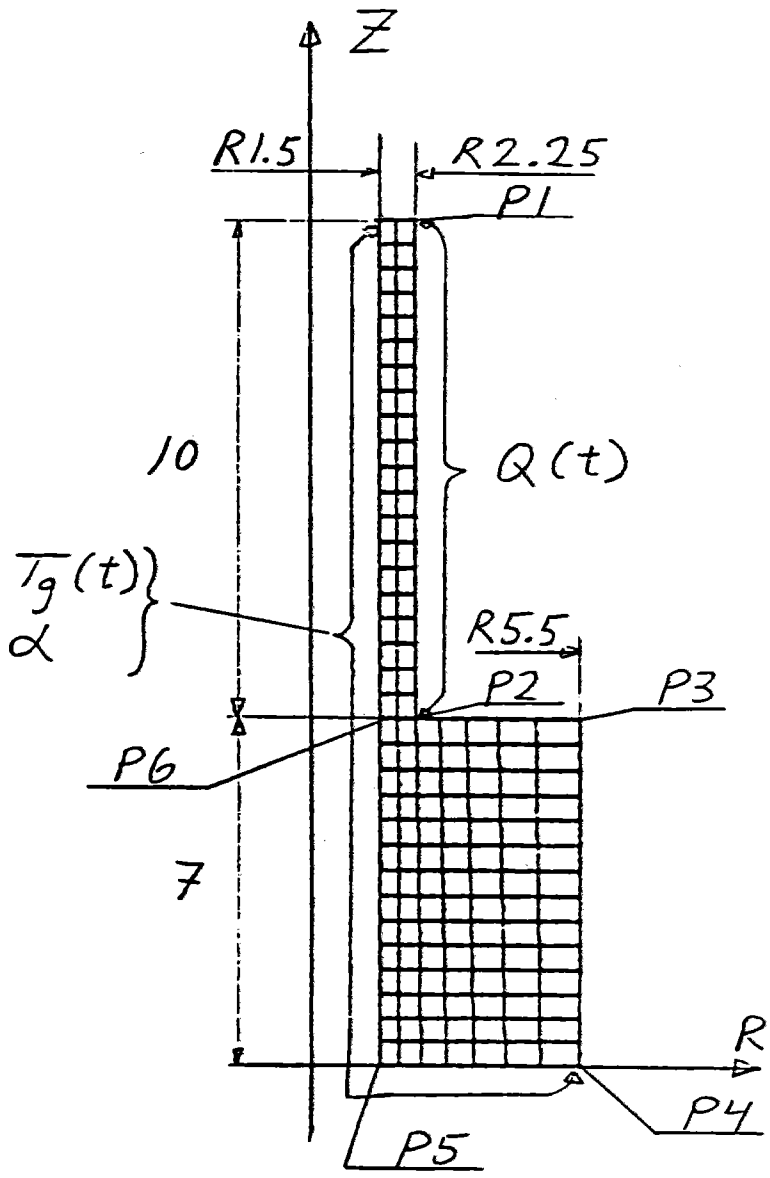

Figure 5-9 Finite-Element Model of the Tube-Manifold Junction

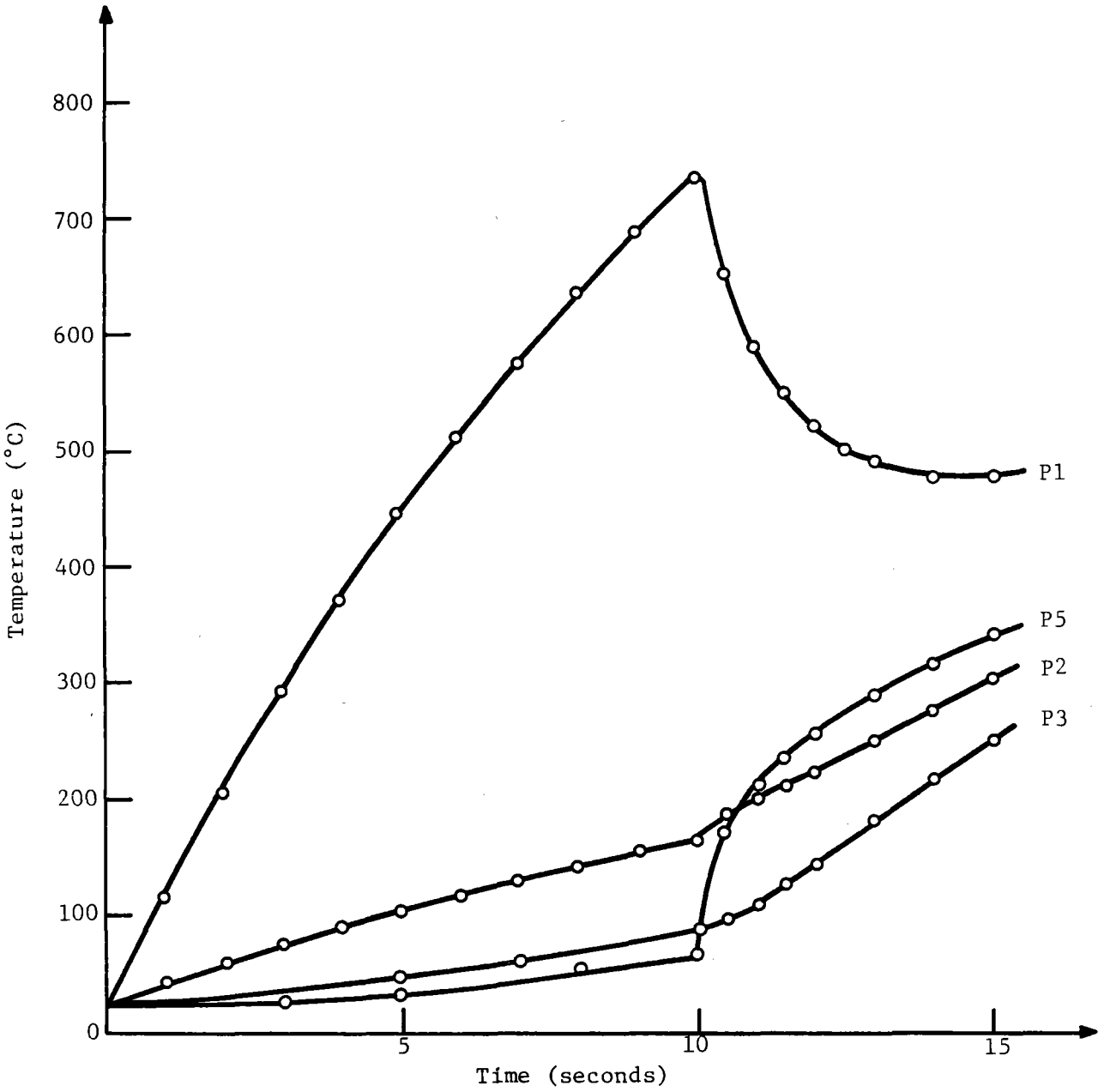

Figure 5-10 Temperature as a Function of Time in Some Points on the Tube-Manifold Junction

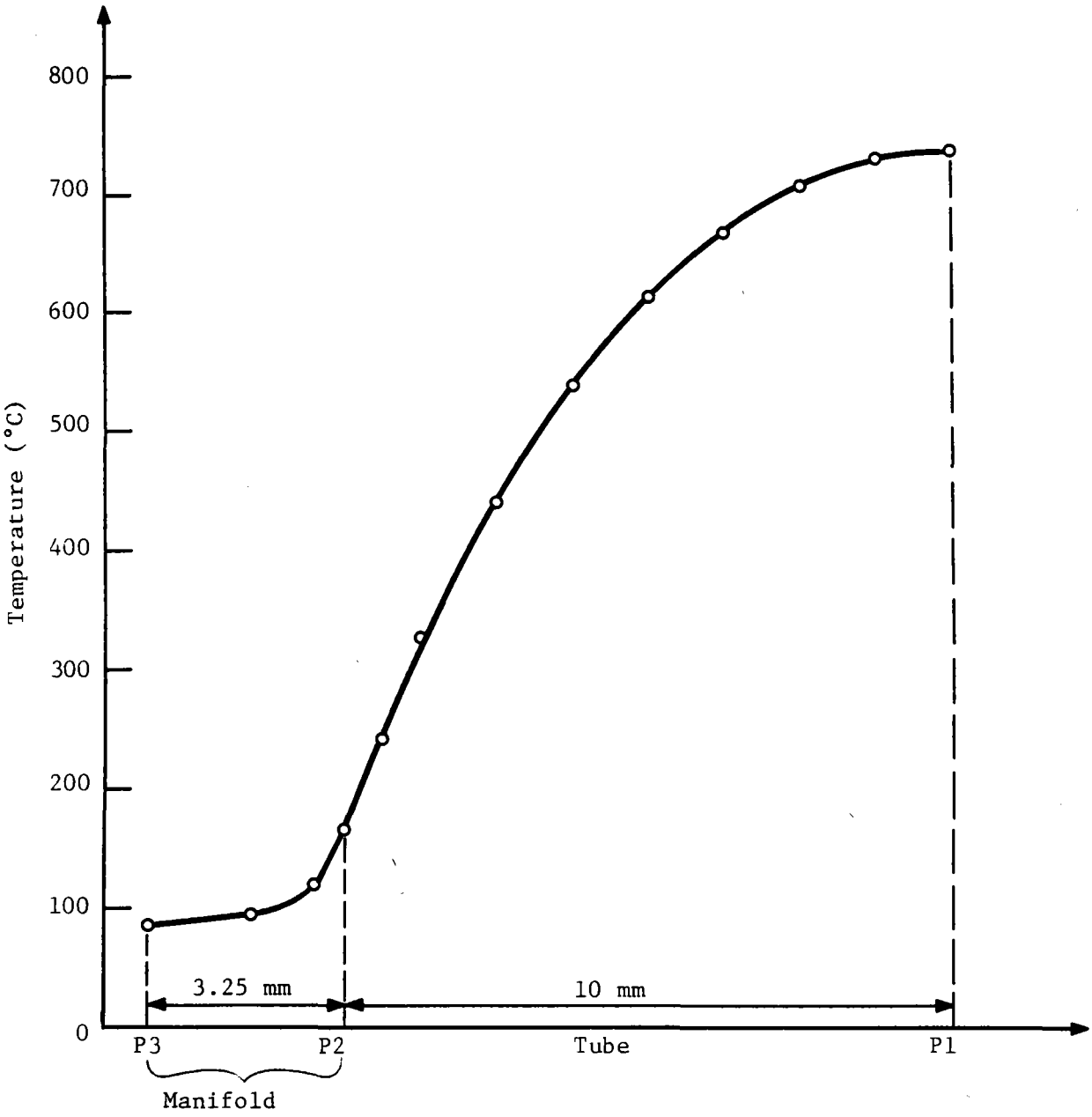

Figure 5-11 Temperature Distribution Along the Line P3 -> P2 -> P1 on the Tube-Manifold Junction at t = 10 seconds

Transient Stress Distribution

A stress analysis was done based on the results from the transient thermal analysis. Figure 5-12 shows the equivalent stress (according to von Mises Yield Criterion) as a function of time in the critical points of the structure. The maximal stress in the tube occurred in point P6 after 10 seconds, just before the cranking of the engine started. The maximal equivalent stress in this point was 233 N/mm^2 with the following stress components:

$\sigma_Z = 200\ N/mm^2$
$\sigma_R = 13\ N/mm^2$
$\sigma\alpha = -62\ N/mm^2$.

The maximal stress in the manifold occurred in point P2 after 10 seconds. The maximal equivalent stress is 188 N/mm^2 with the following components:

$\sigma_Z = -48\ N/mm^2$
$\sigma_R = -223\ N/mm^2$
$\sigma_\alpha = -70\ N/mm^2$.

Comparison With Analytical Solutions

The maximal equivalent stress in point P5 was 157 N/mm^2 at t = 10.5 seconds. The stress evaluation was not done for every time-step in the solution and at this point it appeared as if the maximal stress value had been missed. Therefore, in order to get an approximative value, a comparison was done based on a thermal shock approach. For such cases an analytical solution exists for homogenous flat plates. It is then assumed that the plate is initially at a uniform temperature and is suddenly exposed to the hot gas. In this case the material temperature in the region P4 → P5 is 65°C at time, t = 10 seconds. The gas temperature is 450°C, which gives a temperature step, $\Delta T = 385°C$. The surface heat transfer coefficient, $\alpha = 2000\ W/m^2/°C$ and the wall thickness is 4 mm. This gives a maximal stress of -187 N/mm^2, which is approximately the same as in point P2.

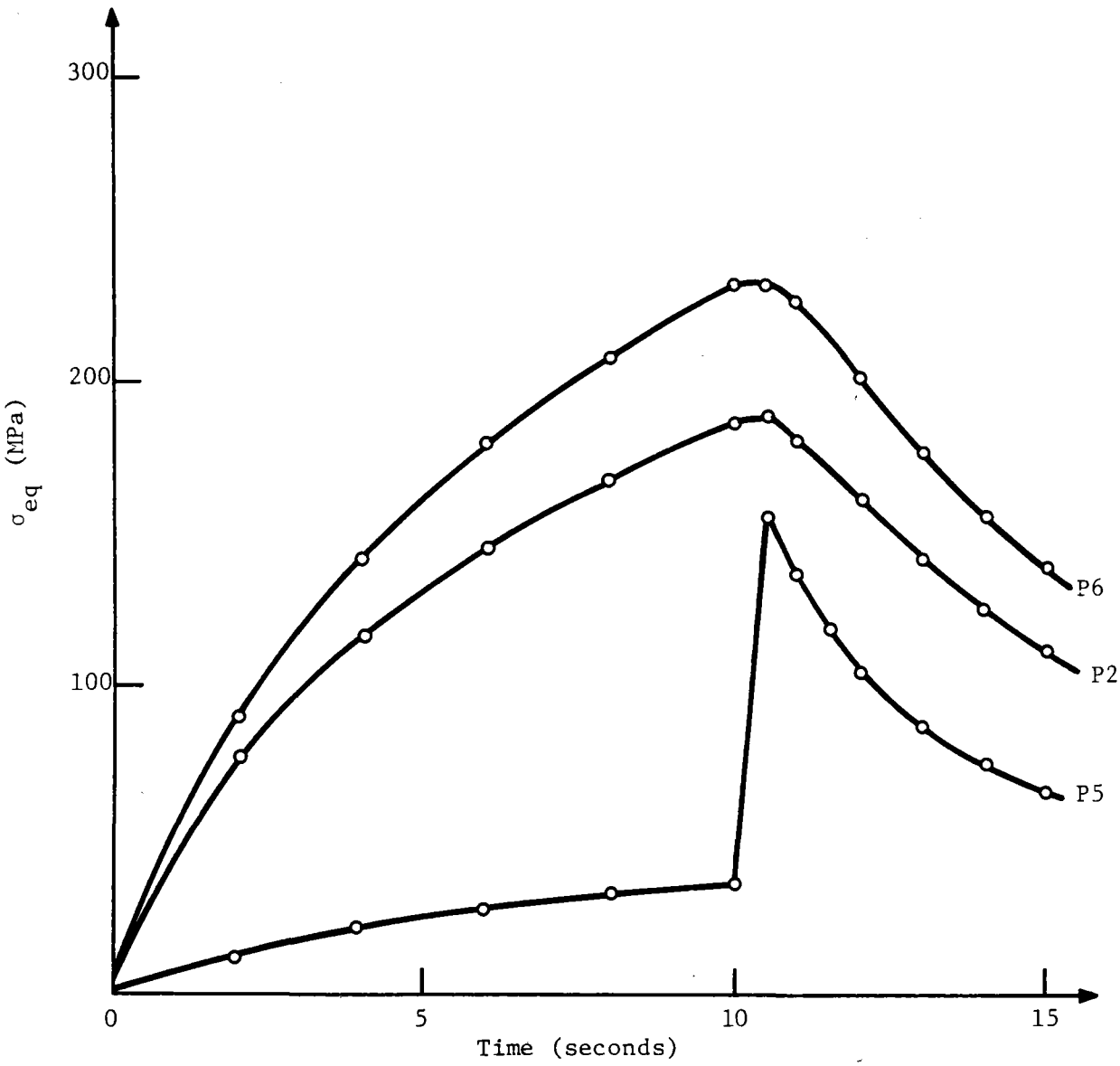

Figure 5-12 Equivalent Stress as a Function of Time for Points at the Tube-Manifold Junction

Life Time Estimations

The maximal stress range in the heater tube was 233 N/mm2, corresponding to the stress cycle σ = (116.5 ±116.5) N/mm^2. The temperature in the critical point was approximately 200°C. The available strength properties of CG-27 was based on bar testing and some of the data are listed below.

	RT	1000°F (538°C)
Yield strength (MPa)	931	952
Ultimate tensile strength (MPa)	1414	1296

Consequently, the maximal stress is well below the yield strength of the material.

Fatigue Data (bar)

R.T.: (345 ±336) MPa → 431,000 cycles
(275 ±269) MPa → ∞ cycles

1000°F (538°C): (379 ±322) MPa → 424,000 cycles
(310 ±265) MPa → ∞ cycles

The data above indicates that the safety factor against high cycle fatigue is greater than 2. The maximal stress range in the manifold was 188 N/mm2, mainly due to a high compressive stress in the radial direction. The strength properties of XF-818 are listed below.

	RT	800°C
Yield strength (MPa)	312	269
Ultimate tensile strength (MPa)	500	427

The maximal stress in the manifold is below the yield strength of the material. Fatigue data on XF-818 at 800°C have been generated within the Material Testing Program. The evaluated stress amplitude of ±94 N/mm^2 can be compared to the fatigue curve, which gives the following result, 335,000 cycles with a safety factor of 1.5 on stress. The requirement is in the order

of 10^4 cycles for this start-up related loading condition, and consequently the analysis has not given any reason to consider the tube-manifold junction as a critical area from the thermal transient point of view.

5.2.2 The Manifold

Transient Loading Conditions

For the manifolds an interesting load situtation occured when rotation of the engine started and the inner surfaces of the manifold were exposed to the hot gas. The temperature function of the gas was represented by an instant temperature step from RT to 450°C, followed by a slow temperature increase to 600°C, obtained after 20 seconds. The surface heat transfer coefficient was 2000 $W/m^2/°C$ during the whole transient. (Material property data are the same as for the tube-manifold junction).

Finite Element Models

Two different finite element models were used to study the thermal transients in the manifold. Both models are shown in Figure 5-13. Model 1 represents the upper part of the manifold, to which the heater tubes are brazed. The brazed part of the tube is included in the model. For symmetry, only a part of the manifold top has been modelled. The purpose was to study the temperature as a function of time in the area between the holes. This temperature function can then serve as one of the load inputs to the next model. Model 1 consists of isoparametric plane elements with 8 nodes. The circular surfaces were exposed to the gas temperature function described in the preceding paragraph, and the transient material temperature was evaluated.

Finite element model No. II represents a cross section of the manifold. The model consists of isoparametric plane strain elements with 8 nodes. The thickness is 5.5 mm, but the elements, in the central upper part of the manifold have been given a reduced thickness in order to take into account the reduced stiffness due to the holes. For the sake of symmetry, only half a model has been analyzed. The central upper part of the model corresponding to the material between the holes in model 1, was forced to follow the

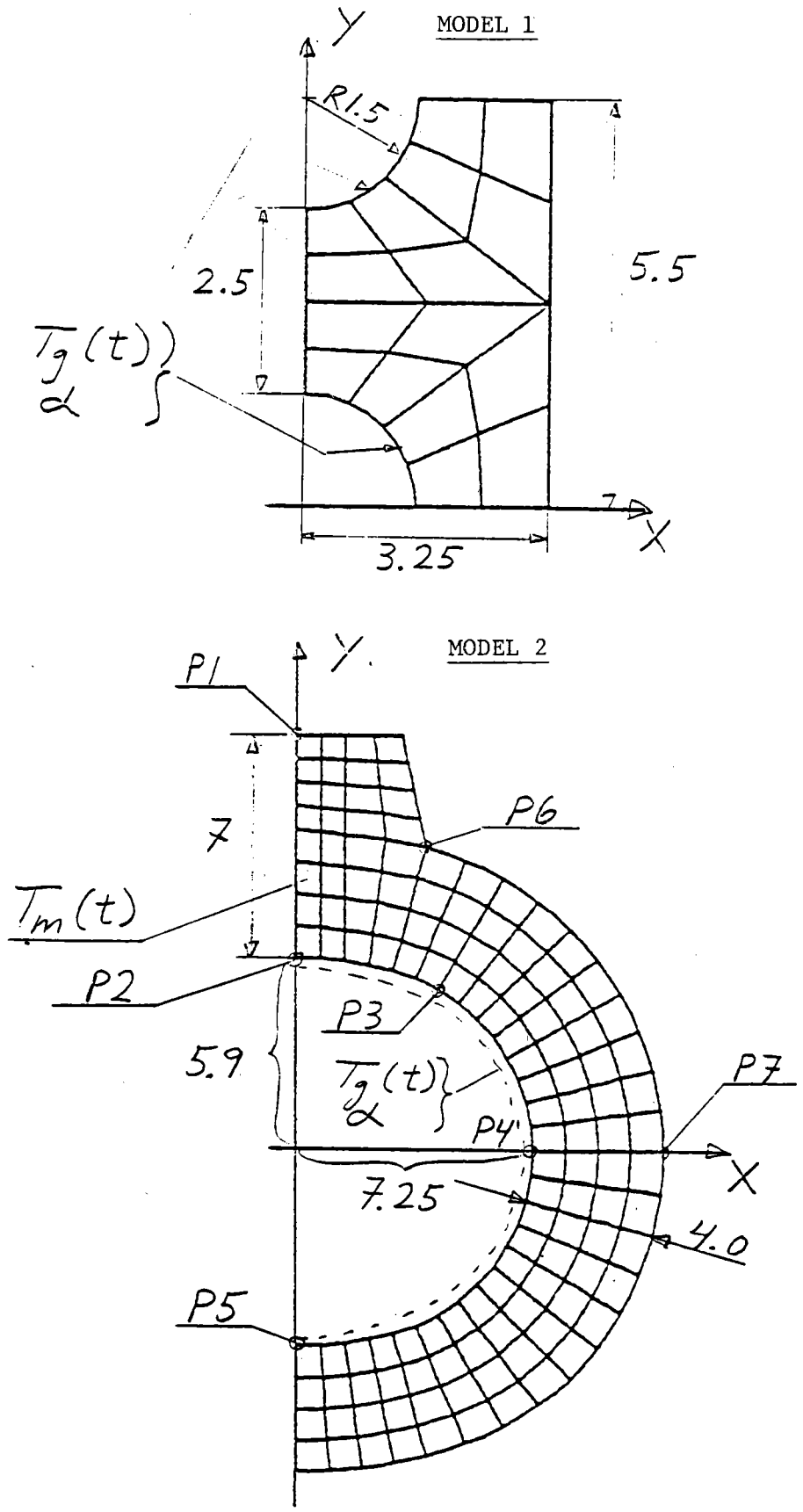

Figure 5-13 Finite Element Model of the Manifold

temperature function evaluation based on model 1. The inner surface of the manifold was exposed to the gas temperature function described earlier in combination with the surface heat transfer coefficient of 2000 $W/m^2/°C$.

Transient Temperature Distribution

Figure 5-14 shows the temperature distribution in the ligament between the holes after 2.0 seconds. Also the mean temperature T_m (t) as a function of time is shown. This temperature function was used for the elements in the ligament region of model No. II. Figure 5-15 shows the temperature as a function of time for different points in model II.

Transient Stress Distribution

A stress analysis was done based on the results from the transient thermal analysis. Figure 5-16 shows the equivalent stress (according to von Mises Yield Criterion) as a function of time for some interesting points in model II. The maximal stress was compressive and occurred in point P3 after 2.0 seconds. The maximal equivalent stress in this point was 200 N/mm^2 with the following stress components:

$$\sigma_x = -176 \ N/mm^2$$
$$\sigma_y = -67 \ N/mm^2$$
$$\tau_{xy} = 91 \ N/mm^2.$$

The maximal equivalent stress in tension was 136 N/mm^2 in point P6.

Comparison With Analytical Solutions

A comparison was done based on a thermal shock approach, in which the manifold was compared with a flat plate with the same thickness. The plate was initially at a uniform temperature of 20°C. Suddenly it was exposed to the hot gas, which had a temperature of 450°C. With a surface heat transfer coefficient of 2000 $W/m^2/°C$, the maximal stress was -209 N/mm^2, which can be compared with the maximal principal stress -228 N/mm^2, which was evaluated based on the finite element model No. II.

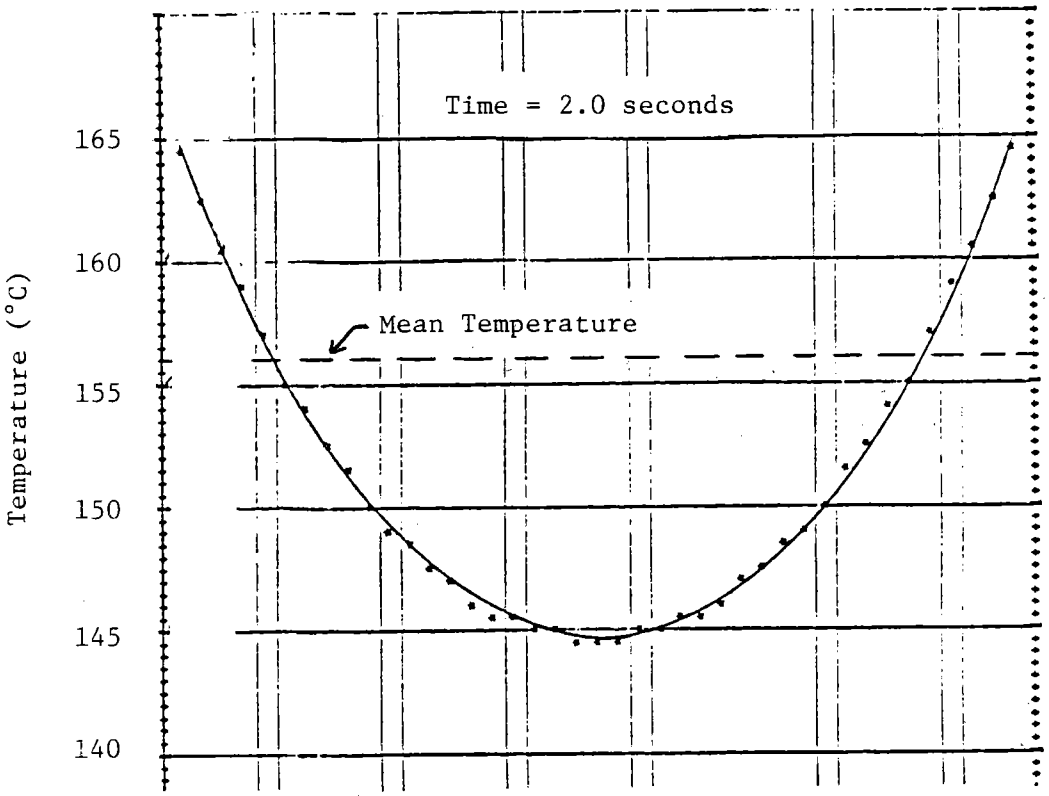

Temperature Distribution after 2.0 Seconds in the Ligament Between the Holes in the Manifold

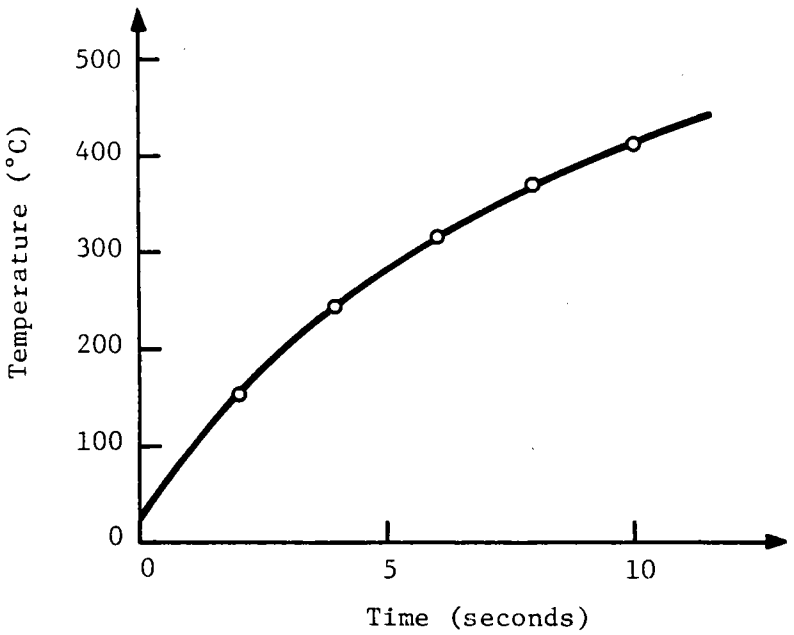

Figure 5-14 Mean Temperature as a Function of Time Between the Holes in the Manifold

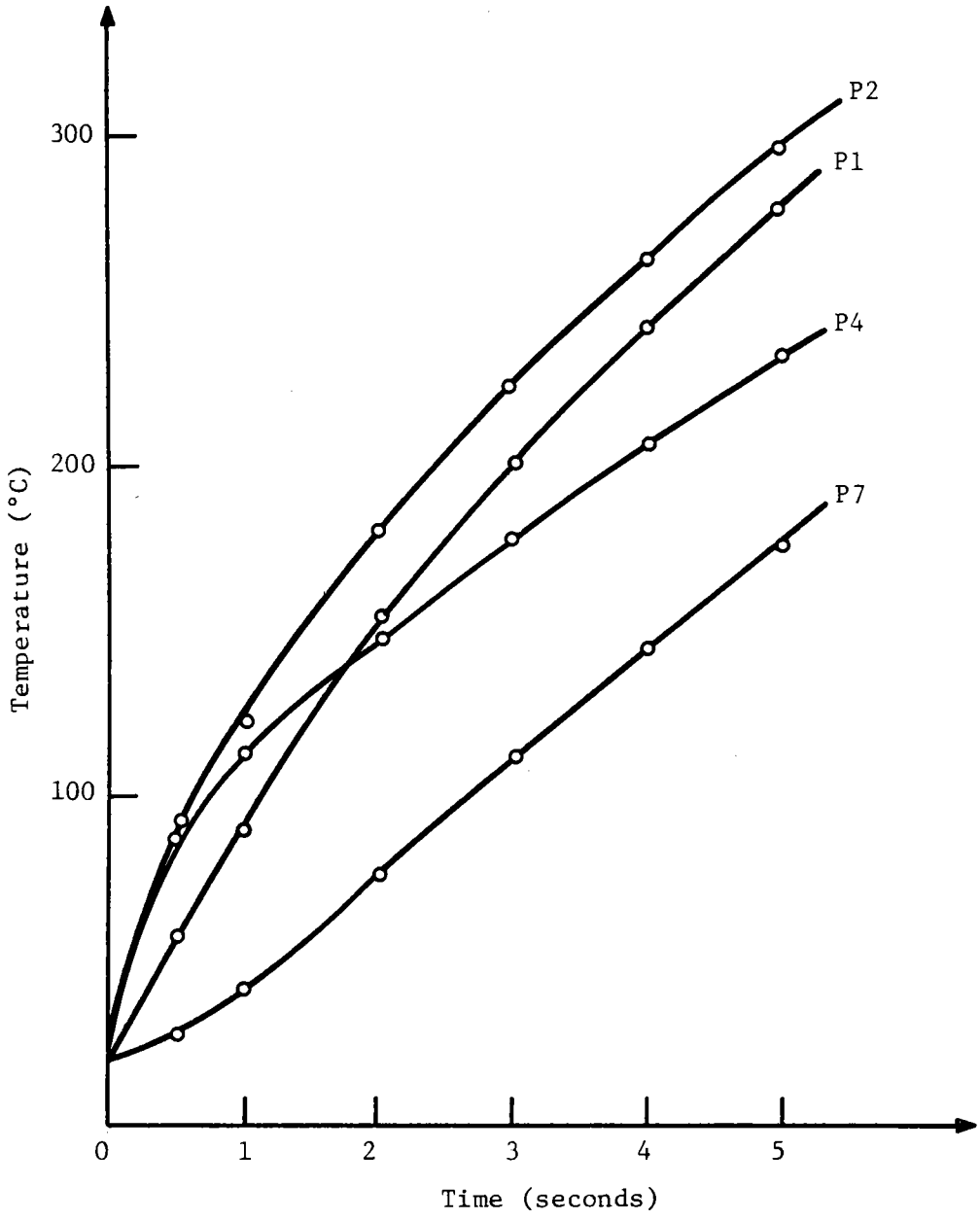

Figure 5-15 Temperature as a Function of Time for Points in the Manifold

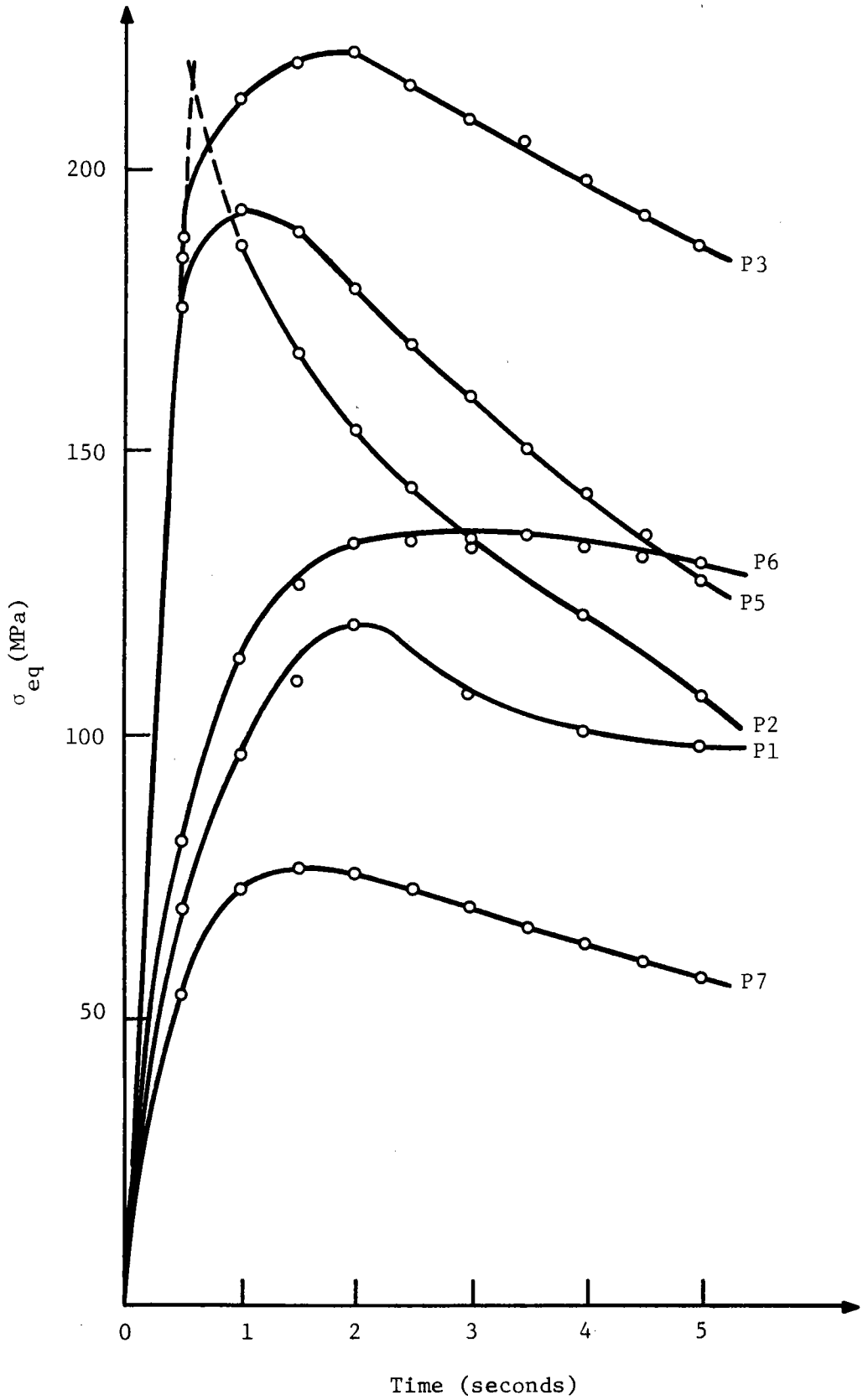

Figure 5-16 Equivalent Stress as a Function of Time for Points in the Manifold

Life Time Estimations

The maximal stress range in the manifold was 200 N/mm^2. It occurred in point P3 after 2.0 seconds and the material temperature was approximately 160°C. The maximal stress is compressive and well below the yield strength of XF-818. The maximal stress range was compared to fatigue data on XF-818 at 800°C. With a safety factor of 1.5 in stress, the number of cycles was 42,400. This can be compared with the requirement, which is in the order of 10^4 cycles. Consequently, the analysis has shown that no low-cycle fatigue problems are to be expected due to the start-up transients.

5.2.3 The Heater Housing

Transient Loading Conditions

When cranking of the engine starts, the inner surface of the heater housing is exposed to the hot working gas. In this transient thermal analysis, the same gas temperature step from R.T. to 450°C followed by a slow temperature increase to 600°C, which is reached after 20 seconds. During the analysis the inner surface was exposed to the gas temperature from the top and down to a point located at the top plane of the regenerator matrix (from point P0 to point P3 in Figure 5-16). The surface heat transfer coefficient was 2000 $W/m^2/°C$ during the transient. The initial temperature was 20°C in the housing. (Material property data is identical to that which was explained earlier.)

Finite Element Model

The finite element model is shown in Figure 5-17. It is an axisymmetric model consisting of 156 isoparametric axisymmetric elements with 8 nodes. The total number of D.O.F. was 1,158.

Transient Temperature Distribution

The transient thermal analysis covered the first 35 seconds of engine rotation. Figure 5-18 shows the temperature as a function of time for some

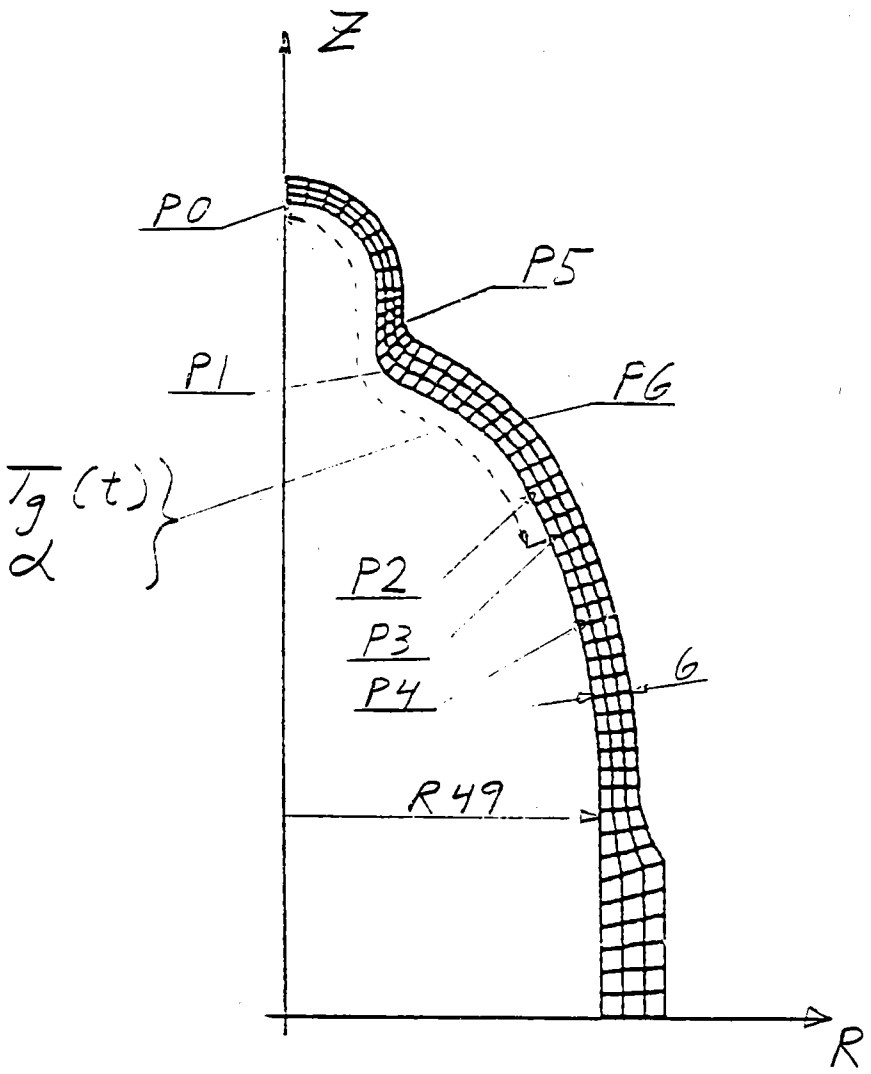

Figure 5-17. Finite-Element Model of the Heater Housing

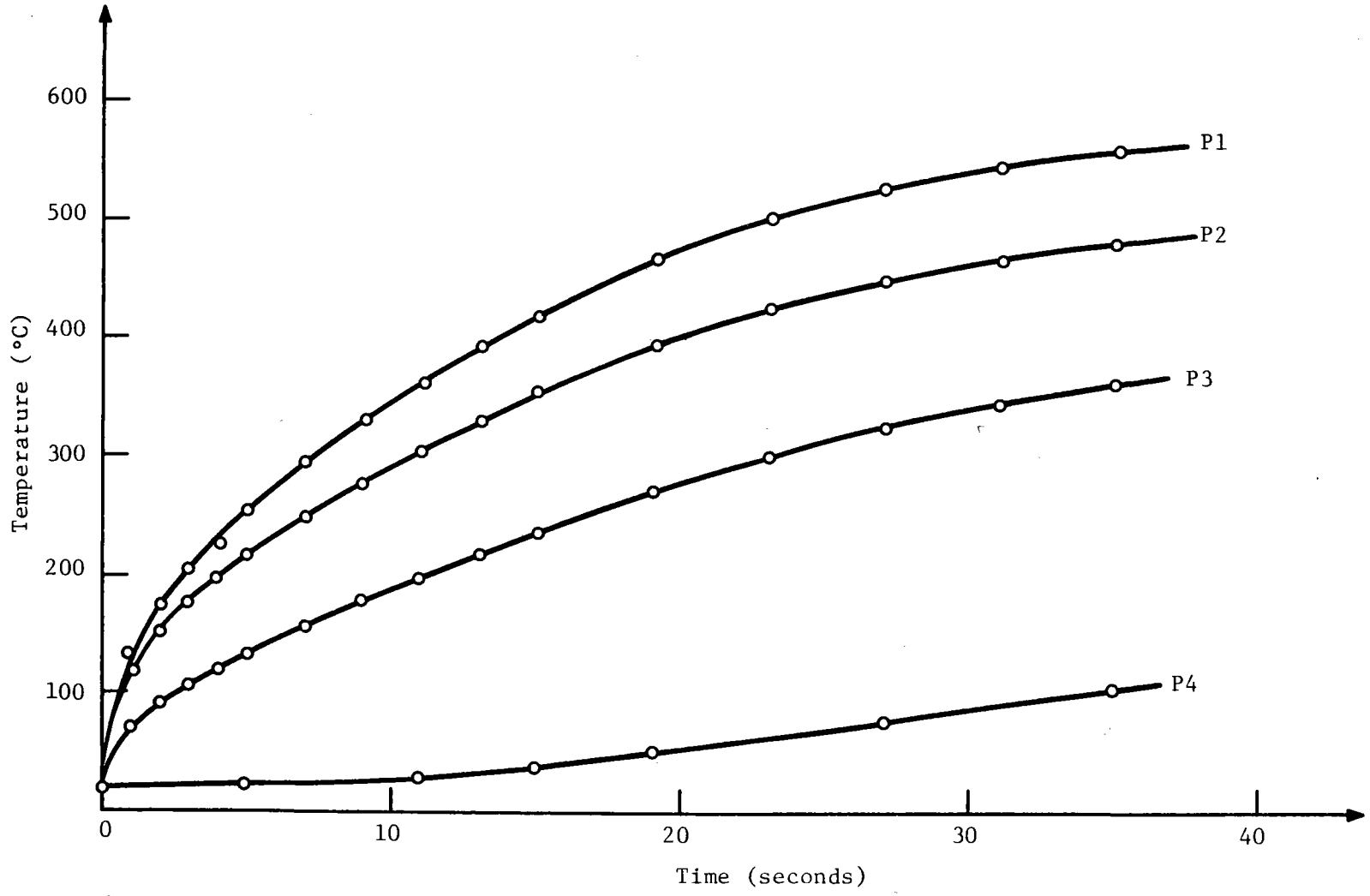

Figure 5-18 Temperature as a Function of Time for Points on the Heater Housing

points in the heater housing. Figure 5-19 shows the temperature distribution along the inner surface at two different times, t = 5, and t = 19 seconds.

Transient Stress Distribution

A stress analysis was done based on the results from the transient thermal analysis. Figure 5-20 shows the stress distribution after t = 5 seconds along the inner and outer surface of the housing. Figure 5-21 shows the stress distribution after t = 19 seconds. The plotted stress component is the equivalent stress according to von Mises Yield Criterion. Figure 5-22 shows the equivalent stress as a function of time for some points on the heater housing.

Comparison With Analytical Solutions

A comparison was done based on a thermal shock approach, in which the pressure vessel wall was compared with a flat plate with the same thickness. The plate initially had a uniform temperature of 20°C. Then one surface suddenly was exposed to the hot gas with a temperature of 450°C. With a surface heat transfer coefficient of 2000 $W/m^2/°C$, the maximal stress was -320 N/mm^2 for a wall thickness of 7.0 mm.

Life Time Estimations

The maximal equivalent stress during the thermal transient was 374 N/mm^2. It occurred in point P2 after 19 seconds and the material temperature was then approximately 400°C. The stress was compressive with the following components:

$$\sigma_R = -79 \text{ N/mm}^2$$
$$\sigma_\alpha = -426 \text{ N/mm}^2$$
$$\sigma_Z = -265 \text{ N/mm}^2.$$

The yield strength of XF-818 at 400°C is approximately 290 N/mm^2, which means that the yield strength is exceeded by 30%. The maximum stress range of 374 N/mm^2 was compared to fatigue data on XF-818 at 800°C. The number of cycles to failure was then 2,900 with a safety factor 1.5 on stress. Without the safety

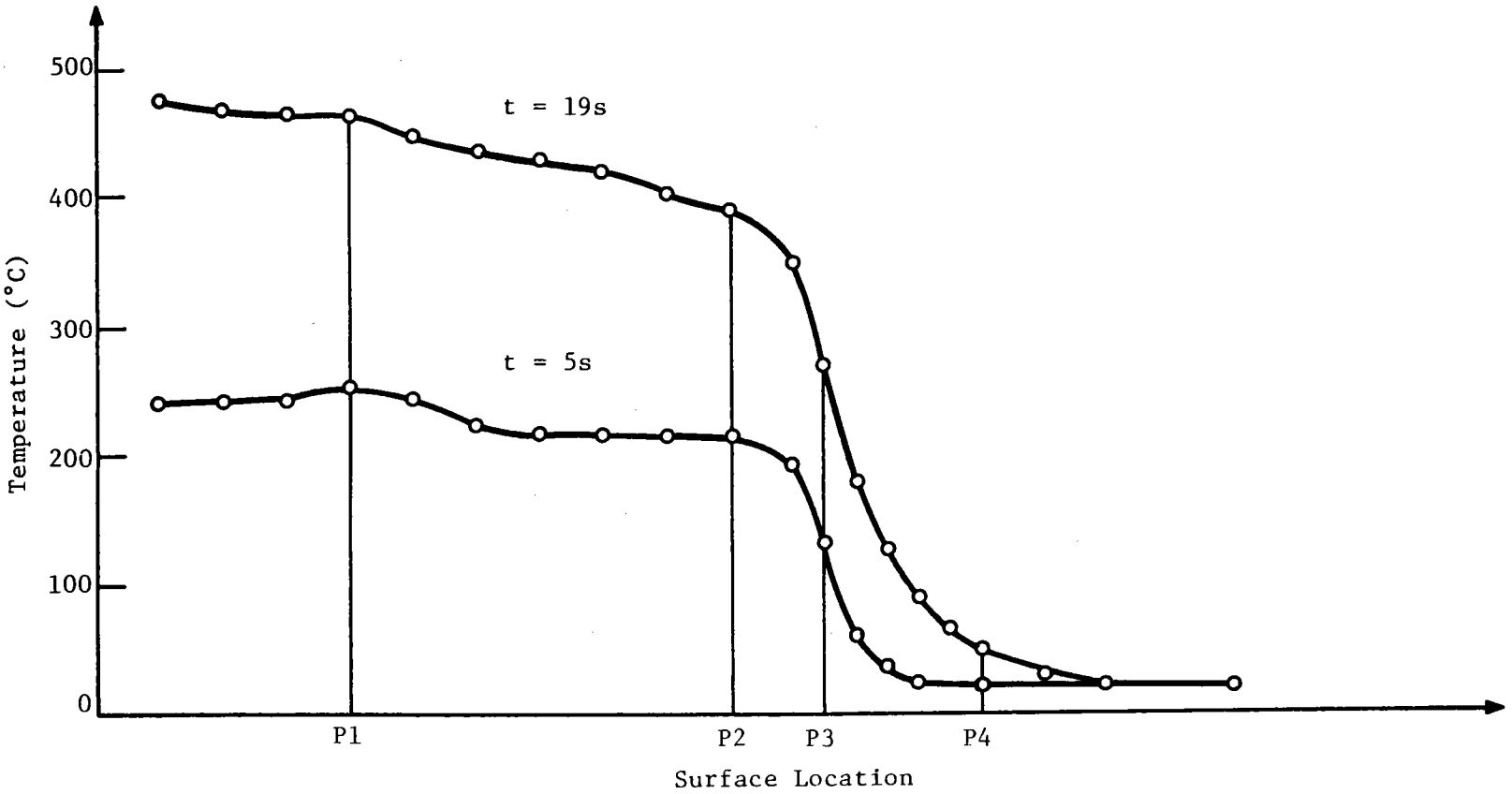

Figure 5-19 Temperature Distribution Along the Inner Surface at Different Times

factor, the number of cycles was 2×10^4. The required number of start/stop cycles in the engine is in the order of 10^4. Thus, based on this analysis, it has not been possible to verify a crack-free life in 10^4 cycles with a proper safety factor. However, the analysis is partly based on assumptions, which of course increase the uncertainty in the result. Therefore, the most important value of this analysis lays in the possibility to compare this result with the corresponding results from the Mod I and Mod I Update heaters, which have been analyzed based on the same assumptions. Such a comparison and also the uncertainties in the analyses are further discussed in the next paragraph.

Comments

The effect of thermal transients during start-up of the engine has been studied earlier in the regenerator housings of the Mod I and Upgraded Mod I. The same analysis procedure and the same assumptions have been used in all cases. This means that the results in terms of stress ranges ($\Delta\sigma$) and number of cycles to failure (N) can be compared for the different engines. The uncertainties in the comparisons are considerably less than in the absolute levels. Figure 5-23 illustrates the improvements from the thermal transient point of view for the different designs. The figure shows the increase in crack-free life expressed in number of cycles. The line N (1.0) represents the estimated number of cycles without any safety factor and N (1.5) the same but with a safety factor 1.5 on the stress. The line $N = 10^4$ indicates the requirement level. The line $\Delta\sigma$ represents the maximal stress range due to the thermal transient for the different designs. The maximal stress range in the hot end of the housings should not exceed the yield strength of the material in order to avoid creep ratcheting effects. The line σ_y indicates the yield strength of XF-818 at 400°C. In the 1983 RESD, the analysis resulted in a life prediciton very close to the requirement. Whether the requirements from the thermal transient point of view are fulfilled, is partly dependent on the uncertainties in the analysis, as noted below.

The temperature function was based on gas temperature measurements in a heater tube during a start of the Mod I engine. The gas temperature as a function of time probably looks different at a point near the regenerator matrix.

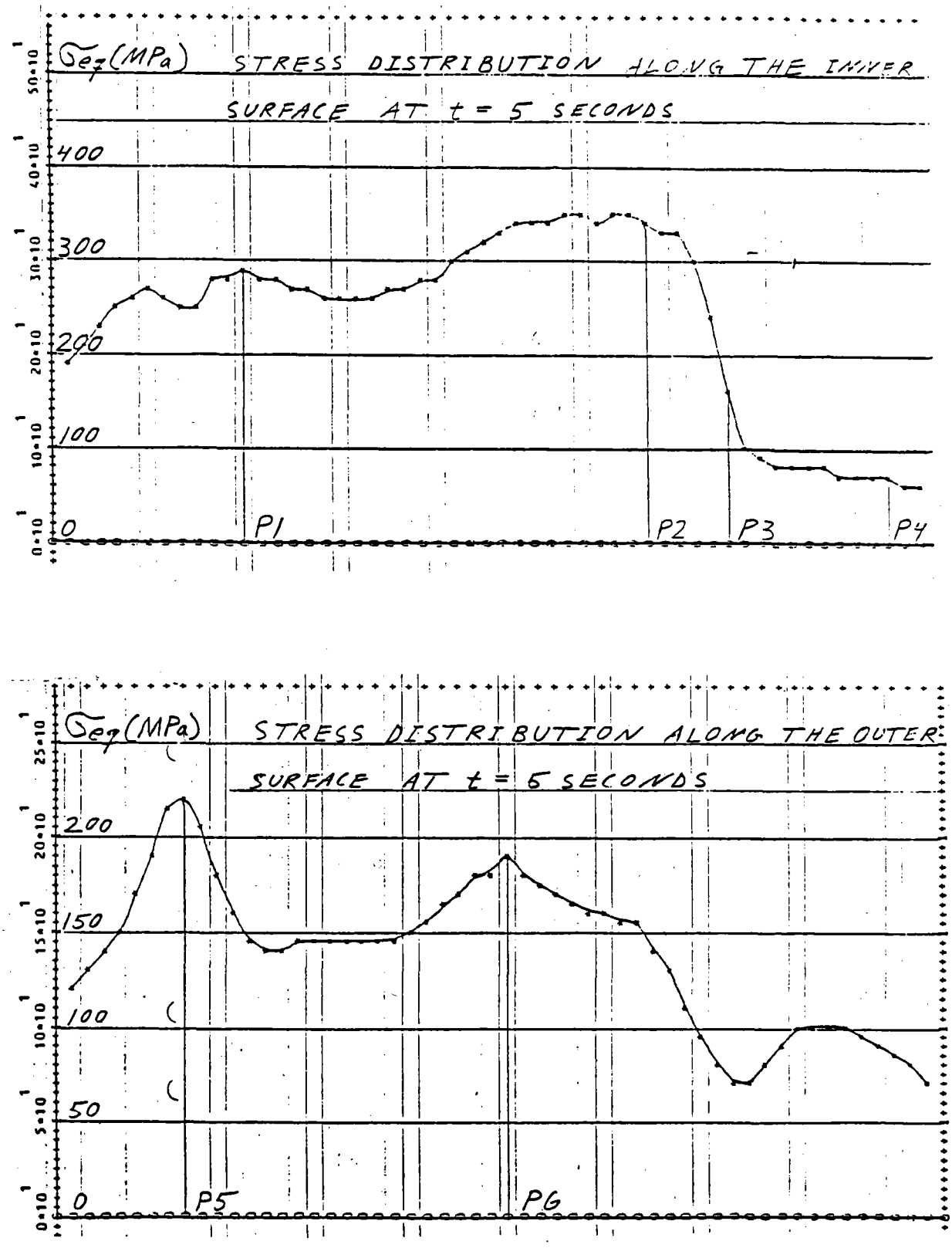

Figure 5-20 Stress Distribution After 5 Seconds

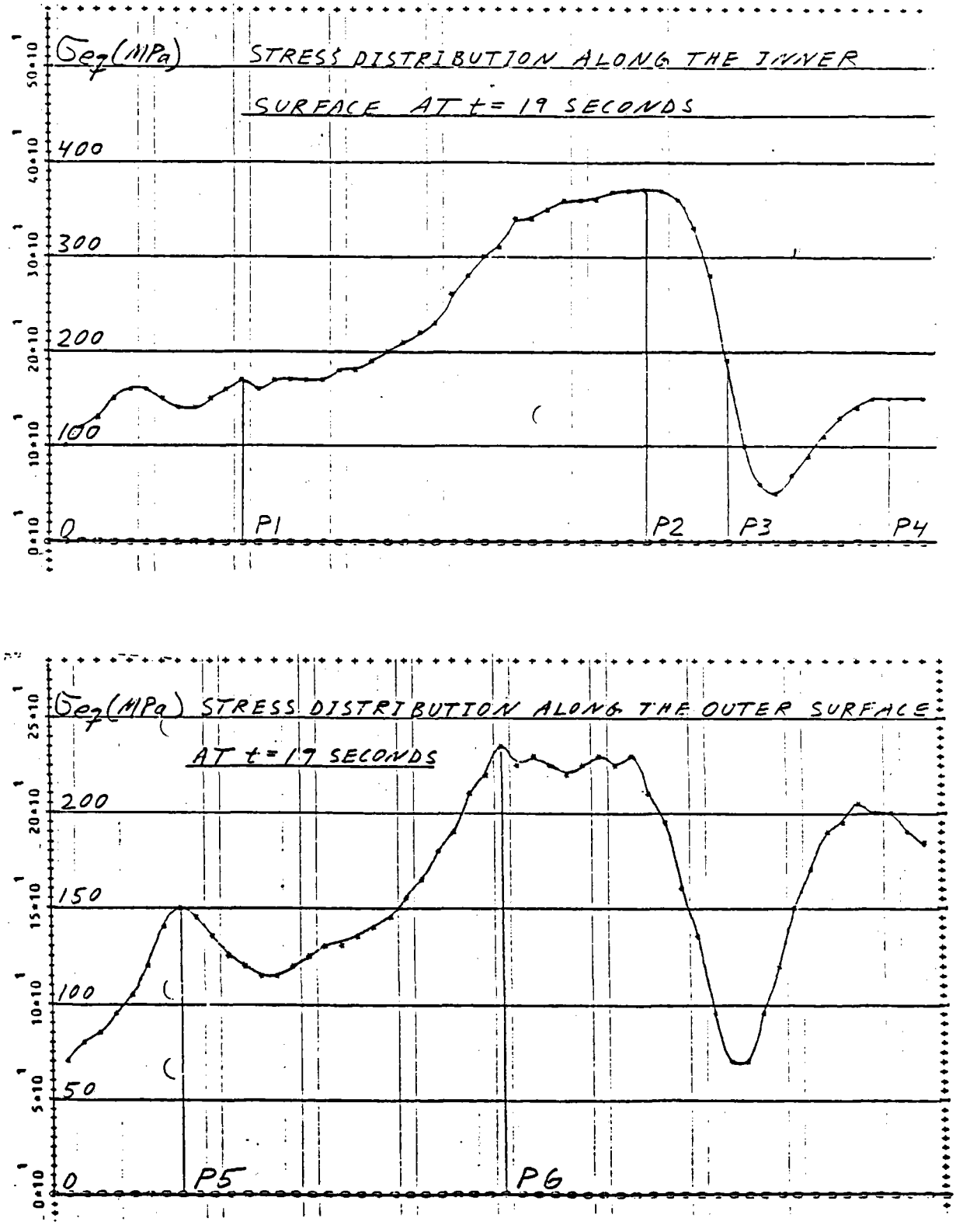

Figure 5-21 Stress Distribution After 19 Seconds

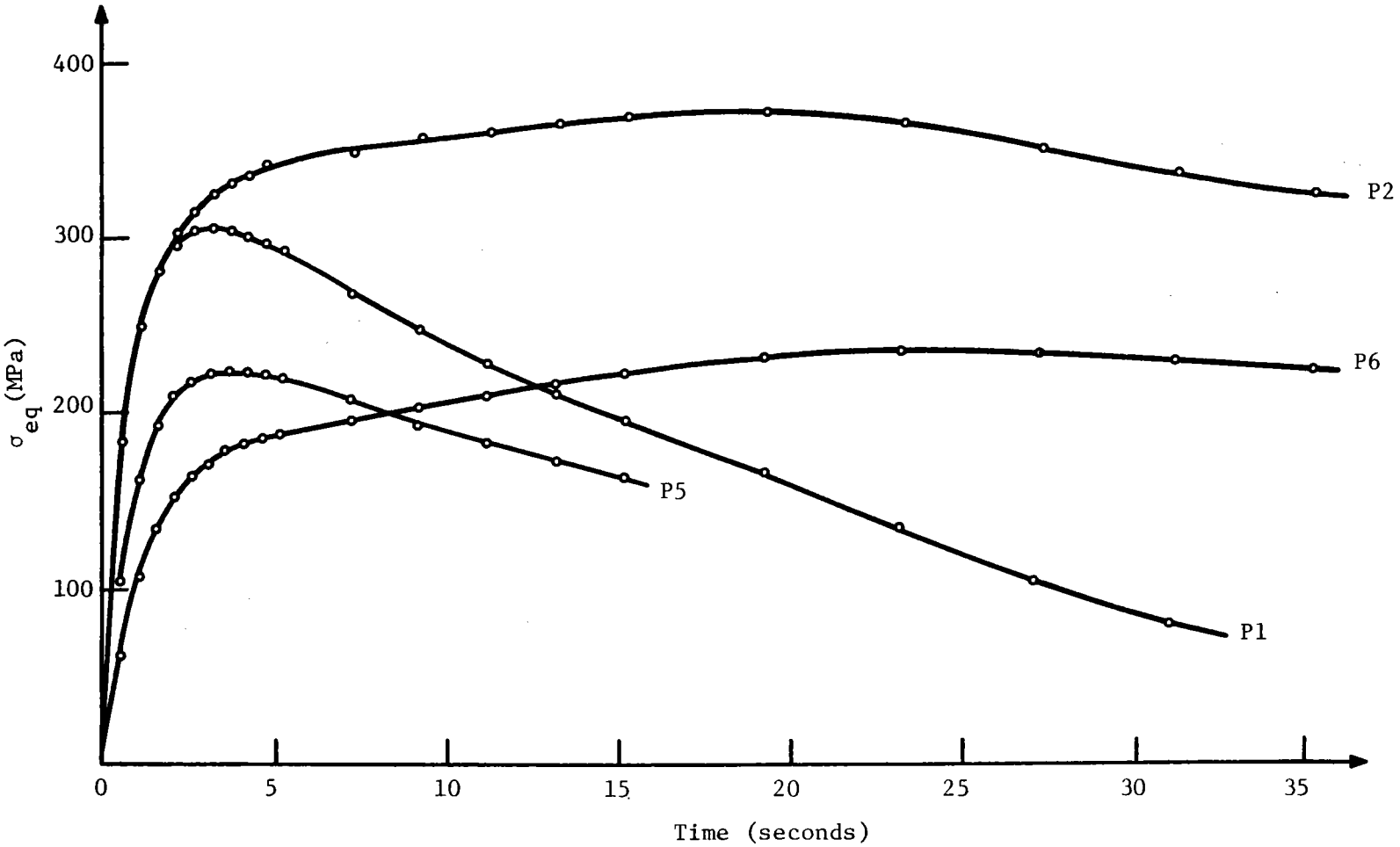

Figure 5-22 Equivalent Stress as a Function of Time for Points on the Heater Housing

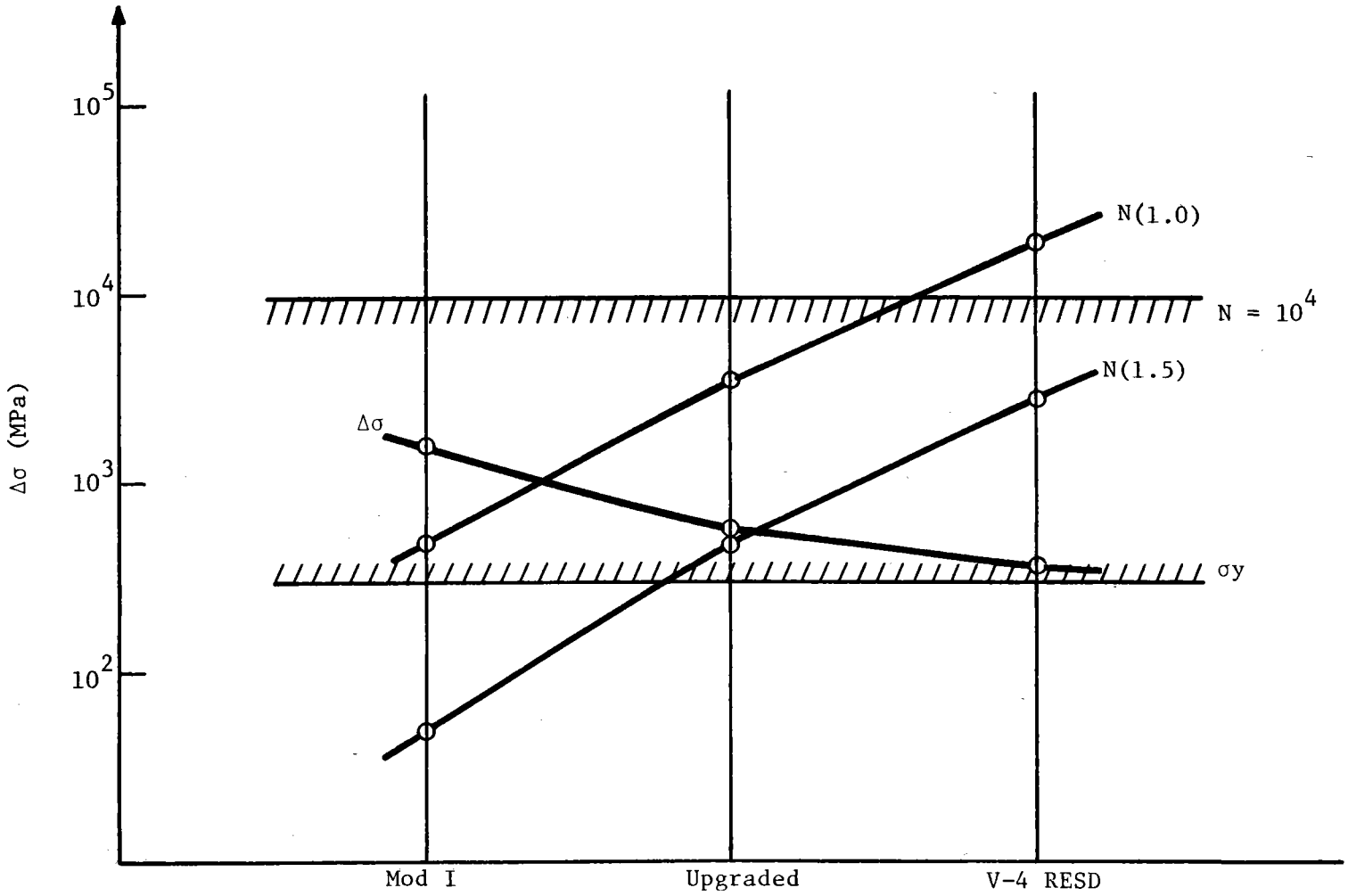

Figure 5-23 A Comparison Between Different Designs of Heater Housings Based on Life Predictions Related to Start-Up Transients

The surface heat transfer coefficient depends on pressure, speed, temperature, geometry, and so on. This means that it varies from point to point and also with time. In the analysis this coefficient was kept constant.

In the analysis model, the inner surface of the top and down to the upper surface of the regenerator matrix was exposed to the hot gas. No heat exchange between the regenerator and the pressure vessel wall was considered. This resulted in a steep axial temperature gradient in the pressure vessel during the start-up transient and the effect from the stress point of view was an increase in the stress level.

Most of the material properties used in the analysis are temperature dependent. This was not considered in the analysis, which was based on constant material properties corresponding to a mean temperature.

The analysis results, in terms of stress ranges, were compared to fatigue data of XF-818 at 800°C. However, when the maximal stress range occurred, the material temperature did not exceed 400°C. The fatigue curve was generated at a mean stress equal to zero

$$\pm \frac{\Delta\sigma}{2}$$

but the maximal stress from the analysis was compressive

$$\left(- \frac{\Delta\sigma}{2} \pm \frac{\Delta\sigma}{2} \right)$$

The fatigue curve is based on test specimens in a membrane stress condition, but the critical points in the pressure vessel have high bending stresses. The material strength properties of XF-818 were generated based on test specimens cast at Bulten-Kanthal in Sweden. Recently tested XF-818 specimens cast in the U.S. have shown higher strength properties than those cast at Bulten-Kanthal. Consequently, it seems possible to improve the strength properties of XF-818 by using a more optimal casting technique. All these material-related uncertainties work in the same direction, namely, they indicate that the predicted life time could be under-estimated.

The high compressive stresses during the thermal transient will be reduced somewhat due to the internal pressure. The primary membrane stress has a safety factor of 1.5 to the yield strength of the material. At a temperature of 400°C the yield strength of XF-818 is approximately 290 N/mm^2. This means that the maximal primary membrane stress is 193 N/mm^2 for an internal presure of 20 MPa. A starting pressure in the engine of 5 MPa gives a primary membrane stress approximately equal to 50 N/mm^2 and consequently this is a rough estimation of the reduction in the compressive stresses.

5.3 Stress Analysis of a Heater Tube During a Start-Up Transient With an Unfavorable Heat Flux Distribution

A cross section of a heater tube has been analyzed for a start-up transient with an extreme heat flux distribution around the tube. The cross section was analyzed based on the finite element method. The model is shown in Figure 5-24. Isoparametric plane strain elements were used, and for symmetry, only a half model was used. The heat flux distribution was extremely unfavorable because all heat was put into the tube from one side while the other side was thermally isolated. The heat flux was 300 kW/m^2.

Figure 5-25 shows the temperature as a function of time in some different points at the tube surface. After 10 seconds, the temperature was 800°C at one side of the tube and 670°C at the other side. This figure also shows the temperature distribution around the tube after 10 seconds.

Figure 5-26 shows the stress distribution in the tube after 10 seconds. The equivalent stress (according to von Mises Yield Criterion) is about 54 N/mm^2 in point P6. Consequently, even a transient loading condition based on an extreme heat flux distribution gives a maximum stress, which is considerably lower than the yield strength of the tube material.

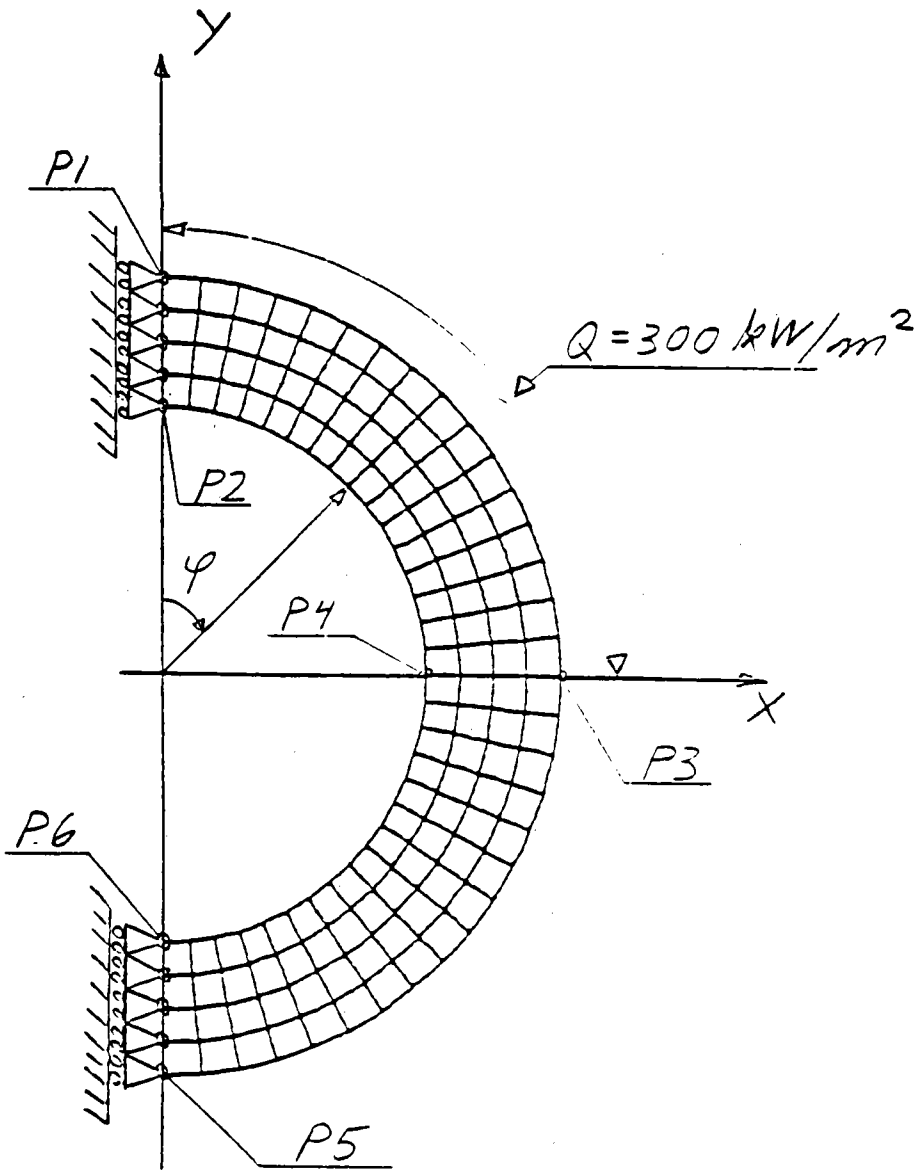

Figure 5-24 Cross Section of a Heater Tube

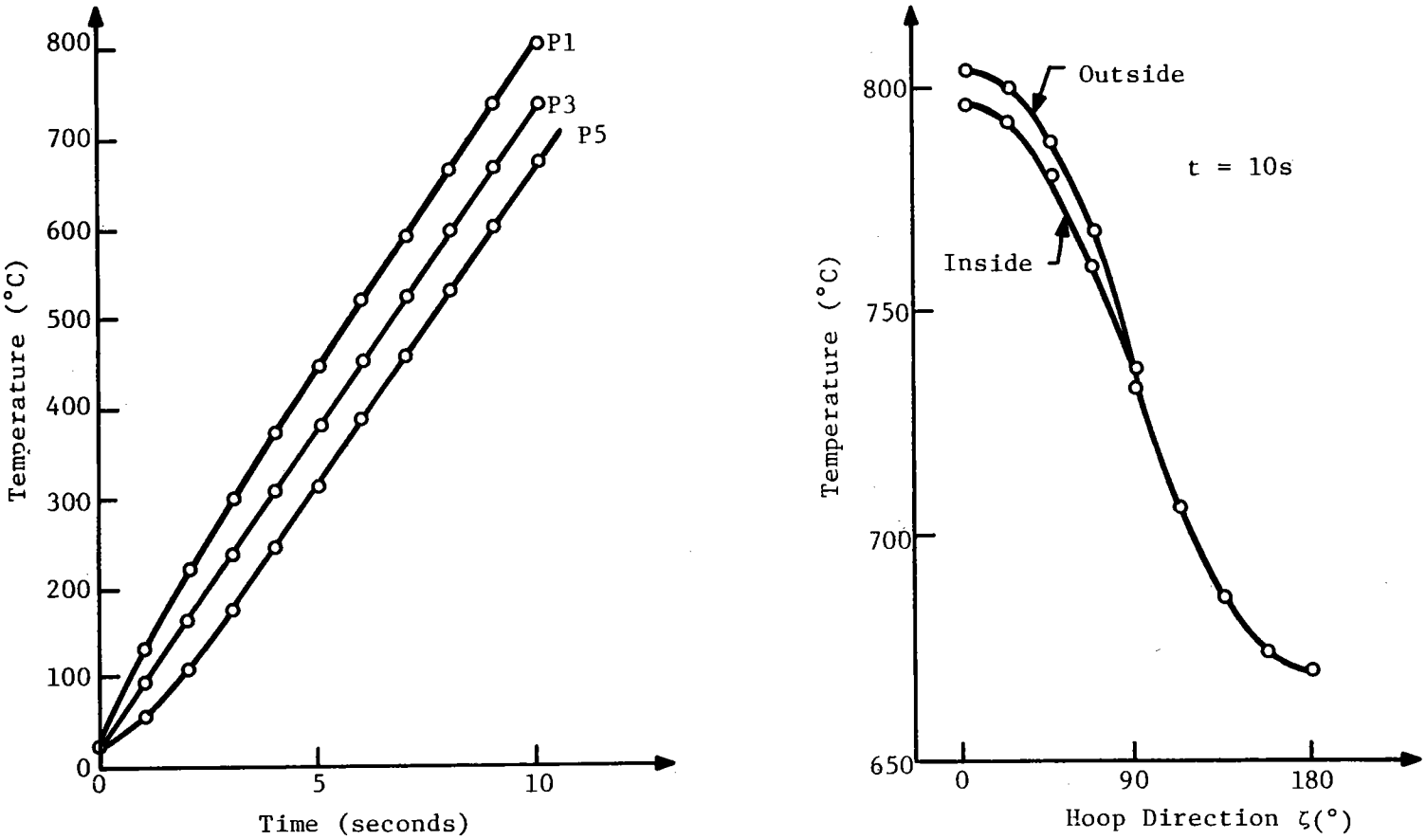

Figure 5-25 Heater Tube Temperature Distribution

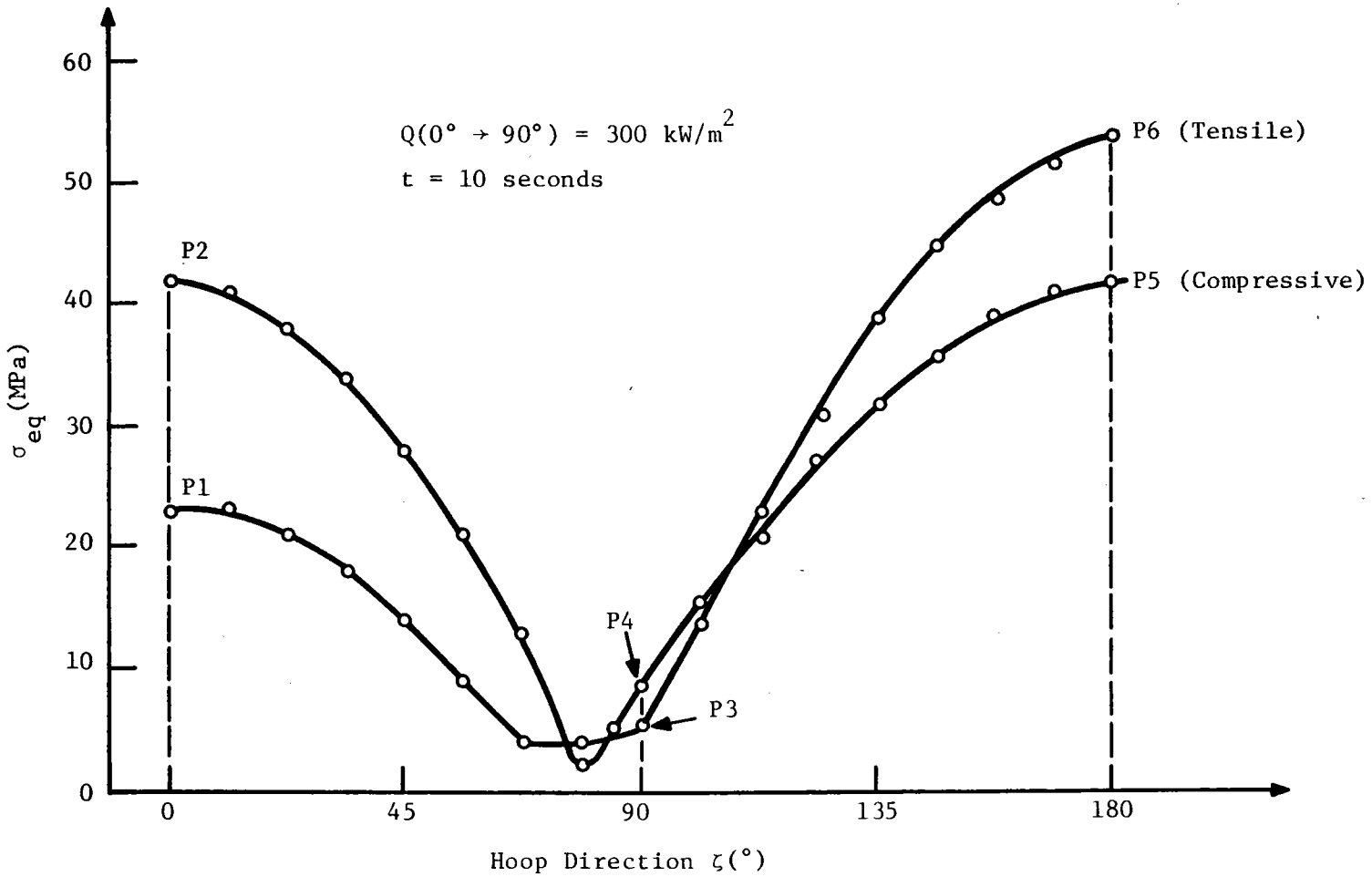

Figure 5-26 Stress Distribution in a Heater Tube

6.0 VEHICLE INSTALLATION AND AUXILIARIES

6.1 Vehicle Description

The reference vehicle is based on the (X-Body) General Motors Pontiac Phoenix currently in production. For the installation study, the current engine compartment and vehicle-mounted auxiliaries (brake, etc.) have been assumed. The X-Body uses a transversely mounted engine arrangement in a rather short (fore-aft) compartment. The engine is bolted to a transfer case/transmission casting, which wraps around and under the engine giving output shafts parallel to and behind the engine centerline. The power train unit with steering rack is mounted on a subframe that bolts to the unit body structure. Suspension is by McPherson Strut with the attendant large, tall towers for mounting.

The combination of power unit subframe, unit body rails, and suspension towers creates severe limitations on compartment width at certain levels. Maximum effective compartment width at the engine output shaft centerline is ~860 mm, of which 300 mm are occupied by the transmission cover, leaving just 560 mm from the transmission bell housing flange to the far side rail. Fore-aft spacing is also tight. At the vehicle centerline, there are ~120 mm to either side of the output shaft center between the transmission casing and front cross member. Height availability is 500 mm from converter center to hoodline. Compare these dimensions: 560 L, 240 W, 500 H to the appropriate measures for the Upgraded Mod I (540 L, 310 W, 590 H) or RESD 1981 (462 L, 310 W, 490 H). The comparable dimensions for the 1983 RESD are 530 L, 170 W, and 460 H (canted).

Installation and auxiliary arrangement studies have been completed; engine-mounted auxiliaries assumed for the studies are:

- Variable Displacement Air Pump
- Alternator
- Air Conditioning Compressor
- Power Steering Pump
- Starter/Upstart Motor Combination

- Water Pump
- Oil pump
- Atomizer Air Compressor
- Hydrogen Compressor.

Also, there are vehicle-mounted units consisting of:

- Hydrodgen Storage Bottle (4 liter)
- Power Brake Assembly
- Electronics Package
- Cooling Fan and Radiator.

The larger-than-standard radiator used for the 1981 RESD is also used in the 1983 RESD. The objective of the studies is to provide a possible installation arrangement, including the auxiliaries above, with minimal modifications to non-Stirling components. 1981 RESD required moving the radiator 25 mm forward, and the front cross member 90 mm forward. Also, an interference with the upper bell housing over the torque converter existed. Auxiliary arrangements and drives have been designed for maximum clearance and serviceability within the package constraints imposed.

6.2 1983 RESD Installation

6.2.1 Side View (Engine Front)

Figure 6-1 shows the installation of the 1983 RESD in the engine compartment of a General Motors X-Body vehicle. In this view from the engine front, the arrangement of auxiliaries is best seen. The hydrogen compressor is driven directly from its own throw on the crankshaft, and its bore is directly cast into the engine block. All other major auxiliaries on the engine are driven by a common poly-V ribbed serpentine belt. The main sheave diameter is 90 mm. The water pump is bolted to the block face and driven on the back of the belt through an 80-mm wheel. The power-steering (P/S) pump is rib side driven through an 80-mm wheel, but note that the unit is installed on the far side of the belt plane from the engine. This does not, however, require any

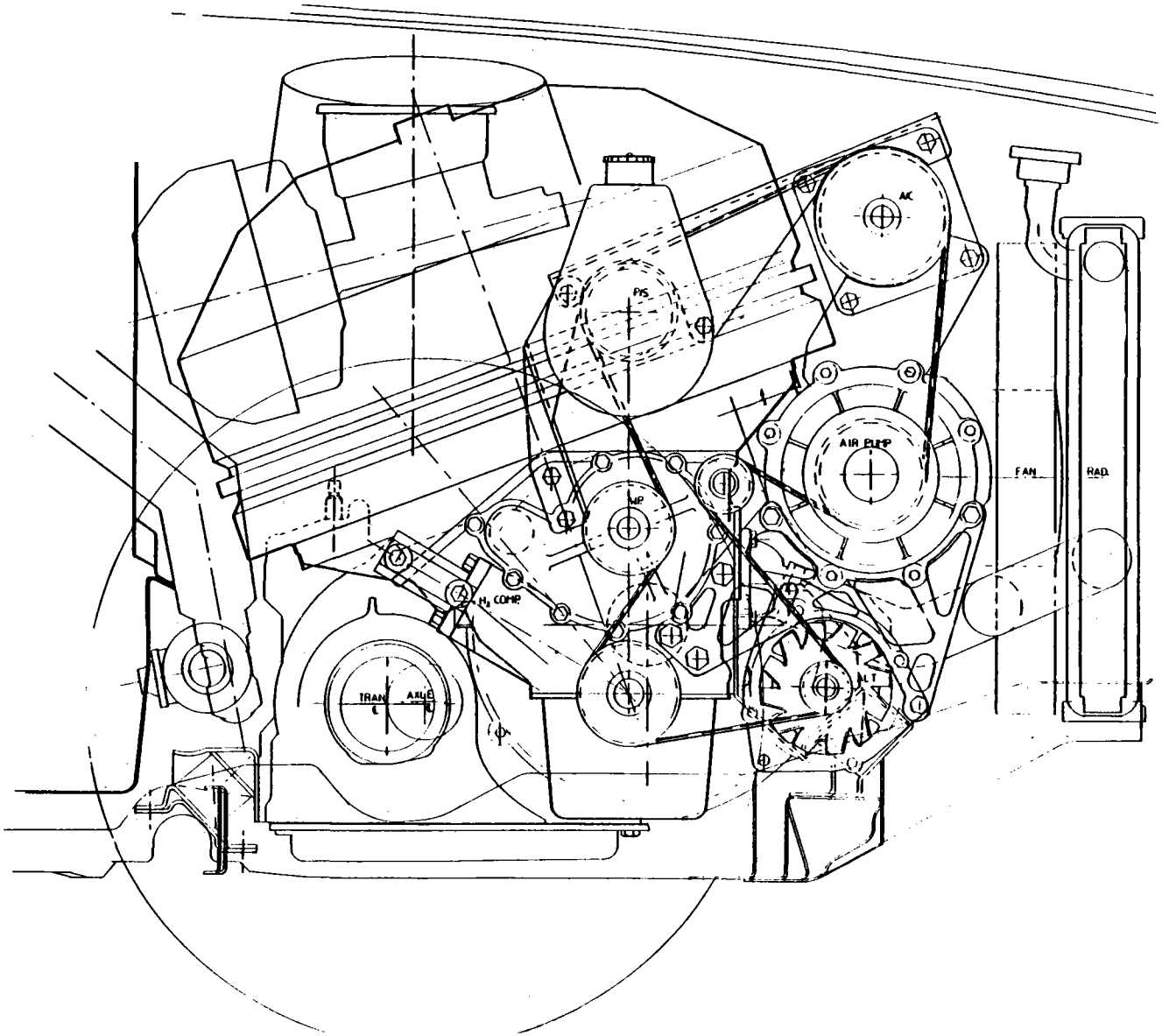

Figure 6-1 1983 RESD Installation Side View

disassembly for belt changing, as the pump support brackets are all external to the belt loop.

The air-conditioning (A/C) compressor is mounted to the air pump and triangulated to the steering pump for rigidity. It is driven by the rib side of the belt on a 120 mm wheel. Note that the optional accessories (P/S and A/C) are packaged uppermost, leaving a compact arrangement for the basic assembly. Note also that eliminating P/S or A/C does not require altering the belt path (though a shorter belt is obviously required), but removing both does require an additional idler/tensioner that can mount to P/S bracket bolts above the water pump.

The air pump is mounted directly to the block just under the external heat system where it provides inlet air to the circular manifold at two locations 180° apart (at each end of the engine). These feed locations correspond to pinch points in the manifold where the heater head housings of the end cylinders (1 and 3) come close to the manifold. These local pinches are then used as diffuser guides to minimize locally high airflow at the inlets. The air pump is driven at engine speed on the rib side of the belt through a 90 mm pulley. The alternator is mounted to block and air pump through a common cast alloy bracket for maximum rigidity and bearing life. The wheel diameter is 40 mm. A tensioner/idler assembly is required for the poly-rib belt. This function is combined with the atomizer air compressor and mounted directly to the block between water and air pumps. The wheel diameter is 45 mm, giving a high speed to the compressor adequate even at idle.

To meet power requirements for these drives, belt sizing was done according to minimum requirements from DAYCO, belt manufacturers. The unit "degree ribs" is used to describe the product of wrap angle and belt width. This parameter is a measure of power capacity. Using the belt path shown in Figure 6-1, the minimum belt width is calculated to be 9 ribs (see Table 6-1). A standard, 10-rib 24-mm wide belt is shown. From Figure 6-1, no interferences with existing compartment or components are indicated.

TABLE 6-1

BELT CHARACTERISTICS

Auxiliary	O-Rib Required	Wrap Shown	Minimum Rib
(Crankshaft)	1080 Rib Side	120°	9
Water Pump	450 Flat Side	60°	9
Power Steering	510 Rib Side	90°	6
Air Conditioning	540 Rib Side	120°	5
Air Pump	540 Rib Side	110°	5
Alternator (55A)	480 Rib Side	120°	4
Alternator (65A)	660 Rib Side	120°	5

6.2.2 Top View

Figure 6-2 shows the 1983 RESD installation from above. This view clearly shows the offside location of the P/S pump, the location of the hydrogen bottle, and the coolant hose connections; the enlargement of the radiator is also shown. The electric fan is somewhat larger in diameter and depth than is standard for IC engines, so a larger motor is fitted. Peak power requirements are estimated to 3 kW (4.0 hp) for the fan at peak engine power with no ram air. A high-speed motor with reduction is used to provide this power at low weight. No interferences are found in this view.

6.2.3 Front View (Engine Side)

Figure 6-3 shows the 1983 RESD installation as viewed through the radiator in front. Overall package clearance is very clearly shown here. No loss in ground clearance occurs; no frame rail interference is indicated; no suspension interference occurs; no hood interference occurs.

6.2.4 Mock-Up

During the value-engineering follow-up to the downsized RESD study, a mock-up of the 1983 engine was constructed and fitted to the X-Body transaxle (see Figure 6-4). It was through this exercise that the packaging concepts in the 1983 RESD installation were developed, including auxiliary arranagement, feasibility of canted installation, and transmission interface.

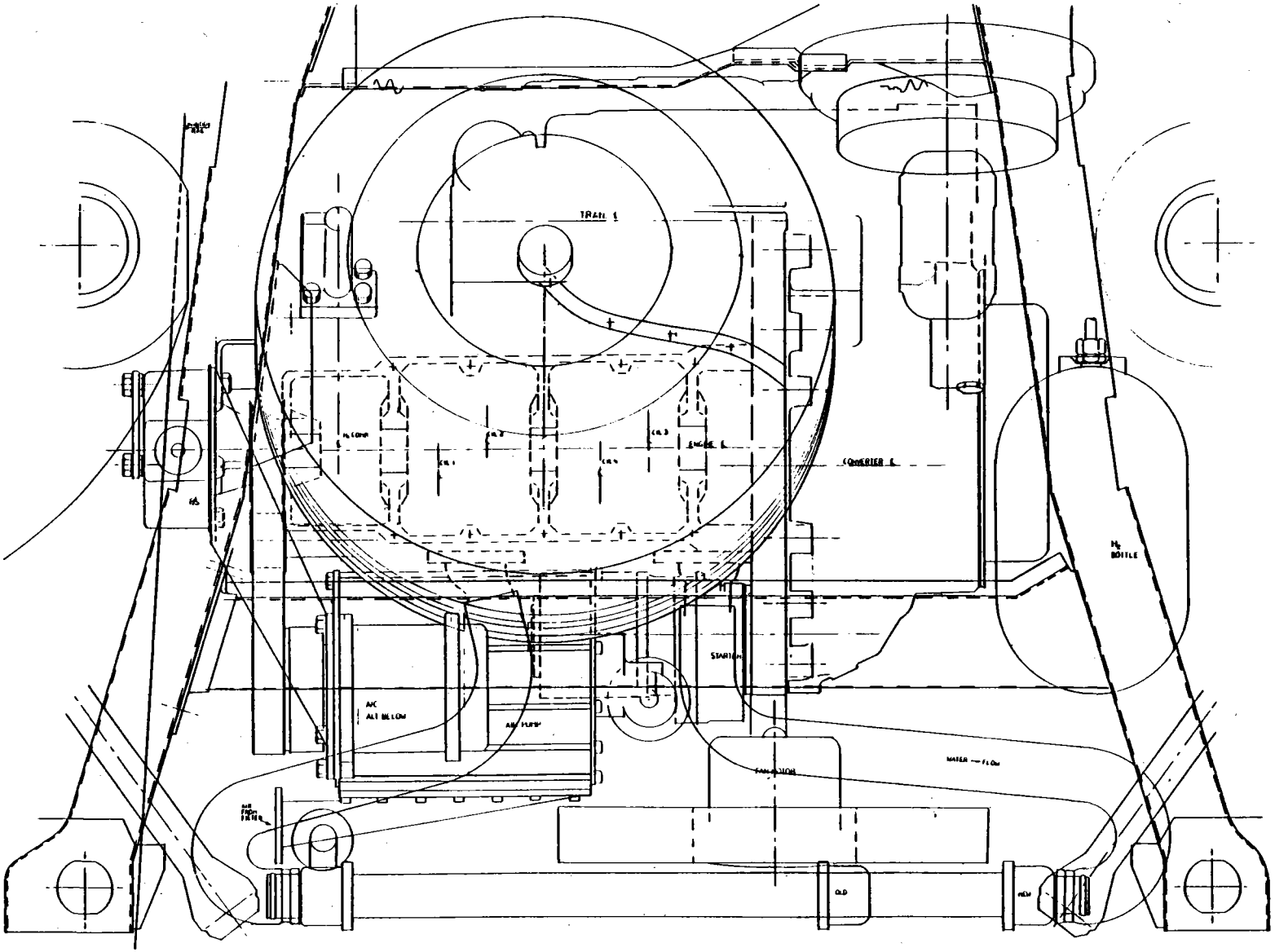

Figure 6-2 1983 RESD Installation Top View

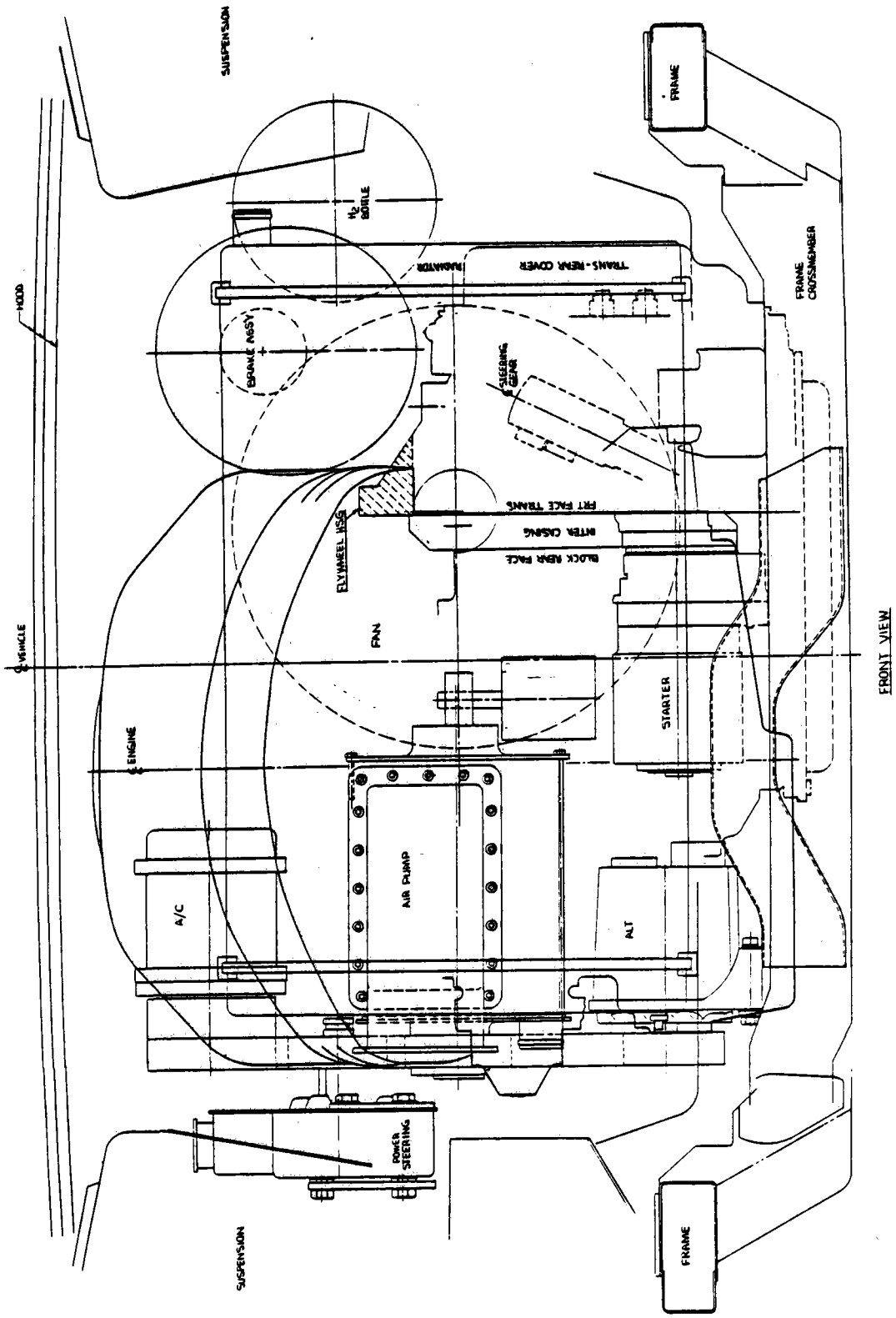

Figure 6-3 1983 RESD Installation Front View

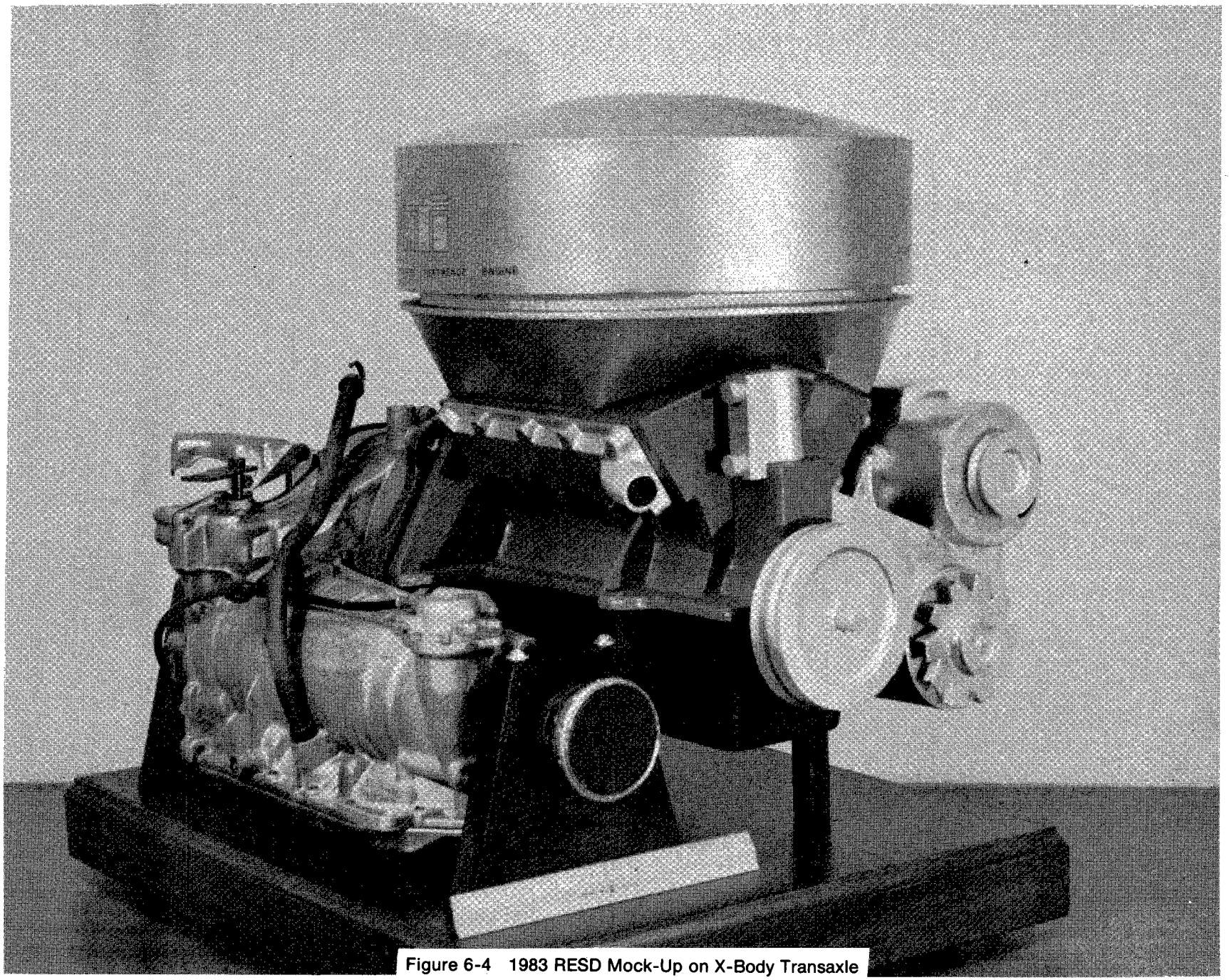

Figure 6-4 1983 RESD Mock-Up on X-Body Transaxle

7.0 ENGINE PERFORMANCE

In this section, the optimization and thermodynamic analysis of the 1983 RESD is shown in comparison with the 1981 RESD and the Mod 1.

7.1 Code Description, Validation and Upgrade

7.1.1 Stirling Code Validation

The Stirling engine code has been upgraded via an analytical follow-up of the measured Mod I performance. This work covered test results from both BSE and SES separate drive unit motoring tests; hence, drive unit friction, Stirling-cycle performance, and EHS performance were subjected to the analysis. Correlation between measured and calculated performance together with Stirling thermodynamic analysis lead to good agreement between calculated and measured performance after some updating of code and input. In the 1983 RESD analysis this upgraded code and standard input set-up is used.

7.1.2 Piston Ring Leakage

In the predictions used for the 1981 RESD study (Ref. 1) no piston ring leakage was explicitly included in the analysis due to the lack of data. Now this effect is included and its level is a result of the Mod I correlations. This causes the engine efficiency, especially at low speeds, to decrease relative to the 1981 RESD predictions, thus increasing the speed for maximum efficiency.

7.1.3 Thermal Hysteresis

Modelling of the thermal hysteresis in the dome gap and some other volumes has been improved, giving a truer response on certain geometric changes.

7.1.4 Tests and Analysis of Reference Engine Regenerators

Smaller regenerators, sized according to previous RESD optimizations, were tested in a P-40 engine. Test results indicate that these smaller, and hence cheaper, regenerators are acceptable in this typical part-load application.

7.1.5 Heat Conduction Loss Through an Annular Partition Wall

Some analytical effort has been devoted to this problem. The axial temperature profile on the cylinder side of this wall has been estimated. Once this temperature profile is given, the loss can be calculated. Thermodynamic analysis, also by means of third-order Stirling code simulations, has been done in order to achieve the performance impact from a certain heat energy dissipation pattern into the regenerator area. Also, results from P-40R tests have been analyzed. Considerations concerning the extent to which the dome gap can prevent this heat dissipation have been made. As a result of this work, an estimate of possible radial heat conduction loss was made; however, a more precise thermodynamic prediction of this loss requires more work. It is also recommended that the P-40R engine be tested with different types of partition walls before the final design is frozen.

7.2 Optimization and Component Performance

7.2.1 Operating Conditions

Working gas:	Hydrogen
Maximum working gas mean pressure:	15 MPa
Maximum engine speed:	4000 rpm
Heater tube outer skin temperature:	820°C
Coolant top tank temperature:	50°C
Rated maximum SES power:	60 kW (80 hp)
Optimization part-load point:	12 kW (16 hp) @ 2000 rpm

7.2.2 External Heat System (EHS)

The external heat system uses the sonic fuel nozzle system. The CGR combustor system is used, but a ceramic preheater replaces the former metallic preheater.

7.2.3 Auxiliaries

The SES is equipped with the following auxiliaries, as far as the power load is concerned; together they represent the auxiliary power consumption:

Auxiliary	Power Consumption
Hydrogen Compressor	Figure 7-1
Burner Blower	Figure 7-2
Sonotek Nozzle	30 Watts
Alternator	Figure 7-3
Cooling Water Pump	Figure 7-4
V-Belt Losses, not accounted for elsewhere	Figure 7-5

The lubricating oil pump is from now on included in the engine friction for practical reasons.

7.2.4 Engine Friction

In the analytical model, the engine friction losses emanate from:

- Piston rings
- Piston rod seals
- Drive unit.

The drive unit, in turn, consists of:

- Bearings
- Crossheads
- Synchronizing/step-up gear
- Oil pump
- Oil seals.

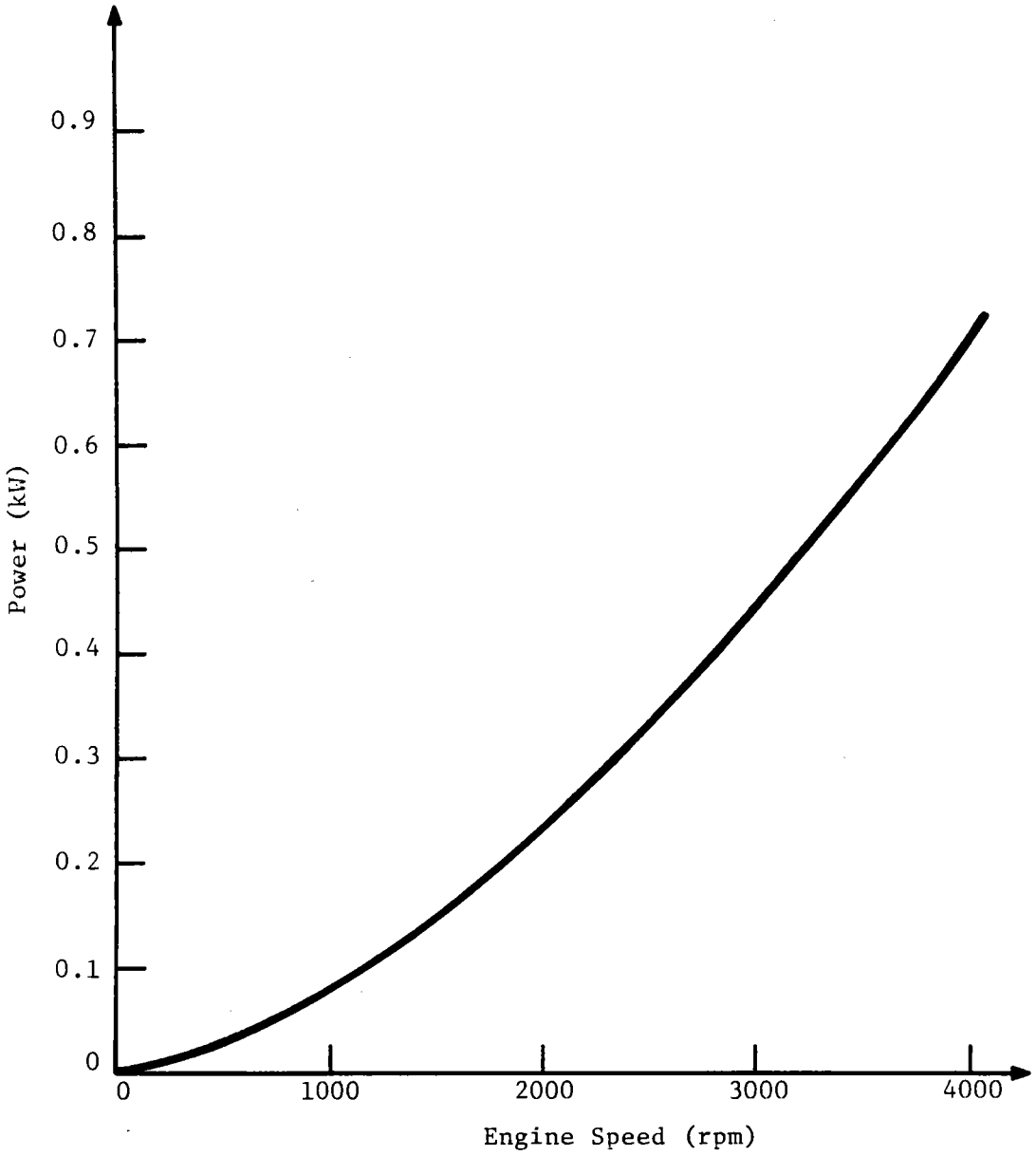

Figure 7-1 RESD Working Gas Compressor Power Consumption versus Engine Speed (Comp. Inactive)

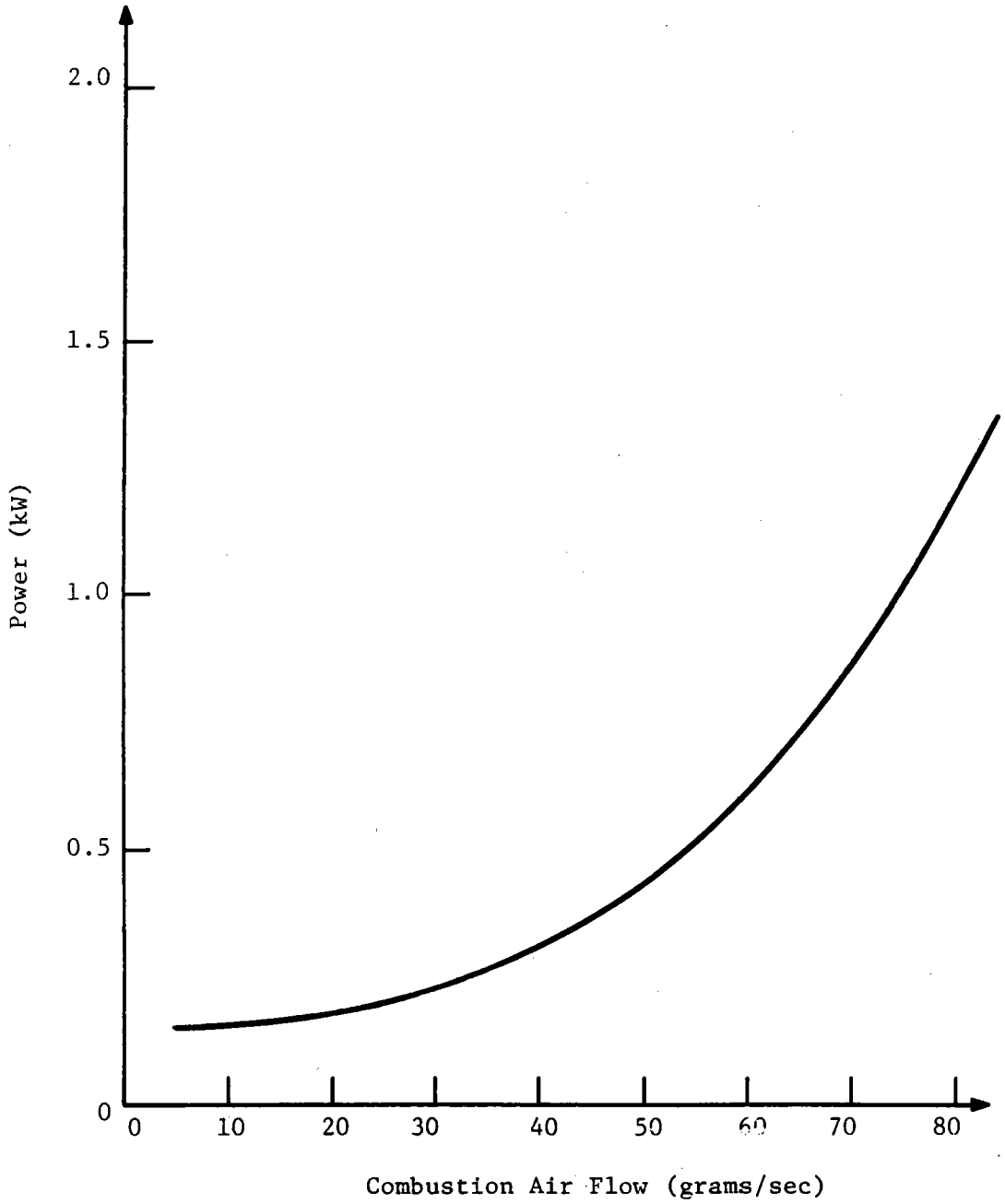

Figure 7-2 RESD Blower Power Consumption versus Combustion Air Flow Rate

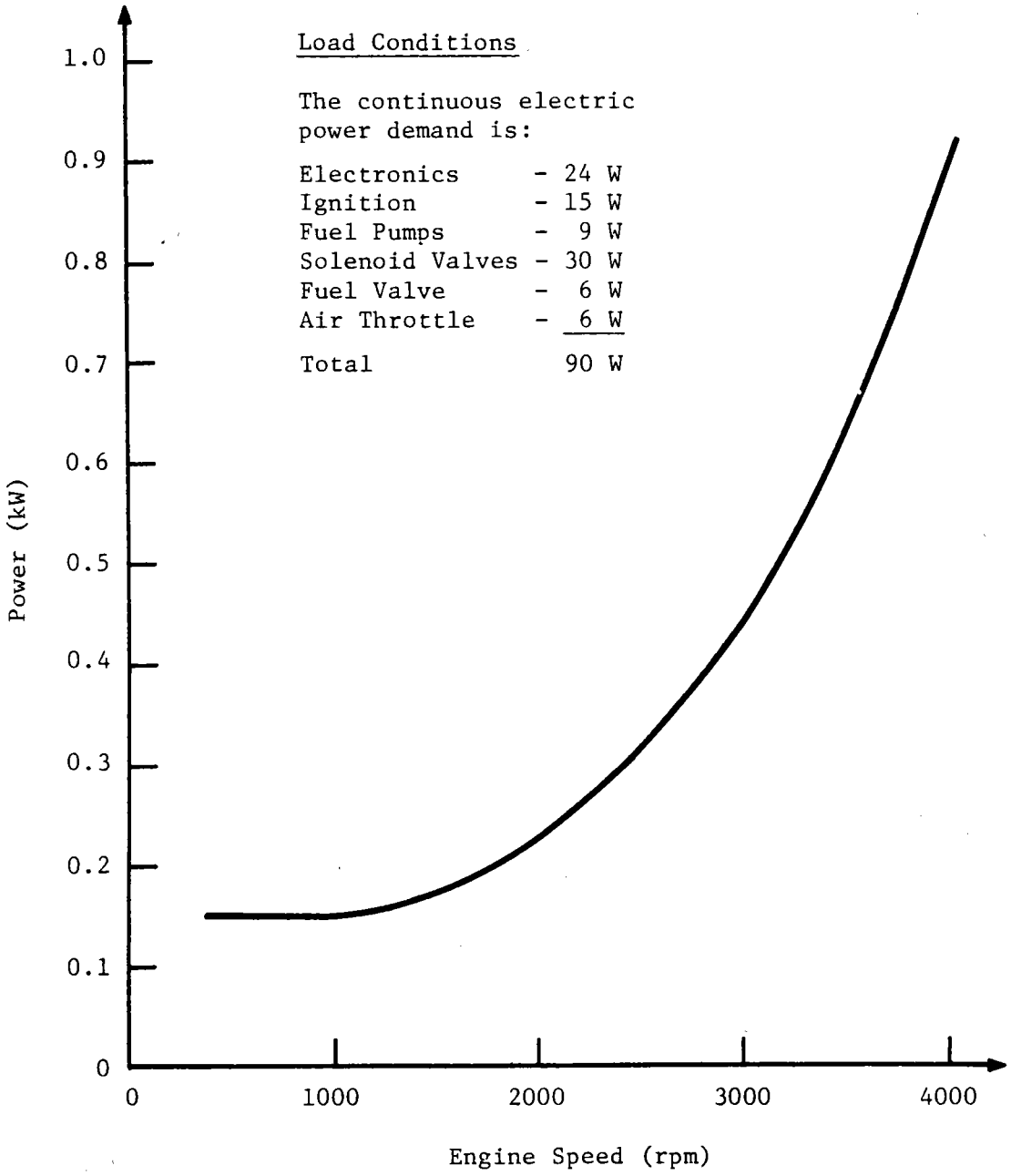

Figure 7-3 RESD Alternator Power Consumption versus Engine Speed

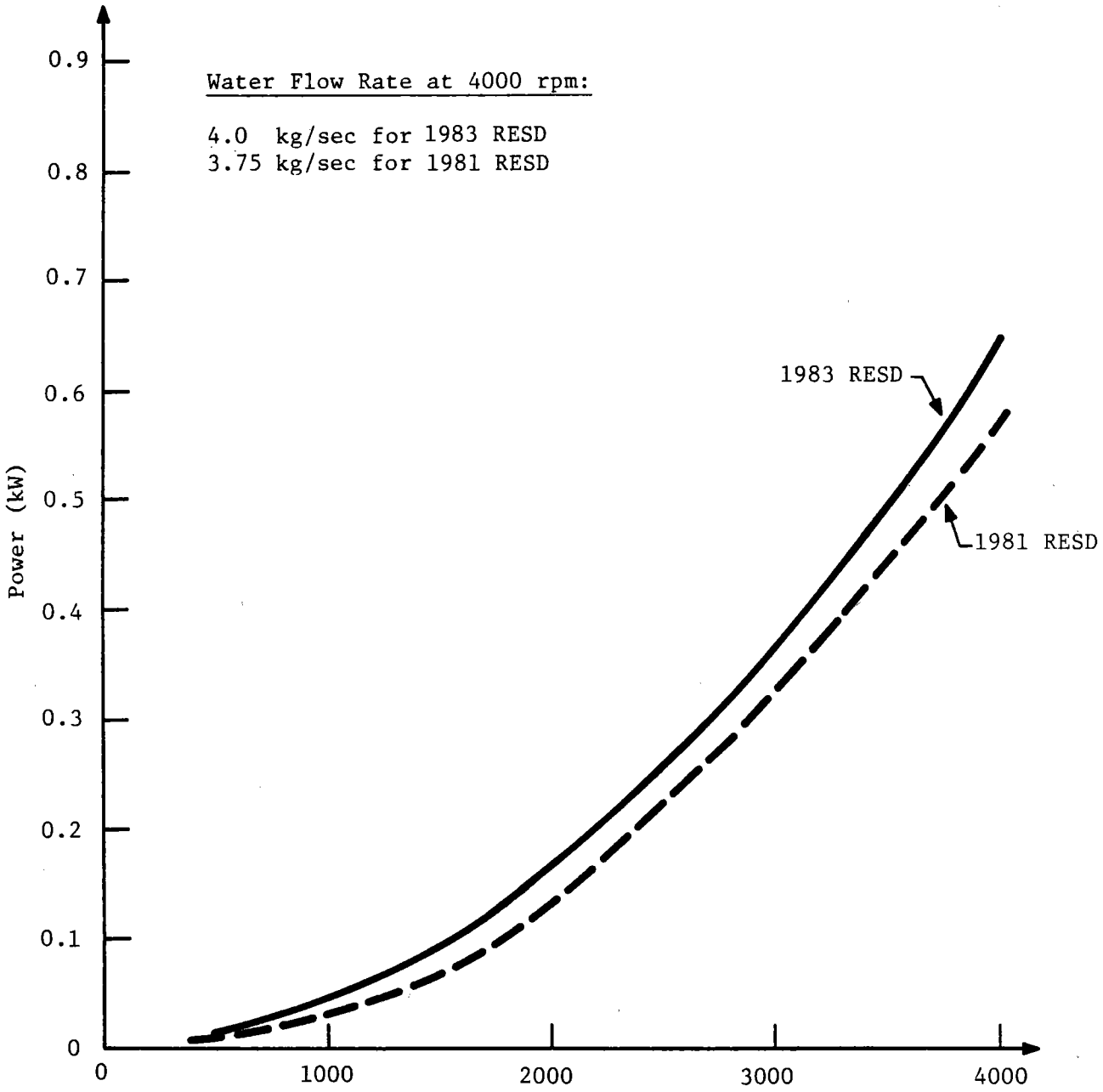

Figure 7-4 RESD Water Pump Power Consumption versus Engine Speed

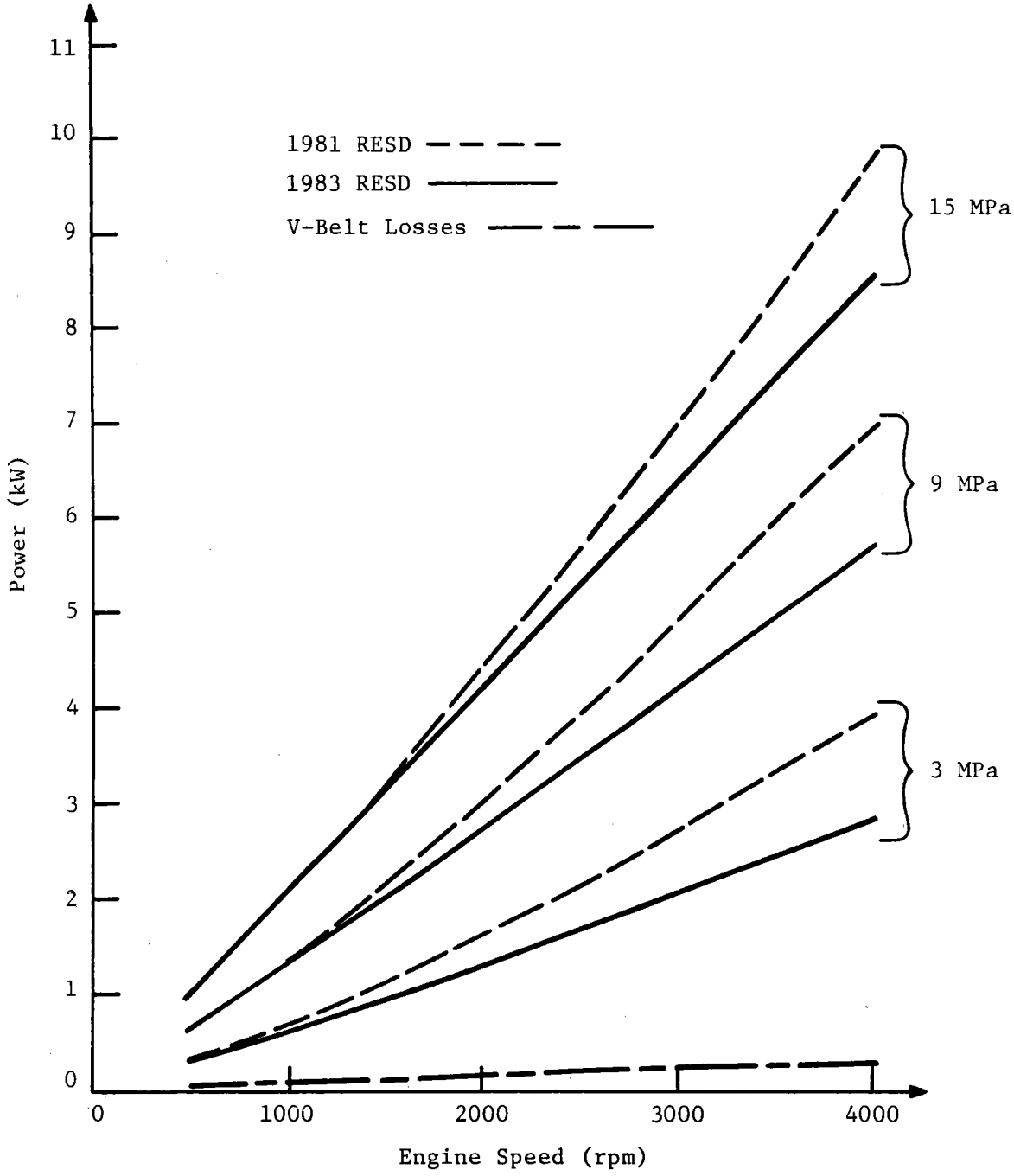

Figure 7-5 RESD Friction and V-Belt Losses versus Engine Speed at 3, 9, and 15 MPa Mean Pressure (Lubricating Oil Shaft Seals Included in the Friction)

Bearings

The 1983 RESD concept uses rolling-element bearings, similar to the drive unit of an Upgraded Mod I. The friction power consumption of these bearings is calculated by means of data given in the SKF a bearing catalogue.

7.2.5 Optimization Features and Conditions

The following list of items present the features and conditions associated with optimization:

- Optimization operating points as previously described in Section 7.2.1
- The optimization function used is vehicle mileage. The optimization defines engine geometry for highest mileage; the effect of cold start penalty is included
- External heat system efficiency versus fuel flow according to Figure 7-6. Lambda schedule according to Figure 7-7.
- Auxiliary load characteristics according to Figures 7-1 through 7-5, the water pump power being a function of actual cooler flow resistance.
- Friction losses calculated for the rolling-element bearing dimensions and friction being a function of calculated piston forces.
- Piston ring leakage calculated for a leakage gap deducted for the Mod I, which means $\geq$1.5 kW ($\geq$2.0 hp) at 15-MPa mean pressure.
- Cylinder/regenerator housing wall thicknesses calculated in proportion to housing diameter, with the proportionality constant being design dependent, according to FEM analysis.

- Piston stroke fixed to 30 mm.

General Considerations

The partition wall is assumed to consist of an inner layer of 3-mm partially stabilized zirconia oxide (heat conductivity 2.5 W/m°C) and an outer shell of

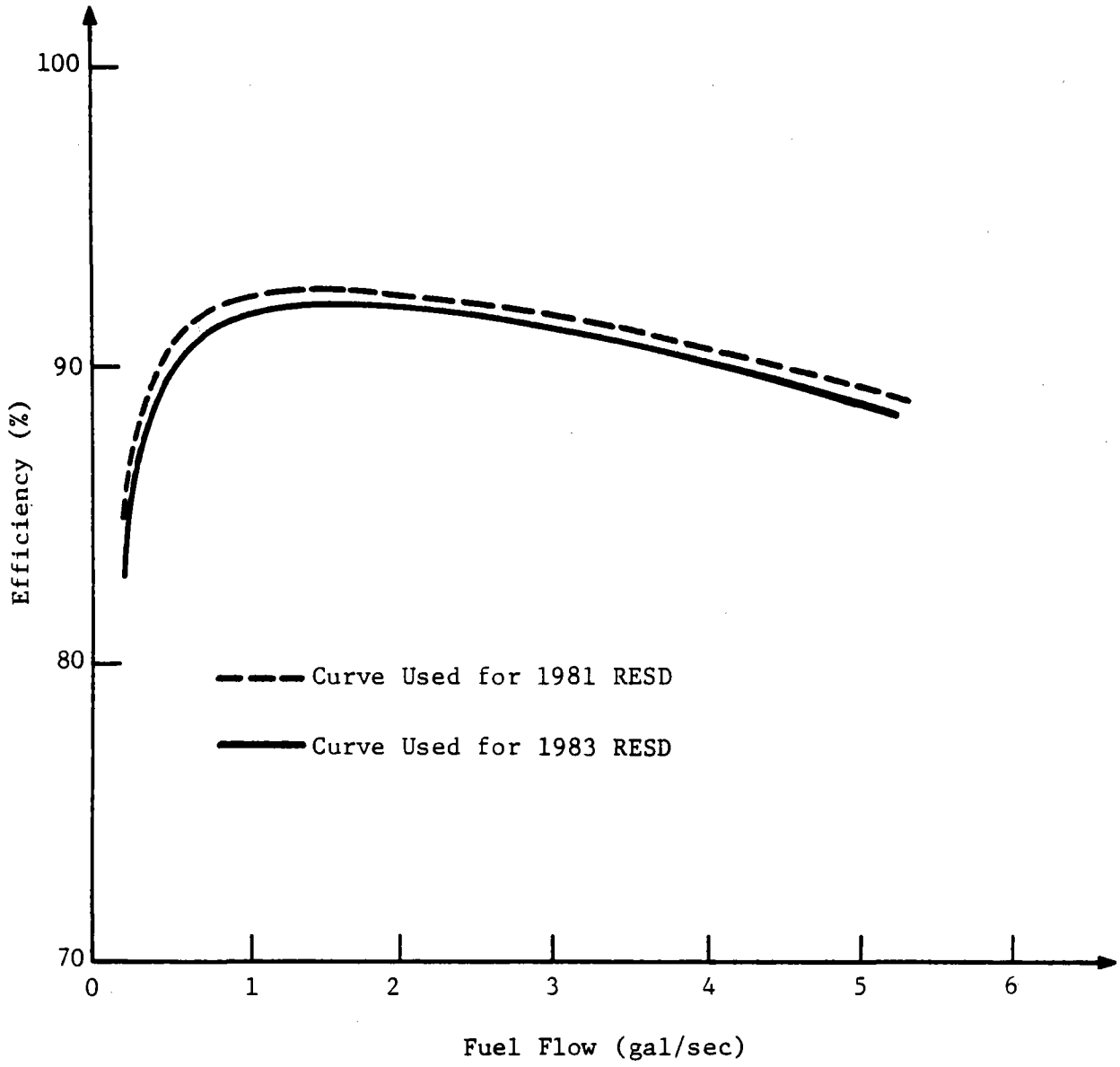

Figure 7-6 RESD External Heat System Efficiency versus Fuel Flow

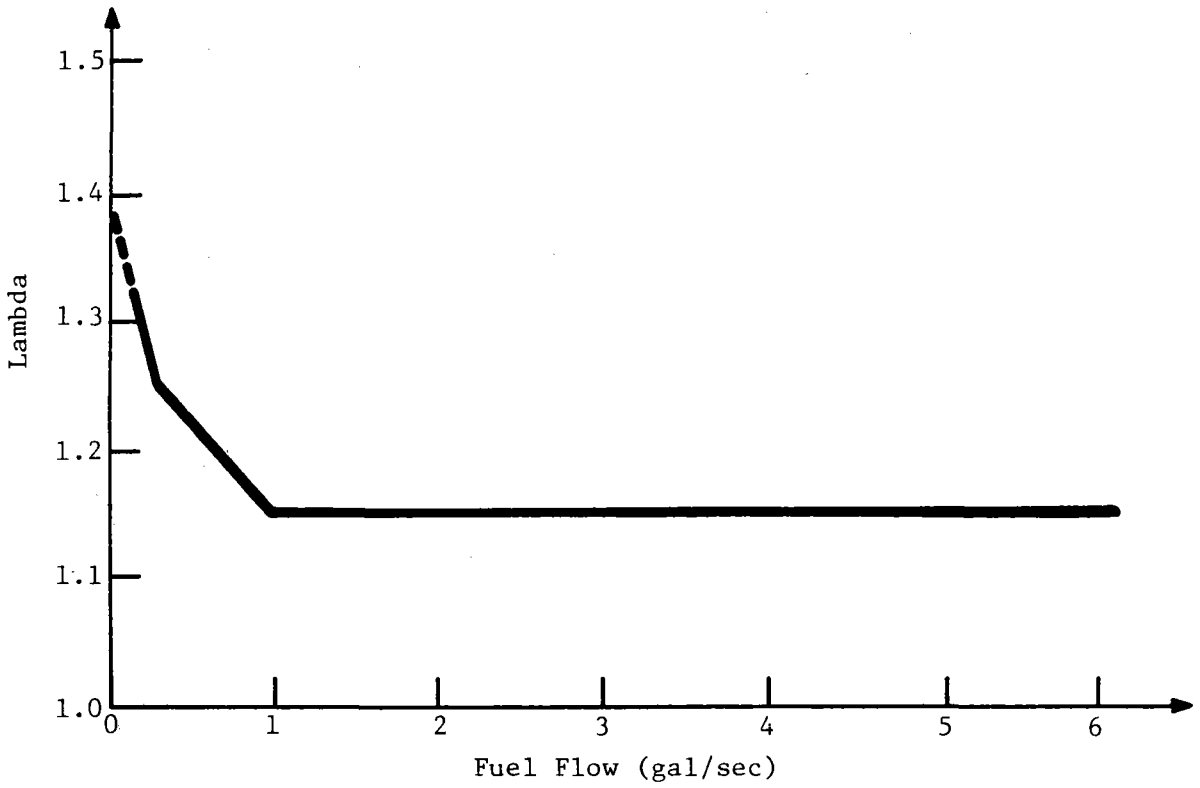

Figure 7-7 RESD Lambda versus Fuel Flow

1-mm stainless steel. Radial heat conduction loss through this wall (from cylinder to regenerator) has been assumed to be 0.25 kW (0.33 hp) per cycle, independent of the engine load.

The impact of the working gas flow distribution through the regenerator due to the manifold effect from the annular duct under the cooler has been included in the optimization code. Hence, the cross section of this duct directly affects the calculated regenerator efficiency.

7.3 Optimization Results

7.3.1 Engine Presentation

After several optimization runs, the work resulted in the development of the 1983 RESD with sequence number 717-00 (1983AR).

The sequence number of the 1981 RESD engine is sequence number 344-00. The same engine, re-evaluated with the upgraded code and standard input set-up, is denoted as the Updated RESD.

The performance of the 1983 RESD compared to the original 1981 RESD and the reevaluated 1981 RESD is shown on Table 7-1. Figures 7-8 and 7-9 graphically present engine performance for the 1983 RESD and the original 1981 RESD.

TABLE 7-1

PERFORMANCE OF OPTIMIZED ENGINES

(Power in kW, Efficiency in %, Speed in rpm)

Operating Point	Optimization		
	Old 344-00	Updated 344-00	V-4 AR 719-00
Full Load Point (p = 15 MPa, n = 4000 rpm)			
Indicated power	73.3	79.4	69.8
Friction	9.8	9.8	6.3
Auxiliaries	3.4	3.6	3.4
Net power	60.1	66.0	60.2
Ext. heat system efficiency	90.5	90.2	90.3
Net efficiency	34.2	35.6	34.6
Part Load Point (P = 12 kW, n = 2000 rpm)			
Indicated power	14.9	14.8	14.3
Friction	2.1	2.0	1.4
Auxiliaries	0.8	0.8	0.9
Net power	12.0	12.0	12.0
Ext. heat system efficiency	91.7	91.7	92.3
Net efficiency	37.6	37.6	37.3
Heat conduction loss*	1.6	1.6	2.6
Maximum Efficiency Point (p = 15 MPa)			
Engine Speed	1100	1300	1350
Indicated Power	24.8	25.9	28.1
Friction	2.3	2.7	2.0
Auxiliaries	0.4	0.5	0.6
Net power	22.1	25.9	25.5
Ext. heat system efficiency	92.4	92.5	92.8
Net efficiency	43.5	42.5	42.2
Low Load Point (p = 5 MPa, n = 1000 rpm)			
Indicated Power	7.9	7.8	7.2
Friction	0.9	0.9	0.6
Auxiliaries	0.4	0.4	0.4
Net power	6.6	6.5	6.2
Ext. heat system efficiency	89.8	89.8	90.7
Net efficiency	36.4	35.4	33.9

*Redefined since "old predictions"

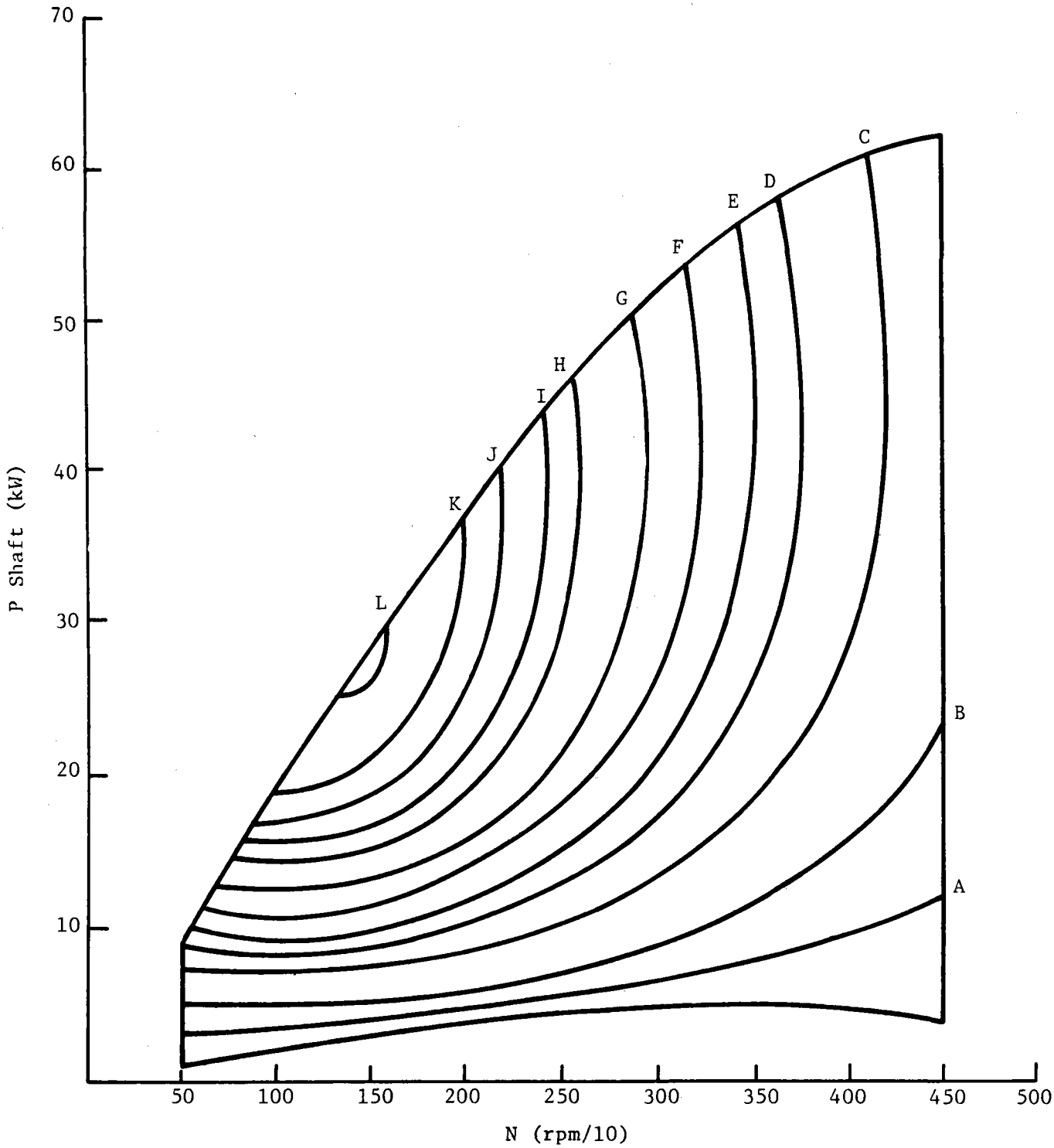

A = 25.0	D = 36.0	G = 39.0	J = 41.0
B = 30.0	E = 37.0	H = 40.0	K = 41.5
C = 34.0	F = 38.0	I = 40.5	L = 42.0

Figure 7-8 1983 RESD: Net Efficiency Isolines (%)

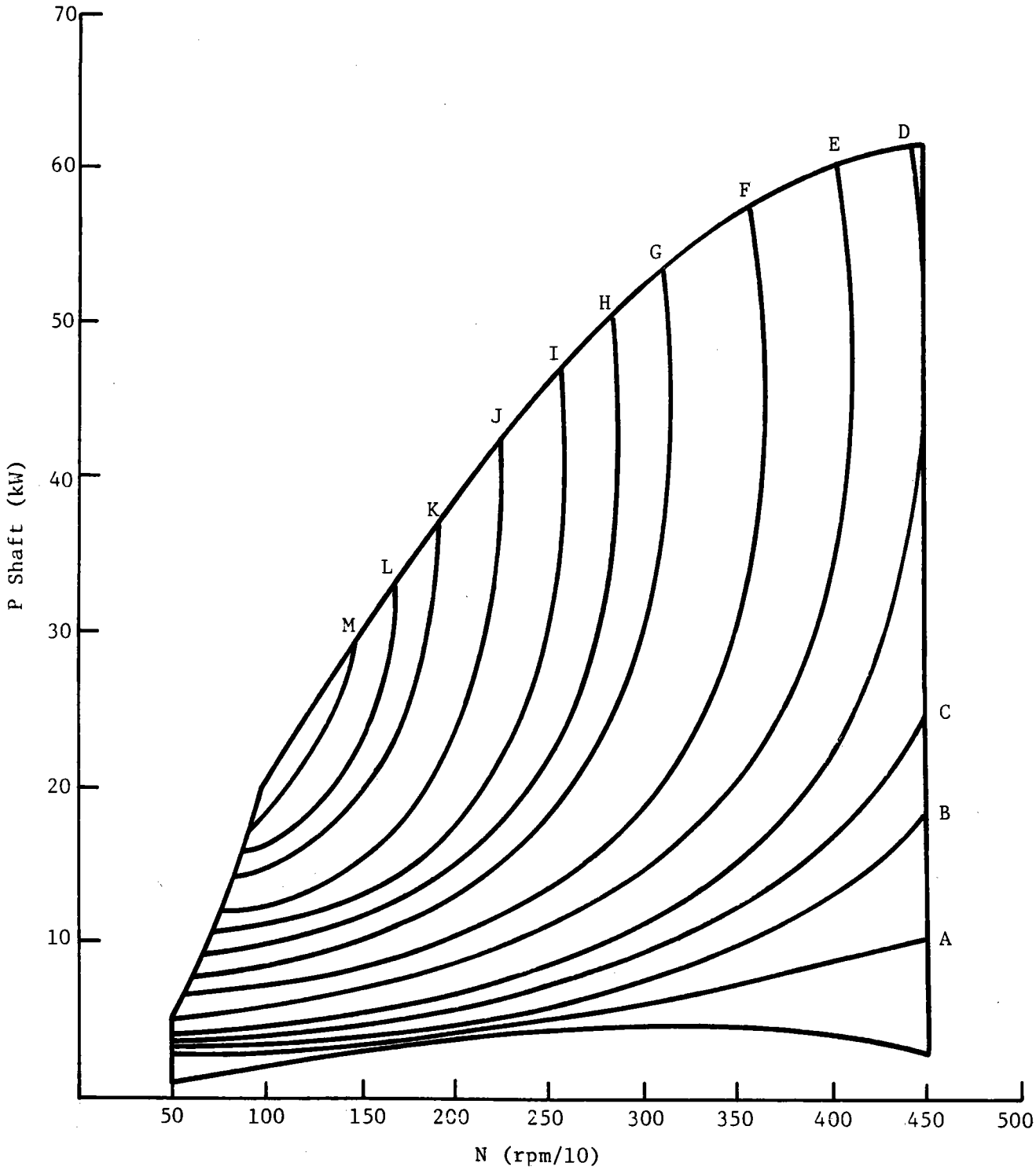

A = 24.0	D = 32.0	G = 33.0	J = 41.0	M = 43.0
B = 28.0	E = 34.0	H = 39.0	K = 42.0	
C = 30.0	F = 36.0	I = 40.0	L = 42.5	

Figure 7-9 1981 RESD: Curves of Constant Net Efficiency (%)

8.0 MTI VEHICLE CODE VALIDATION

The usefulness of sophisticated computer codes is directly related to the users' confidence to predict absolute values. The MTI Vehicle Simulation Program has continually undergone validation studies since it became operational. Actual versus predicted mileage has always agreed quite well; both spark-ignition and Stirling-engine mileage have been predicted with success. These validation studies have been reported in previous RESD Design Reviews, and in the Commercialization Enhancement Program report. The latest validation was conducted on the Mod I Lerma vehicle. Prior to vehicle testing, mileage numbers (and NO_x emissions) were predicted. Lerma test data and predictions are shown in Table 8-1.

Cold-Start Penalty

The EPA CVS urban test consists of six phases (see Figure 8-1).

1. 12-hour Cold Soak: Vehicle must be allowed to come to thermal equilibrium at room temperature 12 hours prior to test.

2. Cold Transient: Vehicle is started and run through the first 505 seconds of the urban driving cycle, filling emission Bag 1.

3. Cold Stabilized: Emissions sampling is switched from Bag 1 to Bag 2, and the vehicle is operated from 505 to 1372 seconds of the urban driving cycle. The engine is switched off.

4. Hot Soak: Vehicle is allowed to "soak" for 10 minutes.

5. Hot Transient: Vehicle is restarted and operated again through the first 505 seconds of the urban driving cycle, filling emission Bag 3.

6. Hot Stabilized: This phase is not actually accomplished, i.e., it is assumed to be equal to the Cold Stabilized Phase.

TABLE 8-1

MOD I LERMA TEST DATA

	Urban				Highway	Combined
Description	HC g/mi	CO g/mi	NOx g/mi	Mileage mpg	mpg	mpg
9/21 Test	.230	3.40	.960	19.90	31.70	23.90
9/24 Test	.290	3.30	.900	18.80	32.10	23.20
9/25 Test	.250	3.20	.840	19.20	32.40	23.50
Standard Deviation	.025	0.082	.049	0.45	0.29	0.29
Mean	.260	3.30	.900	19.30	32.10	23.50
Projections	--	--	.840	19.10	30.00	22.80

11.1 hp at 50 mph DPA

3750 lb IW Setting

2.73 Axle Ratio

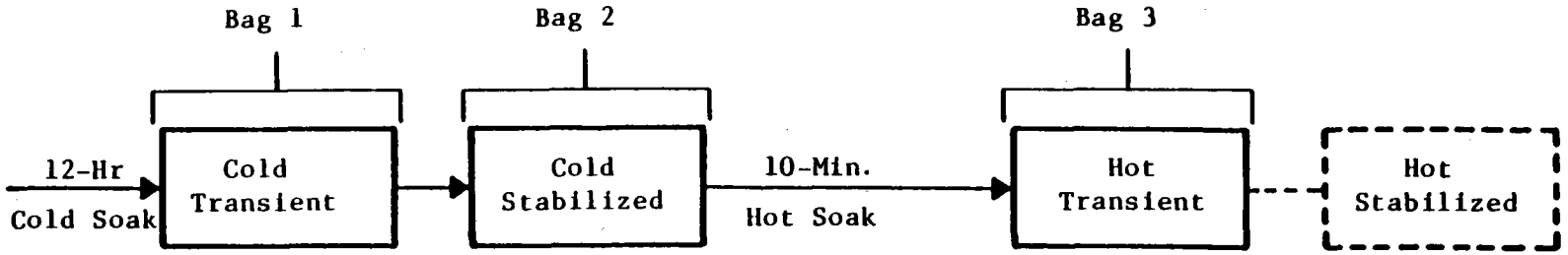

Fuel Consumed M_C M_S M_H (M_S)

$$\text{Estimated mpg} = \frac{\text{Distance}}{43(M_C+M_S) + .57(M_H+M_S)} = \frac{\text{Distance}}{.43M_C + .57M_H+M_S}$$

EPA Test

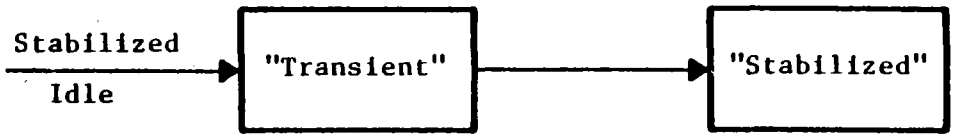

M_T $M_{S'}$

$$\text{"Cold Start" Penalty} = .43(M_C-M_T) + .57(M_H-M_T) + (M_S-M_{S'})$$

$$\text{Estimated mpg} = \frac{\text{Distance}}{CSP + M_T + M_{S'}}$$

811685

Figure 8-1 Cold-Start Penalty Test

Urban mileage, now referred to as "estimated mpg," is calculated as shown in Figure 8-1, which also shows a test to measure the cold-start penalty. First, the official EPA test is run to determine estimated mpg, then the transient and stabilized phases are rerun, beginning with an engine at stabilized idle. The cold-start penalty can be obtained using the formulas shown, and can be broken down further. The following definitions are offered to make discussion easier.

Cold-Start Penalty (CSP) - The mass of fuel that must be added to the fuel consumed on the urban cycle when calculated from steady-state maps, or when run with a stabilized engine at the beginning of the cold and hot cycles.

Cold-Start Fuel Consumption (CSFC) - The amount of fuel consumed by the engine during cold start-up, plus the amount of fuel used to achieve stabilized idle fuel flow, minus the stabilized idle fuel flow for an equal amount of time.

Hot-Start Fuel Consumption (HSFC) - The amount of fuel consumed by the engine during a hot start (restart after 10 minutes of shutdown), plus the amount of fuel used to achieve stabilized idle fuel flow, minus the stabilized idle fuel flow for an equal amount of time.

If we look at the equation for the cold-start penalty:

$$CSP = 0.43\ (M_C - M_T) + 0.57\ (M_H - M_T) + (M_S - M_S'),$$

and assume $M_S - M_S' = 0$, then according to the definitions, we see that:

$$CSFC = M_C - M_T, \text{ and } HSFC = M_H - M_T.$$

Substituting back into the equation for the cold-start penalty:

$$CSP = 0.43(CSFC) + 0.57(HSFC).$$

To arrive at the CSP for the Mod II engine, the relationship between stored heat and cold start penalty is used. The CSFC represents (analytically) the amount of fuel required to raise the temperature of the engine hot parts from

ambient to operating temperatures. Documentation of this relationship between stored heat and CSP has been accomplished via vehicle testing with the upgraded Mod I engine. The calculated stored heat for the Upgraded Mod I is 12.15 MJ, which corresponds to 283 grams of CSFC. Measured CSFC in vehicle tests averaged 274 grams. For the purpose of estimating Mod II CSFC, the stored heat value has been used directly. The stored heat for the Mod II is 10.32 MJ which corresponds to a CSFC of 241 grams. HSFC has been estimated by calculating the energy loss during the 10 minute hot soak, with the following criteria:

- 300 rpm motoring speed
- All auxiliaries decoupled except H_2O pump and combustion air blower
- Fan and electronics supplied from battery
- Combustion air blower operating at zero mass flow.

The calculated HSFC for this hot soak is 66 grams. The CSP for the Mod II is then expected to be:

$$CSP = 0.43\ (241) + 0.57\ (66) = 141 \text{ grams}$$

The 1983 RESD concept was modelled with the RESD vehicle on the MTI Vehicle Simulation Program. Table 8-2 lists the important features of the RESD vehicle. Previous RESD optimizations provided the base to build on. The previous shift schedule was retained; however, the transmission utilized was an automatically shifted 4-speed transmission without torque converter. Final drive ratio was optimized to attain a 15.0-second 0-60 mph acceleration. Urban, highway, and combined mileages are listed in Table 8-3, along with diesel combined mileage.

TABLE 8-2

RESD VEHICLE SPECIFICATION

Note: Complete vehicle specification published as
MTI Report No. 79ASE54TS1 Rev. 4

General	
Model, Year	1983 4-Door Hatchback Pontiac Phoenix
EPA Class	Mid-Size
Maximum Passengers	2 Front/3 Rear
Vehicle Weights	
Curb Weight	1304.5 kg (2870 lb)
Test Weight	1440.9 kg (3170 lb)
EPA Inertia Weight	1420.4 kg (3125 lb)
Road Load	
Rolling Resistance Coefficient	0.0095 (road) 0.0110 (dyno)
Rolling Radius at 72.4 km/h (45 mph)	302.7 mm (0.993 ft) (846 rev/mile)
Air Drag	5.37 kW at 80.4 km/h (7.20 hp at 50 mph)
Drag Coefficient	0.417
Frontal Area	21.34 ft^2
Total Road Load	8.37 kW at 82.4 km/h (11.22 hp at 50 mph)
EPA DPA Setting (includes 10% A/C penalty)	5.414 kW at 80.4 km/h (17.26 hp at 50 mph)

TABLE 8-2 (Cont'd)

Transaxle	
Type	Modified GM THM 440 (4-speed automatically shifted
Gear Ratios	
Engine/Torque Converter	1.40
First	2.92
Second	1.55
Third	1.00
Fourth	0.704
Final Drive	3.64
Shift Schedule	Optimized for Stirling Engine
Accessories	Power Steering/Brakes, Air Conditioning
Accessory Loads	P/S, B, Electric Cooling Fan, Transaxle Front Dump
Acceleration Performance	
0-60 mph Time	15.0 sec
50-70 mph Time	9.7 sec
0-100 ft Time	4.5 sec
Top Speed	>100 mph

TABLE 8-3

RESD VEHICLE FUEL ECONOMY PERFORMANCE

		IC	V-4
Urban w/o CSP	(mpg)		41.3
Cold-Start Penalty	(g)		141
Urban	(mpg)		32.3
Highway	(mpg)		56.9
Combined Mileage	(mpg)	31.0	40.1
Combined Mileage Diesel Fuel	(mpg)		46.1

9.0 RISK ASSESSMENT

The risk assessment presented in Tables 9-1 through 9-8 is a pseudo-objective evaluation of the probability of success in accomplishing the objectives of the RESD based on the level of technology presently embodied in the Mod I engine.

The 1983 RESD represents a substantial increase in the technology level of the program because all experience to date has been on the modular "U" design. In preparing this assessment, input was solicited from all of the sepcialists responsible for the development of this technology. In addition to their input, an evaluation was made as to whether the development would be available in a timely manner, what backup designs were available, and their associated penalty.

After determination of the key performance (power, efficiency, and emissions) and design factors (durability, weight, cost, and packaging), and their risks, relative weighting was made of their impact on achieving the overall objectives. This weighted risk was then assumed to determine the relative performance and design risk.

In this risk assessment, more importance was given to the accomplishment of performance goals than in past assessments due to the radical change from a modular "U" design to an integral "V" design.

The major conclusion of this assessment is that although the risk level is high (61.1%), it is consistent with a high-technology R&D program aimed at providing a revolutionary engine technology to industry with a cost-competitive engine system while maintaining significant performance advantages.

TABLE 9-1

RISK

The probability of achieving program design and performance objectives in the annular engine is based on:

- the foundation of Mod I engine/system experience;

- current state of technology:

  - rigs (Component, HTP-40, P-40R, P-40 Seals, TTB), and
  - engines (Mod I, Updated Mod I);

- development of technology by 1986 within the constraints of:

  - the Work Plan, and
  - the budget

TABLE 9-2

PROGRAM AND SUPPORTIVE OBJECTIVES

	Mod I (Actual)	RESD	
		Goal	Proj.
Engine/Vehicle System			
Combined Fuel Economy (mpg)	23.50	40.3	40.1
Emissions			
CO (g/mile)	3.30	3.40	
HC (g/mile)	0.26	0.41	
NO_x (g/mile)	0.90	0.40	
Particulates (g/mile)	--	0.20	
Reliability (hours)	--	3500	
Engine			
Vehicle Basis	81 Lerma	84 Phoenix	
Inertia Weight (lbs)	3750	3125	
Part-Power Efficiency (%)	31.00	37.4	37.3

TABLE 9-3

ENGINE CHARACTERISTICS

	Mod I	Upgraded Mod I	March, 1981 RESD	May, 1983 RESD
Power (kW)	53.80	58	60	60
(hp)	72.10	78	80	80
Temperature (°C)	720	820	820	820
Weight (lbs)	688	580	397	382*
Specific Weight (lbs/hp)	9.50	7.50	4.90	4.75
Part-Power Efficiency (%)	31.00	33.00	37.70	37.3
Maximum Efficiency (%)	37.40	39.00	43.50	42.2

*Includes alternator and power-steering pump.

TABLE 9-4

DESIGN COMPARISON

	Mod I	Upgraded Mod I	March 1981 RESD	May 1983 RESD
Operating Temp. (°C)	720	820	820	820
Part-Power Optimization	No	Yes	Yes	Yes
Heater Head	Canister	Domed Canister	Canister	Annular
Heater Tubes	Involute	Involute	Involute	Hairpin
Heater Head Material	HS31/N155	XF-818/CG27	XF-818/12RN72	XF-818/CG27
Combustor Loading (kW/l)	40	40	53	38
Combustor	EGR	EGR	Prevaporized	CGR
Fuel Nozzle	Air Atomized	Air Atomized	Non Air Atomized	H_2O Cooled, Low-Flow Air Atomized
Preheater Diameter (in.)	29.5	23.2	27.1	20.9
Preheater	Welded Metallic	Welded Metallic	Folded Metallic	Ceramic Block
Regenerator Matrix	Screen	Screen	Screen	Screen
Cooler	Stainless Steel Tubes	Stainless Steel Tubes	Stainless Steel Tubes	Carbon Steel Tubes
Cold Engine System	Modular	Modular	Modular	Integral
Main Seal	PL w/Capseal	PL w/Capseal	PL w/o Capseal	Double Angle w/o Capseal
Piston Rings	Double Split/Solid	Double Split/Solid	Double Solid	Single "H"
Seal System	P_{min}	P_{min} Liner	P_{min}	-
Engine Drive	Journal	Rolling Element	Red Journal	Rolling Element
Power Control	Moog MPC	Moog MPC	Moog MPC	Rotary MPC
Air/Fuel Control	K-Jetronic	Electronic	Electronic	Closed-Loop Electronic
Blower	Centrifugal	Centrifugal	Centrifugal	Positive Displacement
Auxiliaries				
- Servo Oil	Yes	Yes	Yes	No
- Air Throttle	Yes	Yes	Yes	No
- Combined Starter/ Upstart Motor	No	No	No	Yes

TABLE 9-5

RESD RISK ASSESSMENT (PERFORMANCE)

Performance Factors*	Effect on Achieving RESD Goal: Engine Tests	Tech. Dev.	Overall Risk	Comments
820° Cycle Optimization (P, E)	H	L	M	Mod I Predictions Excellent
Annular Design (P, E)	L	H	H	P-40R Tests Indicate Slight Efficiency Penalty
Partition Wall (P, E)	L	H	H	Additional QE Loss
CGR Combustor (E, I)	L	M	M	Many Options Available
Low Flow Air Atomizer Nozzle (I)	M	M	M	-
Main Seal (No Capseal) (P, E)	M	M	M	New Designs Promising
Single "H" Piston Ring (P, E)	L	H	H	Major Factor in Efficiency
Rolling-Element Drive (P, E)	H	L	L	Utilized in Upgraded Mod I
Simplified Auxiliaries (P, E)	L	H	M	-

*P = Power, E = Efficiency, I = Emissions

TABLE 9-6

RESD RISK ASSESSMENT (DESIGN)

Design Factors*	Effect on Acheiving RESD Goals: Engine Test	Tech. Dev.	Overall Risk	Comments
Heater Head (D, W, C)	L	M	H	Upgraded Mod I Manufacture Successful
V-Block (W, C)	L	M	M	Design Complexity
Alternative Materials (C, D)	M	L	L	Underway in Upgraded Mod I
Preheater (C)	M	M	H	Major Cost Impact
Regenerator (C)	L	H	H	Mod I Design
Cooler (C)	M	H	M	Low Cost Design
Lightweight Piston (W)	M	M	M	Design Risk
Main Seal (D)	M	M	H	Key to 3500 hr Life
Single "H" Piston Ring (D)	M	H	H	-
Controls (D,W,C)	M	H	M	Proven in Upgraded Mod I
Simplified Auxiliaries (D,W,C,S)	H	H	M	Substantial Weight/ Cost Impact

*D = Durability, W = Weight, C = Cost, S = Packaging.

TABLE 9-7

RESD RISK ASSESSMENT SUMMARY

Factors	Relative Contribution 0 - 100 Scale	Risk	Totals
Performance - Represents 40% Risk			
820° Optimization	10	M	
Annular Design	25	H	
Partition Wall	12	H	
CGR Combustors	8	M	
Low-Flow Air Atomized Nozzle	5	M	
No Cap Seal	5	M	
Single "H" Piston Ring	15	H	
Drive	10	L	
Simplified Auxiliaries	10	M	62.1
Design - Represents 60% Risk			
Heater Head	15	H	
V-Block	15	M	
Alternative Materials	5	L	
Preheater	15	H	
Regenerator	5	H	
Cooler	10	M	
Drive Components	5	M	
Main Seal	10	H	
Single "H" Piston Ring	5	H	
Controls	10	M	
Simplified Auxiliaries	5	M	60.5

Risk = 0.4 (62.1) + 0.6 (60.5) = 61.1 Weighted Risk = 61.1

TABLE 9-8

RESD RISK

(Based on Mod I Technology)

	January, 1980 (%)	March, 1981 (%)	May, 1983 (%)
Design Risk	66.5	59.5	60.5
Weighting	70	70	60
Performance Risk	58.6	37	62.1
Weighting	30	30	40
Total Risk	64	53	61.1

10.0 MANUFACTURING COST ANALYSES

10.1 Approach

- The manufacturing cost study was performed by an independent contractor (Pioneer Manufacturing Engineering) with the following criteria:

  - Estimate manufacturing (transfer) cost of the 1983 RESD in 1984 economics for an annual production volume of 300,000 each.

  - Estimate the manufacturing cost of engine controls and auxiliaries in 1984 economics.

  - Perform manufacturability analyses of major parts and operations affecting the manufacturing costs.

10.2 Cost Analyses Data

The data used for the cost analyses included:

- Latest drawings and information as of April 1983;
- Pioneer 1981 RESD cost analysis;
- Vendor information from machinery manufacturers, foundries and their representatives;
- MTI interim manufacturing cost-estimating guidelines; and,
- manufacturing figures in 1984 economics.

10.3 Basis of the Cost Analyses

The manufacturing cost analyses included:

- Material and labor
- Setup costs
- Inbound freight
- Manufacturing scrap

- Perishable production tools
- Rework
- Standard factory overheads
- Depreciation of capital equipment and tooling
- Maintenance, repairs, and other factors.

The manufacturing cost did not include:

- R&D amortization
- General administration
- Sales and shipping costs
- Profits
- Start-up cost
- Inventory costs
- Interest on work in progress.

10.4 Parts Selection Methodology for Cost Analyses

The parts were subject to "ABC" analysis where the "A" parts were $\geq$75% of the total cost, "B" parts were $\geq$20% of the total cost, and "C" parts accounted for the rest of the total cost. "A" and "B" parts were cost-estimated; the cost of "C" parts was extrapolated.

10.5 Conclusion of Manufacturing Cost Analyses

The major factors considered for recommendation regarding manufacturing cost and manufacturability were

- Suited for volume production on transfer line/automated machines
- Less vulnerable for production scrap and rework
- Easy to assemble and test
- Less number of components
- Uniform components to the extent possible.

The recommendations resulting from the manufacturing cost analyses indicated that the V-4 RESD was suitable for high-volume production.

10.6 Summary of Manufacturing Costs

A summary of the Pioneer manufacturing cost study is presented in this section. The basic Stirling engine cost is presented in Table 10-1, with the cost of major subassemblies identified. Manufacturing costs for the complete Stirling engine system which includes controls and auxiliaries is given in Table 10-2. Total first cost, including vehicle integration requirements, is given in Table 10-3, and life cycle costs are given in Table 10-4. First costs and life cycle costs for the 1983 V-4 RESD are compared to the comparable IC and Diesel engines. It should be noted that the Stirling costs are competitive with these current systems.

TABLE 10-1

COST SUMMARY - BASIC ENGINE COMPONENTS
1983 RESD

Component	Cost
Preheater Assembly	$ 88.48
Combustor Assembly	39.25
Cylinder Head Assembly	161.72
Regenerator Assembly (4/Engine)	197.96
Gas Cooler Assembly	76.52
Piston/Piston Rod Assembly	62.12
Engine Block	56.89
Crosshead/Connecting Rod Assembly	32.58
Crankshaft	31.01
Main Bearings	12.00
Oil Sump Assembly	6.58
Lube Oil Pump Assembly	14.66
Water Pump Assembly	28.60
TOTAL	$808.37
"Matured" Cost (85%)	$687.11

TABLE 10-2

COST SUMMARY - STIRLING ENGINE SYSTEM
1983 RESD

Controls and Auxiliaries	Cost
Control Block Assembly*	$ 101.00
Hydrogen Storage Vessel	40.80
Electronic Package*	82.00
Starter System	48.00
Alternator	70.70
Combustion Air Blower*	86.03
Air Fuel Control*	98.06
Hydrogen Compressor*	31.38
Rotary Control Valve*	53.57
Water Pump - After Cooler (with Motor and Controls)	15.00
Transducers* - Pressure (2)	80.00*
TOTAL (Controls and Auxiliaries)	$ 706.54
"Matured" Cost (85% of * Items plus the unfactored remaining parts)	$ 626.73
"Matured" Basic Engine Cost	$ 687.11
TOTAL "Matured" Stirling Engine System Cost	$1313.84

TABLE 10-3

SUMMARY COSTS
TOTAL VEHICLE PROPULSION SYSTEM FIRST COST
1983 RESD FWD PASSENGER CAR

Vehicle Integration Component	Cost
Radiator Coolant System	$ 57.33
Exhaust System	26.73
Battery	37.20
Radiator Fan System	18.75
Power Steering	33.05
Automatic Transmission	421.25
Air Conditioner	80.75
Instruments	2.40
Final Assembly Labor	25.58
TOTAL	$ 703.04
TOTAL "Matured" Stirling Engine System Cost	$1313.84
TOTAL First Cost	$2016.84

TABLE 10-4

LIFE CYCLE COST (LCC)

	Stirling	I.C.	Diesel
Installed Cost	$2017.00*	$1802.00	$2198.00
Annual Depreciation	403.00	360.00	440.00
Annual Interest (6.5%) (Not Earned)	131.00	117.00	143.00
Fuel	730.00	973.00	1148.00
Lube	15.00	15.00	15.00
Tuneup	20.00	30.00	30.00
Spark Plugs	1.00	5.00	--
Fuel Injection Cleaning	--	--	30.00
Oil Change/Filter	15.00	20.00	20.00
Fuel Filter	--	--	16.00
H_2 Charge	26.00	--	--
Annual Charges	1341.00	1502.00	1842.00
x 5 = LCC	6705.00	7510.00	9210.00
Miles Per Gallon	40	30	23

100,000 Miles - 5 Years - 13% Interest

Fuel: $1.46 - Unleaded
$1.32 - Diesel

4.7L Diesel Used (Smallest American) Equivalent HP to SES. and I.C.

Engine Description	kW	Displacement	Cylinders
Stirling - RESD V-4 Mark V	60	N/A	V-4
I.C.	68	2.5L	L-4
Diesel	63	4.7L	V-6

Insurance Costs Assumed to be the Same

NOTE: If Diesel mpg = 40

	Stirling	I.C.	Diesel
TOTAL LCC	$6705.00	$7510.00	$6770.00

(Installed Cost Relatively Insensitive to Engine HP)

Installed Cost	Engine	Control	Integration	Total
Stirling	$687.00	$627.00*	$ 703.00	$2017.00
I.C.	$ 577.00		1227.00	1802.00
Diesel	1180.00		1068.00	2258.00

*These are "Matured" Costs

1. Report No.	2. Government Accession No.	3. Recipient's Catalog No.
NASA CR-174674		

4. Title and Subtitle	5. Report Date
Automotive Stirling Engine Development Program RESD Summary Report	May 1984
	6. Performing Organization Code
7. Author(s)	8. Performing Organization Report No. 84ASE356DR3/84TR11
	10. Work Unit No.
9. Performing Organization Name and Address Stirling Engine Systems Division Mechanical Technology Incorporated 968 Albany-Shaker Road Latham, New York 12110	11. Contract or Grant No. DEN 3-32
	13. Type of Report and Period Covered Design Report
12. Sponsoring Agency Name and Address U.S. Department of Energy Office of Vehicle and Engine R&D Washington, D.C. 20545	14. Sponsoring Agency ~~Code~~ Report No. DOE/NASA/0032-23

15. Supplementary Notes

Final Report. Prepared under Interagency Agreement DE-AI01-77CS51040. Project Manager, William K. Tabata, Energy Technology Division, NASA Lewis Research Center, Cleveland, Ohio 44135.

16. Abstract

This is the final report compiling a summary of the information presented and discussed at the May 1983 Automotive Stirling Engine (AES) Reference Engine System Design (RESD) review held at the NASA Lewis Research Center. The design of the engine and its auxiliaries and controls is described. Manufacturing costs in production quantity are also presented. Engine system performance predictions are discussed and vehicle integration is developed, along with projected fuel economy levels.

17. Key Words (Suggested by Author(s))	18. Distribution Statement
Automotive Stirling engine Reference Engine System Design (RESD) RESD Manufacturing costs RESD system performance	Unclassified - Unlimited Star Category 85 DOE Category UC-96

19. Security Classif. (of this report)	20. Security Classif. (of this page)	21. No. of pages	22. Price*
Unclassified	Unclassified	221	A10

*For sale by the National Technical Information Service, Springfield, Virginia 22161

☆ U.S. GOVERNMENT PRINTING OFFICE: 1984 - 759-100/10408